TECHNISCHE UNIVERSITÄT MÜNCHEN

Ingenieurfakultät Bau Geo Umwelt

Lehrstuhl für Ingenieurgeologie

Tracing fluids involved in the formation of bentonite deposits

Mathias Hendrik Köster

Vollständiger Abdruck der von der Ingenieurfakultät Bau Geo Umwelt der Technischen Universität München zur Erlangung des akademischen Grades eines Doktors der Naturwissenschaften genehmigten Dissertation.

Vorsitzender:

Prof. Dr. Florian Einsiedl

Prüfer der Dissertation:

1. apl. Prof. Dr. Hans Albert Gilg

2. Prof. Lynda B. Williams, Ph.D.

3. Prof. Dr. Martin Elsner

Die Dissertation wurde am 16.11.2017 bei der Technischen Universität München eingereicht und durch die Ingenieurfakultät Bau Geo Umwelt am 24.04.2018 angenommen.

This page is intentionally left empty

Abstract

New petrographic, mineralogical, and chemical evidence is presented regarding the fluids involved in the formation of bentonite deposits. The main focus is placed on the genesis of bentonite deposits in Southern Germany that formed from rhyolitic ashes in a terrestrial, non-arid setting. The use of boron contents and boron isotope values of smectites from bentonite deposits of various formational settings for tracing fluids involved in bentonite deposit formation is discussed.

Petrographic, X-ray diffraction and stable isotope analyses of authigenic carbonates in bentonites in Southern Germany reveal that dolomites and calcites formed in-situ in pedogenic, palustrine, and groundwater settings. The carbon and oxygen isotope values of the authigenic carbonates imply a C3-plant-dominated carbon source and a formation from evaporated meteoric waters. Main and trace element data, and $^{87}Sr/^{86}Sr$ of dolomites, calcites, and smectites indicate that evaporated Sr- and Mg-rich surface water was involved in bentonitisation and dolomite formation in palustrine and some pedogenic settings. However, Sr-poor groundwater with a lower molar Mg/Ca around 1 and a stronger silicate weathering component was involved in bentonite and calcite formation in strictly pedogenic and groundwater settings. The $^{87}Sr/^{86}Sr$ and molar Mg/Ca of the smectite interlayers suggest a later cation exchange with waters having more radiogenic Sr sources and lower molar Mg/Ca. The strontium isotope analysis of one smectite residue without a detrital illitic component and cogenetic palustrine dolomites indicates a rapid onset of bentonitisation and dolomite formation after ash deposition.

Prompt gamma neutron activation analysis and secondary ion mass spectrometry of smectites from various bentonite deposits reveal that smectites show fixed boron concentrations of 0.2 to 196 µg/g. Sodium bentonites have higher boron concentrations (> 30 µg/g) than Mg- or Ca-bentonites. The boron content of smectites is strongly influenced by an interstratified illitic component that requires the use of modified fluid-mineral boron partitioning coefficients for interpretation. Bentonites formed from fluids with < 0.1 µg/g B to more than 100 µg/g B. Smectites from terrestrial settings have negative $\delta^{11}B$ values whereas smectites from marine settings have highly variable $\delta^{11}B$ values, indicating that also marine bentonites formed from fluids influenced by strong water-rock interaction in the continental crust, and not from unmodified seawater. The $\delta^{11}B$ values of smectites also suggest that most Na-bentonites, but also some Mg- and Ca-bentonites, preserve the original interlayer occupancy.

The isotope geochemistry of strontium and boron in smectites and carbonates from bentonites is well suited for tracing fluids involved in the genesis of clay mineral deposits and later overprints. The geochemical systems have a high potential for studying the formational settings of swelling clay minerals and fluid flow in sedimentary basins as well as crystalline rocks close to the surface. They are therefore important criteria for the evaluation of disposal sites for highly active nuclear waste.

Zusammenfassung

In dieser Dissertation werden neue petrographische, mineralogische und geochemische Erkenntnisse zu Fluiden präsentiert, die zur Entstehung von Bentonitlagerstätten beigetragen haben. Hierbei wird der Schwerpunkt auf die Genese der süddeutschen Bentonite gelegt, die sich in einem terrestrischen, nicht-ariden Milieu aus rhyolitischen Aschen gebildet haben. Darüber hinaus werden Borgehalte und Borisotopenwerte von Smectiten aus Bentonitlagerstätten verschiedener Entstehungsräume bezüglich der involvierten Fluiden diskutiert.

Authigene Karbonatminerale in süddeutschen Bentoniten stehen im Mittelpunkte der Untersuchungen zu den an der Lagerstättenbildung beteiligten Fluide. Petrographische, röntgenographische und stabile Isotopen-Analysen an Dolomit und Kalzit ergeben, dass sich die Karbonate in-situ in pedogenen, palustrinen und Grundwasser-gesättigten Milieus gebildet haben. Die stabilen Kohlenstoff- und Sauerstoffisotopendaten der authigenen Karbonate indizieren eine von C3-Pflanzen dominierte Kohlenstoffquelle und die Beteiligung von durch Verdunstung modifizierten meteorischen Wässern. Die Haupt- und Spurenelementuntersuchungen sowie Strontiumisotopenanalysen an Dolomit, Kalzit und Smectit deuten darauf hin, dass eingedampfte Oberflächenwässer mit hohen Sr- und Mg-Gehalten auf Grund der Verwitterung von detritischen Karbonaten an der Bentonit- und Dolomitentstehung im palustrinen und pedogenen Umfeld beteiligt waren. Allerdings waren Sr-ärmere Grundwässer mit einem molaren Mg/Ca von etwa 1 und mit einer stärkeren Silikatverwitterungskomponente an der Bentonitisierung und Kalzitbildung in strikt pedogenem Umfeld und im Grundwasserbereich involviert. Die Strontiumisotopenverhältnisse und molaren Mg/Ca-Werte der Smectit-Zwischenschichten deuten auf einen späteren Kationenaustausch mit Wässern mit radiogenerem Sr, aber niedrigen Mg/Ca hin. Die Strontiumisotopenanalyse einer Smectit-Probe ohne detritischen illitischen Anteil und der kogenetisch gebildeten palustrinen Dolomite weisen auf einen schnellen Beginn der Bentonitisierung und Dolomitbildung kurz nach der Ablagerung des vulkanischen Ausgangsmaterials.

Die Prompt-gamma Neutronenaktivierungs- und Sekundärionen-Massenspektrometrie-Analyse von Smectiten verschiedener Bentonit-Lagerstätten zeigen, dass die Smectite nicht austauschbare Borgehalte von 0.2 µg/g bis 196 µg/g besitzen. Bentonite mit einer Na-dominierten Zwischenschichtbelegung zeigen höhere Borgehalte (> 30 µg/g) als Ca- oder Mg-Bentonite. Die Borkonzentration wird jedoch auch von kleinen Mengen illitischer Komponenten beeinflusst, die es nötig machen modifizierte Fluid-Wasser Bor-Verteilungskoeffizienten zwischen Smectit und dem Fluid bei der Interpretation der Daten zu benutzen. Bentonite wurden von Wässern mit einer Borkonzentration von < 0.1 µg/g bis mehr als 100 µg/g gebildet. Smectite aus terrestrischen

Lagerstätten besitzen durchwegs negative $\delta^{11}B$-Werte, wohingegen Smectite aus marinen Ablagerungsräumen stark variable $\delta^{11}B$-Werte aufweisen. Dementsprechend müssen auch viele marine Bentonite durch die Interaktion mit Wässern mit starker Fluid-Gesteinsinteraktion mit kontinentaler Kruste entstanden sein, und nicht ausschließlich durch unmodifiziertes Meerwasser wie bisher angenommen. Die $\delta^{11}B$-Werte verschiedentlich behandelter Smectite belegen, dass Na-Bentonite und einige Ca- und Mg-Bentonite ihre ursprüngliche Zwischenschicht-Kationenbelegung bewahrt haben könnten.

Die (Isotopen-)Geochemie von Strontium und Bor in Smectiten und assoziierten Karbonaten von Bentoniten eignet sich hervorragend dazu die an der Entstehung und auch möglicher Überprägung der Tonlagerstätten beteiligte Fluide zu charakterisieren. Die beiden geochemischen Systeme besitzen daher auch ein großes Potential für Studien zum Bildungsmilieu von quellfähigen Tonmineralen und auch generell zu Fluidbewegungen in Sedimentbecken und oberflächennahem Kristallin. Sie haben daher auch Bedeutung zur Beurteilung der Sicherheit von Endlagern für hochradioaktive Abfälle.

Acknowledgements

First of all I would like to sincerely thank my doctoral supervisor Prof. Dr. H. Albert Gilg for offering me the chance to research at the Department of Engineering Geology of the Technical University of Munich. He was a constant source of inspiration and continuously supported me.

Prof. Dr. Kurosch Thuro made it possible to work at the Department of Engineering Geology for the majority of my doctoral studies, and I am deeply grateful for this opportunity. Furthermore, I would like to express my gratitude towards Katharina Holzhäuser who was a never ending source of help and moral support during long laboratory hours, to Vladimir Ruttner who always had a helping hand, as well as to my tutor Dr. Christoph Mayr for his cordial friendship and the carbonate stable isotope measurements. I am very grateful for the fruitful research cooperation with Dr. Stefan Hölzl at the ZERIN RiesImpaktMuseum, Lynda B. Williams, Ph.D. at Arizona State University, Dr. Petra Kudejova and Dr. Zsolt Revay at the FRM II research neutron source, Dr. Jürgen Bär at the Universität der Bundeswehr München, as well as Dr. Klaus Simon at the University of Göttingen.

Most of the research presented in this study would have been impossible without the cordial help and access granted to bentonite deposits by Ulrich Boehnke and Martin Ziegenaus at S & B Industrial Minerals (now Imerys), and Bernhard Ratzke at Clariant (former Süd-Chemie).

I also want thank Florian Duschl for introducing me into TUM and especially to Dr. Michael Rieder for being a wonderful teacher and role model during my first courses and field trips.

Dr. Reiner Dohrman and Dr. Stefan Kaufhold at the BGR, as well as Prof. Dr Laurence Warr at the University of Greifswald supplied several sodium bentonites from their collection, and together with Dr. Georg Grathoff offered plenty of advice during the DTTG Workshop 2013 in Karlsruhe.

I am deeply grateful for receiving funding from the Society of Economic Geologists SEG Student Research Fellowship 2012 which was essential in kick-starting my doctoral research, and being awarded the Clay Minerals Society Student Research Grant 2014 which was instrumental for a successful boron isotope study.

Last but not least I want to thank Dr. Tim Yilmaz for proof reading some chapters of my dissertation.

Table of contents

This page is intentionally left empty

CHAPTER ONE

1. Introduction and motivation

Sodium-, Mg- and Ca-bentonites are important industrial commodities used in various applications (Grim & Güven, 1978; Robertson, 1986; Murray, 2007) that show an overwhelming variety of features, starting with their colour and texture (Figure 1.1) and spanning to intrinsic material properties such as the interlayer cation occupancy, layer charge distribution, cis- and trans-vacant octahedral sites of dioctahedral smectites, particle shape, and many others (Odom, 1984; Grim & Güven, 1978).

Fig. 1.1: Variously coloured and textured bentonite samples from around the globe.

The formation of Na-, Mg- and Ca-bentonite deposits has been the subject of geoscientific research for more than a century (Knight, 1897, 1898; Ross & Shannon, 1926; Grim & Güven, 1978), but uncertainties regarding the origin and formation of bentonites with different interlayer cation occupancies have not yet been fully resolved (Grim & Güven, 1978; Christidis & Huff, 2009). The type (marine, meteoric, hydrothermal, etc.) and composition (salinity, Mg/Ca, etc.) of the fluid(s) involved in the alteration and devitrification of the (usually) volcanic parent material is largely unconstrained, just as the origin of Mg- and Ca-ions for the smectitisation of unfavourably silica-rich volcanic rocks (Christidis, 2008; Christidis & Huff, 2009) – especially in strictly non-marine depositional and formational environments.

The following pages include an introduction into the depositional environments (chapters 2 – 2.1) and a review of the genesis of bentonites (chapter 2.2), i.e. bentonites *sensu strictu* formed by the

alteration and replacement of a volcanic parent material (chapters 2.2.1 – 2.2.2), and bentonites *sensu lato*, i.e. smectite-rich cays formed by the precipitation from a fluid or the replacement of non-volcanic rocks (chapters 2.2.3 – 2.2.4). An outline of carbonates in bentonites precedes (chapter 2.3) the current state of art on the formation of bentonite deposits in the Landshut region (chapters 2.4 – 2.4.3), as well as a short summary of other bentonite deposits in Bavaria (chapters 2.4.4 – 2.4.5) and Southern Germany (chapter 2.4.6).

A description of all sample processing and analytical methods (chapter 3) such as X-ray diffraction analysis (XRD), thermal ion mass spectrometry (TIMS), prompt gamma neutron activation (PGAA) or secondary ion mass spectrometry (SIMS), as well as sample origin (chapter 4) which could not be included in the three published or submitted manuscripts (chapters 5 – 7) is also presented.

The doctoral research itself is centred on articles published in the Clay Minerals Journal, and another manuscript in preparation for submission, and has two thematic focus points.

One, the formation of bentonite deposits in the Landshut region in Southern Germany (chapters 5 – 6). In the Landshut region, bentonites are found in a strictly non-marine terrestrial depositional and formation setting (Ammon, 1901; Unger et al., 1985a ,b; Vogt, 1980; Ulbig, 1994, 1999; Gilg, 2005; Aziz et al., 2008, 2010). The absence of seawater incursions during deposition and bentonitisation, and also during the entire time-span since the Miocene make the Bavarian bentonites an interesting target for the examination of a purely terrestrial depositional and formational scenario. Indirect marine "contamination" from saline groundwater or salt dissolution brines can also be excluded because of the lack of evaporite-bearing deposits in the North Alpine Foreland Basin (Lemcke, 1973; Unger, 1996).

Two, the fluids involved in the formation of Na-, Mg- and Ca-bentonite deposits in various depositional environments around the globe (chapter 7). Bentonites from North and South America, in the vicinity of the Mediterranean Sea, as well as the Caucasus region are part of this project, as well as the bentonites from Southern Germany. The B concentrations and $\delta^{11}B$ values of smectites from bentonites are used in this study to determine the B contents and $\delta^{11}B$ values of the smectite-forming fluid, and as tools to estimate the chlorinity/salinity of the solutions and the B origin (e.g. seawater or continental waters). Boron is used because it is especially suitable to distinguish marine from non-marine B sources (e.g. Swihart et al., 1986; Vengosh et al., 1991), and thus has potential to resolve whether bentonites formed in marine or non-marine depositional or formational settings.

The aim of the following discussions thus is to address these topics by focusing on the formation of the carbonate-rich Bavarian bentonite deposits (chapters 5 – 6), and later on applying the gained insights to bentonites from bentonite deposits around the globe (chapter 7).

CHAPTER TWO

2. State of the art

Bentonites are clay rocks predominantly comprised of clay minerals of the smectite group (mostly montmorillonite) with a distinct and exchangeable interlayer cation occupancy (Grim & Güven, 1978; Eisenhour & Brown, 2009; Christidis & Huff, 2009; Clay Minerals Society, 2016). Bentonite was defined by Ross & Shannon (1926) as a clay "*formed by the devitrification and the accompanying chemical alteration of a glassy igneous material, usually tuff or volcanic ash*" but Grim & Güven (1978) use a more general definition that classifies any clay primarily consisting of smectite as bentonite. The name was suggested by Knight (1897, 1898) based on deposits of soapy clay in the Cretaceous Fort Benton unit in Wyoming, USA. It was originally called mineral soap and/or "taylorite" (Knight, 1897, 1898).

The term "bentonite" may be used differently around the world as bentonites are sold under various historic-traditional and commercial names (Robertson, 1986). Bentonites *sensu lato* also include K-bentonites that are non-swelling clay rocks of volcanogenic origin but that are mostly composed of illitic material due to K-uptake and illitisation (Grim & Güven, 1978; Huff, 2016).

The worldwide occurrence and volcanogenic origin make bentonites useful tools for tephrochronology, sequence stratigraphy, radiometric age dating, and the correlation of sedimentary strata (Grim & Güven, 1978; Christidis & Huff, 2009). The presence of bentonites in Triassic to sub-recent sedimentary strata indicates that the smectitisation of volcanic rocks is a common geological process (Grim & Güven, 1978; Elzea & Murray, 1990, 1994; Eisenhour & Brown, 2009) affecting volcanic ash and tuff of acidic to basic compositions (Knechtel & Patterson, 1962; Grim & Güven, 1978; Fischer & Schmincke, 1984; Christidis & Dunham, 1993, 1997). The influence of the parent material on the mineral and chemical composition of bentonite is, however, rather variable (Christidis, 1998, 2006, 2008).

One of the most important aspects of bentonites are the exchangeable cations in the smectite interlayer, its high swelling capacity, and unusual rheological properties that make bentonite a highly valued economic commodity. Bentonites dominated by exchangeable Na-, Mg- or Ca-ions (and to a minor degree other ions) are recognised, and the result of natural cation exchange reactions (Odom, 1984). The exchangeable cation occupancy has a drastic effect on bentonite properties such as viscosity or swelling behaviour (Odom, 1984; Güven, 2009). Bentonites (or more accurately the smectites) can be artificially modified by soda or acid activation, or intercalated with organic molecules

(i.e. organo-bentonites) to design specific properties. Both natural and modified bentonites are used in specialised applications such as cat litter, hazardous and nuclear waste disposal, oil field drilling muds, fining agents for vegetable oils, wine, juice or beer, paper making, iron ore pelleting, as well as ingredients in cosmetics and pharmaceuticals (Grim & Güven, 1978; Murray, 2007).

2.1 Depositional environments

Bentonite deposits are mostly associated with Cretaceous to Pleistocene aqueous depositional environments (Grim & Güven, 1978), with exceptions present in Triassic to sub-recent rocks. Although the majority of bentonite deposits are part of marine sedimentary strata it is not uncommon for bentonites to be found in terrestrial depositional settings such as lakes or wetlands (Grim & Güven, 1978; Elzea & Murray, 1994; Christidis & Huff, 2009). The deposition of volcanic ash and coarser pyroclastic rocks can therefore take place in a wide range of environments from the immediate vicinity to its volcanic source to purely sedimentary environments without obvious volcanic sources (Grim & Güven, 1978; Gilg & Rocholl, 2009; Christidis & Huff, 2009). The depositional environments – or more accurately their distance to the volcanic source – can be used to classify bentonites as distal bentonites in sedimentary environments tens to hundreds of kilometres form the next volcanic source, and proximal bentonites formed by the alteration of volcanic rocks in the immediate vicinity of a volcanic centre (Gilg & Rocholl, 2009).

Examples of distal bentonites are located in the Cretaceous marine shales of Wyoming and Montana (Knechtel & Patterson, 1956, 1962; Slaughter & Early, 1965; Grim & Güven, 1978; Elzea & Murray, 1990), Eocene-Oligocene clastic to marly marginal-marine sediments that host the Otay bentonite near San Diego in California (Cleveland, 1960; Berry, 1991, 1999), in marine calcareous sediments of the Cretaceous Lower Greensand in England (Hallam & Selwood, 1968; Bradshaw, 1975; Grim & Güven, 1978; Robertson, 1986), and in Miocene fluviatile-lacustrine marls, sands and gravels in Southern Germany (e.g. Vogt, 1980; Ulbig, 1994, 1999). These distal bentonites formed from areal extensive but thin (< 10 m) air-fall tephra, and are preserved as small lenticular bodies, horizons or (dis)-continues beds of a few centimetres to several meters thick. In general, bentonites and volcanic ash may be hosted by sedimentary rocks such as sands and gravels, conglomerates, sandstones, shales, clays, calcareous sands, marls, limestones, cherts, other tuffs or tephra, diatomaceous earths or tonsteins. Distal bentonites are therefore not restricted to any special host-rock (Grim & Güven, 1978; Elzea & Murray, 1994). The volcanic parent materials of distal bentonites in sedimentary environments are mostly acidic in composition (Grim & Güven, 1978).

Well-known proximal bentonites are the Pleistocene deposits on Milos Island in Greece (Wetzenstein, 1972; Christidis et al., 1995; Decher et al., 1996; Christidis, 2008; Christidis & Huff, 2009) and the Miocene deposits of Cabo de Gata in Spain (Delgado, 1993; Caballero et al., 2005). These proximal deposits formed in the immediate vicinity to their volcanic source (Gilg & Rocholl, 2009) and are intensely associated with pyroclastic flows, tuffs and other volcanic rocks. The volcanic rocks were erupted subaqueously, deposited in seawater or on land as air-fall deposits, or as volcanic flows. Proximal deposits can therefore be part of both terrestrial and marine settings but are dominated by volcanic features (Caballero et al., 2005; Christidis & Huff, 2009). The parent rocks range from rhyolitic to basaltic in composition (Delgado, 1993; Christidis et al., 1995; Christidis, 2008).

Some bentonite deposits, however, are exceptions to this classification because they do not fit into a distal versus proximal scheme. These are Mg-rich smectites such as saponite, hectorite, stevensite or mixed-layer minerals that form in saline-alkaline lakes (Ames et al., 1958; Norton, 1965; Galán & Castillo, 1984; Christidis & Huff, 2009) or as the result of lateritisation processes in (sub-)-tropical climates (Trescases et al., 1981; de Oliveira et al., 1992; Albrecht, 2011).

2.2 Alteration and formation mechanisms

Smectites *per se* form in many environments such as in soils, in seawater or hydrothermal systems. However, most bentonite deposits are formed by the alteration of a glassy volcanic material (Weaver & Pollard, 1973; Grim & Güven, 1978; Galán, 2006). The alteration of the volcanic material, usually volcanic glass, to bentonite is brought about by the action of one or more fluids during diagenesis, contact metasomatism, hydrothermal activity or hydrolysis by percolating waters (Grim & Güven, 1978; Christidis & Huff, 2009). It is not uncommon for glass shards to be preserved at various degrees of alteration (Grim & Güven, 1978; Weaver, 1989). The timing of bentonitisation is not fully resolved (Grim & Güven, 1978). Smectites formed in Pliocene-Pleistocene to sub-recent marine sediments indicate that smectite and bentonite formation can be a relatively fast process (Cole & Shaw, 1983; Naish et al., 1993; Berry, 1999). Grim & Güven (1978), Christidis (2008) and Christidis & Huff (2009) summarised the mechanisms of bentonite formation in the following four categories.

2.2.1 Diagenetic alteration of volcanic glass

The in-situ alteration of ash, tuff or pyroclastic rocks is the most common mode of formation especially for distal bentonite deposits in the form of thin, stratiform horizons (Grim & Güven, 1978;

Gilg & Rocholl, 2009). The diagenetic alteration process can be sub-divided into a very early alteration related to soil formation, in lakes or wetlands close to the surface and shortly after deposition, and late diagenesis during sediment burial and alteration by basinal fluids. The alteration process is controlled by the permeability and porosity of the ash and host-rocks, as well as by the expulsion of pore-waters through compaction and/or gravitational-driven fluid flow. The alteration fluids are marine or meteoric pore-waters, formation waters and brines, surface water in lakes, or groundwater (Grim & Güven, 1978; Christidis & Huff, 2009; Gilg & Rocholl, 2009). Well-known examples are the probably late diagenetic bentonites in Cretaceous marine sediments of the Western Interior Seaway in Wyoming and Montana (Knechtel & Patterson, 1956, 1962; Elzea & Murray, 1990, 1994; Bertog et al., 2007) and early diagenetic bentonites formed during soil formation hosted in Miocene sediments of the North Alpine Foreland Basin in Southern Germany (Vogt, 1980; Unger et al., 1985a, b; Unger et al., 1990; Ulbig, 1994, 1999).

2.2.2 Hydrothermal alteration of volcanic glass

The hydrothermal and the deuteric alteration of volcanic and igneous material as described by Grim & Güven (1978) takes place in proximal depositional settings (Gilg & Rocholl, 2009). The hydrothermal alteration of volcanic rocks is brought about by the circulation of hot fluids through faults and fracture zones; whereas hot water, gases and vapours sustained by and within a cooling volcanic rock body after emplacement are the driving factors for the deuteric alteration path. Hydrothermal and deuteric alteration are therefore allochthonous and autochthonous processes respectively, but difficult to distinguish because of the strong similarities of the alteration processes (Grim & Güven, 1978; Christidis & Huff, 2009). Hydrothermal alteration is related to the convective flow of marine, meteoric or magmatic fluids at temperatures of up to 90°C (Decher et al., 1996), whereas higher emplacement temperatures (300°C to 800°C; Cas & Wright, 1988) are involved in the initial phases of the deuteric alteration (Christidis, 2008; Christidis & Huff, 2009). The principal mechanisms of “ore” control in both processes are fracture zones, as well as the permeability and porosity development in the volcanic rock masses after emplacement (Christidis & Huff, 2009; Gilg & Rocholl, 2009). Bentonite deposits formed by hydrothermal or deuteric processes often are thick (> 60 m), irregular or stratiform fracture-related bodies. The Miocene deposits of Cabo de Gata in Spain (Delgado, 1993; Caballero et al., 2005) and the Pleistocene bentonites on the island of Milos in Greece (Christidis et al., 1995; Decher et al., 1996; Christidis, 2008) are typical examples.

2.2.3 Smectite precipitation in lakes and sabkha environments

A number of bentonites were assigned by Grim & Güven (1978) to a "miscellaneous and uncertain mode of origin" and are defined by the absence of volcanic glass, the lack of textures indicating the former presence of volcanic material, and a lack of a volcanic source(s) (Grim & Güven, 1978; Christidis & Huff, 2009). Bentonites of this category do not fit into a classification of distal versus proximal settings because it is only applicable to volcanic-related bentonites - but not to chemical precipitates (Gilg & Rocholl, 2009). These bentonites are characterised by the presence of trioctahedral smectites such as saponite, hectorite or stevensite that preferentially form in terrestrial, saline-alkaline lacustrine environments. Bentonite formation occurs either by the replacement of other clay minerals (Gac et al., 1977; Galán & Castillo, 1984) and carbonates (Hay et al., 1986; Chahi et al., 1999), or by direct chemical precipitation from the water column (Darragi & Tardy, 1987; Furquim et al., 2008). Although trioctahedral smectites are often ascribed to arid climate conditions they also form in strongly evaporative, wet tropical climates (Furquim et al., 2008). The Hector deposit in San Bernardino County in California (Ames et al., 1958), the stevensite deposits in Morocco (Faust et al., 1959) and the Pantanal wetlands in Brazil (Furquim et al., 2008) are characteristic examples.

2.2.4 Laterite formation

In addition to the categories used by Christidis (2008) and Christidis & Huff (2009) it should be noted that smectite-rich clays also form during the development of laterites. Although not widely known for having the potential for bentonites, laterites are included in the "miscellaneous and uncertain mode of origin" by Grim & Güven (1978), citing a deposit of bentonite in Precambrian igneous and metamorphic rocks of the Barmer district, India (Siddiquie & Bahl, 1965). These "non-volcanogenic" bentonites form during the lateritisation of acidic to basic rocks in stable tectonic regimes subject to tropical climate. The formation of large, smectite-rich bodies at the base of laterite profiles is, however, somewhat unusual (Aleva, 1994; Tardy, 1997) and is the result of the complex interaction of alkaline fluids, a silica- and Mg-rich setting, and insufficient leaching conditions during the mobilisation of alkali and alkali earth elements (Harder, 1977; Patel, 1987). Smectite formation in laterites therefore preferentially affects Mg-bearing minerals such as olivine, amphiboles or pyroxenes (Nahon et al., 1982) and is more frequently encountered in basic rock types (de Oliveira et al., 1992). Lateritic bentonites formed from basaltic rocks and in tropical weathering conditions are known from the Kutch, Gujarat and Barmer regions in India (Siddiquie & Bahl, 1965; Patel, 1987; Sharifabadi, 1992). In

contrast, smectite-rich laterites formed from ultramafic to acidic rocks in the highlands of North-eastern Brazil are related to weathering during a semi-arid tropical climate and inhibited drainage (Trescases et al., 1981; Moreira, 1984; de Oliveira et al., 1992; Albrecht, 2011).

2.2.5 Summary of criteria for bentonite formation

Several factors are critical for the formation of bentonites and independent of a volcanic or non-volcanic origin. The temperature of the alteration fluid such as formation waters (Wyoming) and groundwater (Bavaria) is rather low but may reach up to 90°C or 100°C in hydrothermal systems such as in Milos in Greece (Delgado, 1993; Decher et al., 1996; Cadrin et al., 1995; Caballero et al., 2005; Gilg, 2005). The bentonitisation of glassy volcanic material involves a hydration reaction with the alteration fluid, requires the presence of Mg ions (Harder, 1972), a high Mg^{2+}/H^{+} activity ratio, and the release of silica and alkali ions from the glass (Grim & Güven, 1978; Caballero et al., 1992; Christidis et al., 1995; Christidis & Dunham, 1997). Bentonite formation therefore requires large water-rock ratios for the mobilisation of silica, alkali and alkaline earth elements (Caballero et al., 1992; Christidis, 2001). The composition of the parent material can but must not have an influence on the chemical and mineral composition of the bentonite (Grim & Güven, 1978; Caballero et al., 1992; Christidis et al., 1995) and many high-quality bentonite deposits formed from rocks of unfavourable chemical composition, i.e. silica-rich and poor in alkali earth elements (Grim & Güven, 1978; Christidis, 2008). This indicates that bentonites form in (mostly) open hydrological systems that supply the elements necessary for the alteration of the volcanic rocks (Caballero et al., 1992; Christidis, 2008). Low water-rock ratios, e.g. due to low permeability and insufficient drainage in closed hydrological systems, will favour the precipitation of zeolites. It is therefore not uncommon for zeolites to occur in bentonites subject to poor drainage conditions (Hay, 1966; Christidis, 2001; Hay & Sheppard, 2001). The hydrological regime and chemical composition(s) of the fluid(s) are, however, the most important factors determining the composition and formation of bentonites (Grim & Güven, 1978; Caballero et al., 1992; Christidis & Huff, 2009).

2.3 Carbonate-bearing bentonite deposits

Many bentonite deposits contain authigenic carbonate minerals in the form of disseminated calcite (Knechtel & Patterson, 1956, 1962; Grim & Güven, 1978; Delgado, 1993; Decher et al., 1996; Christidis & Dunham, 1993; Christidis et al., 1995). Dolomite can, however, also be characteristic for some

bentonite districts such as in Southern Germany (Vogt, 1980; Unger & Niemeyer, 1985a, b; Ulbig, 1994, 1999); whereas siderite has been documented in bentonites in England (Ufer et al., 2008), the Zhangpenggou deposit in China (Tang, 2005) and in the green, bentonitic clays of Kärlich in Germany (Heinzmann & Mörs, 1994; Thüns, 2012; Wostatek, 2014). Further examples of bentonite deposits with mostly authigenic calcite but sometimes dolomite are found in Wyoming in Montana (Knechtel & Patterson, 1956, 1962) and Otay in California (Cleveland, 1960) in the United States of America, Milos Island in Greece (Decher et al., 1996), and Cabo de Gata in Spain (Delgado, 1993; Delgado & Reyes, 1993). The origin of carbonates in most bentonite deposits is uncertain (Grim & Güven, 1978). However, the presence of calcite and dolomite in both distal (Wyoming, Bavaria) and proximal (Cabo de Gata, Milos) deposits suggests that carbonate formation is a common process and not restricted to one specific environment.

The genetic relationship of carbonates with bentonitisation has only been systematically investigated in Cabo de Gata in Spain (Delgado, 1993; Delgado & Reyes, 1993) and Milos Island in Greece (Decher et al., 1996). These proximal deposits are located in marine depositional environments in the vicinity of the Mediterranean Sea and formed through the hydrothermal heating and convection of hot fluids in volcanic complexes (Delgado, 1993; Delgado & Reyes, 1993; Decher et al., 1996; Christidis, 2008). Seawater is therefore considered as the main alteration fluid in these deposits (Christidis & Huff, 2009). Oxygen and carbon isotope studies indicate that in both cases carbonates did form from mixed marine-meteoric waters at temperatures of 30°C to 90°C (Delgado, 1993; Delgado & Reyes, 1993; Decher et al., 1996). Carbonates and smectites have $\delta^{18}O$ values inconsistent with precipitation from the same fluid (Delgado & Reyes, 1993; Decher et al., 1996). Sedimentological evidence in the Cabo de Gata region further points to dolomite formation during subaerial exposure but the involvement of seawater or variably mixed waters in bentonite formation (Delgado, 1993), a systematic genetic link of bentonite and carbonate formation in these deposits is therefore unlikely.

2.4 Bentonite deposits in the North Alpine Foreland Basin

Bentonite deposits and sub-economic bentonite occurrences (Fig. 2.1) are found throughout the North Alpine Foreland Basin associated with Miocene sediments of the Upper Freshwater Molasse (UFM), the uppermost of four sedimentary sequences that comprise the Cenozoic sedimentary infill of the North Alpine Foreland Basin (NAFB). The UFM consists of fluviatile-lacustrine gravels, sands and marls (Lemcke, 1973, 1988; Doppler et al., 2005; Maurer & Buchner, 2007; Aziz et al., 2010) and contains both pre- and post-Riesian volcanic tuff and bentonite horizons (Fiest, 1989; Ulbig, 1994,

1999; Aziz et al., 2008, 2010). Only the post-Riesian main bentonite horizon in the Landshut region (Fig. 2.1) hosts deposits sufficiently large to be of economic interest today, although bentonites have been mined at several locations in Southern Germany. The more than 200 individual deposits of main bentonite horizon (Weinig, 1987; Ulbig, 1994, 1999) constitute the largest bentonite district in Central Europe, with an annual production of about 350,000 t/a, and a mining history dating back 110 years (Ammon, 1901; Ulbig, 1994, 1999).

2.4.1 Bentonites in the Landshut region

The Landshut bentonite deposits (Fig. 2.1) are located in a 40 by 10 km wide tectonic block of the NAFB bordered by NW-SE striking fault zones of a basement high known as the *Landshut-Neuöttinger Hoch* (Unger, 1981, Weinig, 1987; Unger, 1999; Aziz et al., 2008, 2010). The fault zones were active during the Permian and Cretaceous and were possibly re-activated during the Tertiary (Lemcke, 1973).

The westward dewatering (Lemcke, 1973) clastic environment of the NAFB is characterised by sediments of an anastomosing to braided river system (Schmid, 2002; Maurer & Buchner, 2007) with extensive floodplains, wetlands, high groundwater levels in topographic depressions, or oxbow lakes (Schmid, 2002). The UFM in the Eastern part of the NAFB is characterised by sand- and gravel-rich sediments with minor marls, and received significant clastic input in the form of crystalline and sedimentary rocks from the Alps, the Bohemian Massif, and the Swabian Alb (Lemcke, 1988; Unger, 1996; Frisch et al., 1998). With an estimated overburden of 200 to 300 m, the UFM was not subject to significant burial or high temperatures (Lemcke, 1973; Ulbig, 1999).

The presently mined deposits are limited to the 14.7 ± 0.2 Ma old “main bentonite horizon” (Aziz et al., 2010) in the upper part of the fluviatile *Nördlicher Vollschotter* (NV) sand and gravel unit and floodplain sediments of the *Sand-Mergel-Decke* (SMD) (Vogt, 1980; Unger & Niemeyer, 1985a, b; Unger et al., 1990) and occur as small, irregular lenses of variable size (Vogt, 1980; Ulbig, 1999; Aziz et al., 2010) about 10 to 30 m above the ejecta layer of the Early Badenian Ries meteorite impact.

Ulbig (1994) proposed that two types of bentonite deposits formed in different morphological locations to explain sedimentological and depositional differences. The more common deposits of the *Hochlage* (topographic high) are often carbonate-rich clays with marly to clayey footwalls of the SMD, whereas the *Tieflage* (topographic low) deposits are usually hosted by sand or gravel, have a higher detritus but lower carbonate content, and may contain basal kaolinite-rich beds or kaolinite aggregates (Ulbig, 1994). All fine-grained host-sediments and some gravels show various stages of palaeosol development and are rich in authigenic carbonate (Schmid, 2002). However, deposits in topographic

lows can be devoid of carbonates. Intermediate forms of the two types exist. All deposit types are discordantly, i.e. erosionally, capped by younger sediments.

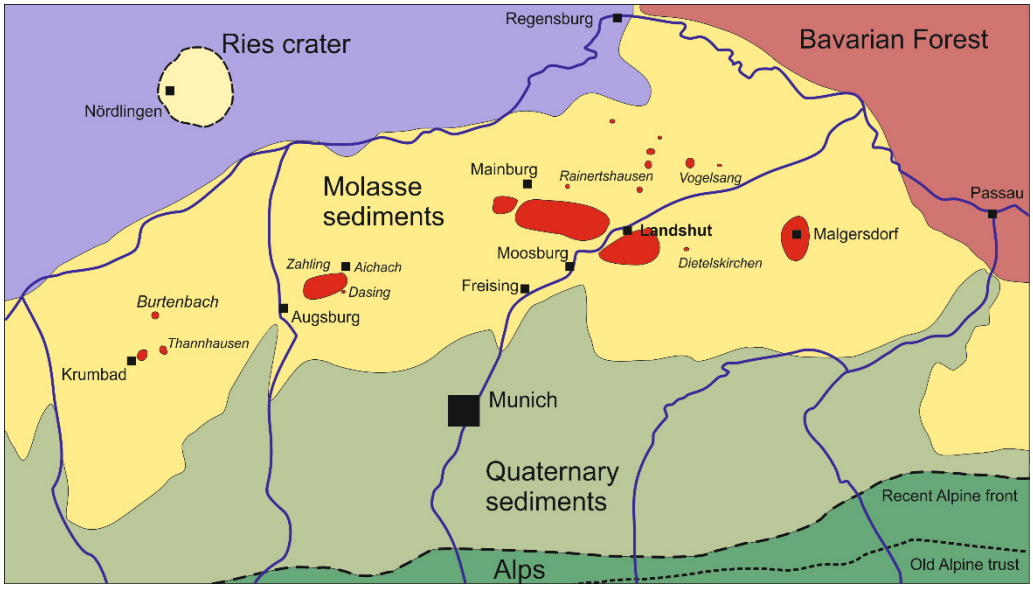

Fig. 2.1: Bentonite districts and isolated bentonite occurrences in Bavaria and other regions. Dark red = bentonite districts, yellow = Tertiary sediments, red = igneous rocks, grey = Quaternary and glacial cover sediments, and green = various rocks of the Alps, according to Ulbig (1994) and Freudenberger & Schwerd (1996).

2.4.2 Dolomite- and calcite-bearing bentonites in the Landshut region

Authigenic carbonates and carbonate-rich sediments are a wide-spread phenomenon in the Miocene Upper Freshwater Molasse (UFM) and were deposited or formed in fluviatile-lacustrine, pedogenic, palustrine and/or groundwater settings (Hofmann, 1973; Fiest, 1989; Schmid, 2002; Maurer & Buchner, 2007; Aziz et al., 2010). The low $\delta^{18}O_{V\text{-}PDB}$ and low $\delta^{13}C_{V\text{-}PDB}$ values of authigenic calcite nodules and sediments confirm carbonate precipitation from meteoric waters in lakes, soils and groundwater (Huber, 2001; Schmid, 2002; Maurer & Buchner, 2007). The $\delta^{18}O_{V\text{-}PDB}$ values are consistent with meteoric precipitation during Miocene climate conditions (Böhme et al., 2001; Böhme et al., 2007; Héran et al., 2010; Bauer et al., 2016).

Many calcite- and dolomite-rich sediments have been documented in pre- and post-Riesian horizons of the UFM (Graup et al., 1981; Horn et al., 1985; Schmid, 2002). The most prominent of these are the dolomite-rich *Süßwasserkalke* in the Landshut and Malgersdorf regions, i.e. freshwater limestones and marls in lacustrine depositional environments and with a pronounced dolomite content at the top (Hofmann, 1973; Unger, 1983, 1991). The *Süßwasserkalke* presumably formed by the leaching of carbonate from detrital carbonate clasts in the *Nördliche Vollschotter-Abfolge* and

subsequent groundwater seepage associated with lakes and wetlands (Unger & Niemeyer, 1985a). Hofmann (1973) suggested that bentonites and *Süßwasserkalke* have a contemporaneous (though not necessarily a common genetic) origin because they share the same lithostratigraphic position in the *Sand-Mergel-Decke*.

Authigenic carbonates associated with bentonite deposits have also been occasionally mentioned (Vogt & Köster, 1978; Unger, 1981; Luft, 1983; Unger & Niemeyer, 1985a, b; Walz, 1991; Ulbig, 1994). Especially the bentonite deposits of the *Hochlage* have a high content of authigenic carbonates (Ulbig, 1994). Unger & Niemeyer (1985a, b) and Ulbig (1994, 1999) describe bentonite deposits in the Landshut and Malgersdorf areas that are dotted with carbonate accumulations and hosted in carbonate-rich marls – mostly likely the *Süßwasserkalke* of Hofmann (1973). Ulbig (1994, 1999), however, ascribed all carbonates to soil forming periods unrelated to bentonite formation. Perhaps as a consequence, very few dolomite-bearing bentonite deposits have ever been documented, and are quickly summarised:

Small lenticular bodies of smectite-bearing dolomite were found in the lower olive-grey bentonite (Fig. 2.2) of the Traich deposit (Unger & Niemeyer, 1985b; Unger et al., 1990). Bentonite-associated carbonates were also documented in the Siegerstetten deposit (Fig. 2.2) south of Landshut. Here, a "calcareous tuff" occurs in blue bentonite. The 10 to 60 cm thick, Mg-rich (probably dolomitic with up to 22.6 wt% $MgCO_3$), micritic and porous carbonate was interpreted by Unger & Niemeyer (1985b) as calcite encrusted algal filaments.

The presence of the Ca-Mg-carbonate dolomite in the *Süßwasserkalke* and the stratigraphically similar bentonites is remarkable because the Ca- and Mg-poor, rhyolitic glass (Ulbig, 1994, 1999; Gilg, 2005; Aziz et al., 2010) requires the addition of large amounts of Mg-ions to form smectite (Harder, 1972; Christidis & Dunham, 1997). The abundance of dolomite as well as smectite therefore necessitates a very large source of Mg-ions, and unusual depositional and formational conditions for a terrestrial and non-arid environment (Maurer & Buchner, 2007; Aziz et al., 2008, 2010).

Additional but indirect indications for a timely or genetic link of carbonate and bentonite are the oxygen stable isotope compositions of smectites from bentonites, pedogenic calcite nodules, and other sediments in the UFM. These materials all have $\delta^{18}O$ values consistent with the formation from meteoric waters and ambient temperatures during the Miocene (Gilg, 2005; Campani et al., 2012; Bauer 2014; Bauer et al., 2016). The abundance of authigenic calcite and dolomite in bentonites and the isotopic composition of authigenic minerals in the UFM therefore suggest that some kind of timely or genetic connection exists between bentonites and bentonite-associated dolomite and calcite.

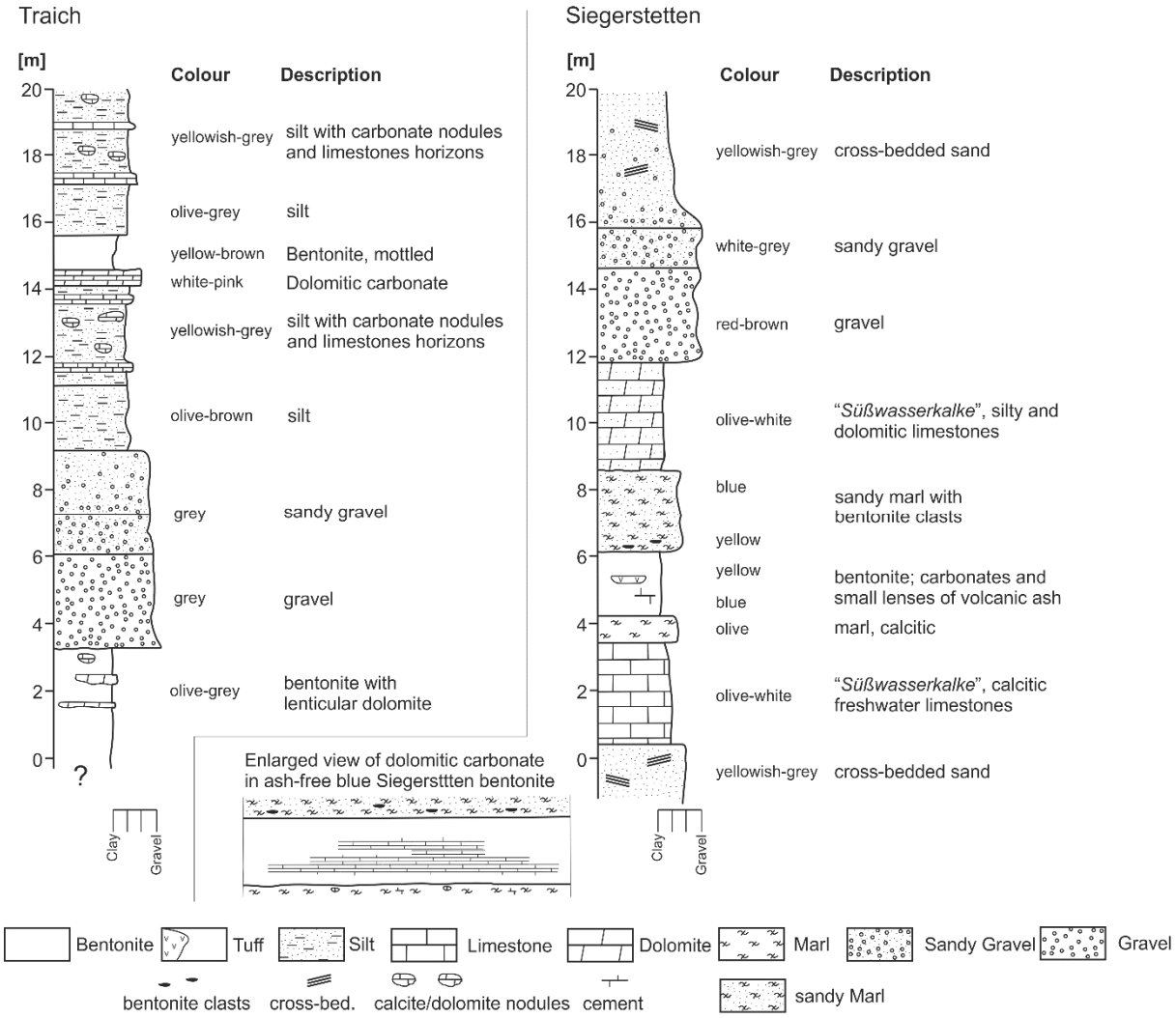

Fig. 2.2: Simplified geological sections of the dolomite-bearing Traich and Siegerstetten bentonite deposits. Redrawn after Unger et al. (1985b) to match the style of geological sections in chapters 5 and 6. Colours are not Munsell colours but colours as used by Unger et al. (1985b).

2.4.3 Open questions on carbonate and bentonite formation in Landshut bentonites

The fluviatile-lacustrine depositional environment of the UFM offers only rough clues for the alteration settings of the volcanic tuff and the formation of bentonites. Previous models for bentonite formation in Bavaria do not discuss bentonite-associated carbonates and provide no satisfactory explanation for the abundance of authigenic dolomite. An intimate spatial association of carbonates and bentonites is, however, obvious from the same previous studies. It therefore seems unlikely that carbonate precipitation in bentonite deposits is completely unrelated to bentonite formation. However, a contemporaneous or cogenetic origin of dolomite, calcite, and bentonite from Mg- and Ca-

poor rhyolitic volcanic ash deposited in a terrestrial depositional environment is rather remarkable, posing several questions:

- What is the formational setting of bentonite, calcite, and dolomite?
- Where did the Mg- and Ca-ions come from?
- What kind of fluid(s) was (were) involved in bentonite, calcite, and dolomite formation?
- What was the chemical composition of the fluid(s) (e.g. salinity, Mg/Ca)?
- Can bentonite and carbonate facies be distinguished using chemical and/or isotopic methods?

2.4.3.1 Mineral composition of the Landshut bentonites and tuffs

The mineral composition of bentonites is dominated by montmorillonite and variable amounts of illite, micas, kaolinite, chlorite, quartz, feldspars, calcite and dolomite, glass shards, pyrite and detrital minerals such as epidote or garnet (Vogt & Köster, 1978; Ulbig, 1994, 1999) and perhaps cordierite (Harr, 1976). The clay fraction of the bentonites is dominated by montmorillonite and various amounts of illite and kaolinite (Ulbig, 1994), as well as traces of quartz, feldspar, chlorite or mixed-layer-minerals (Vogt & Köster, 1978). The heavy minerals in bentonites are concentrated in the > 63 µm fraction (Ulbig, 1994) and include apatite, zircon, ilmenite, magnetite, rutile, tourmaline, disthene, hornblende, titanite, biotite, and sillimanite. The parent material of bentonites, i.e. partially altered tuffs ("*Harte Platte*") have the same mineral composition as bentonites but are characterised by a higher content of volcanic glass, muscovite or biotite, and lower content of smectite (Siegl, 1948; Vogt & Köster, 1978; Ulbig, 1994, 1999). The clay fraction of the tuffs contains mostly montmorillonite, together with variable amounts of illite/muscovite, quartz, kaolinite, as well as mixed-layer-minerals (Ulbig, 1994), probably illite-smectite (Vogt & Köster, 1978). The volcanogenic minerals in bentonites and tuffs confirm a volcanic origin and the detrital minerals indicate the re-deposition of the ash and contamination with clastic sediments (Harr, 1976; Ulbig, 1994, 1999).

2.4.3.2 Stratigraphic position

Although general agreement exists that bentonites belong to the Mid-Miocene Upper Freshwater Molasse (e.g. Doppler et al., 2005; Aziz et al, 2008, 2010), there has been substantial debate regarding the exact eruption, depositional and alteration age. Stratigraphic, faunal, isotopic, and geochemical evidence as well as the heavy mineral assemblages have been used to define the age of the tuff and its stratigraphic position within the UFM. Defining the stratigraphic position is complicated by the

presence of at least five or six, both pre- and post-Riesian tuff and bentonite horizons (Unger & Niemeyer, 1985a, b; Unger et al., 1990; Ulbig, 1994, 1999) and re-sedimentation processes contemporaneous with ash deposition (Harr, 1976; Ulbig, 1994, 1999). There is also considerable regional variation in the distribution and base elevation above sea level of bentonites. Bentonites are found at 490 m a.s.l. in the Mainburg area compared to only 440 m a.s.l. at Landshut (Ulbig, 1994). However, deposits with a base elevation of 442 to 473 m a.s.l. have also been documented in the vicinity of Landshut (Unger, 1991). The main bentonite horizon is therefore located at successively lower elevations further east. The variations in base elevation are most likely the result of active tectonics in the Molasse basin during or after ash deposition (Lemcke, 1973; Ulbig, 1994, 1999). The main bentonite horizon of the Landshut area is, however, clearly located above the ejecta layer (i.e. the *Brockhorizont*) of the Ries impact (Fiest, 1989; Unger et al., 1990; Ulbig, 1994, 1999; Aziz et al., 2008, 2010) in the upper part of the *Nördlicher Vollschotter-Abfolge* (NV) – either within (Hofmann, 1973) or on top of the Sand-Mergel-Decke (SMD) (Unger & Niemeyer, 1985a, b; Unger et al., 1990; Aziz et al., 2008, 2010). The various bentonite-bearing horizons are probably the reason why bentonites and tuff were previously assigned to the Sarmatian (Unger, 1981) and later to the Badenian and/or Sarmatian (Unger & Niemeyer, 1985b) based on evidence corresponding to faunal zones of lithozone 3 (Dehm, 1955). Today, bentonites of the main bentonite horizon are assigned to the Langhian respective the Badenian (Ulbig, 1999) as a part of the *Mittlere Serie* (Dehm, 1955; Ulbig, 1994, 1999). Biostratigraphic evidence places bentonites into mammal zone MN 6 (Heissig, 1989). Identical mammal assemblages in hanging-wall and footwall sediments of the main bentonite horizon indicate that ash deposition occurred in a short time interval (Heissig, 2006).

2.4.3.3 Lithostratigraphy and heavy minerals

The heavy mineral assemblages of Upper Freshwater Molasse sediments has been used to subdivide the UFM into five lithostratigraphic units or lithozones, with L1 being the oldest and L5 the youngest (Unger, 1989, 1991). Although bentonites have been assigned to L3 (Unger, 1981, 1983) it is now evident that the main bentonite horizon is a part of L2, representing a lower Badenian to uppermost Badenian interval (16.8 to 15-14 Ma) corresponding to mammal zones MN 5 and MN 6 (Unger et al., 1985a, b; Heissig, 1989; Unger, 1989; Unger et al., 1990).

Both the bentonite deposits and the *Süßwasserkalke* (Hofmann, 1973; Unger, 1989) are associated with the top of the L2 that is characterised by a predominance of garnet (Harr, 1976; Vogt, 1980; Unger, 1989, 1991) and a high garnet-epidote ratio that can be used to distinguish it from other units (Fiest,

1989; Ulbig, 1994). The high garnet-epidote ratio is characteristic for the main sedimentation cycle of the UFM (Lemcke et al., 1953) and identical in sandy bentonites, sandy-clayey intercalations, and footwall sediments (Ulbig, 1994), confirming biostratigraphy evidence that tuffs were deposited during a short time-interval of L2. However, Harr (1976) and Ulbig (1994) also found variable garnet-epidote ratios that they ascribe to different lithostratigraphic positions of some bentonite deposits and/or variable degrees of mixing with detrital sediments. A detailed heavy mineral study of bentonites and tuffs is, however, missing.

2.4.3.4 Absolute ages for volcanic glasses and bentonites

A series of absolute dating approaches have been used to define the eruption age of the volcanic ash and its deposition in the UFM. Various ages for ash eruption and deposition have been determined and range from 16.12 ± 0.32 Ma to 14.51 ± 0.19 Ma (Storzer & Gentner, 1970; Gubler et al., 1992; Aziz et al., 2008, 2010; Gubler, 2009; Rocholl et al., 2011; Buchner et al., 2013), encompassing both pre- and post-Riesian ages. The Ries impact event, its ejecta layer is located below the main bentonite horizon, has been dated to 15 to 14.6 Ma, with the most likely age being either 14.94 ± 0.07 Ma (Rocholl et al., 2011) or 14.83 ± 0.15 Ma (Jourdan et al., 2012) or 14.74 ± 0.20 Ma (Buchner et al., 2013). The three ages are more or less within analytical error and could be considered identical.

Fission-track dating on volcanic glass from bentonites at Mainburg and Malgersdorf reveal ages of 14.6 ± 0.8 Ma and 14.4 ± 0.8 Ma (Storzer & Gentner, 1970). Glasses from Hachelstuhl at Landshut show $^{40}Ar/^{39}Ar$ ages of 15.21 ± 0.10 Ma and 14.58 ± 0.10 Ma (Aziz et al., 2008, 2010). An age of 14.69 ± 0.19 Ma for the Landshut bentonites is probably the most realistic (Rocholl et al., 2008, 2017). The ages are similar to those of bentonites in Switzerland (Gubler et al. 1992; Gubler 2009). Age discrepancies between individual deposits are most likely related to problems in distinguishing individual deposits and tuff horizons in the UFM (Unger & Niemeyer, 1985a, b; Fiest, 1989; Unger et al., 1990; Gubler et al., 1992; Ulbig, 1994, 1999; Gubler, 2009; Aziz et al., 2008, 2010). Direct radiometric dating of smectite by e.g. the K-Ar, $^{40}Ar/^{39}Ar$ or Rb-Sr has not yet been attempted.

2.4.3.5 Oxygen and hydrogen isotope composition of smectites and glass particles

The oxygen and hydrogen stable isotope values of smectites and glass particles from bentonites reveal that volcanic ash reacted with in meteoric waters to form smectites (Gilg, 2005). The SMOW oxygen and hydrogen isotope values of smectites range from +16.4 to +19.0 ‰ and from -91 to -61 ‰

respectively. There is no apparent difference between bentonites from topographic highs or lows (Ulbig, 1999; Gilg, 2005). The stable isotope values are similar to those of kaolinite deposits in the UFM that are in isotope equilibrium with meteoric waters (Gilg, 2000, 2005; Gilg et al., 2003). Recent studies confirm that the oxygen isotope values of most smectites are consistent with foreland precipitation during the Miocene (Bauer, 2014; Bauer et al., 2016) and formation at ambient temperatures (< 40°C, Gilg, 2005). The hydrogen isotope values of smectites appear to have exchanged with later fluids (Gilg, 2005). The oxygen and hydrogen stable isotope values of volcanic glass particles from bentonites are, in contrast, not consistent with Miocene waters and indicate later isotopic exchange with rather recent and cold, probably Pleistocene, waters (Stichler, 1997; Gilg, 2005).

2.4.3.6 Bentonite parent material and its source

The nature of the parent material of the bentonites and its composition has been debated (Schulz, 1926; Siegl, 1948; Lemcke et al., 1953; Storzer & Gentner, 1970; Herold, 1970; Harr, 1976; Vogt & Köster, 1978; Vogt, 1980; Unger, 1981; Unger et al., 1985a, b; Unger et al., 1990; Ulbig, 1994, 1999; Gilg, 2005; Rocholl et al., 2008; Aziz et al., 2008, 2010). Very early researchers assumed bentonite formation from fluids resulting from weathering reactions in the Bavarian Forrest (Schulz, 1926). However, the tuffs and glass particles in bentonites indicate a glassy material, thus limiting the potential parent material to a volcanic/igneous (Siegl, 1948; Lemcke et al., 1953) or similarly origin.

The discovery that the Ries is a meteorite impact structure and chemical similarities of glassy particles from bentonites with tektites fuelled the hypothesis that bentonites formed from weathered ejecta material (Storzer & Gentner, 1970; Baier, 2009). The impact hypothesis was mainly based on similar but not identical fission track ages of tektites and bentonite glass particles (Storzer & Gentner, 1970) and similarities in the main element composition (Baier, 2009).

Although similar Rb/Sr and $^{87}Sr/^{86}Sr$ were determined for bentonite glasses and Ries tektites, the morphology of the glass particles and gas bubbles therein indicate a volcanic origin (Graup et al., 1981; Horn et al., 1985). Luft (1983) also disagreed with a genetic link of Ries tektites and glass particles based on the similar but not identical strontium isotope ratios and chemical compositions of the < 0.6 µm and > 0.6 µm fractions of bentonites. Bentonite deposits located at stratigraphic positions both below and above the Ries ejecta layer (*Brockhorizont*) also contradict an impact origin (Fiest, 1989; Ulbig, 1994, 1999).

A volcanic origin had been proposed by Siegl (1948) who determined a rhyolitic composition for tuffs from Mainburg. In contrast, Harr (1976) and Walz (1991) suggested volcanic rocks with a rhyolitic

to trachy-andesitic composition. However, both the main and trace element data of glass particles confirm a calc-alkaline, Ca- and Mg-poor, rhyolitic (Ulbig, 1994, 1999; Rocholl et al., 2008; Gilg & Rocholl, 2009) to rhyolitic-andesitic (Vogt & Köster, 1978; Unger & Niemeyer, 1985a; Unger et al., 1990) composition of the volcanic ash. Non-rhyolitic identifications (Harr, 1976; Walz, 1991) were probably the unintentional result of bulk analyses and admixture of detrital material (Gilg, 2005).

The actual source of the volcanic ash was long obscure. Lemcke et al. (1953) suspected a volcanic centre in the Molasse basin but the absence of rhyolitic to andesitic volcanism in the Bavarian Molasse during the Mid-Miocene favours a more distant area: western volcanic centre(s) in the Lake Constance region and Switzerland or volcanic centre(s) in Eastern Europe.

Bulk mineral and chemical analyses of Bavarian bentonites, the Hegau and Swiss bentonites and tuffs seemingly reveal some similarities (Harr, 1976). An eastward decreasing grain size distribution of glass particles, with the largest grain size in the Lake Constance area, and thickness variations of tuff and bentonite beds have been interpreted to suggest a volcanic origin in the West. Ulbig (1994, 1999), Hofmann (1956a, 1965) and Hofmann et al. (1975) therefore proposed volcanic centres in Western Switzerland and the Lake Constance region as the source of the rhyolitic tuffs.

However, the presence of several bentonite horizons in the UFM complicates the determination of regional grain size variations. Ash layers in the Swiss UFM and Hegau area occur at several stratigraphic intervals (Gubler, 2009; Rocholl et al., 2017) and are mostly younger (10.6 to 12.3 Ma; Rahn & Selbekk, 2007) than Bavarian tuffs (14.7 ± 0.2 Ma; Aziz et al., 2010). Additionally, the chemical composition of glass particles (Ulbig, 1994, 1999; Gilg, 2005, Aziz et al., 2010) and < 0.6 µm montmorillonite fractions (Vogt & Köster, 1978) of Bavarian bentonite is not identical with the Zahling-2 tuff (Aziz et al., 2010) at Augsburg nor the deposits in Switzerland. The Ti/Al and Fe/Al allow a clear distinction of Landshut bentonites from other regions (Gilg, 2005; Gilg & Rocholl, 2009).

Several lines of evidence therefore suggest another volcanic source area for the Landshut bentonites. Unger & Niemeyer (1985a) and Unger et al. (1990) argued for a connection of Lower Bavarian bentonites to contemporaneous rhyolitic volcanism in the Pannonian basin and Carpathians. The main element compositions of Mid-Miocene volcanic rocks (Handler et al., 2006; de Leeuw et al., 2013; Lukács et al., 2015) as well as Bavarian tuffs and glasses are similar (Unger & Niemeyer, 1985a) and consistent with the trace element content of Hungarian volcanic rocks (Unger et al., 1990; Harangi et al., 2005; Rocholl et al., 2008). Neodymium isotope ratios of glasses (Rocholl et al., 2008) and volcanic rocks in the Carpathian-Pannonian region (Rocholl et al., 2008; Gilg & Rocholl, 2009) as well as Rb/Sr and $^{87}Sr/^{86}Sr$ of glass particles from bentonites (Graup et al., 1981; Luft, 1983; Horn et al.,

1985) suggest a Carpathian-Pannonian origin, and rule out tektites of the Ries impact as parent material for bentonite formation (Luft, 1983; Horn et al., 1985).

2.4.3.7 Chemical composition of bentonite, tuff, smectite, and glass

The chemical composition of the Landshut bentonites, tuffs, glass particles, and smectites is influenced by the composition of the volcanic glass particles, the leaching of alkali and addition of alkali earth elements, as well as the admixture of detrital material (Harr, 1976; Vogt & Köster, 1978; Luft, 1983; Unger & Niemeyer, 1985a, b; Unger et al., 1990; Walz, 1991; Ulbig, 1994, 1999; Gilg, 2005; Aziz et al., 2008, 2010).

The bulk chemical composition of the bentonites is similar (though not identical) to the smectites. Variations in major element concentrations are most relevant for K_2O and Al_2O_3 content, caused by small amounts of detrital clay minerals or feldspars (Vogt, 1980; Unger et al., 1990; Walz, 1991; Ulbig, 1994) or K-bearing mixed-layer minerals (Vogt & Köster, 1978; Ulbig, 1994). The bulk chemical composition of tuff is largely controlled by the relative amounts of volcanic glass and smectite, as well as variable admixtures of detrital minerals (Unger et al., 1990; Walz, 1991). The tuff therefore has a chemical composition intermediate between pure smectite and pure glass (Ulbig, 1994, 1999).

The silica-, Na- and K-rich glass (Harr, 1976; Ulbig, 1994, 1999; Gilg, 2005; Aziz et al., 2008, 2010) has a calc-alkaline rhyolitic composition. The relatively high water content (~ 4.8 wt%, Ulbig, 1999; 4 to 10 wt%, Gilg, 2005) is positively correlated with silica but negatively correlated to the Na_2O and K_2O contents suggesting an increased loss of alkalis with successive hydration of the volcanic glass (Gilg, 2005). Smectites are therefore strongly depleted in Si_2O, Na_2O and K_2O relative to the fresh, rhyolitic glass (Harr, 1976; Vogt & Köster, 1978; Luft, 1983; Walz, 1991; Ulbig, 1994, 1999; Gilg, 2005), as expected for the preferential removal of silica and alkali elements and the enrichment of Al_2O_3, Fe_2O_3, MgO and CaO during bentonite formation (Ulbig, 1994, 1999; Gilg, 2005).

2.4.3.8 Exchangeable cations

Table 2.4.3 summarises the exchangeable cation occupancy of Lower Bavarian bentonites based on data in Grim & Güven (1978), Ulbig (1994), and Kaufhold & Dohrmann (2008). Bentonites are characterised by a predominance of Ca-ions, a molar Ca-Mg ratio of about 2:1, and very low Na-ion concentrations (Grim & Güven, 1978; Ulbig, 1994). The Ca-Mg ratios and the interlayer cation

composition (except for K) is similar to the chemical composition of ground waters in the UFM (Egger et al., 1983; Ulbig, 1994), suggesting cation exchange reaction during or after bentonitisation.

The exchangeable K in bulk bentonites might be related to the presence of mica. However, an inverse correlation of exchangeable K with smectite content and higher K concentrations in tuffites suggests exchange reactions with the K-rich glass (Ulbig, 1994), as indicated by the presence of K-bearing mixed-layer minerals (Vogt & Köster, 1978; Ulbig, 1994).

Table 2.1: The exchangeable cation occupancy (meq/100g) of bulk bentonites and tuffs in Southern Germany.

Sample	Material	Na^+	K^+	Mg^{2+}	Ca^{2+}	Comment/Source
B16	Bentonite	0.3	2.4	19.8	47.3	Cu-trien method; Kaufhold & Dohrmann, 2008
B25	Bentonite	0.2	1.3	14.6	38.8	Cu-trien method; Kaufhold & Dohrmann, 2008
63	Bentonite	6.0	2.0	33.0	64.0	NH_4-acetate method; Grim & Güven, 1978
64	Bentonite	8.0	1.0	43.0	84.0	NH_4-acetate method; Grim & Güven, 1978
P-1a	Bentonite	0.4	5.7	43.5	87.3	NH_4-acetate method; Ulbig,1994
Vo-W	Bentonite	0.5	9.3	36.5	78.8	NH_4-acetate method; Ulbig,1994
T-1a	Bentonite	0.7	10.9	35.8	68.4	NH_4-acetate method; Ulbig,1994
V-2a	Tuffite	2.6	8.9	28.3	66.1	NH_4-acetate method; Ulbig,1994
T-2a	Tuffite	3.0	7.1	33.5	69.4	NH_4-acetate method; Ulbig,1994
Maz-2a	Tuffite	3.7	10.6	10.4	24.2	NH_4-acetate method; Ulbig,1994
Hö-2a	Tuffite	4.3	14.8	17.3	58.8	NH_4-acetate method; Ulbig,1994
Hö-2c	Tuffite	3.8	11.0	6.9	18.0	NH_4-acetate method; Ulbig,1994
Hö-2d	Tuffite	3.1	9.4	11.2	34.7	NH_4-acetate method; Ulbig,1994

2.4.4 Malgersdorf

The bentonite deposits of Malgersdorf (Fig. 2.1) south of Landau a.d. Isar were the first bentonites to be discovered in Southern Germany (Ammon, 1901) and constitute the most eastern bentonite district (Ammon, 1901; Unger, 1983; Unger & Niemeyer, 1985a; Ulbig, 1994, 1999). Mining ceased in the 1950s (Weinig, 1987; Ulbig, 1994). The bentonites are found at lower elevations than the Landshut bentonites at 425 to 460 m a.s.l. (Schulz, 1926; Batsche, 1957; Unger & Niemeyer, 1985a; Ulbig, 1994, 1999). Although the lithologic and stratigraphic history of the Malgersdorf region differs slightly from the development in the Landshut area in respect to the position of bentonites being in or on top of the *Sand-Mergel-Decke* and more carbonate clasts in the *Nördliche Vollschotter* gravels, bentonites have very similar properties (Herold, 1970; Unger et al., 1990; Ulbig, 1994) such as partially altered tuff horizons (Harr, 1976) and grain sizes of glass particles. The Malgersdorf and Landshut bentonites can be roughly stratigraphically parallelised according to Ulbig (1994), although a detailed parallelisation of the various bentonites and tuffs is still missing (Gilg, 2005). The chemical and mineral compositions of the bentonites, tuffs (Harr, 1976; Ulbig, 1994), smectites (Vogt & Köster, 1978) and glasses are

identical to the Landshut bentonites (Ulbig, 1994) therefore indicating a similar origin. Volcanic glasses from Malgersdorf also have Fe/Al and Ti/Al identical to the Landshut area, further indicating an identical volcanic source (Gilg, 2005). The Malgersdorf bentonites are found at the top or above the *Nördliche Vollschotter-Abfolge* (Ulbig, 1994) in sediments of the *Sand-Mergel-Decke* just as the Landshut bentonites (Batsche, 1957; Herold, 1970; Hofmann, 1973). Observations by Ulbig (1994) place the Malgersdorf bentonites above the ejecta layer of the Ries impact but bentonites underneath the ejecta layer have also been located (Unger et al., 1990). The age of the volcanic glass determined using fission-track data (14.4 ± 0.8 Ma) is, within error, similar to the Landshut bentonites (Storzer & Gentner, 1970; Aziz et al., 2010).

2.4.5 Other bentonite deposits in Bavaria

Although the Landshut and Malgersdorf bentonites are the most important bentonite districts, bentonites are found at several other localities in the Upper Freshwater Molasse in Southern Germany (Ammon, 1901; Lemcke et al., 1953; Harr, 1976; Weinig, 1987; Ulbig, 1994; Aziz et al., 2008, 2010). Small occurrences of bentonite sporadically occur north of Landshut, between Landshut and Malgersdorf (Unger & Niemeyer, 1985a; Ulbig, 1994), and south of Freising (Brunnacker, 1962). Most of these occurrences are sub-economic and often are little more than thin horizons or lenticular bodies found in gravel and sand pits (Unger et al., 1985a; Ulbig, 1994). The clays contain high amounts of illite and kaolinite, and are rather sandy, bentonitic clays instead of pure bentonite (Oeltzschner, 1965; Herold, 1970; Vogt & Köster, 1978; Unger et al., 1985a; Ulbig, 1994).

The sandy, illite- and kaolinite-rich Vogelsang (Fig. 2.1) bentonite has, however, been in production for a short time (Unger et al., 1985a). It is hosted by gravels of the *Nördliche Vollschotter-Abfolge* and according to Ulbig (1994) is probably an equivalent of the Landshut bentonites. The Frontenhausen and Geisenhofen clays contain heavy mineral assemblages indicative of lithozones L2 and L3, i.e. a high garnet content (> 90 wt%) for L2 that is slightly lower in L3 (~ 85 wt% garnet) but with higher amounts of other heavy minerals than in L2. The heavy mineral content would thus be consistent with the stratigraphic position of the main bentonite horizon (Unger et al., 1985a). Trace element concentrations of smectites from localities such as Dietelskirchen (Fig. 2.1) are, however, not identical to the Landshut bentonites (Vogt & Köster, 1978).

Bentonites north of Landshut (Fiest, 1989; Ulbig, 1994) are hosted in gravels of the *Nördliche Vollschotter-Abfolge* below and above the *Brockhorizont* and at elevations of 420 to 480 m a.s.l. (Ulbig, 1994). Bentonites above the *Brockhorizont* might be equivalents of the main bentonite horizon of the

Landshut area, especially in localities such as Rainertshausen (Fig. 2.1) situated only a few km north of the Volkenschwand and Oberviecht deposits that are in the centre of the Landshut bentonite district. The garnet-rich sediments and garnet-epidote ratios of sediments near Rainertshausen corroborate the similarity to the heavy mineral content of lithozone L2 and the main bentonite horizon (Ulbig, 1994).

The Augsburg-Aichach area (Fig. 2.1) west of Munich hosts several bentonite and tuff occurrences at Dasing, Pfaffenzell, Aichach, Unterneul, Unterzell, Laimering, and Zahling (Lemcke et al., 1953; Harr, 1976; Fiest, 1986, 1989; Ulbig, 1994; Aziz et al., 2008, 2010). The Laimering tuff/bentonite close to Unterneul reveals a thin layer of a very fine grained basal bentonite resembling the Landshut bentonites (Fiest, 1989; Ulbig, 1994). Its mineral and chemical composition is similar to the Landshut bentonites (Ulbig, 1994). The deposit is situated above the *Brockhorizont* and is assigned to the main bentonite horizon by Ulbig (1994) based on biostratigraphic evidence (Fiest, 1989; Heissig, 1989). The Unterneul bentonite, however, is below the ejecta layer of the Ries impact (Heissig, 1989; Unger et al., 1990; Ulbig, 1994) – it has been suggested to be a detrital accumulation of smectite because it completely lacks residual glass (Harr, 1976; Aziz et al., 2010).

The rhyolitic glass tuff of Zahling was thought to be an equivalent of the main bentonite horizon (Ulbig, 1994; Heissig, 2006) but recent work suggests an older, pre-Riesian age (16.1 ± 0.3 Ma; Rocholl et al., 2008; Aziz et al., 2010). Although the Zahling-2 tuff is chemically similar to glass particles from the main bentonite horizon it has lower Ti/Al and Fe/Al (Ulbig, 1994, 1999), indicating a more differentiated magma source.

2.4.6. Bentonite deposits outside of Bavaria

Bentonites in the UFM are also found in the Krumbach-Thannhausen area in Swabia (Fig. 2.1) (Lemcke et al., 1953) and have been the target of small-scale mining operations (Unger, 1981; Ulbig, 1994). The Krumbach-Thannhausen bentonites are several meters thick and show beds and lenses of partially altered tuff (Harr, 1976), and are erosionally capped by Quaternary gravels (Ulbig, 1994). The mineral composition is similar to the main bentonite horizon (Harr, 1976; Ulbig, 1994). The bentonites are found at an elevation of 540 m a.s.l. about 40 m above the Ries impact ejecta layer (Scheuenpflug, 1980). Ulbig (1994) allocated them to the Badenian assuming that they belong to a similar horizon as the Landshut bentonites. The glass particles from a tuff in the Krumbach deposit also have a rhyolitic composition (Ulbig, 1994, 1999), trace element concentrations, Ti/Al and Fe/Al very similar to the Landshut and Malgersdorf areas (Ulbig, 1999; Gilg, 2005). However, a parallelisation with the Landshut

bentonites is unlikely in light of $^{40}Ar/^{39}Ar$ ages of glass particles of 15.45 ± 0.1 Ma (Rocholl et al., 2008) and 15.6 ± 0.4 Ma (Aziz et al., 2010). The old ages could be interpreted to indicate that the formation of the Landshut, Malgersdorf, and Krumbach bentonites is related to two or more eruption stages (Aziz et al., 2010).

Small occurrences of bentonite with a thickness of 3 to 6 m are also located in the Hegau and Lake Constance region close to Switzerland (Erb, 1931; Hofmann, 1956a, b; Schreiner, 1976; Bauer et al., 2016). The Hegau bentonites formed from alkaline mafic and phonolitic tuffs or lapilli, or in the case of the *Basisbentonit* from rhyolitic-dacitic material deposited in direct vicinity to their volcanic source during the middle or late Miocene (Hofmann, 1956a, b; Harr, 1976; Sawatzki & Schreiner, 1991). The smectite content of the bentonites varies from 70 to 90 wt%. The smectite-rich Hegau tuffs contain mica, chlorite, kaolinite and carbonates, as well as quartz, sanidine, oligoclase-andesine, apatite, zircon, rutile, amphiboles/pyroxenes, and ilmenite (Hofmann, 1956a, b; Harr, 1976; Bauer et al., 2016). The $\delta^{18}O$ and δD values of smectites from the *Deckentuff* are at the lower ($\delta^{18}O$) respective higher (δD) end of values of Bavarian bentonites, indicating either colder climate or higher precipitation (Bauer et al., 2016). The older, smectite-rich volcanic rocks (*Deckentuff*) have been dated using biotite and apatite K-Ar and fission track data at 14.1 ± 1.0 Ma to 12.8 ± 1.4 Ma (Lippolt et al., 1963; Rahn & Selbekk, 2007). The mineral composition and age excludes these volcanic rocks as a tephra source for the Landshut bentonites, as previously suggested (Ulbig, 1999). However, the *Basisbentonit*, a glass-rich, rhyolitic tuff underlying the *Deckentuff* at Heilsberg/Hegau (Hofmann, 1956a, b; Harr, 1976) has been dated using $^{40}Ar/^{39}Ar$ on glass particles and feldspars at 14.5 ± 0.2 Ma (Aziz et al., 2010), though is distinguishable from the Landshut bentonites based on the lower Ti/Al and Fe/Al. The element ratios are similar to the elemental ratios of the Zahling-2 tuff and Bischoffszell bentonite in Switzerland (Ulbig, 1994; Gilg, 2005).

CHAPTER THREE

3. Materials and sample origin

This chapter discusses the origin of the samples and materials used in sample processing for the studies in chapters 5, 6 and 7. Chapters 5 and 6 focus on bentonite-associated calcite and dolomite; and smectite separates of dolomite- and calcite-bearing bentonites, tuffs and tuffitic sandstone from Southern Germany. Geochemical and mineralogical results of bulk bentonites, smectite separates, and disseminated calcite (and dolomite) from bentonite deposits worldwide are presented in chapter 7.

3.1 Southern Germany

Field work was carried out from 2011 to 2014 in actively mined bentonite deposits located in the Mainburg-Landshut region (see Chapter 2.3). All examined deposits are reclaimed by now, with the exception of the Rehbach deposit. Bentonite deposits were sampled for bentonites, tuffs/sandstone, and carbonates, and documented using vertical sections. Access to deposits was kindly granted by Süd-Chemie AG (now Clariant) and S&B Industrial Minerals (now Imerys).

The dolomites and calcites, bentonites, altered tuffs, and tuffitic sandstone, are from the Gabelsberg, Mittersberg, and Zweikirchen deposits with supplementary dolomite and calcite samples from the Hofen, Rehbach, Hader, and Landersdorf deposits. The carbonate samples were used for carbon and oxygen stable isotope analysis as well as microfacies analysis. A carbonaceous wood fragment from the hanging-wall gravels of the Peterswahl deposit close to Mittersberg was also analysed.

3.2 Worldwide

Whole-rock bentonites and < 0.2 µm smectite separates from bentonite deposits at Landshut (Bavaria) in Southern Germany; Milos Island (Angeria and Zoulias) in Greece; Cabo de Gata (Los Trancos) in Spain; the island of Sardinia (S'Aliderru) in Italy; Pertek in Turkey; Askana in the Republic of Georgia; the Tavush region in Armenia; Bahia (Vitória da Conquista) in Brazil; La Tranquera in the San Juan and Lago Pellegrini in Rio Negro provinces of Argentina; as well as Wyoming (Mowry and Beaver

bentonite at Lowell), Montana (Glasgow), California (Otay) and Nevada (Fallon) in the United States of America (Fig. 3.1) are part of the boron isotope study discussed in chapter 7.

Untreated whole-rock bentonites were provided by H. Albert Gilg (TUM), Gerhard Lehrberger (TUM) and Thomas Albert (Süd Chemie AG, now Clariant), Stefan Kaufhold and Reiner Dohrmann (both BGR), Laurence Warr (University of Greifswald), and Mirela Tsagkari (S&B Industrial Minerals, now working at Arkema). Bentonites from the Landshut region in Southern Germany were collected by myself during field work for chapters 5 and 6.

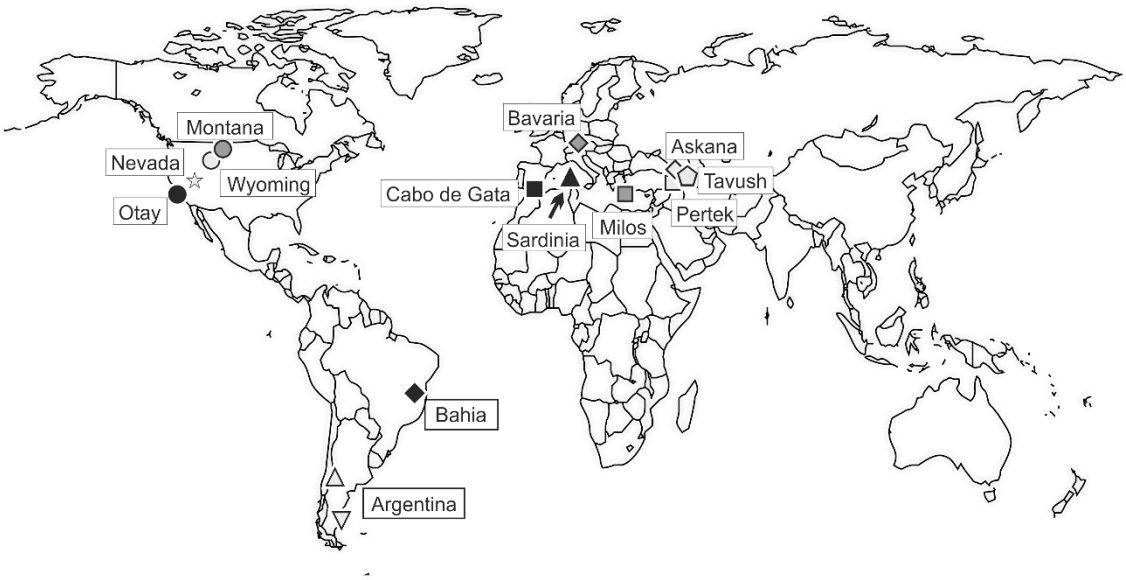

Fig. 3.1: Simplified map of the world showing the locations of the examined bentonite deposits. Light-grey: Na-bentonites, grey: Ca-bentonites, black: Mg-bentonites. The map of the world was plotted with R 3.2.1.

CHAPTER FOUR

4. Methods

The sample processing and analytical methods used to investigate the micromorphology, mineralogical, isotopic, and chemical composition of calcites and dolomites as well as bentonites, tuffs/sandstone, and smectite separates are discussed in this section.

4.1 Overall sample pre-treatment

Samples were stored in polypropylene (PP) bags and manually screened for macroscopic features such as sedimentary fabrics, munsell colour, and carbonates prior to processing. Carbonates, bentonites, tuffs, and sandstone were broken into small pieces (< 10 mm) wearing nitrile gloves, split, and dried in a drying cabinet at 40°C. Carbonates in bentonites and tuffs were manually separated to obtain carbonate-free whole-rock samples.

4.1.1 Dolomite and calcite

Sub-samples of carbonates were used for the preparation of standard petrographic thin-sections, X-ray diffraction and stable isotope analysis. The sub-samples for the latter two methods were dry-ground in an agate mortar until reaching the consistency of very fine flour, passing through a < 6.3 µm sieve without residue.

4.1.2 Whole-rock samples

About 1.8 g of dried whole rocks of bentonite, tuffs, and sandstone were milled for 7 minutes in isopropanol using agate cylinders and a McCrown micronizing mill. Ten wt% of ZnO was added to tuffitic samples to estimate the amount of X-ray amorphous volcanic glass. Some tuffitic samples (Gabelsberg and Zweikirchen) were durable enough for the preparation of standard petrographic thin-sections.

4.1.3 The < 2.0 and < 0.2 µm fractions

The exchangeable cations in the smectite interlayer, the geochemical composition (ICP-MS), strontium (TIMS) and boron isotope, and geochemical analyses (PGAA and SIMS) were determined on "pure" smectites (< 0.2 µm fractions) separated from dried (18 hours at 40°C) but otherwise untreated whole rocks. Smectites were separated using equipment that was cleaned with distilled water and triple-washed with a 1.82 % mannitol solution.

About 5 to 10 g of dried whole-rock bentonites, tuffs and sandstone were dispersed in distilled water (EC < 0.9 µS/cm) using 0.5 litre Kautex polyethylene (PE) bottles, manually shaken and soaked in an ultrasound bath for 15 minutes. Ultrasound treatments were divided in three blocks to prevent excessive heating of the clay suspension. Temperatures of up to 80°C can be reached during excessively long ultrasound baths. Neither ammonium-bearing water for pH control nor dispersants such as sodium pyrophosphate were used during sample processing in order to avoid contamination by trace elements.

The clay suspensions were centrifuged for 95 minutes (including 5 minutes for acceleration and deceleration) at 1650 rpm and a bottle fill height of 10.5 cm to separate the < 0.2 µm fractions. The transparent or slightly turbid liquid was carefully decanted into 0.5 litre PE bowls lined with PE foil. The foil reduced the loss of clay sticking to the bowl and made it easier to retrieve the < 0.2 µm fractions without having to touch them. The liquid was evaporated in a drying cabinet at 40°C. The sample processing is highly dependent on individual sample properties, and anything between 0.05 to 4.0 g of the < 0.2 µm fraction may be obtained during one centrifugation cycle.

The < 2.0 µm fraction of the Clay Minerals Society standard Imt-1 illite was dispersed in distilled water and separated by sedimentation in triple mannitol-washed Atterberg cylinders both for prompt gamma neutron activation analysis and X-ray diffraction analysis.

4.1.4 Dialyses, cation exchange, and acid ammonium oxalate treatment

The size separation method described above can result in the accumulation of water soluble phases in the < 0.2 µm fractions and thus requires de-salting. Dialysis is a time-intensive but simple and cheap method that does not require a high-speed centrifuge. Samples of less than 50 mg and up to 1000 mg can be processed using only distilled water (D), a 1.82% mannitol (M) solution (Tonarini et al., 1997) and/or a 1 M ammonium acetate (A) solution.

Mannitol is a polyhydric sugar alcohol similar to xylitol or sorbitol that bonds boron to hydroxyl groups, and removes adsorbed boron from clay surfaces (Hingston, 1964). The ammonium exchange re-expands the smectites and removes interlayer B (Zhang et al., 1998). The combined ammonium exchange and mannitol treatment thus can remove both interlayer and absorbed boron with the same reliability as divalent cation exchange treatments (e.g. Williams et al., 2001; Williams & Hervig, 2005, 2006).

A 0.1 M acid ammonium oxalate (AAO) solution was used to remove Fe-hydroxides. The photo-sensitive AAO solution was prepared immediately before sample treatment by mixing the proper amounts of ammonium oxalate and oxalic acid. Although the 0.1 M solution is less effective (i.e. slower) than the original 1 M solution by Schwertmann (1964) its higher pH is less damaging to the clay minerals. Ultraviolet and daylight enhance the reaction (Schwertmann, 1964). The AAO treatment was followed by mannitol-washing identical to the other sub-samples.

The flexible Visking cellulose dialysis tubes (Type 36/32) were watered for four days, the water replaced on a daily basis to remove humectants (e.g. glycerine), and then stored in distilled water to prevent drying.

The overall procedures for distilled water (D), mannitol (M), and ammonium acetate (A) plus mannitol treatment are identical. About 300 mg of the dry < 0.2 µm fraction was weight into 50 ml Nalgene bottles and 25 ml of the respective solution was added to the sample, shaken, and soaked in an ultrasound bath for 15 minutes and then left soaking for 24 hours. The AAO sub-samples were placed in daylight for four days. The suspension was shortly shaken and introduced into the flexible tubes and placed into PE see-through boxes together with two litres of distilled water (EC < 0.9 µS/cm) as buffer solution. The buffer solution was replaced daily until its EC remained constant (0.9 to 1.0 µS/cm), this usually requiring 10 to 14 days. The < 0.2 µm fractions were dried at 40°C and stored in weighing-paper lined PE bags.

4.2 Analytical methods

4.2.1 Polarisation microscopy and microfabric analysis

The microfabrics of carbonates were examined in standard petrographic thin-sections (~30 µm thick) using a polarization microscope (Leica DMLM). Selected samples of each facies were dried at 40°C, dry-cut and hardened in diluted Araldite epoxy resin because even a small smectite content resulted in swelling and bubble formation. Thin-sections were not covered because of that. Removable

glass slides and glycerine were used later on for better image quality. Carbonate facies were identified according to the microfacies classifications of Wright & Tucker (1991), Freytet & Verrecchia (2002) and Alonso-Zarza (2003).

4.2.2 Field emission - scanning electron microscopy and micromorphology

Air-dried and subsequently vacuum-stored (two days) whole-rock samples not hardened with epoxy resin were examined with a field-emission scanning electron microscope (FE-SEM) Zeiss Ultra 55 Gemini with a Bruker XFlash 5030 detector and Quantax Esprit 1.9 software system at the Institut für Werkstofftechnik, Universität der Bundeswehr München. The Zeiss Ultra 55 Gemini is especially suitable for the examination of non-conductive and non-carbon coated materials. Image acquisition was performed at 2.0 or 3.0 kV with a theoretical resolution of 1.7 nm which was lower due to rough, uncoated sample surfaces and material properties. However, EDX measurements of uncoated samples made it possible to distinguish smectite from dolomite by comparing the relative amount of silica, aluminium, calcium, magnesium, and especially carbon.

4.2.3 X-ray diffraction: mineral composition and clay mineral analysis

Random powder mounts of whole-rocks, as well as air-dried, ethylene-glycolated (EG) and heated (550°C) orientated mounts of the < 0.2 µm (and the < 2.0 µm of the Imt-1) fraction were characterised by X-ray diffraction analysis from 2 to 70°2θ (PW 1800, Cu Kα). The instrument was operating at 40 mA and 40 kV with a graphite monochromator, and automatic divergence slit. Powder mounts were quantified by full-pattern Rietveld refinement using BGMNwin 1.8.6. (Bergmann et al., 1998) with an estimated relative error of about 10 wt%. The individual phases were identified manually, and compared to the results of the IDENT software of the Phillips PW 1800, and the database of BGMNwin 1.8.6. Smectites were identified in orientated mounts of the < 0.2 µm fraction based on the migration of the d_{001} reflection from ~12 Å (mostly interlayer Na) or ~14.5 Å (mostly interlayer Ca) in the air-dried state to ~16.5 Å to ~17.5 Å in the EG-solvated state. The calcium and magnesium content and ordering of dolomites and calcites were estimated using the position of d_{104} reflection and the d_{015}/d_{110} intensity ratio (Goldsmith & Graf, 1958; Lumsden & Chimahusky, 1980).

Discrete illite in the < 0.2 µm fractions and its content was estimated using reference intensity ratios (peak areas of d_{001} reflections) of 4 for smectite and 1 for illite. The illite-in-EG-smectite content was determined according to Środoń (1980) using the peak migration method (26° - 28° 2θ and 15° -

18° 2θ). As discrete illite can interfere with the identification of the peak positions (Środoń, 1980), the percent illite-in-EG-smectite was also estimated by comparing the 001/002 and 002/003 positions (Moore & Reynolds, 1997). Using these methods, variable humidity, interlayer composition, and layer charge can yield errors up to 30 % for the illite-in-EG-smectite content (Środoń, 1980).

4.2.4 X-ray fluorescence, handheld: Ca, Sr and Mn content in dolomite and calcite

A handheld ED-XRF Bruker Tracer III-SD with a Rhodium anode and a 10 mm² silicon drift detector was used for the chemical analysis of Ca, Sr, and Mn on a smoothed surface of dolomite and calcite samples. Only the 67 solid carbonate samples were used, their surface smoothed with corundum coated abrasive paper, cleaned with pressurised air and checked for traces of abrasive paper using a binocular. The X-ray spot size was about 3 x 4 mm. Measurements were conducted for 30 seconds operating at 40 kV and 30 µA with the yellow filter (12 mil Al + 1 mil Ti). Spectra were fitted with the ARTAX software (Version 7.4.8.2) and calibrated using ICP-MS results and the international standards BCS393, DWA-1, MAG-1 and NIM-S (Govindaraju, 1989).

4.2.5 Inductively coupled plasma mass spectrometry (ICP-MS) and thermal ionisation mass spectrometry (TIMS): Geochemical composition and Rb-Sr dating

As the mineralogical analyses (chapters 5 and 6) showed that the carbonates contain variable contents of silicates and oxides, only selected silicate-poor carbonate samples were subjected to the acid leach approach. Prior to hydrochloric acid treatment, smectite separates (< 0.2 µm fractions) and carbonates were dialysed with distilled water until the electrical conductivity remained < 0.9 µS/cm, then dried at 40°C, and split.

Carbonates were dissolved in 1N HCl in PTFE beakers and allowed to react for 45 minutes at 20°C. The solution was separated by centrifugation. A two-step procedure using hydrochloric acid was applied to the < 0.2 µm fractions to extract easily leachable and more strongly bound elements in the clay minerals according to a simplified procedure after Chaudhuri & Brookins (1979), Clauer (1979) and Clauer et al. (1982). Smectites were treated with triple distilled 1N HCl for 15 to 20 minutes at 20°C and the solution centrifuged (=“leachate”). The residues were washed additionally for one minute with 1N HCl and three times with triple distilled water to remove excess acid. The residual material (=“residue”) was treated with 6N HCl at 90°C for 12 hours. Leachate and residue were analysed by inductively coupled plasma mass spectrometry (Actlabs Canada, UltraTrace 7: method A).

As the K, Rb and Sr concentrations of method A were in several cases below the detection limit, a second approach (method B) with a prolonged leaching time of 18 hours and a Perkin Elmer DRC II ICP-MS at the Department of Geochemistry, University of Göttingen, Germany was used. The JA-2 was used in method B for external accuracy check and showed an error of less than 10 to 30%. Results were corrected for drift and for major oxygen interferences. Hundred ml 2% HNO_3 with 4 internal standard elements (Be, Rh, In, Re) were added to 1 ml of the leachate and residue solutions.

For Sr isotope analyses, an ion chromatographic column separation with Sr-specific crown-ether resin (Sr-Spec®, EIChroM Industries, USA) was used to extract Sr and to remove interfering elements (Horwitz et al., 1992; Pin & Basin, 1992). The samples were leached according to method A. The Sr isotope ratios of smectites and carbonates were determined using a thermal ionisation mass spectrometer (TIMS, MAT 261.5, Thermo Finnigan, Germany) at the ZERIN Ries Crater Museum, Nördlingen, Germany, using single tungsten filaments. Significant extant Rb was evaporated by controlled preheating before measurement. Isotope mass fractionation during analysis was corrected by referencing to an invariant 88Sr/86Sr value of 8.37521. To check for proper operation of the mass spectrometer, certified reference material (SrCO3, NIST SRM 987) was measured. The mean value during the time of analyses was 0.710211 ± 0.000023 (2sigma_mean; n: 55). Total analytical uncertainty (precision + accuracy) for 87Sr/86Sr in "normal" natural samples is estimated by replicate analyses of in-house standards at < 50 ppm.

A split of sample MB28 (a dolomite) containing illite was reacted 24 hours in 1N HCl at 20°C to determine the influence of leaching time on isotope ratios. The Sr isotope ratio of MB28 increased only slightly from 0.710521 to 0.710541, indicating that leaching time has a negligible effect on Sr isotope ratios of carbonates. “Isochron” ages of smectite leachate and residue pairs and carbonate-smectite residue pairs were calculated using IsoPlot 4.13 (Ludwig, 2008). Ages were calculated using results from method A for leachates and results from method B for residues because the residue Sr content was below the detection limit of method A.

4.2.6 Exchangeable cations: “Cu-trien method”

The exchangeable cations and cation exchange capacity of dialysed (using distilled water) < 0.2 µm fractions were double determined on 0.2g (a) and 0.3g (b) sub-samples at the Bundesanstalt für Geowissenschaften und Rohstoffe (BGR). The material was weight after drying at 105°C and treated with a three times calcite oversaturated Copper-triethylenetetramine (“Cu-trien”) solution. The concentrations of sodium, potassium, magnesium and calcium ions in the exchange solution were

determined by inductively coupled plasma mass spectrometry (ICP-MS). The exchangeable cations, as well as the exchangeable sulphate and chloride content of samples B17, B23, B31 and B51 were previously determined at the BGR (Kaufhold & Dohrmann, 2008; Dohrmann & Kaufhold, 2010).

4.2.7 Carbon and oxygen stable isotopes

Carbon and oxygen stable isotope values were determined for 83 dolomite and calcite samples. Twenty-five mg of carbonate were weighed into glass tubes according to the carbonate mineral content determined by X-ray diffraction analysis and Rietveld refinement.

Stable isotope measurements were performed with a Con-Flow DeltaPlus (Thermo Scientific) isotopic-ratio mass spectrometer linked to a Gasbench II (Museum of Natural Sciences, Berlin, and GeoBio-Center LMU, Munich, Germany). Isotope ratios are reported as δ-values in ‰ relative to V-PDB with an estimated accuracy and precision of ± 0.1 ‰. 103% phosphoric acid was added drop wise to each sample with a syringe. Samples were measured after a reaction time of at least 3 h at 72°C. Standards NBS 18 and NBS 19, and an internal laboratory standard (Solnhofen Plattenkalk: $\delta^{18}O_{V\text{-}PDB}$ of -4.84 ‰ and $\delta^{13}C_{V\text{-}PDB}$ of 0.47 ‰), were included in every batch. All three standards show standard deviations of ± 0.08 ‰ for oxygen and ±0.07 ‰ for carbon. The $\delta^{18}O$ values of dolomite were corrected using a phosphoric acid fractionation factor of 1.00986 at 72°C (Rosenbaum & Sheppard, 1986).

4.2.8 Prompt gamma neutron activation analysis: PGAA

The boron concentrations and chemical composition of the < 0.2 µm fractions from 21 bentonite samples were determined at the research neutron source FRM II Heinz Maier-Leibnitz Zentrum in Garching, Germany in cooperation with Dr. Petra Kudejova and Dr. Zsolt Revay.

Prompt gamma neutron activation analysis is a non-destructive techniques that offers very low detection limits of < 0.05 ppm for boron determination due to its large neutron capture cross section. Hydrogen also has a large neutron cross section that makes it is possible to normalise all samples as H_2O-free, making a comparison of boron concentrations feasible. The ammonium content in ammonium exchanged samples was determined by allocating the corresponding amount of hydrogen atoms to each nitrogen atom.

About 50 to 300 mg of the < 0.2 µm fractions – constituting up to five sub-samples of untreated (U), distilled water-washed (D), mannitol-washed (M), ammonium exchanged plus mannitol-washed (A) and AAO-treated (F) material – were sealed into 25 µm thick PTFE foil. Each PTFE bag was weighed.

The fluorine to carbon ratio of the PTFE foil makes it possible to subtract these elements (C and F) from the measured concentrations in fluorine-free samples. The PTFE bags were placed into the neutron beam with no extra collimator and irradiated in a vacuum (0.3 mbar) for 1 to 2.5 hours. Each sample was irradiated with cold neutrons (25 K) at a flux of $3.8*10^8$ to $2.0*10^{10}$ n cm^2/s providing a neutron spectrum with an average energy of 1.83 MeV. The gamma spectra were detected by a Compton-suppressed spectrometer using a 60% HPGe detector coupled with a surrounding BGO scintillator.

The PTFE foil, PE foil, mannitol powder, ammonium acetate, and distilled water stored for one week in a closed Kautex PE bottle and a closed Nalgene bottle were also irradiated (Table 4.1).

Table 4.1: Boron concentrations and other trace elements in the equipment and chemicals, in µg/g.

Material	Al_2O_3	Cl^-	Pb	B
PTFE foil	0.16	0.29	7000	0.39
PE foil	0.12		12000	0.19
Mannitol powder	0.13	7.0	13000	0.25
Ammonium acetate	0.21		4.1	0.79
water in old PE bottle		0.7		0.52
water in new PE bottle		0.7		0.61

4.2.9 Secondary ion mass spectrometry: SIMS

Boron isotope values were determined at the SIMS lab of the Arizona State University in Tempe, Arizona in cooperation with Lynda B. Williams, Ph.D. Although SIMS is not able to provide the high precision results as e.g. TIMS (Tonarini et al., 1997) it has a much better spatial resolution. It is therefore possible to assess the variation in boron isotope values at different spots on the same sample (Chaussidon et al., 1997; Williams, 2000). The lower precision of the SIMS is in part compensated by the very large boron isotope variation in natural fluids and minerals (-40 to +70 ‰ $\delta^{11}B$; e.g. Swihart et al., 1986; Vengosh et al., 1992). The boron isotope ratios were determined using a Cameca IMS 6f with a defocused oxygen ion beam with a spot size of 30 µm resulting in a more homogenous sputtering of the sample surface. The Cameca was calibrated for $^{10}BH^+$ interferences as the boron hydride may interfere with ^{11}B measurements because of its very similar atomic mass (Fig. 4.3). Further information for boron isotope analysis can be found in Hervig (1996) and Chaussidon et al. (1997).

The procedures of Williams (2000) were used for boron analysis of the smectite separates. Up to four mannitol-washed and/or ammonium exchanged smectite sub-samples were dispersed in boron-free distilled water and pipetted onto boron-free glass slides. The Imt-1 illite of the Clay Minerals Society was used as a reference and pipetted onto the centre of each glass slide. An average $\delta^{11}B$ value

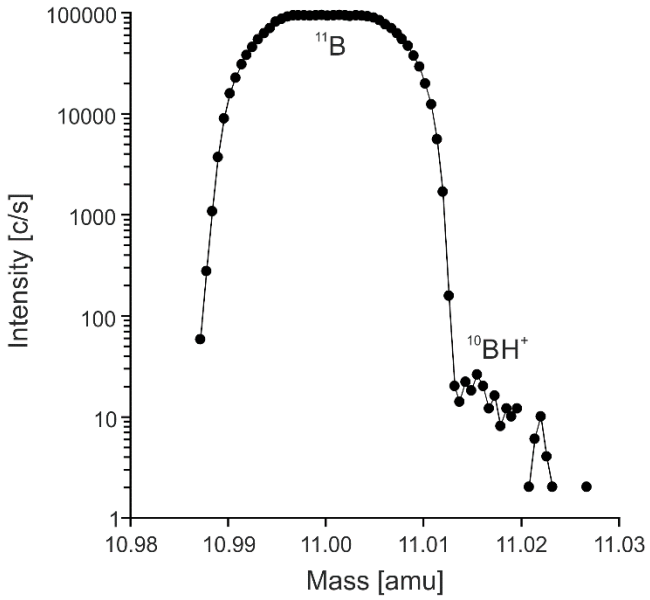

Fig. 4.1: The separation of ^{11}B from ^{10}BH^{+} by high-mass resolution.

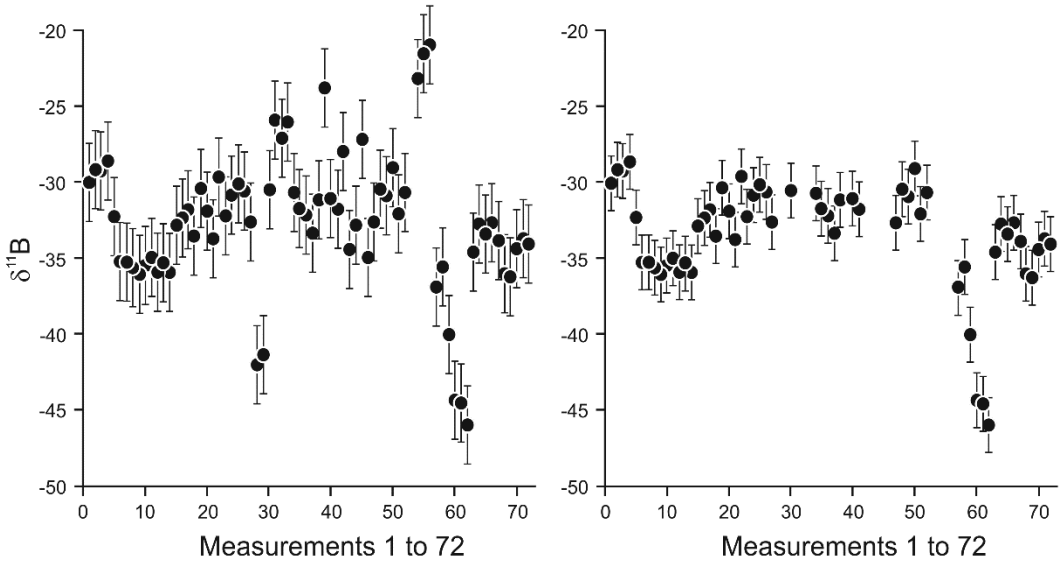

Fig. 4.2: Variation in instrumental mass fractionation (IMF) in the clay mineral standard Imt-1. Left: IMF uncorrected for fluctuations in current, manual errors, or instrumental drift. Right: The IMF used for defining areas of stable IMF for boron isotope analysis.

of -9.0 ‰ relative to standard NBS SRM 951 was applied. The -9.0 ‰ value lies between δ^{11}B values of -8.66 ‰ and -9.86 ‰ determined according to Tonarini et al. (1997) (Williams, 2000). The Imt-1 was measured before and after each sample to determine the instrumental mass fractionation (IMF), which varied between -29.1 ‰ to -46.0 ‰ (excluding outliers) during the measurement campaign. Blocks of (almost) stable IMF (Fig. 4.4) were used to calculate the δ^{11}B value of the smectites reported as $\delta^{11}B = [((^{11}B/^{10}B_{sample})/(^{11}B/^{10}B_{standard})-1)*1000]$-IMF.

CHAPTER FIVE

5. Pedogenic, palustrine and groundwater dolomite formation in non-marine bentonites (Bavaria, Germany)

Published in Clay Minerals – Journal of Fine Particle Sciences: Köster M. H. & Gilg H. A. (2015) Pedogenic, palustrine and groundwater dolomite formation in non-marine bentonites (Bavaria, Germany), Clay Minerals, v. 50, p. 163-183.

This research project was designed by Mathias H. Köster with input from Prof. Dr. H. Albert Gilg (Technische Universität München). Field work in bentonite mines was carried out by Mathias H. Köster with the help of three bachelor students. Mathias H. Köster performed the sample processing, the microfabric analysis, the SEM imaging, and the X-ray diffraction analysis. Sample weighing and processing for carbonate stable isotope measurements was done by Mathias H. Köster, the stable isotope measurements were performed by PD Dr. Christoph Mayr (Ludwig-Maximilians Universität München & Friedrich-Alexander-Universität Erlangen-Nürnberg). Mathias H. Köster drafted and wrote the initial manuscript, with some editing, revisions and data verification by Prof. Dr. H.Albert Gilg. Mathias H. Köster brought the manuscript into its final shape and submitted it to the Clay Minerals Journal.

Abstract

Dolomite and calcite in Bavarian bentonites, southern Germany, were investigated using petrography, field-emission scanning electron microscopy and stable isotope geochemistry to explore the role of authigenic carbonate formation during bentonitization. Pedogenic, palustrine and groundwater carbonates were distinguished on the basis of X-ray diffraction, micromorphological and stable isotope analysis. The $\delta^{13}C_{V\text{-}PDB}$ and $\delta^{18}O_{V\text{-}PDB}$ values of dolomite range from –8.0‰ to –6.1‰ and –5.4‰ to –3.4‰ respectively. Calcites show a range from –11.9‰ to –8.1‰ for carbon and from –9.1‰ to –6.2‰ for oxygen. Carbon isotope compositions imply a C3-plant-dominated carbon source

and repeated wetting and drying cycles. The oxygen isotope data points to an evaporation and temperature controlled $\delta^{18}O_{V\text{-}SMOW}$ value of meteoric water of –7.0‰ to –4.8‰. A syngenetic to early diagenetic timing of dolomitization is indicated, suggesting both dolomite and bentonite formation in non-saline, non-arid and repeatedly partially-oxygenated and reducing soil and groundwater environments during pedogenesis.

5.1 Introduction

Bentonite, a versatile and highly priced commodity, is a smectite-rich clay that is commonly formed by alteration of volcanic glass (e.g. Christidis & Huff, 2009). Many world-class bentonite deposits were formed from rhyolitic pyroclastites, although acidic precursor rocks are considered less suitable for bentonitization than intermediate volcanic rocks, such as andesite or latite, due to their high Si to Al ratios and low Mg content (Grim & Güven, 1978; Christidis, 2008). Rhyolitic rocks require intense leaching of silica and alkalis to prevent secondary silica precipitation, as well as the addition of Mg ions to form montmorillonite (Christidis & Dunham, 1997). Thus, many rhyolite-based bentonite deposits are hosted in marine settings. The necessary high water-rock ratios are related either to hydrothermal heating and convection of marine fluids in volcanic complexes for proximal bentonites, e.g. Cabo de Gata, Spain (Delgado, 1993; Delgado & Reyes, 1993), and Milos, Greece (Decher et al., 1996; Christidis, 2008), or to compaction-driven diagenetic fluid flow of marine pore waters in sedimentary basins for distal bentonites, e.g. Wyoming, USA (Gilg & Rocholl, 2009). Therefore, seawater is generally considered as the main source for Mg in smectite formed from rhyolitic precursor rocks (Christidis & Huff, 2009). In contrast, bentonite deposits in southern Germany are derived from Mid-Miocene rhyolitic ash deposited in a strictly non-marine freshwater environment. These bentonites often contain abundant dolomite and calcite (Vogt, 1980; Unger, 1999; Ulbig, 1999) with a hitherto unknown temporal and genetic relationship.

Dolomite and calcite in bentonites have been investigated systematically only for the proximal deposits of Cabo de Gata, Spain and Milos, Greece. Both bentonite deposits are related to marine depositional environments in the vicinity of the Mediterranean Sea (Delgado, 1993; Delgado & Reyes, 1993; Decher et al., 1996) that could have acted as a source of Ca and Mg. Stable oxygen and carbon isotope studies indicate that in both cases the carbonates did form from hydrothermal mixed marine-meteoric waters at temperatures of about 30 to 90°C (Delgado, 1993; Delgado & Reyes, 1993; Decher et al., 1996). In contrast, carbonate formation in distal non-marine and non-hydrothermal bentonites is still unexplored, but might shed light on smectitization in such an environment.

In this study, we report on the presence of authigenic dolomite and calcite in a non-marine bentonite. Petrographic and isotope geochemical data are used to explore carbonate genesis in this unusual setting and its relationship to bentonitization.

5.2 Geological setting

The Bavarian bentonite deposits near Landshut, Bavaria (Fig. 5.1), form the largest bentonite district in Central Europe with a production of 350 000 t/y and a mining history dating back 110 years (Unger, 1999). The bentonite deposits are located in a 40 km by 10 km wide belt (Fig. 5.1) and are mostly restricted to the Landshut-Neuöttinger Hoch, a tectonic block bordered by NW–SE striking fault zones (Unger, 1999) that were active during the Permian and Cretaceous, that were possibly re-activated during the Tertiary (Lemcke, 1973).

More than 130 individual deposits are hosted in the Mid-Miocene Upper Freshwater Molasse (UFM), the uppermost of four sedimentary sequences that comprise the Cenozoic sedimentary infill of the North Alpine Foreland Basin (NAFB) (e.g. Aziz et al., 2008). The westward dewatering (Lemcke, 1973) clastic sedimentary environment of the NAFB was characterised by meandering rivers, floodplains, high groundwater levels in topographic depressions or oxbow lakes and the formation of gravels, sands and marls (Schmid, 2002). With an estimated overburden of 200 to 300 m, the UFM was not subject to significant burial or high temperatures (e.g. Lemcke, 1973; Ulbig, 1999).

Bentonites in the main bentonite horizon occur as small, irregular lenses of variable size (Vogt, 1980; Ulbig, 1999) hosted by marly floodplain sediments of the Sand–Mergel–Decke (e.g. Aziz et al., 2008) and/or by fluviatile sand and gravel of the uppermost Nördlicher Vollschotter about 10 to 30 m above the ejecta layer of the Early Badenian Ries meteorite impact. Hofmann (1973) showed that the bentonites in the Sand–Mergel–Decke share the same lithostratigraphic position as dolomite-bearing "Süßwasserkalke", freshwater limestones and marls with a pronounced and increasing dolomite content at the top and often with a calcareous base. Non-economic bentonites are also found below the ejecta layer of the Ries impact (Ulbig, 1999). Deposits may be discordantly capped by sandy gravel, silt- and mica-rich sand or more rarely by clayey sediment. All fine-grained host-sediments and some gravels show various stages of palaeosol development and are rich in authigenic carbonate (Schmid, 2002).

Ulbig (1999) proposed two types of bentonite deposits formed in different morphological locations to explain sedimentological differences. While the more common deposits of the "Hochlage" (topographic high) are often carbonate-rich clays with marly to clayey footwalls of the Sand-Mergel-

Decke, the less common "Tieflage" (topographic low) deposits are usually hosted by sand or gravel and may contain basal kaolinite-rich beds or kaolinite aggregates in bentonite (Ulbig, 1999). The deposits in topographic lows can be completely devoid of carbonates. Intermediate forms of the two types also exist.

The blue, green, grey and yellow bentonites show a bed thickness of 0.5 to 8 m, while total thickness of a deposit may reach 10 m due to often intercalated lithified sub-economic horizons of smectite-poor and partially altered tuffite, sandy clay, or silicified bentonite ("Harte Platte"). The mineralogical composition of bentonites is dominated by Ca-montmorillonite and variable amounts of illite/mica, kaolinite, chlorite, quartz, feldspar, calcite and dolomite, apatite, zircon, Fe-Ti-oxides, as well as occasionally glass shards, pyrite and detrital minerals, including epidote and garnet (Vogt, 1980; Ulbig, 1999).

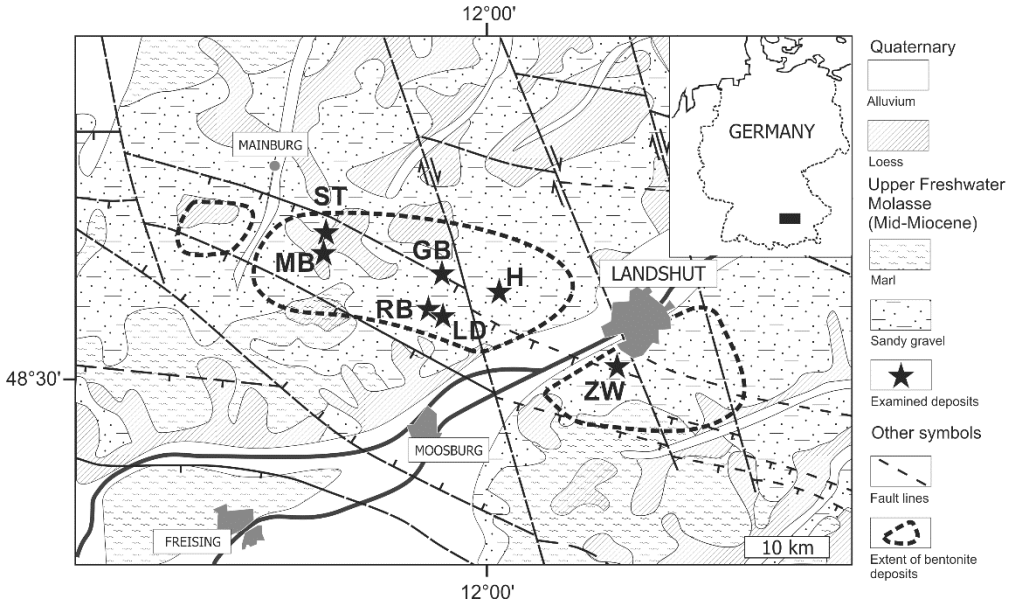

Fig. 5.1: Simplified geological map (modified from Freudenberger & Schwerd, 1996; Unger, 1999) and location of the Bavarian bentonite deposits studied. Reproduced with the permission of the Mineralogical Society of Great Britain & Ireland, from Köster & Gilg (2015).

5.3 Materials and sample origin

Field work was conducted between 2011 and 2014 in seven actively mined bentonite deposits (Fig. 5.1). Deposits are located in the Landshut region, Germany, and include the Zweikirchen (ZW), Gabelsberg (GB), Rehbach (RB), Landersdorf (LD), Mittersberg (MB), Hader (H) and Strass (ST) deposits. 82 carbonate samples were recovered from bentonites. A carbonaceous wood fragment from the

hanging-wall gravels of the reclaimed Peterswahl deposit several kilometres south of Mittersberg was also analysed.

5.4 Methods

Paleosol development with carbonate accumulations in bentonites are recognized based on horizonation, soil fabrics, root casts and redoximorphic features (e.g. Retallack, 1988; Nettleton et al., 2000; Schmid, 2002). Carbonate facies is addressed using the schemes of Wright & Tucker (1991), Freytet & Verrecchia (2002) and Alonso-Zarza (2003). Selected samples of each facies were air-dried and hardened in Araldite epoxy resin and cut. The micro-fabric of carbonates were examined in standard petrographic thin-sections (~ 30 µm thick) using a polarization microscope (Leica DMLM). Air-dried whole-rock samples (not hardened with epoxy resin) were examined with a field-emission scanning electron microscope (FE-SEM) Zeiss Ultra 55 Gemini with a Bruker XFlash 5030 detector and Quantax Esprit 1.9 software system. The EDX measurements of uncoated samples made it possible to differentiate smectite from dolomite by comparing the relative amount of silica, aluminium, calcium, magnesium and especially carbon. The mineralogical composition was investigated by powder X-ray diffraction analysis from 2 to 70°2θ (Phillips PW 1800, Cu Kα). The Rietveld program BGMNwin 1.8.6. was used for phase quantification. The clay minerals were identified additionally on air-dried, glycolated and heated (550°C) oriented mounts. Stable isotope measurements were performed with a Con-Flow DeltaPlus (Thermo Scientific) isotopic-ratio mass spectrometer linked to a Gasbench II (Museum of Natural Sciences, Berlin, and GeoBio-Center LMU, Munich, Germany). Isotope ratios are reported as δ-values in per mil (‰) relative to Vienna Pee Dee Belemnite (V-PDB) with an estimated accuracy and precision of ± 0.1‰. 103% phosphoric acid was added drop-wise to each sample with a syringe. Samples were measured after a reaction time of at least 3 h at 72°C. National Bureau of Standards NBS 18 (carbonatite) and NBS 19 (TS-limestone) and an internal laboratory standard (Solnhofen Plattenkalk: $\delta^{18}O_{V\text{-}PDB}$ of –4.84‰ and $\delta^{13}C_{V\text{-}PDB}$ of -0.47‰), were included in every batch. All three standards show standard deviations of ±0.08‰ for oxygen and ±0.07‰ for carbon. The $\delta^{18}O$ values of dolomite were corrected using a phosphoric acid fractionation factor of 1.00986 at 72°C (Rosenbaum & Sheppard, 1986).

The calcite-CO_2 and calcite-HCO_3^- carbon isotope fractionation factors of Romanek et al. (1992) were used. The carbon isotope fractionation factor of Sheppard & Schwarcz (1970) was applied to estimate the calcite-dolomite fractionation. Deines (2004) showed by theoretical computations that

the high-temperature (100–650°C) dolomite-calcite carbon calibration of Sheppard & Schwarcz (1970) can be extrapolated to low temperatures.

The dolomite-water $^{18}O/^{16}O$ fractionation factor (Eq. 1) for microbial dolomite (Vasconcelos et al., 2005) and the calcite-water fractionation factor (Eq. 2) of Kim & O'Neil (1997) were used to determine the oxygen isotopic composition of water:

$1000\ln\alpha_{dolomite\text{-}water} = 2.73*10^{6}T^{-2} + 0.26$ Eq. 1

$1000\ln\alpha_{calcite\text{-}water} = 18.03*10^{3}T^{-1} - 32.42$ Eq. 2

with T in Kelvin.

5.5 Results

5.5.1 Field relationship

Examined bentonite deposits rest on marl, silt or clayey sand of the Sand-Mergel-Decke and show a sharp footwall contact. One deposit (H) underlain by gravels is most likely in the uppermost Nördlicher Vollschotter gravel. All deposits show a sharp hanging-wall contact and are capped discordantly by younger sediments. Carbonates in bentonites are present as soft and indurated masses, stringers or networks, coalescent nodules, concretions, rhizoliths and cements (Fig. 5.2). Carbonate content increases towards the hanging-wall and root traces are well preserved, especially in partially altered tuffite (Fig. 5.5A) and all bentonites show a distinct horizonation and various states of oxidation. Two typical end-members representative of the wide spectrum of carbonate-bearing bentonites are depicted in Figures 5.2 & 5.4.

5.5.2 Deposits with pedogenic carbonate

In pedogenic-dominated bentonite deposits, dolomite is abundant in strongly mottled bentonite beds especially in the upper part of the deposit (Zweikirchen (ZW) (Fig. 5.2), also LD, ST and H (Fig. 5.1)) where rootlet-associated laminar carbonate networks and carbonate in slickensides are also most frequent. Clastic-filled or dolomite-rich rhizoliths are common in bentonite beds with dolomite nodules. They show well-preserved downward branching root-casts (Fig. 5.5A) and/or ferruginised rootlets. Shrinkage and desiccation cracks are typical features of dolomite nodules (Fig. 5.3A) and are also found in the microfabrics as circumgranular cracks and brecciation features (Fig. 5.3C). Well-preserved root fabrics (Fig. 5.3B), coalescent nodules, occasional peloids, abundant calcite spar-filled

cracks (Fig. 5.3C), aureoled grains and iron/manganese oxide stains (Fig. 5.3A) are characteristic and found in various intensities and amounts in all pedogenic dolomites.

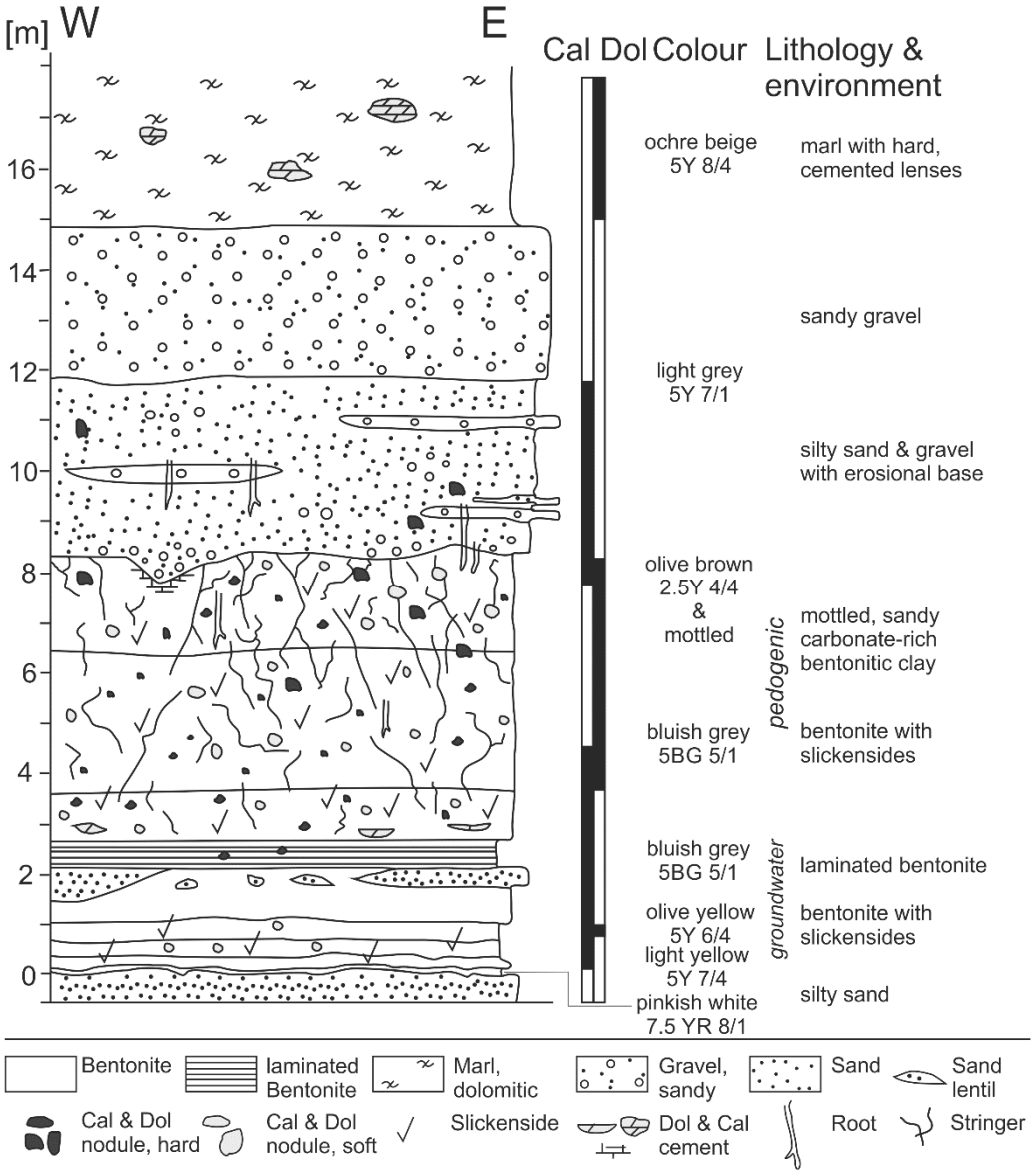

Fig. 5.2: Section of a pedogenic carbonate dominated bentonite (Zweikirchen deposit). Cal = calcite, Dol = dolomite. Reproduced with the permission of the Mineralogical Society of Great Britain & Ireland, from Köster & Gilg (2015).

Dolomite occurs mostly as subhedral and subrhombic grains of 0.5–5 µm or as round, crypto-crystalline, un-coated, non-broken peloids with a diameter of 80–100 µm as defined by Alonso-Zarza (2003). In samples from the ZW deposit, sub-micron sized elongated "rice" grains and aggregates are observed (Fig. 5.3D). They are strikingly similar to dolomite precipitated by moderately halophilic

aerobic bacteria (Sánchez-Román et al., 2011) or to sub-rounded dolomite aggregates in sub-oxic to oxic Pliocene lacustrine dolomite of the La Roda "white earths" in Spain (García del Cura et al., 2001).

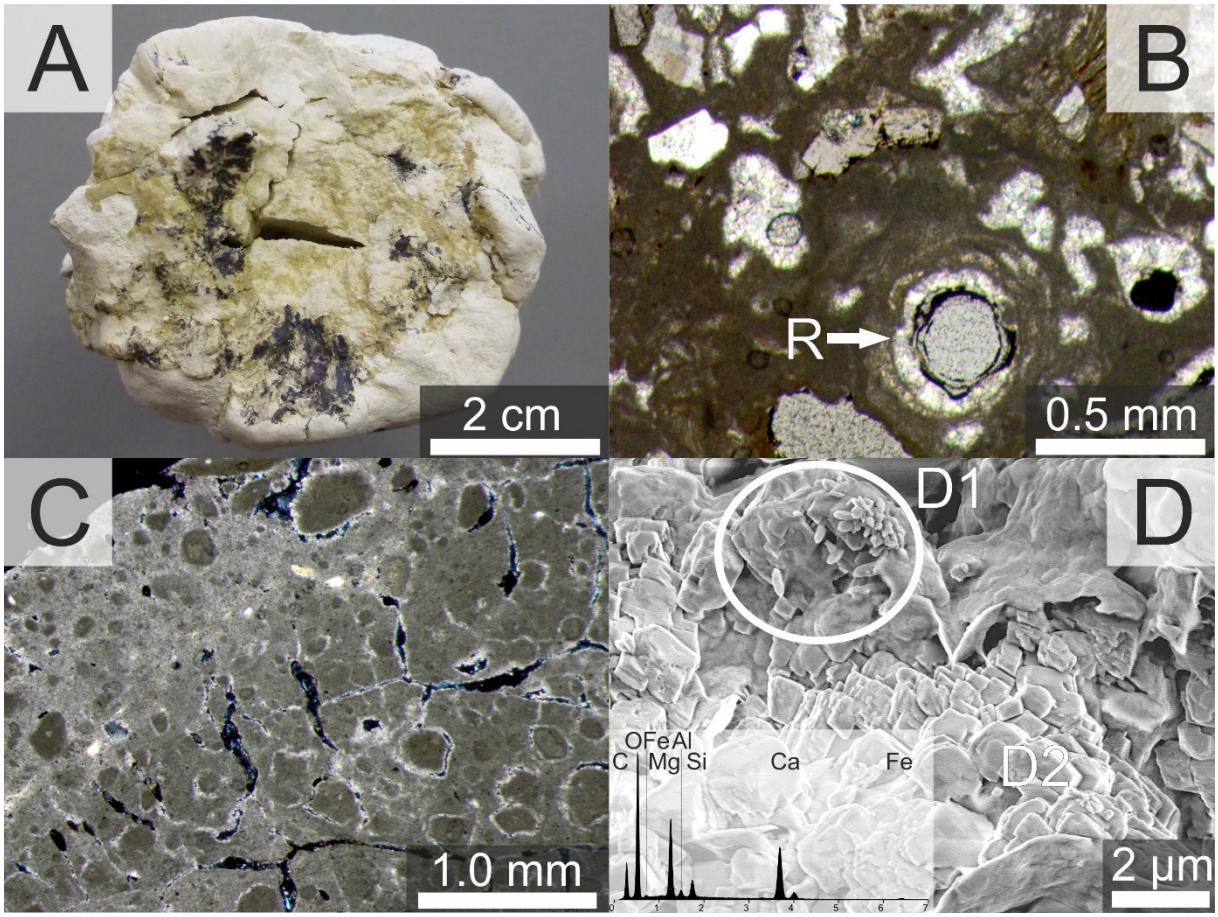

Fig. 5.3: A: Typical cracking and mottling of dolomite nodules. B: Central root (R) channel in micritic dolomite; clay-lined and calcite-spar filled porosity. C: Circumgranular cracks and brecciation fabrics with microspar at the edges. D: Dolomitized sub-micron sized bacteria-like objects (D1) and micritic dolomite (D2). Reproduced with the permission of the Mineralogical Society of Great Britain & Ireland, from Köster & Gilg (2015).

5.5.3 Deposits with palustrine carbonate

In palustrine settings, dolomite (Fig. 5.4) is located in the upper part of bentonites as irregular masses (RB, MB) or as up to 1.0 m thick nodular horizons (GB) with only incipient mottling. These nodular dolomite beds are found exclusively in palustrine settings and consist of hard and soft, slightly mottled carbonate with small rootlet-traces, clay cutans, and grey, carbonate-free clayey patches. Some bentonite deposits with palustrine carbonate (GB) are host to several meters of partially altered tuffite with abundant root casts (Fig. 5.5A). Dolomite-lined root-casts are rarely present in partially altered tuffite (MB). In these deposits (GB, MB) rust-red to yellow joint surfaces penetrate downward

into bentonite. The microfabrics are similar to pedogenic dolomite, but show more intense soil churning and pedoturbation (Fig. 5.5B) through rare shrinkage cracks, crystal-sized mottling, broken bioclasts and tiny, now clay-filled, rootlets.

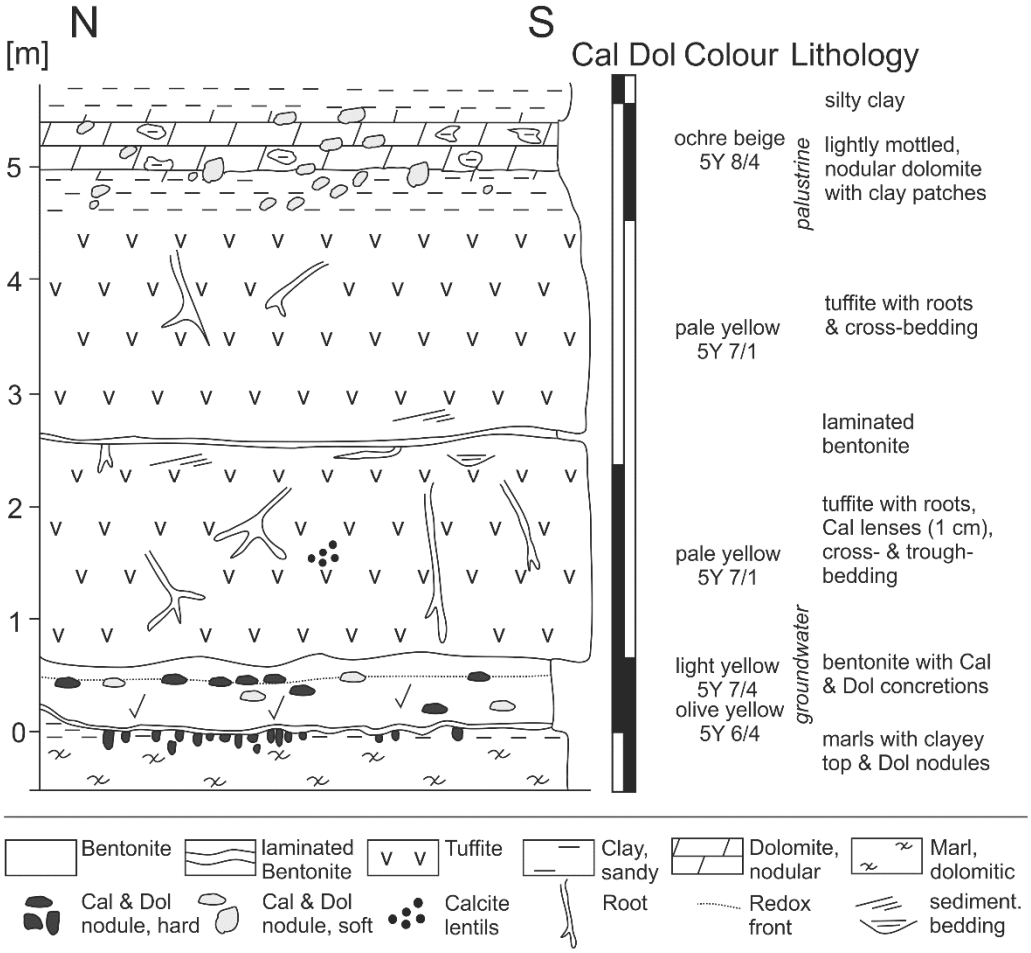

Fig. 5.4: Section of a bentonite deposit dominated by palustrine carbonates (Gabelsberg deposit). Cal = calcite, Dol = dolomite. Reproduced with the permission of the Mineralogical Society of Great Britain & Ireland, from Köster & Gilg (2015).

The micromorphology is also similar to that of the pedogenic facies. An intimate intergrowth of smectite and granular dolomite with a grain size of 50 to 500 nm (Fig. 5.5C) is commonly observed. Primary volcanogenic, detrital and biogenic particles are replaced by granular dolomite and smectite. Smectite coats detrital grains and glass shards with a dense "sod" of flakes and aggregates, probably indicating direct precipitation from solution. The partially altered tuffite contains abundant glass shards, smectite, rare silified plant remains, and small spheres of an undetermined silica phase (Fig. 5.5D), that indicate the mobilization of silica. Smectite can be found originating from within and more commonly growing on the surface of silica globules.

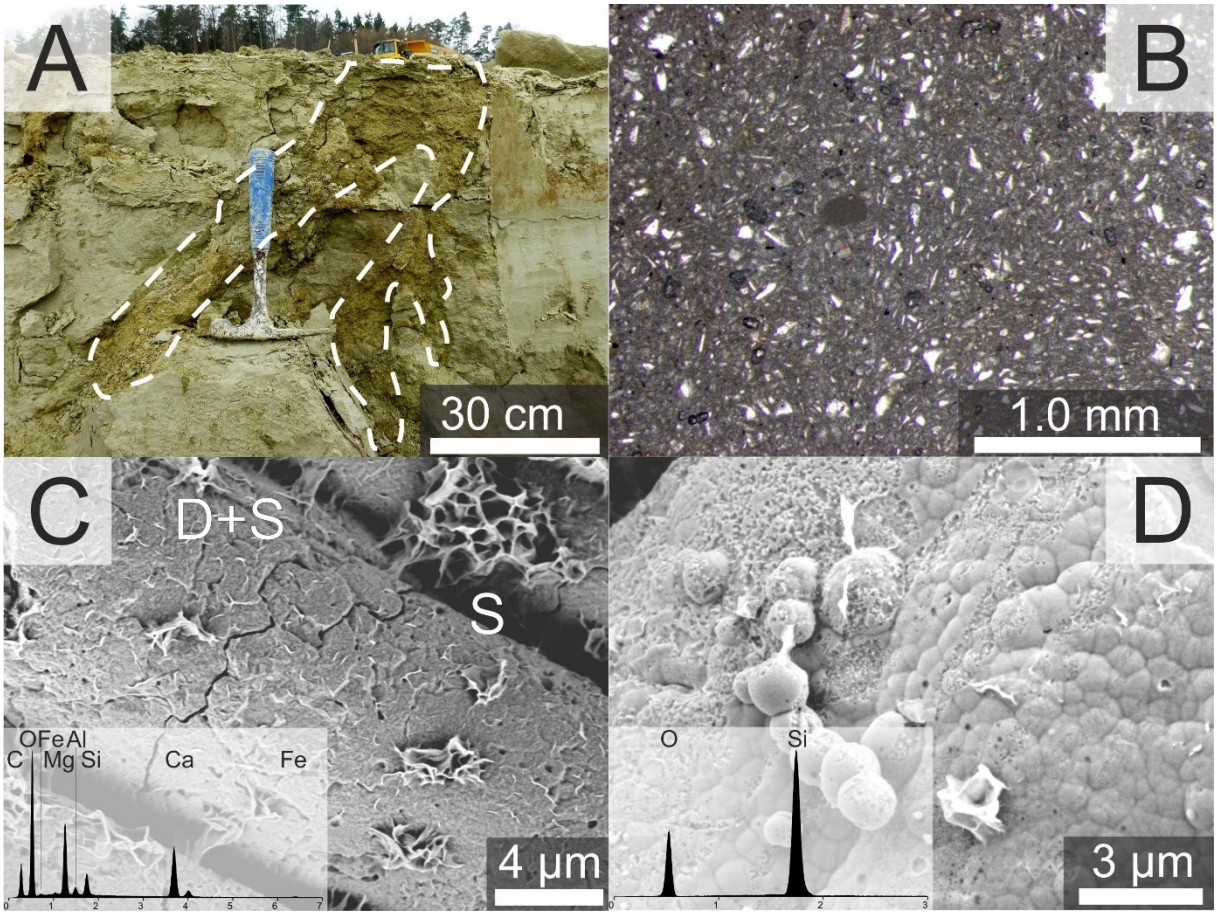

Fig. 5.5: A: Sediment-filled root in partially altered tuffite. B: Soil churning fabrics, calcite in broken bioclasts and voids of dissolved volcanic glass particles. C: Replacement of volcanic grains by granular dolomite and smectite (D+S), partially overgrown by smectite flakes (S). D: Silica globules and smectite in partially altered tuffite. Note the solution pits and smectite crystallization within and on the silica globules. Reproduced with the permission of the Mineralogical Society of Great Britain & Ireland, from Köster & Gilg (2015).

5.5.4 Groundwater dolomite in deposits with pedogenic and palustrine carbonate

Groundwater dolomite can be present in the lower parts (Fig. 5.2 & 4.4) of bentonite deposits (GB, UZ) either in the form of hard, elongated concretions up to 30 cm long with a pronounced core and white, powdery rim, and/or as fine-grained, clayey lenses with rare, aureoled quartz. Both concretions and clayey lenses are composed of cracked clotted micrite (M1) at the centre and dense microspar (M2) along cracks and rim. Cracks and different micrite generations point to a poly-phase formation history (Fig. 5.6A) and a connection of micritisation and cracking. This could either be related to later micritisation of clotted micrite (M1) and/or a second growth episode of concretions and clayey lenses (e.g. Wright & Tucker, 1991). Dolomite appears as rhombohedral crystals that displace residual grains

in Figure 5.6B. The variable grain-size of dolomite rhombs of <1–6 µm, results in a clotted micrite appearance.

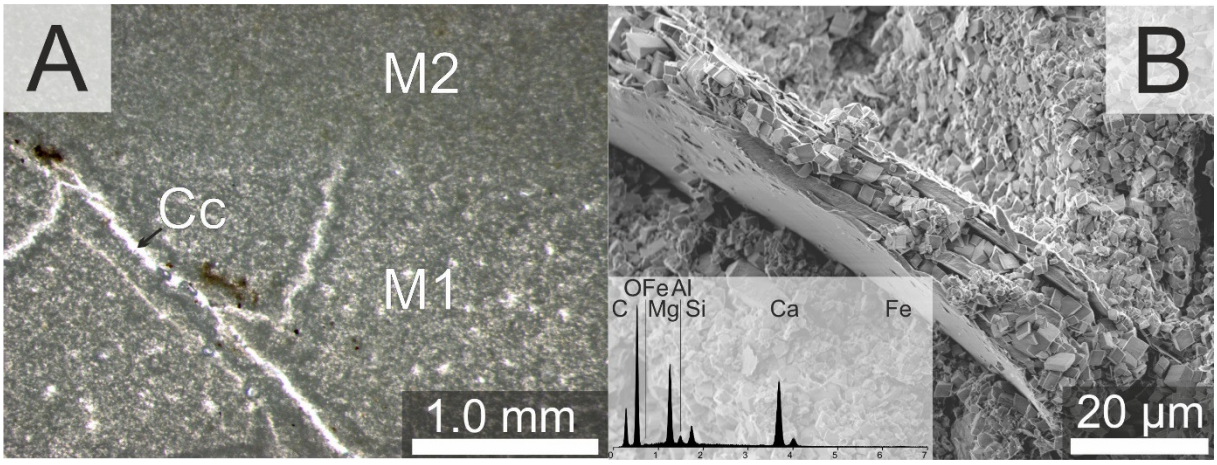

Fig. 5.6: A: Dense (M2) and clotted (M1) micrite generations. Cracks filled with calcite (Cc). B: Well-preserved dolomite rhombs replacing a large mica flake. Reproduced with the permission of the Mineralogical Society of Great Britain & Ireland, from Köster & Gilg (2015).

5.5.5 Pedogenic and groundwater calcite in bentonite deposits

Sub-ordinate calcite is present in some bentonite deposits (LD, H, ST) in varying abundance. While pedogenic calcite is morphologically identical to pedogenic dolomite, groundwater calcite shows some fabrics that are not found in pedogenic and palustrine environments and lack biogenic and desiccation features. In residual, only partially altered glass-bearing tuffite, calcite is found as small (1 cm) lentils or as granular calcite in root casts filled with smectite-rich, sandy sediment. In some bentonite deposits (H, ST), calcite is present as granular "sugary" nodules. The microfabrics of the groundwater calcites show a coarse, turbid calcite-spar, that is either the result of slow crystallization or the recrystallization of a precursor carbonate. Typical de-dolomitization fabrics such as rhomb-shaped open pores or pseudomorphs indicative of the recrystallization of a precursor dolomite are, however, lacking.

5.5.6 Mineralogical composition

X-ray diffraction analysis of the carbonates (Table 5.1, Fig. 5.7) reveals the presence mainly of dolomite and some calcite. The carbonate content was very variable, from 1–99 wt%. Carbonates (Fig. 5.7) contain the same detrital, neoformed and residual volcanic minerals as bentonite and partially

altered tuffite, i.e. smectite, illite/mica, quartz, feldspars, together with traces of kaolinite and chlorite and glass shards. A few of the dolomite nodules in the MB deposit and the partially altered tuffite in the GB deposit contained an undetermined silica phase (Fig. 5.5D). No minerals typical of terrestrial saline conditions, i.e. salts, gypsum, palygorskite or sepiolite were found, nor their dissolution fabrics (e.g. Talbot, 1990; Wright & Tucker, 1991).

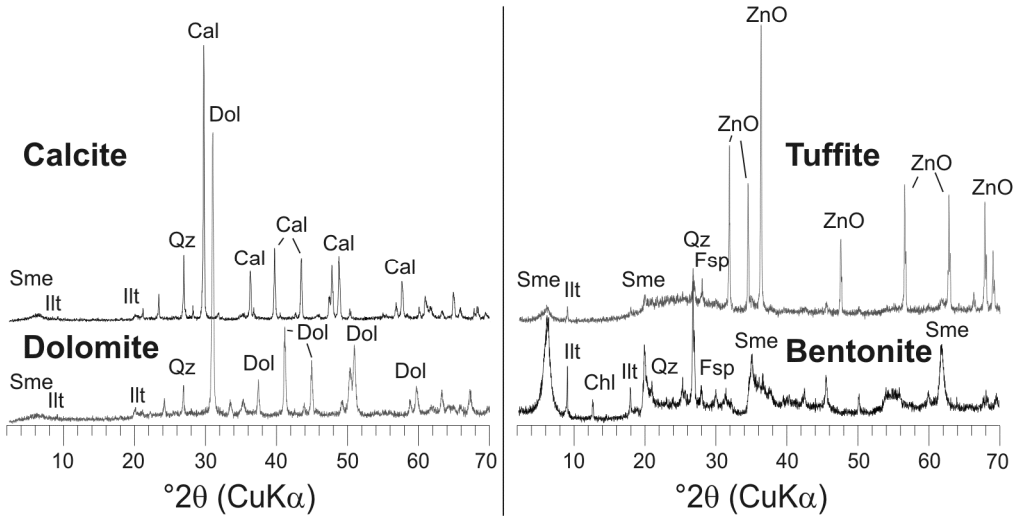

Fig. 5.7: Whole-rock X-ray diffractogram of a calcite (ZW12) and a dolomite (GB10) nodule (left), as well as a tuffite and a bentonite (right). Cal = calcite, Dol = Dolomite, Sme = Smectite, Ilt = Illite/Muscovite, Qz = Quartz, Fsp = Feldspar, Chl = Chlorite, and ZnO = zinc oxide (internal standard). Reproduced with the permission of the Mineralogical Society of Great Britain & Ireland, from Köster & Gilg (2015).

5.5.7 Stable isotopes

Eighty-two carbonate samples were analysed for their carbon and oxygen stable isotope compositions (Table 5.1). The average stable isotope composition of the carbonates is shown in Table 5.2. Stable isotope ratios of calcite- or dolomite-rich end-members (>80 wt%; n=80) were used for a reconstruction of the environment of formation. The few calcite- and dolomite-bearing samples show an intermediate isotope composition (Table 5.1). The carbon and oxygen isotope ratios reveal distinct groups for pedogenic, palustrine and groundwater carbonate as illustrated in Figure 5.8. The small amounts of dolomite and calcite derived from partially altered tuffite are isotopically identical to the carbonate from the bentonite. The carbonaceous wood recovered from the hanging-wall gravels of the Peterswahl deposit had a $\delta^{13}C$ value of –25.2±0.17‰.

Table 5.1: Mineral and stable isotope composition of dolomites and calcites. PED = pedogenic, PAL = palustrine, GW = ground water, XXX abundant, T = traces.

Name	Lithology	Type	$\delta^{18}O$	$\delta^{13}C$	Cal	Dol	Qz	Sme	Ilt/Ms	Kln	Chl	Fsp	Opl-CT	Amorph.
ZWEIKIRCHEN														
ZW031	Bentonitic	PED	-6.5	-8.1	48	5	41	3	3	-				
ZW029	clay	PED	-4.5	-6.6	4	71	11	11	2	-				
ZW027		PED	-6.2	-8.5	33	7	35	15	9	1	T	T		
ZW002		PED	-5.1	-6.8	2	65	15	14	3	1				
ZW026		PED	-5.3	-6.5	0	95	3	1	1	1				
ZW025		PED	-5.4	-6.6	0	99	1	0	0	-				
ZW024		PED	-6.7	-9.0	78	8	6	6	2	-				
ZW023		PED	-5.0	-6.8	0	77	11	8	3	-		T		
ZW034	Bentonite	PED	-6.3	-6.2	4	45	21	24	6	-				
ZW006		PED	-4.9	-6.4	0	47	20	22	8	2				
ZW003		PED	-5.8	-6.6	0	50	28	13	7	1				
ZW005		PED	-5.1	-6.9	0	67	15	9	5	2				
ZW004		PED	-8.3	-10.7	75	1	10	9	4	1				
ZW022		PED	-5.1	-6.6	0	66	16	13	4	-				
ZW021		PED	-6.6	-8.8	60	5	13	15	7	1				
ZW020		PED	-5.1	-6.8	0	86	8	4	3	-				
ZW032		PED	-6.7	-8.9	64	6	8	16	7	-				
ZW018		GW	-6.4	-9.2	60	6	8	20	6	-				
ZW017		GW	-7.2	-9.4	70	0	5	19	6	-				
ZW016		PED	-7.1	-8.8	69	0	5	18	6	2				
ZW015		PED	-6.2	-9.2	75	2	9	8	5	-				
ZW033		PED	-7.4	-9.0	70	0	8	16	6	-				
ZW014		PED	-6.8	-9.2	24	2	6	62	6	-				
ZW013		PED	-3.4	-6.6	0	47	4	31	15	3		T		
ZW012		GW	-8.3	-11.5	80	0	2	15	2	1				
ZW011		GW	-9.1	-11.9	65	0	11	18	6	1	T			
ZW010		GW	-8.1	-11.3	73	0	3	19	3	2				
REHBACH														
RB03	Bentonite	PAL	-4.2	-7.5	3	36	5	50	7	-		T		
RB01		PAL	-4.6	-7.5	3	28	10	49	10	1		T		
RB04		PAL	-4.1	-7.1	0	68	3	24	4	-		T		
RB02		PAL			2	66	4	22	5	2		T		
LANDERSDORF														
LD06	Bentonite	GW	-7.6	-11.8	58	3	4	36	-	-				
LD05		PED	-7.9	-9.5	49	2	4	38	5	2				
LD04		PED	-7.3	-9.6	18	2	8	64	4	4				
LD03		PED	-7.4	-9.7	70	0	4	23	4	0				
LD02		GW	-7.1	-10.9	87	0	2	9	2	0				
LD01		PED	-7.0	-8.3	73	0	7	16	3	1				
GABELSBERG														
GB16	Dolomite	PAL	-3.5	-7.1	0	56	2	37	4	-				
GB34	bed	PAL			4	58	6	27	5	-				
GB32		PAL	-3.9	-7.2	5	53	7	30	6	-				
GB10		PAL	-3.8	-7.1	2	70	4	19	5	-				
GB31		PAL	-6.1	-7.2	4	56	6	28	6	-				
GB09		PAL	-3.8	-7.2	0	56	5	24	15	-				
GB33		PAL	-4.1	-6.9	7	55	5	27	6	-				

Table 5.1: Continued.

Name	Lithology	Type	$\delta^{18}O$	$\delta^{13}C$	Cal	Dol	Qz	Sme	Ilt/Ms	Kln	Chl	Fsp	Opl-CT	Amorph.
GABELSBERG														
GB30		PAL	-5.6	-6.9	7	44	8	33	8	-				
GB08		PAL	-3.5	-7.2	2	63	4	25	6	-				
GB22	Tuffite				3	0	18	68	11	-				
GB21					0	0	10	89	0	-		T		
GB14		GW	-8.1	-10.6	8	0	5	83	3	-				
GB07					0	0	14	79	6	-				
GB06I		GW	-6.7	-11.7	XXX									
GB06II		GW	-6.7	-11.6	XXX									
GB06III		GW	-7.0	-11.7	XXX									
GB06		GW	-6.7	-11.4	45	0	7	37	10	-				
GB15	Bentonite	GW			3	3	6	79	9	-				
GB18		GW	-4.4	-7.1	2	43	3	49	4	-				
GB13		GW	-6.4	-10.8	58	11	4	24	3	-				
GB17		GW	-6.5	-10.8	84	6	1	8	1	-				
GB28		GW	-6.8	-11.0	86	2	1	10	2	-				
GB27		GW	-5.4	-7.4	32	35	4	27	2	-				
GB05		GW	-5.1	-6.4	0	33	4	57	5	-				
GB04		GW	-7.1	-10.9	34	19	4	40	4	-				
GB03		GW	-4.7	-7.1	0	68	2	26	4	-				
UNTERZELL														
UZ03	Bentonite	GW	-7.2	-10.4	85	2	3	8	2	T				
UZ04		GW			3	67	8	15	7	0				
UZ05		GW	-6.8	-9.0	86	0.4	3	7	2	2				
UZ01		GW	-4.8	-6.3	3	70	11	10	6	0				
HADER														
H05	Bentonite	GW			98	0	1		1					
H08		GW	-7.9	-11.1	97	0	1		1					0
H03		PED	-4.9	-7.7	0	48	3	33	7					8
H02		PED	-4.8	-7.3	0	37	3	38	12					9
H01		PED	-4.7	-7.5		58	2	28	4	T				8
H09		PED	-5.2	-6.5	0	37	8	22	20	T				13
H11		GW			XX	0								
H17		GW			XX	0								
H16		GW	-7.7	-11.7	97	0	T	T	T					
H13		GW			XX	0								
H12		PED	-5.5	-6.9	0	54	7	17	12					10
H10		PED	-5.1	-6.1	0	20	8	35	16					21
H15		PED	-5.0	-7.2	0	50	5	19	13					13
H14		PED	-5.0	-7.3	0	73	4	11	5					7
MITTERSBERG														
M29	Tuffite	PAL	-3.6	-7.3	0	65	T	17	3					14
M28	&	PAL	-3.4	-7.4	0	74	T	13	4	T				8
M27	Bentonite	PAL	-4.1	-7.4	0	75	T	13	3					8
M26		PAL			X	XX		XX						
M25		PAL	-4.8	-7.4	0	38	4	39	8	T	3	8		
M19		PAL	-5.0	-6.9	T	29	3	41	13		1			13
M18		PAL	-4.9	-7.4	0	66	3	21	6	1	2	1		
M13		PAL			0	1	3	64	14	1	3	9		4

Table 5.1: Continued.

Name	Lithology	Type	$\delta^{18}O$	$\delta^{13}C$	Cal	Dol	Qz	Sme	Ilt/Ms	Kln	Chl	Fsp	Opl-CT	Amorph.
M17		PAL	-4.2	-7.5	0	55	2	27	4	T				11
M14		PAL	-3.6	-7.3	0	60	2	25	4					9
M12	Tuffite	PAL	-3.8	-7.6	0	67	2	17	4	T				9
M10		PAL	-5.8	-8.0	5	10	3	57	16	1				8
M09		PAL	-4.3	-7.4	0	53	2	10	3					32
M11	Bentonite	PAL	-4.1	-7.0	0	35	18	17	9	1	3	3	6	8
M24	earlier Marl		-4.0	-7.6	0	58	6	13	5				8	10
M23			-3.9	-7.1	0	61	3	5	3				9	19
M08			-4.0	-7.0	0	56	10	14	7		5	6	2	
M07			-4.2	-6.9	0	59	10	10	7		6	6	2	

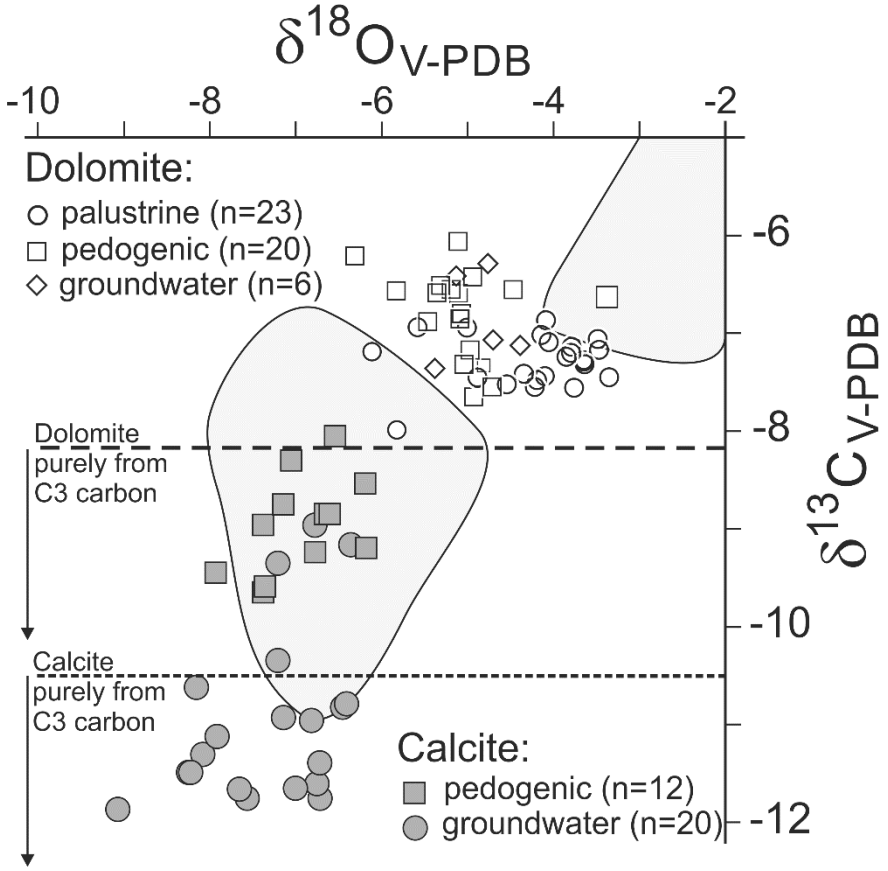

Fig. 5.8: Bivariate plot of oxygen and carbon stable isotope compositions of dolomite and calcite samples documented in Table 5.1. Dolomite and calcite limits, cf. *Carbon stable isotopes below*. Reproduced with the permission of the Mineralogical Society of Great Britain & Ireland, from Köster & Gilg (2015).

Table 5.2: The stable isotope composition of dolomites and calcites.

	$\delta^{13}C_{V\text{-}PDB}$			$\delta^{18}O_{V\text{-}PDB}$		
	mean	min.	max.	mean	min.	max.
Pedogenic dolomite	-6.8 ± 0.4	-7.7	-6.1	-5.1 ± 0.5	-6.3	-3.4
Palustrine dolomite	-7.3 ± 0.3	-8.0	-6.1	-4.3 ± 0.7	-6.1	-3.4
Groundwater dolomite	-6.9 ± 0.4	-7.4	-6.3	-4.9 ± 0.3	-5.4	-4.4
Pedogenic calcite	-9.0 ± 0.5	-9.7	-8.1	-6.9 ± 0.5	-7.9	-6.2
Groundwater calcite	-10.9 ± 0.9	-11.9	-9.0	-7.3 ± 0.7	-9.1	-6.4

5.6 Discussion

Pedogenic dolomite is very rare in the geological record and has been described in the basalt-derived Holocene soils of Hawaii, USA (Capo et al., 2000), the Permian fluviatile-lacustrine clastic sediments in the Ural mountains, Russia (Kearsey et al., 2012), and the Pleistocene petrocalcic soils in Spain (Diaz-Hernandez et al., 2013). Calcite and the small amounts of dolomite in the Cabo de Gata bentonites, Spain, have been described as pedogenic in origin (Delgado, 1993), while the calcite from Milos, Greece is not derived from pedogenic processes (Decher et al., 1996). Dolomite in bentonite has not been examined systematically, but may yield new insights into the conditions and timing of bentonitization.

5.6.1 Carbonate formation and diagenetic setting

Terrestrial carbonates form in fresh to saline waters (Alonso-Zarza, 2003) in association with pedogenesis, activity of microorganisms and the root systems of plants (Wright & Tucker, 1991; Cerling & Quade, 1993) and their fabrics link them to processes closely related to the water table (Alonso-Zarza & Wright, 2010; Armenteros, 2010). Carbonates preserve indicators of palaeosol development, i.e. horizonation, root casts, mottling or gleying (Nettleton et al., 2000) present in practically all of the Bavarian bentonite deposits examined (Figs. 4.2 and 4.4). Pedogenic (soil) and palustrine (lake wetlands) settings are home to deep rooting (Fig. 5.5A) vegetation (Alonso-Zarza, 2003). The preserved root fabrics (Fig. 5.3B), however, indicate that the soils were not permanently water-logged because most roots need oxygen to respire. The absence of permanently water-logged conditions and subsequent oxidation enhances ferruginisation and mottling that are very common in upper bentonite horizons (Fig. 5.2) indicating the redistribution of iron during wet and dry cycles (Retallack, 1988). Nodulisation and pedoturbation (Fig. 5.3B & 4.5C) fabrics due to the formation of curved and planar joint surfaces also point to repeated wetting and drying cycles (Freytet & Verrecchia, 2002). In contrast,

grey clay patches underneath weakly mottled nodular dolomite (Fig. 5.4) indicate gleying and poor drainage (e.g. Freytet & Verrecchia, 2002).

Below the water table, groundwater carbonates form concretions with a diffuse boundary in the more protected phreatic zone (Wright & Tucker, 1991; Alonso-Zarza, 2003). In bentonites, earthy calcite-rich lenses (Fig. 5.2) and concretions (Fig. 5.4) may be present in footwall regions of bentonites, similar to valley calcrete (e.g. Wright & Tucker, 1991). Lenses and concretions are sometimes orientated horizontally along redox fronts between light and dark yellow oxidized bentonite (Fig. 5.4), probably reflecting the position of the water table.

Carbonate microfabrics are classified according to alpha- and beta-fabric end-members (Wright & Tucker, 1991). Alpha-fabrics lack biogenic forms and show a micritic to microsparitic groundmass, displacive growth, floating grains, or crystal-sized mottling. Beta-fabrics are dominated by biogenic features and signs of exposure or desiccation. Typical beta-fabrics are alveolar septal fabrics, circumgranular cracks, roots, coated grains, brecciation and clay cutans (Wright & Tucker, 1991). Intermediate forms of alpha- and beta-fabrics are common (Freytet & Verrecchia, 2002).

The palustrine and pedogenic carbonates in Bavarian bentonites reveal typical beta-fabrics. Palustrine carbonates show pedoturbation and broken bioclasts (Fig. 5.5B) typical for soil churning in wetlands (Freytet & Verrecchia, 2002), but they also show pedogenic fabrics, i.e. coalescent nodules, circumgranular cracks and shrinkage cracks (Fig. 5.3C), indicating soil rotation and desiccation in the vadose zone (Freytet & Verrecchia, 2002; Wright & Tucker, 1991). Alveolar septal fabrics of mineralized root walls (Klappa, 1980) were found in reworked bentonite (Fig. 5.2) and partially altered tuffite with partially spar-filled root voids (Fig. 5.3B) indicating vadose conditions. The intimate growth fabric of granular dolomite and flaky smectite in partially altered tuffite (Fig. 5.5C) point to simultaneous or timely post-formational precipitation of carbonate and clay minerals. Elongated "rice" grains and aggregates that resemble fossil microbial remains are present in pedogenic dolomite (Fig. 5.3D). The size and shape of these grains are similar to either dolomite precipitated by moderately halophilic aerobic bacteria in culture experiments (Sánchez-Román et al., 2011) or to subrounded dolomite aggregates of spherical and oblong-shaped bodies in suboxic to oxic Pliocene lacustrine dolomite of the La Roda "white earths" from Spain (García del Cura et al., 2001). They are quite distinct from the dumbbell-shaped microbial dolomites precipitated in anoxic sulphate-reducing environments (Warthmann et al., 2000; van Lith et al., 2003) or the irregular masses and rods formed by methanogens (Roberts et al., 2004; Kenward et al., 2009). Although there is substantial debate on the nature of these objects, most authors agree on a microbial origin (e.g. Kirkland et al., 1999; Southam & Donald, 1999; Schieber & Arnott, 2003; Pacton et al., 2010; Sánchez-Román et al., 2011).

The groundwater carbonates show typical abiogenic alpha-fabrics. The micrite groundmass records a multi-phase formation and micritisation history (Fig. 5.6A). The lack of porosity indicates a phreatic origin, while euhedral dolomites in clotted micrite and microspar (Fig. 5.6B) show steady formation processes (e.g. Wright & Tucker, 1991).

The macro- and microfabrics provide strong evidence for a syn- to very timely post-depositional formation of carbonates. Smectitization must have commenced shortly before or during carbonatisation in order to explain the microfabrics discovered and their intimate intergrowth. The excellent primary fabric preservation rules out a later diagenetic overprint.

5.6.2 Carbon stable isotopes

The precipitation of soil carbonate is influenced by degassing, dewatering, evaporation, temperature and biological activity (e.g. Cerling, 1984; Wright & Tucker, 1991), but may show a seasonal bias caused by dry or warm periods (Cerling & Quade, 1993; Breecker et al., 2009; Passey et al., 2010). A fluctuating water table will therefore regulate both the decomposition of organic matter and mixing with atmospheric carbon dioxide. During non-water-logged conditions atmospheric exchange is increased, leading to greater $\delta^{13}C$ values close to the palaeo-surface and increased evaporation. While the addition of Ca^{2+}, e.g. from inflowing water, enhances calcite formation, an increase of dissolved carbonate and/or evaporation will favour dolomite precipitation by either raising the CO_3^{2-}/Ca^{2+} and Mg/Ca ratios or the Mg and Ca concentrations (Machel & Mountjoy, 1986). In contrast, water-logged water bodies are less affected by atmospheric exchange and often mirror either the carbon isotope composition of soil organic matter or the external input of dissolved carbonate (Talbot, 1990).

During the Mid-Miocene, C3-plants were the only significant organic carbon source in the UFM with an average $\delta^{13}C$ value of –25.5‰ (Tütken & Vennemann, 2009), similar to our result of -25.2±0.17‰. Based on the mean annual air temperature (MAT), estimated as 15–21°C for the Mid-Miocene (Böhme, 2003; Böhme et al., 2007), calcites should be roughly 15‰ heavier than organic carbon (Cerling & Quade, 1993), suggesting an uppermost limit of calcite $\delta^{13}C$ values formed purely from C3-plant carbon of –10.6‰ (15°C) to –11.3‰ (21°C) (Fig. 5.8). Dolomite formed from C3-plant carbon (Fig. 5.8) only, should therefore have a $\delta^{13}C$ value of –8.2‰ (15°C) to –8.9‰ (21°C).

Dissolved inorganic carbon (DIC) introduced by ground water is another important source of carbonate. For disseminated calcite with $\delta^{13}C$ values of +1.1 to +3.5‰ from Milos, Greece, Decher et al. (1996) suggested that dissolved inorganic carbon was sourced from overlying marine limestone.

Delgado (1993) showed that dolomite in Cabo de Gata bentonite has $\delta^{13}C$ values of –5.8 to +1.8‰, indicating both marine and non-marine sources. In the Molasse basin Mesozoic marine lime and dolostone clasts have $\delta^{13}C$ values between –6.0‰ to +1.5‰, while UFM ground waters show DIC $\delta^{13}C$ values of –15 to –9‰ (Egger et al., 1983). The carbon isotope values of carbonates in bentonites (Fig. 5.9A & B), however, do not match values expected from such soil CO_2 or DIC values alone (e.g. Romanek et al., 1992). The $\delta^{13}C$ values of dolomite and calcite are, therefore, inconsistent with a single carbon source.

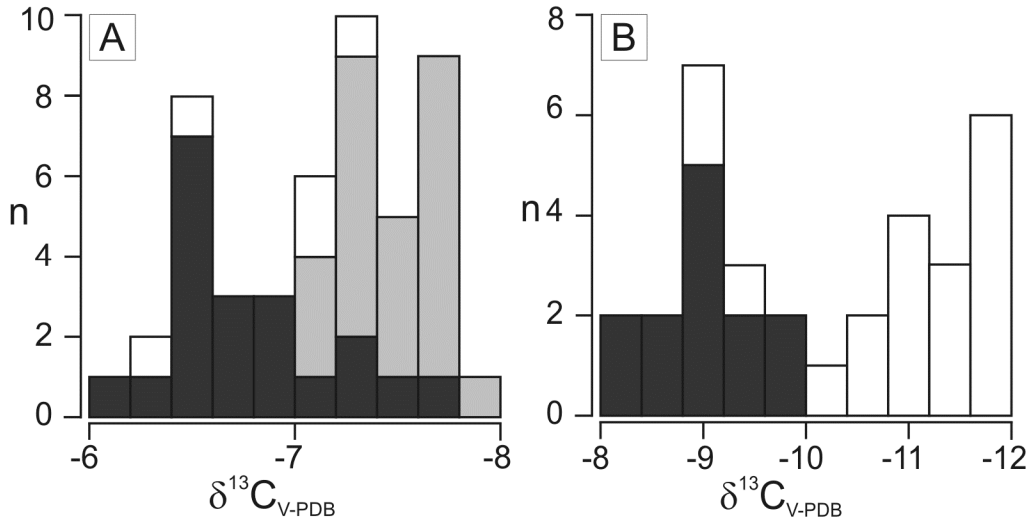

Fig. 5.9: A: Carbon stable isotope histogram of dolomites; pedogenic (black), palustrine (grey), and groundwater carbonates (white). B: Carbon stable isotope histogram of calcites; pedogenic (black) and groundwater carbonates (white). Data from Table 5.1. Reproduced with the permission of the Mineralogical Society of Great Britain & Ireland, from Köster & Gilg (2015).

Considering a soil diffusional enrichment of 4.4‰, a pre-industrial atmospheric $\delta^{13}C$ value of –6.5‰ for the Mid-Miocene (Cerling, 1984, 1991), calcite-CO_2 and calcite-HCO_3^- fractionations of about 10.4‰ and 1‰ (Romanek et al., 1992), a simple mixing model of soil CO_2 with DIC or atmospheric CO_2 could account for the measured $\delta^{13}C$ values. This suggests that $\delta^{13}C$ values are probably the result of a soil CO_2-dominated three component system. In light of field relationships, mottling, shrinkage cracks and carbonate fabrics, a contribution of atmospheric carbon especially in pedogenic facies seems legitimate (e.g. Alonso-Zarza, 2003; García del Cura et al., 2001).

The carbon stable isotope results (Fig. 5.9A & B) are good indicators for fluctuating water levels with repeated changes between reducing wet (water-logging during high stands) and oxygenated dry conditions. These conditions induced carbonate precipitation in warm/dry periods and supported smectite formation in wet periods. Incipient bentonites were settled by C3 vegetation that was the

major source of carbon while minor amounts of carbon were derived from the atmosphere and carbonate-rich UFM groundwater.

5.6.3 Oxygen stable isotopes

Co-precipitated dolomite and calcite that has formed in oxygen isotope equilibrium should display a 3.1–4.4‰ fractionation at temperatures between 15–30°C, which encompasses the estimates for MAT (15.7–20.8°C) and the warm month temperatures (WMTs) of 20.2–28.1°C (Böhme et al., 2007) and should be consistent with the hydrogen and oxygen isotope data for the bentonite smectites (Gilg, 2005; Gilg & Rocholl, 2009; Bauer, 2014). We observed, however, an average oxygen isotope fraction between dolomite and calcite of 1.8‰ for pedogenic carbonates and 2.4‰ for groundwater carbonates (Table 5.2).

The $\delta^{18}O$ frequency distribution of carbonates (Fig. 5.10A & 5.10B) also illustrates a large scatter, indicating variable water compositions, temperatures or water sources. Co-precipitation in equilibrium would also have resulted in a more mixed carbonate composition, however, mixed dolomite-calcite samples are rare. We conclude that the dolomite and calcite must have formed either at different temperatures or in waters of differing isotopic compositions.

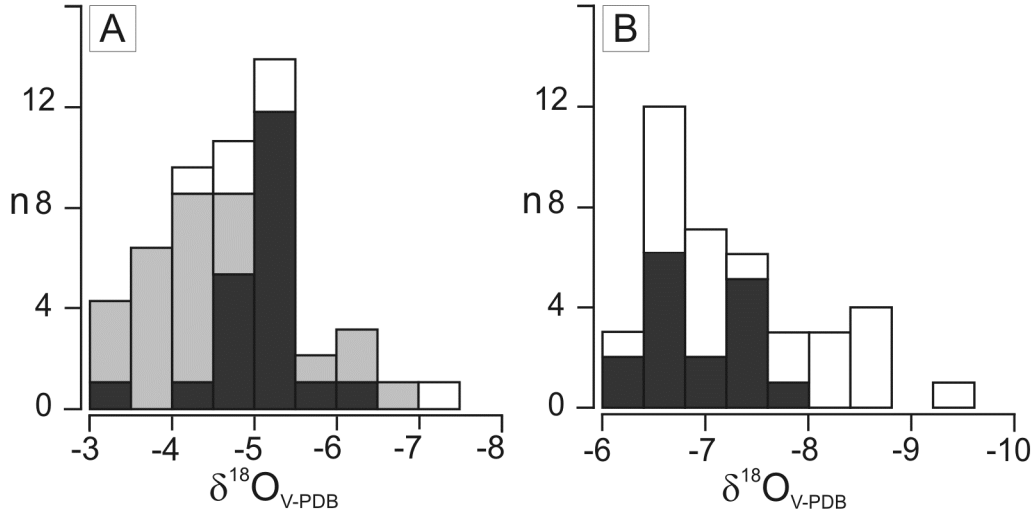

Fig. 5.10: A: Oxygen stable isotope histogram of dolomites; pedogenic (black), palustrine (grey), and groundwater (white). 9B: Oxygen stable isotope histogram of calcites; pedogenic (black), and groundwater (white). Data from Table 5.1. Reproduced with the permission of the Mineralogical Society of Great Britain & Ireland, from Köster & Gilg (2015).

Tütken et al. (2006), Tütken & Vennemann (2009) and Héran et al. (2010) suggest $\delta^{18}O_{V\text{-}SMOW}$ values in the upper soil column and in Mid-Miocene surface waters influenced by surface heating or

evaporation of –5.9±1.7‰ or –5.6±0.7‰ based on mammal and turtle teeth phosphate. Gilg (2000) derived a $\delta^{18}O_{V\text{-}SMOW}$ value of approximately –7‰ for meteoric groundwater from Mid-Miocene kaolinite in Southern Germany. These results show distinct isotopic differences between the paleo-surface and more protected groundwater settings. The latter settings were found in bentonites meeting the conditions described by Hillel (1982), i.e. reduced surface heating and evaporation at depths greater than 200 cm, which best reflect the MATs.

If groundwater calcite did precipitate at MAT and the conditions described above, it would have formed in water (Fig. 5.11) with a mean $\delta^{18}O_{V\text{-}SMOW}$ value of –7.0±0.7‰ (15°C) to –5.7±0.7‰ (21°C; n=20). As indicated by the similar range of $\delta^{18}O$ values (Fig. 5.10B), pedogenic calcite (n=12) formed at similar conditions (Fig. 5.11) with a mean $\delta^{18}O_{V\text{-}SMOW}$ of water from –6.7±0.5‰ (15°C) to –5.4±0.5‰ (21°C), perhaps recording annual calcite formation being less affected by evaporation.

Untypical for extremely evaporative conditions, the ^{18}O values of dolomites are rather low (Fig. 5.8, Fig. 5.10A); lower than palustrine and pedogenic, microbially mediated dolomites formed at aerobic, moderately evaporative conditions in the La Roda white-earths that have dolomite $\delta^{18}O_{V\text{-}PDB}$ values of –3.07‰ to +5.40‰ (García del Cura et al., 2001). Traces of pedogenic dolomite present in Los Trancos bentonite also shows high $\delta^{18}O_{V\text{-}PDB}$ values of between +0.5‰ and +3.3‰ (Delgado, 1993). Both occurrences indicate either more evaporative conditions and the involvement of non-marine water or a hydrothermal component (García del Cura et al., 2001; Delgado, 1993). In contrast calcite $\delta^{18}O_{V\text{-}PDB}$ values of –14.7‰ to –10.6‰ from Milos, Greece, were interpreted to have formed in hydrothermally heated mixed groundwater (Decher et al., 1996).

However, the carbon isotope values in Bavarian deposits show the dominance of soil CO_2 derived from the decomposition of organic matter, suggesting somewhat limited evaporation and degassing in comparison to conditions at La Roda and Los Trancos and the absence of marine waters. Cerling & Quade (1993) also argued that evaporation has little effect on $^{18}O/^{16}O$ ratios of soil water except for extreme environments, e.g. deserts or long surface exposure. Cerling & Quade (1993), Breecker et al. (2009) and Passey et al. (2010) used clumped isotopes to extend this notion and Quade et al. (2013) described a 10–15°C summer bias of carbonate based MATs compared to WMTs, for shallow depths (200 cm). As a consequence the isotopic composition of water in upper soil layers is controlled by temperatures 10–15°C above MAT resulting in conservatively estimated temperatures of 25–31°C. These temperatures reflect ground temperatures slightly above the WMT (20.2–28.1°C; Böhme et al., 2007). Applying these temperatures (Fig. 5.11) in Eq. 1 (Vasconcelos et al., 2005), pedogenic dolomite (n=20) would have precipitated in waters with a similar average isotopic composition as calcites of –6.8±0.6‰ (25°C) to –5.6±0.6‰ (31°C), while palustrine dolomites (n=23) experience stronger

evaporation (e.g. Alonso-Zarza, 2003) and therefore formed in slightly enriched waters of –6.0±0.8‰ to –4.8±0.8‰. The few groundwater (n=5) dolomites would have formed in waters of –6.4±0.3‰ to –5.2±0.3‰, questioning their true groundwater nature and suggesting mixing with downward percolating waters.

The oxygen isotope values of calcite and dolomite are similar to those found by Tütken et al. (2006), Tütken & Vennemann (2009) and Héran et al. (2010) and confirm that carbonates in bentonite formed in meteoric ground and surface waters. The good agreement of calcite with MATs and meteoric water might suggests calcite precipitation throughout the year. In contrast, pedogenic and palustrine dolomite formation were probably intense in hot/dry periods when temperature and evaporation were greatest.

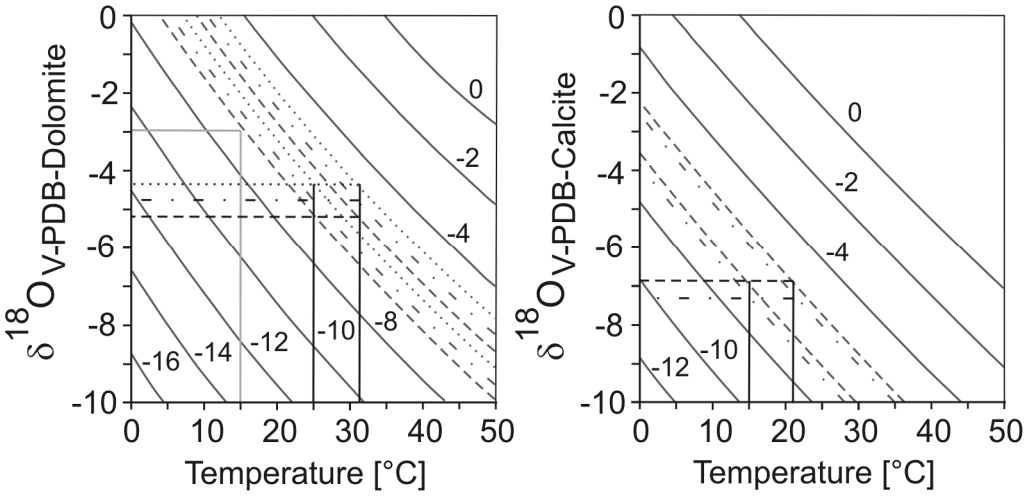

Fig. 5.11: Diagrams of oxygen isotope fractionation for dolomite-water (left) and calcite-water (right). Curves represent water $\delta^{18}O_{V\text{-}SMOW}$ values. Dotted, dotted-dashed and dashed lines represent oxygen isotope data of palustrine, ground, and pedogenic waters. Black solid lines: upper and lower temperature limits (cf. *Oxygen stable isotopes*). Reproduced with the permission of the Mineralogical Society of Great Britain & Ireland, from Köster & Gilg (2015).

5.7 Carbonate formation and its relationship to bentonitisation

Dolomitization and smectitization of Mg-poor rhyolitic ash required the introduction of Mg^{2+} and Ca^{2+} ions (e.g. Folk & Land, 1975; Christidis, 2008). Hydrothermal, strongly evaporated or saline fluids did not exist in the UFM (Vogt, 1980; Ulbig, 1999; Unger, 1999; Schmid, 2002; Aziz et al., 2008). These new stable isotope results confirm that dolomite and calcite in bentonites formed from meteoric waters. The present-day meteoric ground waters in the UFM are of Ca–Mg–HCO_3 type (Egger et al.,

1983, Table 5.3) and similar to Ca–(Mg–)–HCO_3 waters involved in the formation of the Northern Cabo de Gata bentonites, such as Los Trancos (Caballero et al., 2005).

The groundwater in the UFM shows variable Mg^{2+} (0.05 mMol/L to 1.98 mMol/L) and Ca^{2+} (0.05 to 3.35 mMol/L) concentrations and also variable molar Mg/Ca ratios (0.53 to 1.57; Table 5.3) that are consistent with the stability of calcite and in part dolomite (Folk & Land, 1975; Machel & Mountjoy, 1986). The average molar Mg/Ca ratio of the UFM ground waters (~0.86) is in equilibrium with the molar interlayer Mg/Ca ratio in smectites of the Bavarian bentonites (0.51; Grim & Güven, 1978) considering the preferential uptake of Ca relative to Mg in the interlayer of smectites (e.g., Laudelout et al., 1968; Sayles & Mangelsdorf, 1979).

Table 5.3: Composition of ground waters in the Upper Freshwater Molasse (based on Egger et al., 1983).

Water type	Ca-Mg-HCO_3
Mg/Ca ratio (molar)	0.53 to 1.37
pH	7.26 to 9.10
Carbonate alkalinity (CO_3^{2-} or HCO_3^- /Ca^{2+})	>> 2.5
Sulfate (mmol/L)	0 to 0.8
Total Dissolved Solids (mg/L)	280 ± 51

Additionally, the weathering of limestone and dolostone in Molasse sediments (Egger et al., 1983) and the decomposition of soil organic matter (e.g. Talbot, 1990), enhanced carbonate formation by raising the pH and carbonate alkalinity (CO_3^{2-}/Ca^{2+} ratio). Machel & Mountjoy (1986) contended that the increased carbonate alkalinity is equally as important for dolomitization as a high Mg/Ca ratio because it shifts the reaction kinetics towards dolomite. Although sulphate reduction might have enhanced dolomite formation, sulphate is not per se a kinetic inhibitor to dolomite precipitation. The low sulphate concentrations do, however, provide conditions suitable for dolomite precipitation (e.g. Last, 1990; Sánchez-Román et al., 2011). During the Mid-Miocene, Ca–Mg–HCO3– water in the Molasse basin probably was a large reservoir of Mg^{2+} and Ca^{2+} derived from dissolution of limestone and dolostone clasts, cation-exchange with clay minerals (Egger et al., 1983) and possibly silicate weathering. The presence of dolomite in bentonites, therefore, indicates that waters with high carbonate alkalinity and Mg/Ca ratios around 1 percolated through incipient soils and volcanic ash.

5.8 Conclusions

Carbonates in bentonites were examined systematically for the first time and their relationship to bentonitization was explored. The new petrographic and isotope geochemical data show that

pedogenic and palustrine dolomite and calcite are important constituents of non-marine bentonite deposits in Bavaria.

Carbonates formed below and above a fluctuating groundwater table. Plants, ground water and soils provided the biological background, the Mg/Ca ratio and the carbonate alkalinity, respectively, required for dolomite formation in a strictly non-arid environment. Silica globules in the carbonates show that silica mobility and dolomitization were a coeval process, while the intimate intergrowth of smectite and dolomite point to either a syngenetic or at least very timely post-smectitization process. While dolomitization and smectitization started at about the same time it cannot be ruled out that smectitization continued after blanketing of deposits by younger sediment.

Bentonitization of acidic, Mg- and Ca-poor volcanic precursor rocks does not necessarily require the involvement of seawater or saline conditions. It was a terrestrial process driven by Ca–Mg–rich waters influenced by pedogenesis. The strong pedogenic imprint implies that bentonitization occurred soon after deposition on a time scale similar to that of the development of soils.

Acknowledgements

This publication is part of the first author's Ph.D. research at the Lehrstuhl für Ingenieurgeologie at the Technische Universität München, Germany. PD Dr. Christopher Mayr at the section of Paleontology & Geobiology of the Ludwig-Maximilians-Universtität and Dr. Ulrich Struck at the Museum of Natural History in Berlin enabled the stable isotope analyses. We are grateful for access to bentonite mines granted by Bernhard Ratzke, Süd-Chemie AG (now Clariant), and the cooperation of Hans-Ulrich Boehnke, S&B Industrial Minerals. Dr. Jürgen Bär, Institut für Materialwissenschaften, Universität der Bundeswehr München, gave access to the field-emission scanning electron microscope. Also acknowledged is bachelor student Adrian Richter for field work and XRD analyses from samples of the Mittersberg and Hader deposits. We are grateful for the efforts of the two reviewers whose comments improved the manuscript considerably and the useful remarks of the editor. This study was supported financially by the Society of Economic Geologists', SEG Graduate Fellowship Award 2012.

CHAPTER SIX

6. A strontium isotope study of dolomite-bearing bentonite deposits in Bavaria (Germany)

Published in Clay Minerals – Journal of Fine Particle Sciences: Köster M.H., Hölzl S. & Gilg H.A. (2017) A strontium isotope and trace element geochemical study of dolomite-bearing bentonite deposits in Bavaria (Germany), v. 52, Clay Minerals, p. 161-190.

The research project was designed by Mathias H. Köster with advice from Prof. Dr. H. Albert Gilg (Technische Universität München). The field work was carried out by Mathias H. Köster with the occasional assistance of three bachelor students. Mathias H. Köster performed the sample processing, the microfabric analysis, and the X-ray diffraction analysis. SEM imaging was done by Mathias H. Köster after instruction by Dr. Jürgen Bär (Institut für Werkstoffkunde, Universität der Bundeswehr München). The handheld XRF measurements were carried out together with H. Albert Gilg but element quantification was done by Mathias H. Köster. Although sample weighing and processing was done by Mathias H. Köster stable isotope measurements were performed by PD Dr. Christoph Mayr (Ludwig-Maximilians Universität München & Friedrich-Alexander Universität Erlangen-Nürnberg). Mathias H. Köster performed the sample digestion and elution of strontium for strontium isotope analysis. Dr. Stefan Hölzl (RiesKraterMuseum Nördlingen) made the measurements of the Sr isotope ratios and advised on the relevant parts of the manuscript. Mathias H. Köster drafted the initial manuscript, with editing, revisions, and data verification by Prof. Dr. H. Albert Gilg and Dr. Stefan Hölzl. M.H. Köster brought the manuscript into its final shape and submitted it to the Clay Minerals Journal.

Abstract

The Landshut bentonites that formed from Ca- and Mg-poor rhyolitic tuffs in a fluviatile-lacustrine depositional environment of the Miocene Upper Freshwater Molasse, Southern Germany, contain abundant palustrine, pedogenic and groundwater carbonates. Geochemical analyses of dolomites,

calcites, and smectites from bentonites of various environments by XRD, TIMS, ICP-MS, and handheld XRF yield new insights into the compositions of fluids and source of imported components involved in carbonate formation and bentonitisation, as well as the timing of bentonite formation. Evaporated, strontium-rich brackish surface water with a molar Mg/Ca of 2 to 5 derived mostly from the weathering of detrital carbonates was involved in dolomite and bentonite formation in palustrine and some pedogenic environments. However, strontium-poor groundwater with a molar Mg/Ca around 1 and a stronger silicates weathering component caused bentonite and calcite formation in strictly pedogenic and groundwater settings. The $^{87}Sr/^{86}Sr$ and molar Mg/Ca in the smectite interlayers indicate later cation exchange with a water having more radiogenic strontium sources and lower molar Mg/Ca. The Rb-Sr data indicate the common presence of detrital illitic phases in the < 0.2 µm fractions of the bentonites. Cogenetic palustrine dolomite and a single smectite residue sample that lacks such a detrital illitic phase provide an age constraint for bentonitisation at 14.7 ± 4.1 Ma identical to primary ash deposition. Thus a rapid onset of bentonitisation of accumulated ash and dolomite formation in evaporation-driven wetland environments is indicated for the genesis of the Landshut bentonites.

6.1 Introduction

Dolomite and calcite are excellent palaeoenvironmental indicators used for reconstructing marine and terrestrial sedimentary environments (Banner, 1995). Dolomite and calcite are also common impurities in bentonite deposits but have rarely been studied in any detail (Knechtel & Patterson, 1956, 1962; Vogt, 1980; Delgado, 1993; Decher et al., 1996; Köster & Gilg, 2015). Mineralogical and stable isotope studies of dolomites or calcites were to date only presented from bentonite deposits in the vicinity of the Mediterranean Sea at Cabo de Gata, Spain, (Delgado & Reyes, 1993; Delgado, 1993) and Milos, Greece (Decher et al., 1996). However, the stable isotope values of carbonates and smectites in these bentonites are often not consistent with precipitation from the same fluid (Decher et al., 1996; Delgado & Reyes, 1993), and together with sedimentological evidence for dolomite formation during later subaerial exposure and the involvement of seawater during bentonite formation (Delgado, 1993) suggest no systematic genetic link of carbonate and bentonite formation.

Recently, Köster & Gilg (2015) provided the first systematic study of carbonates in the terrestrial bentonite deposits in Southern Germany. They showed that authigenic dolomite and calcite can be used to reconstruct the environments of ash alteration. The microfabrics, and $\delta^{13}C$ and $\delta^{18}O$ values of dolomite and calcite reveal that carbonates formed in pedogenic, palustrine and groundwater settings shortly after ash deposition and possibly during the onset of bentonitisation (Köster & Gilg, 2015). The

chemical composition of fluids, i.e. salinity, redox conditions, and source(s) of Mg and Ca ions necessary for wide-spread dolomite and calcite precipitation, as well as bentonitisation, of the Mg- and Ca-poor rhyolitic tuffs (Ulbig, 1999; Gilg, 2005; Aziz et al., 2010) are, however, not well constrained.

Tracing the source(s) of alkaline earth metal ions for bentonite formation is especially problematic because the smectite interlayer is susceptible to cation exchange reactions. Strontium isotope geochemistry has therefore rarely been applied in bentonite studies, the work of Chaudhuri & Brookins (1979) on the Clay Spur and Otay bentonites being a notable exception. They demonstrated that Sr in smectites (Clay Spur: 52.4 – 248.3 ppm; Otay: 48.2 – 117.4 ppm) is mostly (but not exclusively) exchangeable and that Rb is more firmly bound in smectite residues (Clay Spur: 4.1 – 6.9 ppm; Otay: 2.9 – 4.2 ppm). The contrasting $^{87}Sr/^{86}Sr$ of the residues (Clay Spur: 0.710 – 0.712; Otay: 0.712) and leachates (Clay Spur: 0.707; Otay: 0.709) and very low Rb/Sr values in the residues (< 0.08) could be interpreted to suggest a later cation exchange with less radiogenic Sr. Chaudhuri & Brookins (1979), however, did not compare the Sr isotope ratios of smectites to diagenetic carbonates in the Clay Spur (Knechtel & Patterson, 1956, 1962) or Otay (Cleveland, 1960) bentonites.

The intimate association of dolomites and calcites with bentonites in Southern Germany (Köster & Gilg, 2015) is an excellent opportunity for further exploring dolomite and calcite formation in terrestrial bentonite deposits. We aim to ascertain the salinity and Mg/Ca of the involved fluids, the Sr (and by inference Ca and Mg) sources for carbonate and bentonite formation, and the timing of bentonite deposit formation using acid-leach techniques and the Rb/Sr method.

6.2 Geological setting

The Landshut bentonite deposits (Fig. 6.1) are located in a 40 by 10 km wide tectonic block in the North Alpine Foreland Basin bordered by NW-SE striking fault zones of a basement high (Unger, 1981, 1999; Aziz et al., 2010). The presently mined deposits are limited to the 14.7 ± 0.2 Ma old main bentonite horizon (Aziz et al., 2010) in the upper part of the fluviatile Nördlicher Vollschotter (NV) sand and gravel unit and floodplain sediments of the Sand-Mergel-Decke (SMD) formed in an anastomosing to braided river system (Schmid, 2002; Maurer & Buchner, 2007) of the Upper Freshwater Molasse (UFM) (Vogt, 1980; Unger & Niemeyer, 1985a, b; Unger et al., 1990; Ulbig, 1999). Ulbig (1999) invoked topographic “highs” and “lows” to explain sedimentological and depositional differences of bentonites. Topographic “highs” are underlain by marl or clayey sand (SMD) and associated with abundant dolomite and calcite whereas topographic “lows” are characterised by sandy to gravely (NV) footwalls, higher detritus and lower carbonate content (Ulbig, 1999). All deposits are erosionally

capped by younger sediments (Fig. 6.2 & Fig. 6.3) and the hiatus is indicated by pedogenic features in bentonites. Carbonates in bentonites of both settings formed in palustrine, pedogenic or groundwater environments (Köster & Gilg, 2015). The presence of carbonates, partially altered tuffs, and sharp redox fronts evident by distinct colour contacts (e.g. yellow versus blue) of the bentonites are important characteristics for distinguishing depositional and alteration settings of bentonites. Bluish-grey, green-grey, yellow, brown, and mottled redox facies can be differentiated (Vogt & Köster, 1978; Unger, 1981; Unger & Niemeyer, 1985a, b; Unger et al. 1990; Ulbig, 1999; Köster & Gilg, 2015).

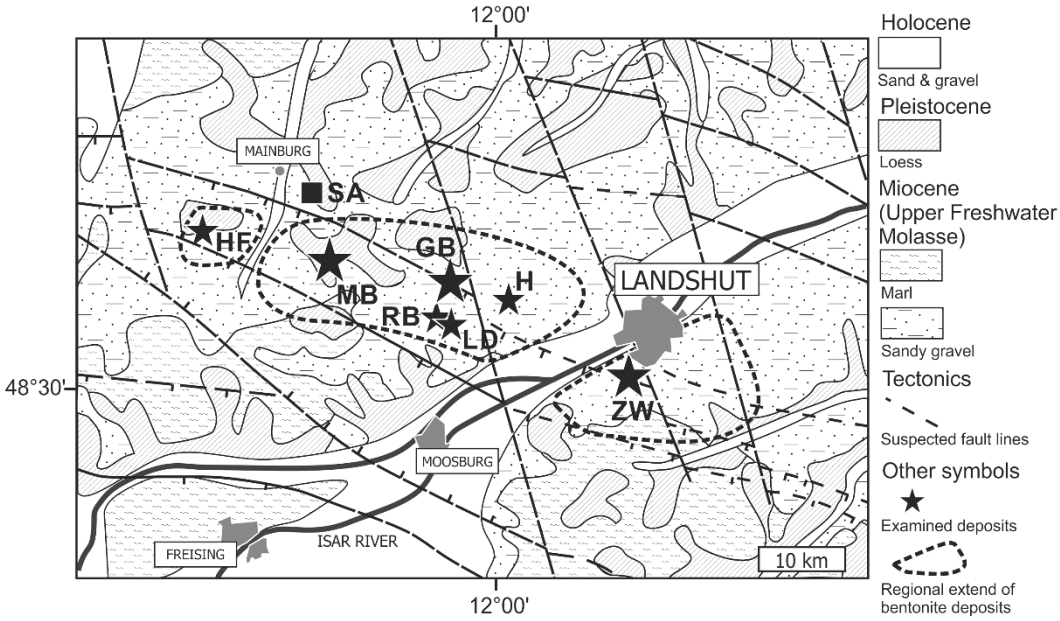

Fig. 6.1: Simplified geological map of the Landshut bentonite deposits (modified from Köster & Gilg, 2015; according to Freudenberger & Schwerd, 1996; Unger, 1999). Stars: Bentonite deposits. ZW – Zweikirchen, GB – Gabelsberg, MB – Mittersberg, LD – Landersdorf, H – Hader, RB – Rehbach, HF – Hofen. Square: Sandelzhausen (SA) fossil locality. Reproduced with the permission of the Mineralogical Society of Great Britain & Ireland, from Köster et al. (2017).

The UFM in the Eastern part of the North Alpine Foreland Basin is characterised by sand- and gravel-rich sediments with minor marls, and received significant clastic input in the form of crystalline and sedimentary rocks from the Alps, the Bohemian Massif, and the Swabian Alb (Lemcke, 1988; Unger, 1996; Frisch et al., 1998). The clasts in sands and gravels comprise quartz, granite, gneiss, and Alpine Bunter sandstone, as well as Mesozoic marine lime- and dolostones among other lithotypes (e.g. Unger, 1991). Lime- and dolostone clasts are derived from various Mesozoic marine carbonate sequences, mainly but not exclusively from the Mid-Triassic Hauptdolomit Formation of the Alps and Jurassic carbonates of the Swabian Alb (Unger, 1991; McArthur et al., 2001; Zorlu, 2007; Geske et al., 2012).

Ground waters in the Upper Freshwater Molasse are characterised by high cation concentrations (Egger et al., 1983). The water chemistry is influenced by carbonate and silicate weathering, as well as cation exchange reactions with clays, that are the source of high Ca^{2+}, Mg^{2+}, and HCO_3^- (and minor Na^+) concentrations in Molasse basin groundwater (Egger et al., 1983; Wagner et al., 2003). The ground waters in the Cenozoic sediments are characterised by variable $^{87}Sr/^{86}Sr$ values compatible with both marine carbonate- and silicate-derived strontium sources (Voerkelius et al., 2010). The Ca-Mg-HCO_3 waters of the Western Molasse basin have low Sr isotope ratios (0.70835 to 0.70965) typical for the weathering of marine carbonates (Waber et al., 2014), whereas waters of the Eastern Molasse basin are characterised by more radiogenic $^{87}Sr/^{86}Sr$ (> 0.71000) related to a combination of carbonate and silicate weathering and an increasing influence of the Variscan basement of the Bohemian Massif (Tütken & Vennemann, 2009).

6.3 Methods

6.3.1 Sample origin

Dolomite and calcite, bentonite, weakly altered tuff and quartz-rich tuffitic sandstone, originate from the Gabelsberg (GB), Mittersberg (MB) and Zweikirchen (ZW) deposits, Southern Germany (Fig. 6.1). Additional carbonate samples are derived from the Hofen (HF), Rehbach (RB), Hader (H), and Landersdorf (LD) deposits (Fig. 6.1). With the exception of new samples from Hofen, dolomite and calcite samples have been previously studied by Köster & Gilg (2015). The lithostratigraphic positions of the 67 bulk carbonate samples used for handheld XRF analysis are documented in Appendix 6.2.

6.3.2 X-ray diffraction

Carbonates were dry-ground in an agate mortar. Whole rocks of bentonite and tuffitic samples were ground in isopropanol using a McCrown micronizing mill. As internal standard, 10 wt% of ZnO was added to estimate the amount of amorphous volcanic glass in tuffitic samples. The < 0.2 µm fractions (i.e. almost “pure” smectites) were separated from bulk aliquots of bentonite and tuff by centrifugation. Random powder mounts, as well as air-dried and ethylene-glycolated (EG) orientated mounts of the < 0.2 µm fractions were characterised by X-ray diffraction analysis from 2 to 70°2θ (Phillips PW 1800, Cu Kα). The Ca and Mg content, and cation ordering (i.e. the segregation of Ca and Mg into separate sheets) of dolomite were estimated using the d_{104} reflection and the d_{015}/d_{110}

intensity ratio (Goldsmith & Graf, 1958; Lumsden & Chimahusky, 1980). Powder mounts were quantified by full-pattern Rietveld refinement using BGMNwin 1.8.6. with an estimated relative error of about 10 wt%. Discrete illite was detected in the < 0.2 µm fraction of three tuff samples and its content was estimated using a reference intensity ratio (peak areas of d_{001} reflections) of 4 for smectite and 1 for illite. The percentage of illite layers interstratified in smectite was determined according to Środoń (1980) using the peak migration method (26° – 28° 2θ and 15°– 18° 2θ). As discrete illite can interfere with the determination of the peak positions (Środoń, 1980), the percentage of illite layers interstratified in smectite was also estimated by the difference between the positions of 001/002 and 002/003 (Moore & Reynolds, 1997). Variable humidity, interlayer composition, and layer charge can be problematic in determining the percentage of illite interstratified in smectite using these methods and we estimate a relative error of about 30 % for the interstratified illite in smectite content (Środoń, 1980).

6.3.3 Hydrochloric acid treatment and isotope geochemistry

As our mineralogical analyses (Köster & Gilg, 2015, their Table 1) show that the authigenic carbonates in bentonites contain variable contents of silicates and oxides (i.e. clays, micas, feldspars, Fe- and Mn-minerals) we selected carbonate samples with a high carbonate content and low content of all other minerals, and applied an acid leach approach. Prior to the hydrochloric acid treatment, both the carbonates and the < 0.2 µm fractions of bentonites were dialysed with distilled water to remove absorbed elements until the electrical conductivity remained < 0.9 µS/cm, then dried at 40°C, and split.

The carbonate samples were dissolved in 1N HCl in teflon beakers and allowed to react for 45 minutes at 20°C. The solutions obtained from the dissolution of the carbonates were separated by centrifugation.

We followed a simplified method for the treatment of the < 0.2 µm fractions (smectites) according to Chaudhuri & Brookins (1979), Clauer (1979) and Clauer et al. (1982) involving a two-step procedure. In the first step we applied a weak hydrochloric acid treatment to extract the easily leachable exchangeable and adsorbed elements. The second step involved a stronger acid attack to liberate more strongly bound elements, e.g. in illitic components and octahedral positions. Smectites were first treated with triple distilled 1N HCl for 15 to 20 minutes at 20°C and the solution centrifuged (=“leachate”). The residual material (=“residue”) was washed additionally for one minute with 1N HCl and three times with triple distilled water to remove excess acid. The residue was then treated with

6N HCl at 90°C for 12 hours to extract the more strongly bound elements. Leachate and residue were analysed by inductively coupled plasma mass spectrometry (Actlabs Canada, UltraTrace 7; method A). As the Rb and Sr concentrations of method A (and K), were in several cases below the detection limit but essential for the Sr isotope analysis, we used a second approach (method B) with a prolonged leaching time of 18 hours and a Perkin Elmer DRC II ICP-MS at the Department of Geochemistry, University of Göttingen, Germany. The JA-2 standard (Japanese Andesite 2) was used in method B for external accuracy check and showed an error of less than 10 to 30% relative to its average chemical composition (Imai et al., 1995). Results were corrected for drift caused by non-ionised material collecting on the detector leading to the erroneous counting of photons as ions, and for major oxygen interferences caused by argon from the plasma combining with oxygen interfering with the reliable detection of ions of a certain element. Hundred ml 2% HNO_3 with 4 internal standard elements (Be, Rh, In, Re) were added to 1 ml of the obtained leachate and residue solutions.

For Sr isotope analyses, the < 0.2 µm fractions (smectites) were leached according to method A and the carbonates were dissolved using 1N HCl for 45 minutes at 20°C, as for the chemical analysis. The solutions were centrifuged to remove solids. An ion chromatographic column separation with Sr-specific crown-ether resin (Sr-Spec®, EIChroM Industries, USA) was used to extract Sr and to remove interfering elements such as Ca, Ba or Rb (Horwitz et al., 1992; Pin & Basin, 1992). Columns were pre-cleaned with 6.5N HNO_3, 6N HCl and triple-distilled H_2O, and flushed with 6.5N HNO_3 after introduction of the sample solution. The Sr was finally eluted with 0.05 HNO_3.

The Sr isotope ratios of smectites and carbonates were then determined using a thermal ionisation mass spectrometer (MAT 261.5, Thermo Finnigan, Germany) in the ZERIN-lab at the Ries Crater Museum Nördlingen, Germany, using single tungsten filaments. Significant extant Rb (its ionisation temperature is lower than for Sr) was evaporated by controlled preheating before measurement because traces of ^{87}Rb would interfere with the correct determination of the $^{87}Sr/^{86}Sr$. Isotope mass fractionation during analysis was corrected by referencing to an invariant $^{88}Sr/^{86}Sr$ value of 8.37521. To check for proper operation of the mass spectrometer, certified reference material (SrCO3, NIST SRM 987) was measured and showed a mean $^{87}Sr/^{86}Sr$ of 0.710211 ± 0.000023 (2sigma of the mean; n = 55) during the time of analyses. The total analytical uncertainty (precision + accuracy) for $^{87}Sr/^{86}Sr$ in natural samples is estimated by replicate analyses of in-house standards (a red wine) at < 50 ppm to verify the reproducibility of the complete sample processing chain from digestions, extraction to measurement.

A split of sample MB28 (a dolomite) containing illite was reacted 24 hours in 1N HCl at 20°C to determine the influence of leaching time on isotope ratios. The Sr isotope ratio of MB28 increased only

slightly from 0.710521 to 0.710541, indicating that leaching time has a negligible effect on Sr isotope ratios of carbonates.

Table 6.1: Mineral composition of carbonates, bentonite and tuff whole-rocks (WR) and the < 0.2 µm fractions used for Sr isotope analyses. ped = pedogenic, pal = palustrine, gw = groundwater.

Sample	Facies	Material	Type	Rock colour	Cal	Dol	Qz	Sme	Ilt/Ms	Kao/Chl	Fsp	Opl-CT	Am.
Zweikirchen													
ZW26	ped	Dolomite	WR	mottled	T	95	3	1	1	1			
ZW25	ped	Dolomite	WR	mottled	T	99	1						
ZW23	ped	Dolomite	WR	mottled	T	77	11	8	3				
ZW20	ped	Dolomite	WR	mottled		86	8	4	3				
ZW18	gw	Calcite	WR	bluish-grey	60	6	8	20	6				
ZW17	gw	Calcite	WR	bluish-grey	70		5	19	6		T		
ZW16	gw	Calcite	WR	bluish-grey	69	T	5	18	6	2			
ZW50		Bentonite	WR	bluish-grey		T	6	76	8	3	6		
ZW50		Bentonite	< 0.2 µm	bluish-grey			T	>99	T				
ZW39		Sandstone	WR	white-blue			54	24	3	1	10	8	
ZW39		Sandstone	< 0.2 µm	white-blue			T	94	16		T		?
ZW48		Bentonite	WR	yellowish		T	6	79	9	3	4		
ZW48		Bentonite	< 0.2 µm	yellowish			T	>99	T				
Mittersberg													
MB28	pal	Dolomite	WR	greenish-grey		74	1	13	4	1	T	8	
MB27	pal	Dolomite	WR	greenish-grey		75	1	13	3			8	
MB18	pal	Dolomite	WR	greenish-grey		66	3	21	6	1		3	
MB12	pal	Dolomite	WR	greenish-grey		67	2	17	4	1		9	
MB38		Tuff	WR	greenish-grey			2	19	3	2	2		73
MB38		Tuff	< 0.2 µm	greenish-grey			T	90	10				?
MB34		Bentonite	WR	greenish-grey			3	83	4	6	4		
MB34		Bentonite	< 0.2 µm	greenish-grey			T	>99					
Gabelsberg													
GB10	pal	Dolomite	WR	whitish-beige	2	63	4	25	6				
GB08	pal	Dolomite	WR	whitish-beige	1	56	5	24	15				
GB07	pal	Dolomite	WR	whitish-beige	2	70	4	19	5				
GB41		alt. Tuff	WR	greenish-grey		T	9	56	28		2		5
GB41		alt. Tuff	< 0.2 µm	greenish-grey			T	>99	T				?
GB37B		Tuff	WR	beige			6	25	4	2	4		60
GB37B		Tuff	< 0.2 µm	beige			T	XXX	X				
GB35A		Bentonite	WR	yellowish			T	94	2		4		
GB35a		Bentonite	< 0.2 µm	yellowish			T	>99					

Cal = calcite, Dol = dolomite, Qz = quartz, Sme = smectite, Ilt/Ms = illite and/or muscovite, Kao/Chl = kaolinite or chlorite, Fsp = feldspar, Am. = X-ray amorphous (volcanic glass), XXX > 95 %, X < 5%, T = traces (< 1 %).

"Isochron" ages of smectite leachate and residue pairs (the < 0.2 µm fractions) and carbonate-smectite residue pairs were calculated using IsoPlot 4.13 (Ludwig, 2008). The Rb/Sr ages were calculated using results from method A for leachates and results from method B for residues because the residue Sr content was below the detection limit of method A. The decay constant used in the age

calculations (Table 6.4) is $\lambda^{87}Rb = 1.42*10^{-11}$/yr. The Sr and Rb concentrations were determined by ICP-MS, as described earlier in the text.

6.3.4 Handheld X-ray fluorescence analysis

A handheld ED-XRF Bruker Tracer III-SD with a rhodium anode and a 10 mm² silicon drift detector was used for chemical analysis of Ca, Sr, and Mn on a smoothed surface of carbonate samples. Spot size is about 3 x 4 mm. Measurements were conducted for 30 seconds operating at 40 kV and 30 µA with the yellow filter (12 mil Al + 1 mil Ti). Spectra were fitted with the ARTAX software (Version 7.4.8.2) and calibrated using our ICP-MS results and the international standards BCS393, DWA-1, MAG-1 and NIM-S (Govindaraju, 1989). Average absolute errors (1 SD) are ± 3.4 wt% for CaO, ± 45 µg/g for Sr, and ± 744 µg/g for Mn.

6.4 Results

6.4.1 Geological sections and sedimentary fabrics

Bentonite deposits (Fig. 6.2 and Fig. 6.3) from pedogenic-groundwater (ZW, LD, H) and palustrine (MB, GB, HF, RB) settings were distinguished based on the lithostratigraphic position of carbonates, carbonate mineralogy, microfabrics, stable isotope composition, and colour (Köster & Gilg, 2015). The samples used for Sr isotope analysis are illustrated in Figure 6.2.

Palustrine dolomites are characterised by nodular replacement beds (Fig. 6.4a), few but large nodules, dolomite-lined root moulds, and soil churning (Köster & Gilg, 2015). Pedogenic dolomites and calcites are characterised by hard and soft nodules, earthy masses, as well as stringer networks. Substantial calcite-spar can be found in shrinkage cracks of pedogenic calcites (Fig. 6.4c). Groundwater carbonates form concentric or nodular masses of clotted micrite and limpid calcite-spar (Fig. 6.4d). Based on colour, three redox facies are distinguished: reduced blue bentonite, intermediate green, and oxidised yellow bentonite. Blue bentonites commonly contain pyrite (Fig. 6.4b) and appear either homogeneous or laminated because of detrital mica (Fig. 6.4e). Green and yellow bentonites were solely encountered as homogenous clay (Fig. 6.4f). Root traces and sedimentary fabrics are seldom preserved in bentonites. Partially altered tuff, however, shows excellent fabric preservation of deep reaching roots (Köster & Gilg, 2015), altered volcanic glass shards (Fig. 6.4g) and silicified plant remains (Fig. 6.4h).

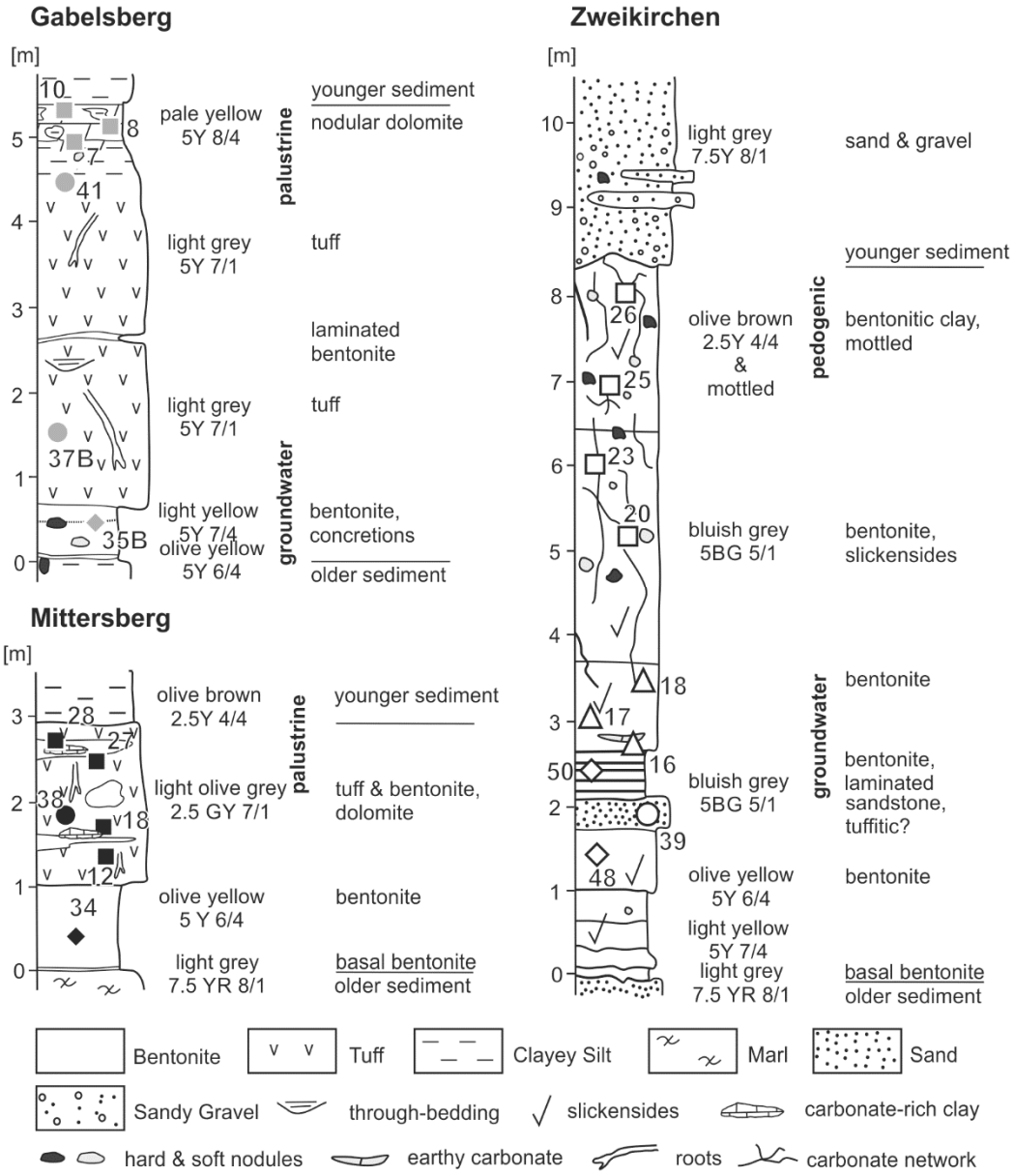

Fig. 6.2: Geological sections and sedimentary structures of the Gabelsberg (GB), Mittersberg (MB) and Zweikirchen (ZW) deposits. The samples used for ICP-MS and TIMS analysis are shown in the sections as squares (dolomite), triangles (calcite), diamonds (bentonite) or circles (partially altered tuff and a tuffitic sandstone [ZW39]) with sample numbers. Reproduced with the permission of the Mineralogical Society of Great Britain & Ireland, from Köster et al. (2017).

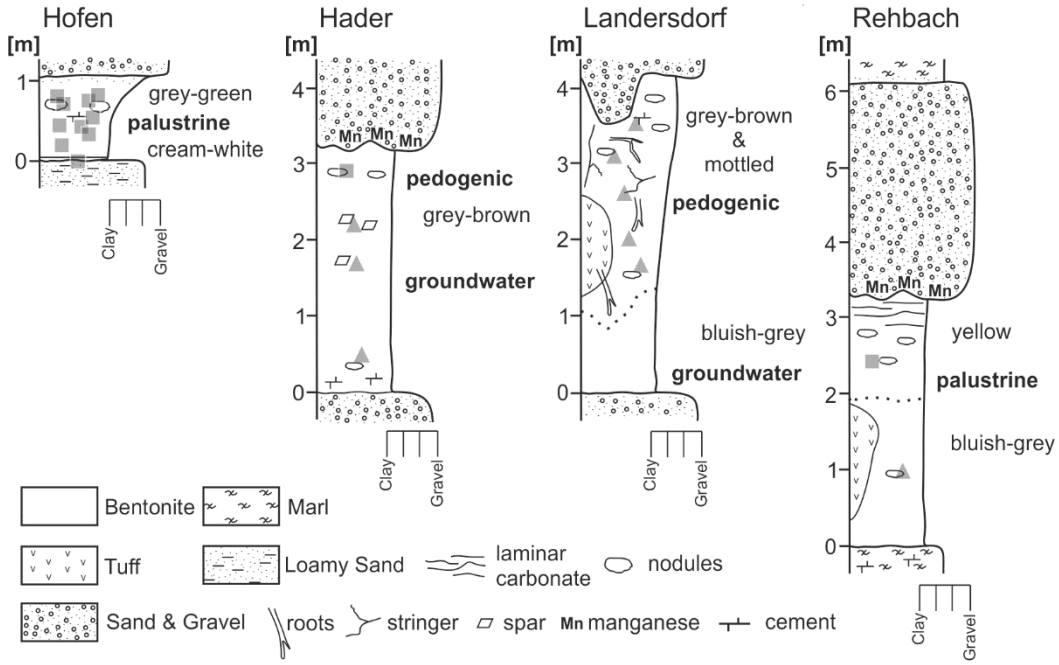

Fig. 6.3: Simplified geological sections with major sedimentary structures and carbonate accumulations in the Hofen (HF), Hader (H), Landersdorf (LD) and Rehbach (RB) deposits. Squares and triangles: p-XRF sample localities. Hofen base: ~1 cm cream-white basal bentonite layer ("Rahm"). Reproduced with the permission of the Mineralogical Society of Great Britain & Ireland, from Köster et al. (2017).

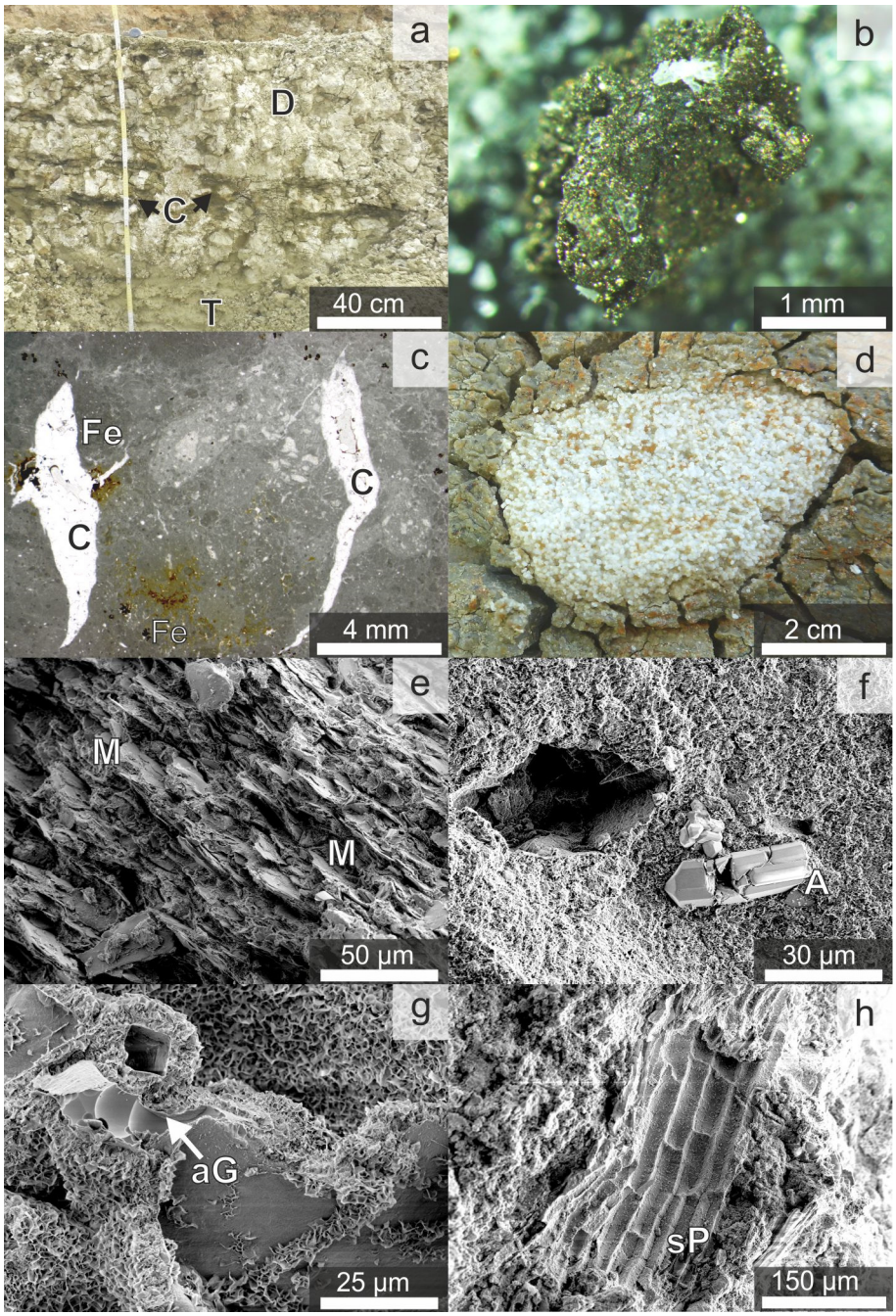

Fig. 6.4: Bentonite and carbonate fabrics. A. Nodular palustrine dolomite (D) with clay patches (C) and partially altered tuff (T) in the Gabelsberg deposit (GB07, 08, 10). B. Pyrite from bluish bentonite beds in the Rehbach deposit. C. Calcite-spar (C) in shrinkage cracks with mottles of hematite and goethite (Fe) in the Landersdorf deposit. D. Sugar-like groundwater calcite in the Hader deposit. E. Bluish-grey (ZW50) bentonite with detrital mica (M) and F. Yellow bentonite (ZW48) with apatite crystal (A) both from Zweikirchen G. Almost completely altered volcanic glass (aG) with primary fabric preservation and H. Silicified plant remains (sP) with preserved cell-walls both from the Gabelsberg deposit (GB37B). Reproduced with the permission of the Mineralogical Society of Great Britain & Ireland, from Köster et al. (2017).

6.4.2 Mineralogical composition

The mineralogical compositions of carbonates and the < 0.2 µm fractions of bentonites and tuffs are shown in Table 6.1 and Table 6.2. Well-defined peaks at 2.892 to 2.905 Å and at 3.022 to 3.029 Å are characteristic for calcium-rich dolomite and Mg-enriched calcite. The d_{015} and d_{110} cation ordering reflections confirm the actual dolomite character and reveal a moderate degree of order (Fig. 6.6; I_{015}/I_{110}: 0.38 – 0.68). The calcium-rich composition and moderate cation ordering favour a primary origin of dolomite (Last, 1990).

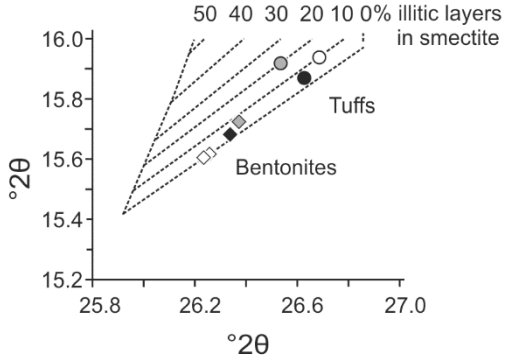

Fig. 6.5: Percentage of interstratified illite in smectite of the < 0.2 µm fractions according to Środoń (1980). Diamonds: bentonite smectites; circles: tuff smectites. Mittersberg (black), Gabelsberg (grey) and Zweikirchen (white) deposits. Reproduced with the permission of the Mineralogical Society of Great Britain & Ireland, from Köster et al. (2017).

Dioctahedral smectite (d_{060}; 1.50 to 1.49 Å) is the main constituent of bentonite and tuff, with variable amounts of mica/illite, kaolinite, chlorite, quartz, feldspar, volcanic glass, pyrite, goethite and hematite. Orientated, air-dried and ethylene-glycolated < 0.2 µm fractions expand upon EG-treatment from 14.7 Å to 17.3 Å. Some < 0.2 µm samples (Table 6.2) contain traces of discrete illite/mica visible as a small, low-angle reflection (001; ~ 10 Å). The < 0.2 µm fraction of strongly altered tuff (GB41) is composed of R0 illite(0.2)/smectite. Tuffitic whole-rock samples (GB37B) and < 0.2 µm fractions of tuff (GB41, MB38) and tuffitic sandstone (ZW39) contain higher contents of discrete illite/mica, quartz, or opal-CT than bentonite. The percentage of interstratified illite in smectite of the < 0.2 µm fractions is illustrated in Fig. 6.5.

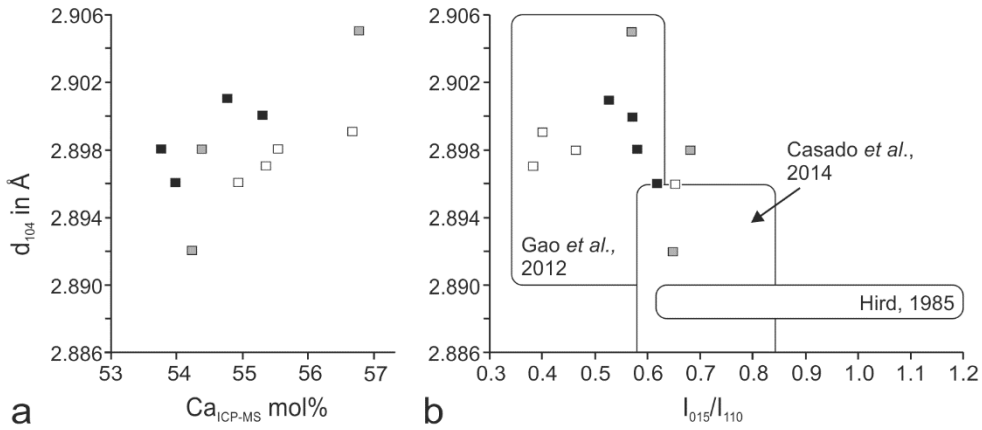

Fig. 6.6: Calcium content, d_{104} positions, and cation ordering of dolomites. A. The d_{104} reflection versus calcium content. B. Dolomite d_{104} versus the I_{015}/I_{110} intensity ratios. Gao et al. (2012): Silurian, marine-overprinted lacustrine Ca-dolostones; Casado et al. (2014): Miocene lacustrine/palustrine Mg-dolomites; Carboniferous vein dolomites for comparison (Hird, 1985). Pedogenic: white (ZW); palustrine: black (MB) and grey (GB). Reproduced with the permission of the Mineralogical Society of Great Britain & Ireland, from Köster et al. (2017).

Table 6.2: Discrete illite and interstratified illite content of the < 0.2 µm fractions. The error for the interstratified illite in smectite content is estimated at 10 % to 30 % (Środoń, 1980), and an estimated 25 % for discrete illite.

Sample	**Host lithology**	**% discrete illite**	**2°theta** Smectite d_{003}	**2°theta** Smectite d_{005}	**% Illite in Smectite** Środoń (1980)	**Δd2** Smectite 001/002-002/003	**% Illite in Smectite** Moore & Reynolds (1997)
ZW39	Tuff	~ 16	15.93	26.69	11	5.74	23
ZW48	Bentonite		15.62	26.25	1	5.40	4
ZW50	Bentonite		15.61	26.25	1	5.38	3
MB34	Bentonite		15.68	26.33	1	5.42	6
MB38	Tuff	~ 10	15.87	26.63	12	5.48	9
GB41	Tuff	~ 11	15.92	26.53	19	5.60	16
GB35A	Bentonite		15.72	26.35	8	5.28	0

6.4.3 Chemical composition of dolomite and calcite

The ICP-MS analyses of carbonates (Table 6.3) confirm the XRD results and reveal dolomites with Mg/(Mg+Ca) molar ratios of 0.45 ± 0.01 (n=11) and calcites with Mg/(Mg+Ca) molar ratios of 0.04 ± 0.02 (n=3). The trace element compositions of carbonates from the various environments show significant differences. Strontium concentrations in dolomites exceed that of most island dolomites (Budd, 1997) and are highest in palustrine dolomites (536 – 1120 µg/g) that have Rb concentrations (4.8 – 9.5 µg/g) similar to pedogenic dolomites (Table 6.4). The Mn content (305 – 580 µg/g) is not well pronounced, and Th and U concentrations are elevated. Palustrine dolomites also have elevated Li (13

– 20 µg/g) and Ba (63 – 110 µg/g) concentrations (Table 6.3). Pedogenic dolomites reveal intermediate Sr (208 – 368 µg/g) and Rb (1.4 – 8.5 µg/g) concentrations, and Mn content (357 – 1700 µg/g; Table 6.3 and Table 6.4). Calcites display much lower Sr (66 – 126 µg/g) but higher Rb (10.6 – 13.3 µg/g) and very high Mn (2880 – 4729 µg/g) concentrations (Table 6.3; Table 6.4).

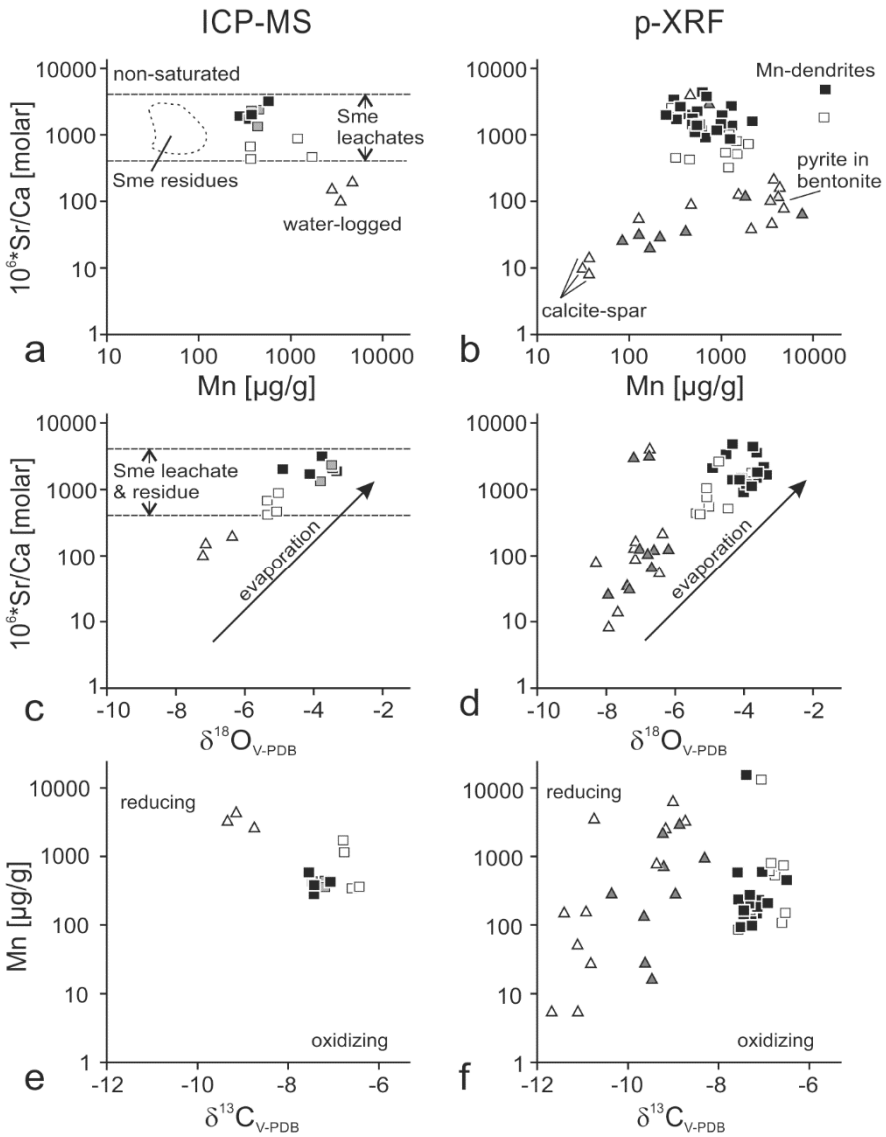

Fig. 6.7: Geochemical data of carbonates used for Sr isotope analysis using an HCl-leach method (left side) and of bulk samples using portable XRF (right side). A and B. Sr/Ca versus Mn content. C and D. Sr/Ca versus $\delta^{18}O$ values (Köster & Gilg, 2015). E and F. Mn content versus $\delta^{13}C$ values (Köster & Gilg, 2015). Squares: palustrine (black and grey) and pedogenic (white) dolomite. Triangles: groundwater (white) calcite. Note: Not all samples measured by p-XRF were analysed for stable isotopes. Reproduced with the permission of the Mineralogical Society of Great Britain & Ireland, from Köster et al. (2017).

The Ca, Sr, and Mn concentrations determined by handheld XRF (Chapter 6 - Appendix 6.2) are dominated by carbonates, but are in part influenced by included silicates or oxides. They are used to compare a larger number of samples (Fig. 6.7a-f) on the basis of their 10^6*(Sr/Ca) molar ratios, denoted here as Sr/Ca_m, and Mn content. The Sr/Ca_m and Mn contents measured by XRF are consistent with ICP-MS results (Fig. 6.7a-f). Dolomites show negatively correlated Sr/Ca_m and Mn content, while calcites display a positive but less distinct correlation of Sr/Ca_m and Mn content. High Sr/Ca_m of dolomites and calcites are related to high $\delta^{18}O$ values (Fig. 6.7c-d), whereas Mn contents and $\delta^{13}C$ values show a more complicated relationship (Fig. 6.7e-f).

6.4.4 Rare earth element patterns

The rare earth element plus yttrium (REE+Y; Chapter 6 - Appendix 6.1) patterns (Fig. 6.8) were normalised against post-Archean Australian shale (PAAS, Nance & Taylor, 1976) as recommended by Bau & Möller (1992) for sedimentary environments. Both pedogenic and palustrine dolomites, as well as groundwater calcites show a slight enrichment of heavy REE ($LREE_{PAAS}$ ~ 0.5 – 0.1 and $HREE_{PAAS}$ 1.0 – 1.1) indicating the remobilisation of HREE, and complexation in carbonate-rich waters (Möller et al., 1984). Palustrine dolomites have small negative Ce and Eu anomalies suggesting slightly oxidising conditions, and/or inheritance from the fluid phase interacting with detrital rocks. In contrast, pedogenic dolomites and groundwater calcites display positive and negative Ce and Eu anomalies, suggesting variable redox conditions in soil and groundwater settings.

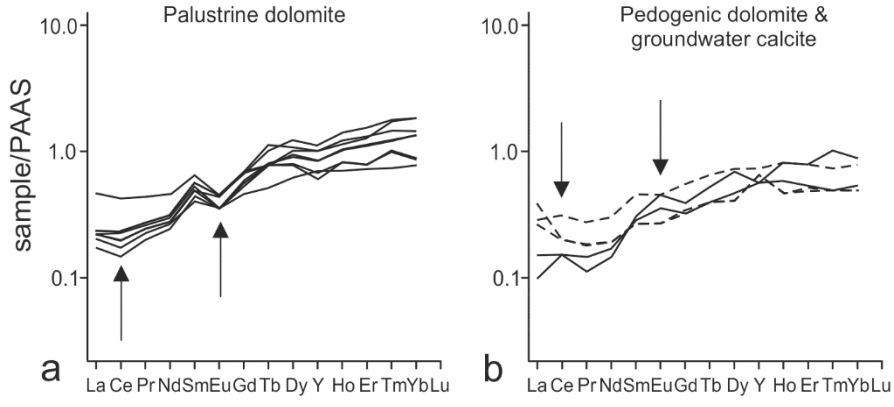

Fig. 6.8: REE+Y patterns of HREE-enriched dolomites and calcites. A. Negative Ce and Eu anomalies (arrows) in palustrine dolomite. B. Pedogenic (solid line) and groundwater calcite (dashed line) with variable Ce and Eu anomalies (arrows). Reproduced with the permission of the Mineralogical Society of Great Britain & Ireland, from Köster et al. (2017).

6.4.5 Chemical composition of smectites

The chemical compositions of the smectite (< 0.2 µm fraction) leachates and acid-treated residues of bentonites, tuffs and sandstone are shown in Table 6.3 and Table 6.4. The first step (method A) of the 1N and 6N HCl treatment revealed that Ca and Mg are the main leachable elements with an average molar Mg/(Mg+Ca) ratio of 0.43 ± 0.11, consistent with previously reported exchangeable cation compositions (Grim & Güven, 1978; Ulbig, 1994). The leachates also contain Sr (7.0 – 90.1), Rb (0.3 – 4.1 µg/g), as well as traces of As, Ba, Cu, Pb and V.

Smectite residues (method A) have a low MgO (1.2 – 1.9 wt%) and very low CaO content (0.1 wt%) that corresponds to a Mg/(Mg+Ca) molar ratio of 0.96 to 1.00 confirming the partial dissolution of smectite octahedral layers, and possibly suggesting the presence of trace amounts of carbonate not detected by XRD or traces of residual calcium in the smectite interlayer. The acid treatment of residues liberated variable Fe (11.4 – 19.7 mg/g) but very low SiO_2 (< 1.3 wt%) concentrations indicating that tetrahedral layers were only partially dissolved. Smectite residues from palustrine deposits (GB and MB) have an elevated Li content of ~ 20 µg/g (Table 6.3).

The 18 hour acid treatment of smectite residues (method B) liberated Sr (1.0 – 3.7) and Rb (7.8 – 22.6 µg/g). The Rb and K contents are positively correlated (r^2 = 0.85), suggesting that Rb is located in discrete illite or an interstratified illitic component. In both methods A and B, sample GB35A showed anomalously low Sr and Rb contents. GB35A has one of the lowest percentages of interstratified illite in smectite (Table 6.2) and was prone to clumping during treatment, possibly leading to an insufficient acid attack on the already low Sr and Rb content in illitic components.

The “total” Sr contents (Leachate + Residue; mean: 29.4 ± 27.6 µg/g, 1 SD) of smectites slightly exceed previous results (Vogt & Köster, 1978; mean: 19.5 ± 4.8 µg/g, 1 SD) of Na-exchanged smectites treated with 0.1 M EDTA and 0.1 N ammonium solution, probably because these treatments removed exchangeable strontium. The Sr content of residues (mean: 2.7 ± 1.0 µg/g, 1 SD) is rather low. A “total” Rb content of 16.9 ± 5.5 µg/g (Leachate + Residue) was extracted, mostly located in the residues (14.4 ± 4.9 µg/g, 1 SD; Table 6.4). This is less than those reported by Vogt & Köster (1978; 31 ± 12 µg/g, 1 SD), indicating the partial extraction of Rb from smectite residues. Strontium is thus more easily extractable from absorbed and exchangeable positions (65 to 97%) whereas Rb is more firmly fixed in the residues (77 to 93%), similar to the results from Clay Spur and Otay bentonites (Chaudhuri & Brookins, 1979).

Table 6.3: Geochemical composition of carbonates, smectite leachates and residues according to method A. The detection limit of K according to method A was 5000 µg/g. The K content of smectites was determined using method B. L = leachate, R = residue, * = discrete illite in sample, n.d. = not determined. ped = pedogenic, pal = palustrine, gw = groundwater. Arsenic < 10 µg/g for carbonates and < 60 µg/g for smectites.

Sample	Mat.	MgO	CaO	SiO_2	TiO_2	Al_2O_3	P	S	Ba	Co	Cs	Cu	Fe	Ga	K	Li	Mn	Na	Pb	Te	Th	U	V
		wt%	wt%	wt%	wt%	wt%	wt%	wt%	µg/g	µg/g	µg/g	µg/g	µg/g	µg/g	µg/g	µg/g	µg/g	µg/g	µg/g	µg/g	µg/g	µg/g	µg/g
ZW26	Dol	19.2	32.6	0.3	<0.03	0.2	<0.03	0.11	18	1.0	0.0	<4.0	<3000	0.0	n.d.	<6	373	<500	3	<10	0.4	3.0	10
ZW25	Dol	19.4	35.3	0.0	<0.03	0.0	<0.03	0.13	42	1.2	0.6	<4.0	<3000	1.5	n.d.	<6	357	<500	4	<10	0.5	4.6	30
ZW23	Dol	15.3	26.6	0.6	<0.03	0.3	<0.03	0.09	51	2.4	0.4	<4.0	<3000	0.8	n.d.	<6	1210	<500	19	<10	1.5	4.1	20
ZW20	Dol	16.5	28.4	0.7	<0.03	0.4	0.03	0.10	57	2.6	0.3	13	4000	0.9	n.d.	<6	1700	900	20	<10	0.8	4.1	10
ZW18	Cal	1.9	38.8	0.7	<0.03	0.3	0.08	0.14	56	1.6	0.6	9	<3000	1.0	n.d.	<6	4720	900	15	<10	1.2	3.3	20
ZW17	Cal	0.8	39.5	0.5	<0.03	0.2	0.06	0.14	34	1.3	0.5	<4.0	<3000	0.6	n.d.	<6	3550	<500	10	<10	1.2	1.1	10
ZW16	Cal	1.2	43.2	0.4	<0.03	0.2	0.03	0.16	65	2.2	0.5	6	<3000	0.7	n.d.	<6	2880	<500	29	<10	1.0	1.6	20
ZW50 L	Sme	0.5	0.7	0.2	<0.03	0.1	<0.03	<0.05	12	1.8	<0.02	13	<3000	<0.4	n.d.	<6	<9	<500	4	<10	0.9	<0.2	120
ZW50 R	Sme	1.5	0.1	0.1	0.03	5.5	<0.03	<0.05	<6	6.1	1.1	16	19590	6.8	605	<6	40	<500	15	250	7.1	<0.2	500
*ZW39 L	Sme	0.4	0.5	0.1	<0.03	0.1	<0.03	<0.05	32	<0.04	<0.02	12	<3000	<0.4	n.d.	<6	<9	<500	10	<10	0.7	1.0	80
*ZW39 R	Sme	1.9	0.1	0.3	<0.01	5.9	<0.03	<0.05	20	3.8	1.7	14	13870	5.8	2000	<6	40	<500	5	250	4.3	0.9	460
ZW48 L	Sme	0.4	0.4	<0.1	<0.03	<0.09	<0.03	<0.05	62	<0.04	<0.02	<4.0	<3000	<0.4	368	<6	<9	<500	6	<10	0.5	0.5	110
ZW48 R	Sme	1.2	0.1	0.1	0.03	3.7	<0.03	<0.05	20	1.8	0.7	14	16150	8.2	863	<6	40	<500	7	250	5.2	<0.2	470
MB28	Dol	12.1	20.4	0.7	<0.03	0.5	0.03	0.08	65	1.7	0.3	6	<3000	1.3	n.d.	13	305	<500	8	<10	2.3	5.8	30
MB27	Dol	15.0	25.7	1.1	<0.03	0.7	<0.03	0.09	74	2.3	0.4	8	<3000	1.2	n.d.	15	365	<500	10	<10	3.0	5.8	20
MB18	Dol	14.0	22.7	1.3	<0.03	0.7	<0.03	0.08	105	3.0	0.6	11	<3000	1.2	n.d.	14	386	500	18	<10	3.8	2.3	20
MB12	Dol	14.2	23.1	1.2	<0.03	0.7	<0.03	0.08	88	2.2	0.4	8	<3000	1.2	n.d.	16	580	600	11	<10	2.8	5.6	20
*MB38 L	Sme	0.3	0.5	0.3	<0.03	0.3	<0.03	<0.05	34	<0.04	<0.02	5	<3000	<0.4	n.d.	<6	<9	<500	5	50	0.6	0.0	190
*MB38 R	Sme	1.7	0.1	0.1	0.05	5.1	<0.03	<0.05	30	3.2	0.9	20	11400	8.2	585	20	60	<500	11	250	5.0	<0.2	480
MB34 L	Sme	0.3	0.7	<0.1	<0.03	<0.09	<0.03	<0.05	10	<0.04	<0.02	<4.0	<3000	<0.4	n.d.	<6	<9	<500	2	50	0.6	<0.2	190
MB34 R	Sme	1.9	0.1	0.2	0.05	5.8	<0.03	<0.05	0	6.3	0.4	12	19700	9.2	836	20	60	<500	10	250	8.2	<0.2	480
	Sme																						
GB10	Dol	14.3	26.0	0.7	<0.03	0.3	0.11	0.09	63	1.4	0.4	9	<3000	1.1	n.d.	15	437	< 500	3	<10	2.1	7.1	20
GB08	Dol	17.2	28.4	1.3	<0.03	0.9	0.06	0.10	84	5.5	0.5	8	<4000	1.2	n.d.	20	451	800	10	<10	2.7	13.6	20
GB07	Dol	15.4	25.5	1.3	<0.03	1.2	0.04	0.09	110	7.4	0.4	7	<4000	2.3	n.d.	19	372	800	8	<10	1.6	10.2	10
GB41 L	Sme	0.3	0.9	0.1	<0.03	0.3	<0.03	<0.05	8	<0.04	<0.02	5	<3000	<0.4	n.d.	<6	<9	<500	2	50	0.6	0.8	130

Table 6.3: Continued.

Sample	Mat	MgO	CaO	SiO_2	TiO_2	Al_2O_3	P	S	Ba	Co	Cs	Cu	Fe	Ga	K	Li	Mn	Na	Pb	Te	Th	U	V
		wt%	wt%	wt%	wt%	wt%	wt%	wt%	µg/g	µg/g	µg/g	µg/g	µg/g	µg/g	µg/g	µg/g	µg/g	µg/g	µg/g	µg/g	µg/g	µg/g	µg/g
GB 41 R	Sme	n.d.	n.d.	n.d.	n.d.	n.d.	n.d.	n.d.	n.d.	n.d.	n.d.	n.d.	n.d.	n.d.	2118	n.d.	n.d.	n.d.	n.d.	n.d.	n.d.	n.d.	n.d.
*GB37B L	Sme	0.2	0.9	0.1	<0.03	<0.09	<0.03	<0.05	29	0.7	<0.02	8	<3000	0.5	n.d.	<6	<9	<500	3	<10	0.7	0.4	130
*GB37B R	Sme	1.8	0.1	0.1	0.07	4.6	<0.03	<0.05	40	4.4	1.8	27	16100	7.6	1013	20	100	<500	5	240	5.1	0.4	490
GB35A L	Sme	0.3	0.7	<0.1	<0.03	<0.09	<0.03	<0.05	6	<0.04	<0.02	<4.0	<3000	<0.4	61	<6	<9	<500	<0.2	<10	0.2	<0.2	100
GB35A R	Sme	n.d.	n.d.	n.d.	n.d.	n.d.	n.d.	n.d.	n.d.	n.d.	n.d.	n.d.	n.d.	n.d.	35	n.d.	n.d.	n.d.	n.d.	n.d.	n.d.	n.d.	n.d.

6.4.6 Rb-Sr isotope results

The data reveal a systematic increase of Rb/Sr (Table 6.4) and $^{87}Sr/^{86}Sr$ but a decrease of Sr concentrations from dolomites via calcites to smectite leachates and residues (Table 6.4; Fig. 6.10). The lowest Rb/Sr and $^{87}Sr/^{86}Sr$ are found in palustrine dolomites (0.005 – 0.013, 0.71042 – 0.71113; Table 6.4) from Gabelsberg and Mittersberg, with slightly higher values in pedogenic dolomites from Zweikirchen (0.006 – 0.37, 0.71105 – 0.71135; Table 6.4). Groundwater calcites from Zweikirchen have higher Rb/Sr and $^{87}Sr/^{86}Sr$ (0.097 – 0.177, 0.71138 – 0.71154) than the pedogenic dolomites from the same locality (Fig. 6.10; Table 6.4). In the Gabelsberg and Mittersberg deposits, the Rb/Sr (0.011 – 0.471) and $^{87}Sr/^{86}Sr$ (0.71108 – 0.71160) of smectite leachates are higher than in associated dolomites but in part exceeded by the values of smectite leachates from the Zweikirchen deposit (0.034 – 0.137, 0.71231 – 0.71285; Table 6.4). The Rb/Sr and $^{87}Sr/^{86}Sr$ (0.333 – 14.000, 0.71401 – 0.72286) of the smectite residues are even higher but without systematic differences (Fig. 6.10). Illite-rich samples reveal the highest Rb/Sr and $^{87}Sr/^{86}Sr$ (Table 6.4). Smectite leachate-residue pair model ages range from 11.8 to 35.5 Ma. Their initial $^{87}Sr/^{86}Sr$ vary between 0.71091 and 0.72161 (Table 6.4). The highest initial $^{87}Sr/^{86}Sr$ were determined in illite/mica-poor sample ZW50 which has a low Rb/Sr (2.108). The L-R pair ages (Table 6.4) are mostly older than the rhyolitic ash (14.7 ± 0.2 Ma; Aziz et al., 2010), indicating the frequent presence of detrital illitic material in the < 0.2 µm fractions (Table 6.2). The only sample that does not contain detrital micaceous material (MB34) yields a L-R model age of 11.8 ± 1.5 Ma (Fig. 6.9).

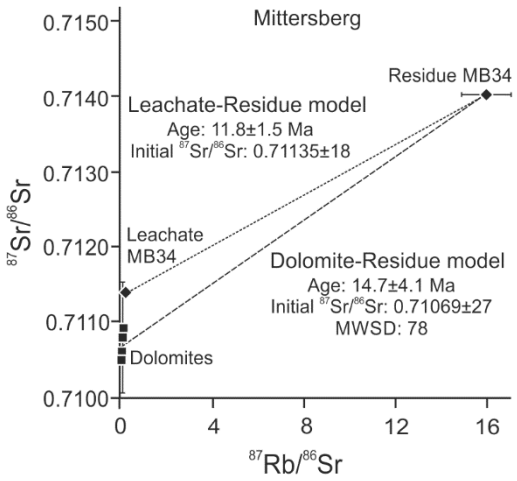

Fig. 6.9: Isochron plot of the Mittersberg deposits showing Rb-Sr data of dolomites (MB12, 18, 27 and 28) and smectite residue (MB34). The smectite leachate-residue pair is included for comparison. Squares: dolomite; diamonds: smectite from bentonite. Reproduced with the permission of the Mineralogical Society of Great Britain & Ireland, from Köster et al. (2017).

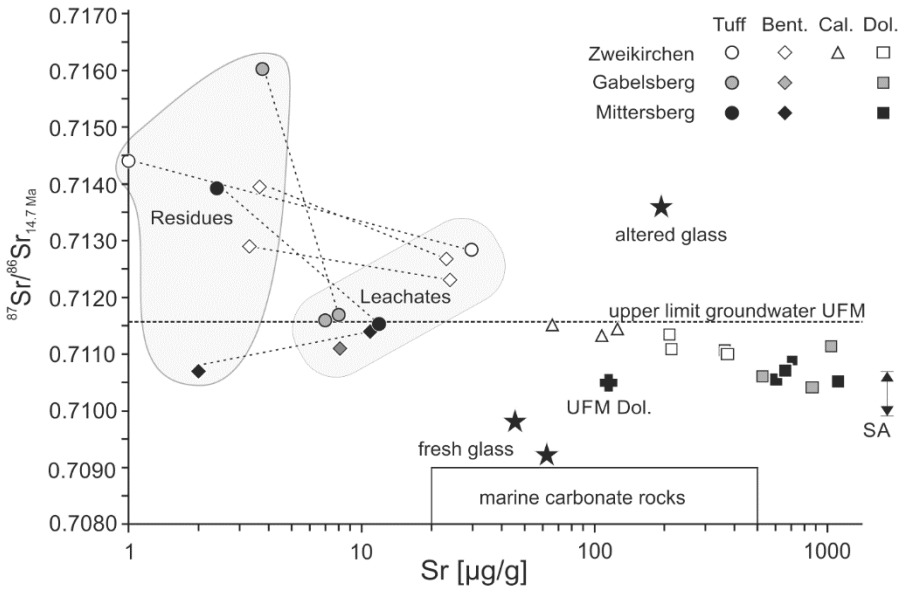

Fig. 6.10: The Sr concentrations plotted against Sr isotope ratios at 14.7 Ma of carbonates and smectites, compared to previous studies in the North Alpine Foreland Basin. Thin-dashed lines connect smectite leachate-residue pairs. Stars: volcanic glass shards, black cross: dolomite in the UFM (Graup et al., 1981); SA: Sr isotope ratio range of Sandelzhausen fossil mammal teeth enamel (Tütken & Vennemann, 2009); box – Mesozoic marine carbonates (McArthur et al., 2001; Zorlu, 2007; Geske et al., 2012). Upper limit of shallow (< 150 m) groundwater in the UFM (~ range 0.7080 to 0.712), according to data in Eichinger et al. (2007), Voerkelius et al. (2010) and Tütken et al. (2006). Reproduced with the permission of the Mineralogical Society of Great Britain & Ireland, from Köster et al. (2017).

As all leachates from the separated clay fractions have more radiogenic strontium isotope ratios than the associated early diagenetic carbonates and as this strontium is located in an exchangeable position of the smectite, the isotope composition of the leachates may not be representative for the initial $^{87}Sr/^{86}Sr$ during smectite formation. We therefore determined an isochron age using early diagenetic palustrine dolomites and the smectite residue (< 0.2 µm fraction) of a bentonite from Mittersberg (MB34) that does not contain detrital illitic components (Fig. 6.9). The calculated dolomite-smectite residue age of 14.7 ± 4.1 Ma is identical to the eruption age of the volcanic ash at 14.7 ± 0.2 Ma (Aziz et al., 2010) and its initial $^{87}Sr/^{86}Sr$ of 0.71069 (Table 6.4; Fig. 6.9) is identical to the average Sr isotope value (0.71070; based on values in Table 6.4) of palustrine dolomites.

Table 6.4: Rb and Sr content of carbonates (method A) and smectites (methods A and B), as well as Sr isotope ratios (method A) and leachate-residue model ages, including discrete (Ilt) and interstratified illite (Ilt/Sme) content according to Środoń (1980) and in brackets according to Moore & Reynolds (1997). Sme = Smectite, L = leachate, R = residue, A = method A, B = method B, * = discrete illite-rich samples.

Sample No.	Material	Rb	Sr	Rb/Sr	$^{87}Rb/^{86}Sr$	1 SD	$^{87}Sr/^{86}Sr$	2sigma	$^{87}Sr/^{86}Sr_{initial}$	L (A) + R (B) model		Ilt	Ilt/Sme
		µg/g	µg/g				measured	mean	at 14.7 Ma	Age [Ma]	$^{87}Sr/^{86}Sr_{initial}$	%	%
Zweikirchen													
ZW26	Dolomite	1.4	216	0.006	0.019	0.001	0.71108	0.000012					
ZW25	Dolomite	8.5	368	0.023	0.067	0.004	0.71107	0.000024					
ZW23	Dolomite	8.3	368	0.023	0.065	0.004	0.71105	0.000157					
ZW20	Dolomite	7.7	208	0.037	0.107	0.007	0.71135	0.000023					
ZW18	Calcite	13.3	126	0.106	0.306	0.020	0.71148	0.000020					
ZW17	Calcite	11.7	66	0.177	0.513	0.033	0.71154	0.000018					
ZW16	Calcite	10.6	109	0.097	0.282	0.018	0.71138	0.000013					
ZW50 L, A	Sme/Bentonite	1.4	23.0	0.061	0.176	0.011	0.71268	0.000019					
ZW50 R, A	Sme/Bentonite	7.0	<10				0.71522	0.000017					
ZW50 R, B	Sme/Bentonite	7.8	3.7	2.108	6.106	0.397	0.71522	0.000017	0.71395	30.2±4.6	0.71261±14		1 (3)
*ZW39 L, A	Sme/Tuff	4.1	30.0	0.137	0.396	0.026	0.71285	0.000013					
*ZW39 R, A	Sme/Tuff	23	<10				0.72286	0.000015					
*ZW39 R, B	Sme/Tuff	14.0	1.0	14.000	40.581	2.638	0.72286	0.000015	0.71440	17.6±2.3	0.71275±10	16	11 (23)
ZW48 L, A	Sme/Bentonite	1.3	24.0	0.054	0.157	0.010	0.71231	0.000041					
ZW48 R, A	Sme/Bentonite	8.0	<10				0.71537	0.000009					
ZW48 L, B	Sme/Bentonite	3.1	90.1	0.034	0.100	0.006	0.71231	0.000041					
ZW48 R, B	Sme/Bentonite	14.0	3.3	4.242	12.288	0.799	0.71537	0.000009	0.71281	17.7±2.9	0.71229±30		1 (4)
Mittersberg													
MB28	Dolomite	5.3	606	0.009	0.025	0.002	0.71059	0.000021					
MB27	Dolomite	7.8	686	0.011	0.033	0.002	0.71079	0.000020					
MB18	Dolomite	9.5	714	0.013	0.039	0.003	0.71090	0.000014					
MB12	Dolomite	6.9	1120	0.006	0.018	0.001	0.71052	0.000010					
MB12-24h	Dolomite						0.71054	0.000014					
*MB38 L, A	Sme/Tuff	3.1	12.0	0.258	0.748	0.049	0.71151	0.000025					
*MB38 R, A	Sme/Tuff	11.0	<10				0.71708	0.000014					

Table 6.4: Continued.

Sample No.	Material	Rb µg/g	Sr µg/g	Rb/Sr	$^{87}Rb/^{86}Sr$	1 SD	$^{87}Sr/^{86}Sr$ measured	2sigma mean	$^{87}Sr/^{86}Sr_{initial}$ at 14.7 Ma	L (A) + R (B) model Age [Ma]	$^{87}Sr/^{86}Sr_{initial}$	Ilt %	Ilt/Sme %
*MB38 R, B	Sme/Tuff	12.6	2.4	5.250	15.209	0.989	0.71708	0.000014	0.71391	27.1±3.8	0.71123±19	10	12 (9)
MB34 L, A	Sme/Bentonite	0.9	11.0	0.082	0.237	0.015	0.71139	0.000017					
MB34 R, A	Sme/Bentonite	4.0	<10				0.71401	0.000010					
MB34 R, B	Sme/Bentonite	11.0	2.0	5.500	15.929	1.035	0.71401	0.000010	0.71069	11.8±1.8	0.71135±18		1 (6)
Gabelsberg													
GB10	Dolomite	5.5	536	0.010	0.030	0.002	0.71061	0.000024					
GB08	Dolomite	6.5	1050	0.006	0.018	0.001	0.71113	0.001170					
GB07	Dolomite	4.8	874	0.005	0.016	0.001	0.71042	0.000024					
*GB41 L, A	Sme/altered Tuff	1.5	8.0	0.188	0.543	0.035	0.71167	0.000027					
*GB 41 R, B	Sme/altered Tuff	18.9	2.4	7.875								11	19 (16)
*GB37B L, A	Sme/Tuff	3.3	7.0	0.471	1.365	0.089	0.71160	0.000017					
*GB37B R, A	Sme/Tuff	20	<10				0.71961	0.000016					
*GB37B R, B	Sme/Tuff	22.6	3.8	5.947	17.234	1.120	0.71961	0.000016	0.71602	35.6±5.0	0.71091±21		
GB35A L, A	Sme/Bentonite	<0.8	<8				0.71108	0.000026					
GB35A L, B	Sme/Bentonite	0.3	27.8	0.011	0.031	0.002	0.71108	0.000026					
GB35A R, A	Sme/Bentonite	0.3	0.9	0.333		0.001							8 (0)

6.5 Discussion

Our geochemical data of dolomite, calcite and smectite in the Landshut bentonites provide some new insights into the fluid compositions and cation source(s) during carbonate formation and bentonitisation in a terrestrial environment. Köster & Gilg (2015) suggested that the fluids responsible for carbonate formation and possibly bentonite formation of the Landshut bentonites were broadly similar to present-day Ca-Mg-HCO_3^- groundwater in the UFM (molar Mg/Ca: 0.53 – 1.37; CO_3^{2-}/Ca^{2+}: 2.50 – 9.85, rarely ~ 25; Egger et al., 1983). However, the unusual high Sr concentrations of bentonite-hosted dolomites (up to 1120 µg/g; Table 6.4) observed in this study are difficult to reconcile with an unmodified freshwater composition (TDS: 0.28 g/L; Egger et al., 1983). Strontium-rich dolomites are often attributed to marginal marine lagoons, microbial-mediation or strongly evaporative environments (e.g., Sánchez-Román et al., 2011) where Sr content and Sr/Ca_m broadly correlate with salinity (Banner, 1995). Marine or terrestrial evaporite deposits with sulphates or halides, however, are absent in the North Alpine Foreland Basin and the UFM was never subject to marine incursions (Lemcke, 1973; Unger, 1996). Strontium-rich carbonate formation in saline environments during the Mid-Miocene have very rarely been reported in the North Alpine Foreland Basin. The alkaline-saline lake in the Mid-Miocene Ries impact crater (Arp & Wiesheu, 1997) and calcitic saline soils with minor dolomite and palygorskite at Mergelstetten (Kallis et al., 2000) are notable exceptions with the formation of carbonates with more than 2000 µg/g Sr. Evaporation processes, as expected in a palustrine setting, therefore must have played a significant role for dolomite formation in the Landshut bentonites.

6.5.1 Salinity and Mg/Ca of the dolomite and calcite forming water

The correlation of Sr/Ca_m with $\delta^{18}O$ values of the dolomites ($r^2 = 0.84$; Fig. 6.7c+d) indicates evaporation (Gasse et al., 1987; Banner, 1995) and suggests that the salinity of the water that precipitated dolomites is also correlated with Sr/Ca_m and Sr content (Folk & Land, 1975; Banner, 1995). The presence of lithium solely in Sr-rich palustrine dolomites (13 – 20 µg/g; Table 6.3) additionally implies elevated salinities (Gaines, 1980). The dolomites in the Landshut bentonites have Sr concentrations rather similar to carbonates from fresh to brackish lakes in the Palaeogene Madrid basin (202 – 496 µg/g Sr, Sr/Ca_m: 250 – 640; Bustillo et al., 2002), the Miocene La Roda 'white earths' (494 – 834 µg/g Sr, Sr/Ca_m: 1000 – 1500; García del Cura et al., 2001), both in Spain, or the Holocene lake sediments of the Northern Sahara (1033 – 3246 µg/g Sr, Sr/Ca_m: 1640 – 5580; Gasse et al., 1987).

The Sr/Ca_m of dolomite and calcite in the Landshut bentonites can be derived from those of shallow groundwater in the UFM (Wagner et al., 2003; Eichinger et al., 2007; Kainzmaier et al., 2007) using established Henderson and Kracek distribution factors for calcite (0.03 ± 0.2, Banner, 1995), non-stoichiometric dolomite (D_{Sr} = 0.0118 + ΔCa * 0.0039), and a high D_{Sr} of 0.051 for palustrine dolomite (Vahrenkamp & Swart, 1990), taking rapid precipitation and evaporation into account (Gaines, 1980; Lorens, 1981; Banner, 1995). A specific Sr-rich precursor phase such as Sr-rich aragonite (Tucker & Wright, 1990; Anadón et al., 2002) in the form of Charophyta remains in palustrine dolomite (Köster & Gilg, 2015) is therefore not required. Moreover, most Charophyta species are composed of calcite (Tucker & Wright, 1990) and residual aragonite or its dissolution fabric has never been observed in bentonites (Vogt, 1980; Köster & Gilg, 2015). In addition, bioclast-bearing (Gabelsberg) and bioclast-poor dolomites (Mittersberg) have identical Sr concentrations and $^{87}Sr/^{86}Sr$ (Table 6.4; Fig. 6.10) indicating the same Sr sources.

Sánchez-Román et al. (2011) recently reported high Nernst (22 – 37), and Henderson and Kracek Sr partition coefficients (0.12 – 0.22) for microbial-mediated dolomites. Dolo-micritic grains and aggregates resembling microbial remains were observed in the Landshut bentonites (Köster & Gilg, 2015). The low cation ordering d_{015}/d_{110} ratios of dolomite, its non-stoichiometric composition, and framboidal pyrite in bluish bentonite (Fig. 6.2; Fig. 6.4b; Ulbig, 1994) that could be related to bacterial sulphate reduction (e.g. van Lith et al., 2003) might be suggestive of microbial mediation for dolomite formation. Nonetheless, dolo-micrite also forms by rapid inorganic precipitation (Banner, 1995). Granting that microbial activity certainly occurred in palaeosols of the UFM (Schmid, 2002) and probably was beneficial for dolomite formation (e.g. Sánchez-Román et al., 2011), we still consider it a minor factor for the observed Sr enrichment in the palustrine dolomites, as the $\delta^{13}C$ values (-7.3 ± 0.3 ‰, 1 SD; Köster & Gilg, 2015) of dolomites are inconsistent with typical organic derived microbial carbon isotope values, i.e. too low for fermentation processes but slightly too high for sulphate reduction (Nelson & Smith, 1996), and oxygen isotope enrichments cannot be explained.

Assuming a starting salinity (TDS) of 0.28 g/L in water (Egger et al., 1983), a Sr/Ca_m of ~ 80 (Wagner et al., 2003) for calcite-precipitating water (Table 6.5) and a linear relationship of salinity with Sr/Ca_m, we calculate salinities of 2.3 to 6.4 g/L during dolomite precipitation, with extreme values of 15.3 g/L in palustrine settings (Table 6.5) most affected by evaporation. These salinities are consistent with dolomite formation in lacustrine environments and in the range of dolomite-precipitating brackish waters of Lake Balaton (0.5 g/L; higher during playa-like periods), Lake Neusiedl (1.5 g/L), and Lake Specchio di Venere (16.0 g/L) (Last, 1990).

As both the molar Mg/Ca and the salinity of the fluid exert a major control on dolomite precipitated from it (Folk & Land, 1975) even in non-evaporite-bearing environments (Last, 1990) we can use our results to estimate the molar Mg/Ca of the dolomite precipitating water using the Mg/Ca–salinity relationship of Folk & Land (1975). We derive a molar Mg/Ca of 2 to 5, assuming that factors such as temperature, alkalinity or pH are either negligible or constant. The molar Mg/Ca is consistent with dolomite-forming lacustrine environments such as Lake Balaton during dry periods (1.5 – 3.5; Tompa et al., 2014) and water in its sediment pore-space (7 – 12; Müller et al., 1972), and water of Lake Neusiedl (7.9; Schroll & Wieden, 1960), suggesting that our Mg/Ca estimates are realistic. The molar Mg/Ca of 2 to 5 for dolomite precipitating water is also coherent with the calcium-rich composition of dolomites (Folk & Land, 1975).

Table 6.5: 10^6*(Sr/Ca) ratios of calcites and dolomites, and salinities derived using a freshwater salinity of 0.28 g/L for waters precipitating calcite (from Egger et al., 1983).

	Median	Mean	Min.	Max.	Median	Mean
	10^6*(Sr/Ca) molar				SAL (g/L)	
Pedogenic calcite	81	78	27	128	0.28	0.28
Groundwater calcite	83	88	9	224	0.28	0.28
Palustrine dolomite	1513	1837	894	4379	5.30	6.43
Pedogenic dolomite	534	651	435	1042	1.87	2.28

The molar Mg/Ca of water in pedogenic and groundwater settings precipitating calcite was determined using a linear temperature-dependant relationship that relates the Mg/Ca of calcite to that of the water it formed from (Last, 1980). We additionally used the salinity–Mg/Ca diagram of Folk & Land (1975) to estimate the Mg/Ca of calcite precipitating water. These two methods yield molar Mg/Ca of 0.8 to 1.8 at 15°C to 31°C (Köster & Gilg, 2015) and of 1.0 respectively. Both results are consistent with the Mg/Ca of waters in the UFM (range 0.53 – 1.37; Egger et al., 1983), indicating that calcites in bentonites precipitated from largely unmodified soil and groundwater.

6.5.2 Redox sensitive elements

Dolomites and calcites from oxidised, intermediate and reduced (Fig. 6.2, Fig. 6.3) bentonites have highly contrasting Mn concentrations with calcites generally being enriched in Mn relative to dolomites (Table 6.3). The contrasting compositions of calcites and dolomites suggests distinct fluid compositions as the preferential inclusion of Mn into Mg-sites would produce rather Mn-enriched dolomite (Kretz, 1982) if they formed from the same fluid.

Pyrite-bearing blue bentonites from the Zweikirchen deposit contain groundwater calcites that are highly enriched in Mn (2880 – 4720 µg/g) but have low U concentrations (Table 6.3). As Mn^{2+} is water-soluble in reducing environments whereas uranium is not, calcites will be enriched in Mn^{2+} if precipitated from such water but will incorporate little uranium. The composition of our calcites therefore indicates reducing conditions and/or a high Mn availability, and possibly slow precipitation rates (Rimstidt et al., 1998; Dromgoole & Walter, 1990), as suggested by low $\delta^{13}C$ values (Fig 6e-f) and redox limits (~ 200 µg/g Mn) defined by Lohmann (1988). However, the large range of Mn concentrations (37 – 4839 µg/g) in calcites examined by p-XRF (Fig. 6.7a-f; Appendix 6.2) suggests highly variable redox conditions during calcite formation in bentonites, as indicated by variable REE+Y patterns (Fig. 6.8b) and contrasting Ce anomalies, with negative Ce anomalies indicating less reducing to oxidising conditions (Möller et al., 1984; Bau & Möller, 1992). The presence of Mn-poor calcite-spar (Appendix 6.2; Fig. 6.4d) in grey-brown bentonite from Hader (31 – 282 µg/g; Fig. 6.3) and calcites with high and low Mn concentrations in yellow bentonites of Gabelsberg and Zweikirchen (Appendix 6.2, Fig. 6.2) confirms later oxidation events because Mn-rich calcites cannot form simultaneously with oxidised (yellow) bentonite. So although Mn-rich calcites in pyrite-bearing blue bentonites are indicative of some cogenetic calcite and bentonite formation in reducing waters, Mn-rich and Mn-poor calcites in oxidised bentonites require contrasting redox conditions for their formation (Tucker & Wright, 1990; Lohmann, 1988), and indicate at least two calcite generations.

The down-section increasing Mn concentrations (353 – 1700 µg/g; Table 6.3) in pedogenic dolomites of the Zweikirchen deposit point to increasingly reducing conditions and higher Mn availability in soils with depth, consistent with positive Ce anomalies and REE+Y patterns (Fig. 6.8b). We note that groundwater calcites in the lower parts of the Zweikirchen deposit have even higher Mn concentrations (2880 – 4720 µg/g) than pedogenic dolomites (Möller et al., 1984; Bau & Möller, 1992) at the same locality, consistent with increasingly reducing conditions with depth.

Palustrine dolomite have the lowest Mn concentrations (305 – 580 µg/g; Table 6.3) and show less pronounced (MB) or absent (GB) down-ward trends in Mn content. The Mn concentrations and low $\delta^{13}C$ values of the palustrine dolomites (-7.3 ± 0.3 ‰, 1 SD; Köster & Gilg, 2015) are similar to lacustrine La Roda 'white earths' formed in oxic to suboxic environments (García del Cura et al., 2001). The systematically negative Ce anomalies (Fig. 6.8a) and high U concentrations (2.3 – 13.6 µg/g; Table 6.3) thus point to rather oxidising conditions during dolomite precipitation.

6.5.3 Strontium provenance for carbonates

Dolomites, calcites and the smectite leachates have all very low Rb/Sr and the measured $^{87}Sr/^{86}Sr$ (Table 6.4) do therefore not require any age corrections. The $^{87}Sr/^{86}Sr$ of the Sr-rich palustrine dolomites from the two studied deposits about 12 km apart are very homogeneous (0.71052 – 0.71113) and only slightly less radiogenic than the pedogenic dolomites from the Zweikirchen deposit (0.71105 – 0.71135). Both are significantly more radiogenic than the unaltered volcanic glasses (~0.7098) at 14.7 Ma that contain only 40 µg/g Sr (Horn et al., 1985) and therefore indicate that Sr and by inference also Ca and Mg was not derived from volcanic glasses but introduced from the surrounding sedimentary environment. The Sr isotope values of our dolomites are similar to those of early diagenetic dolomite unrelated to bentonite in the UFM (Horn et al., 1985) and mammal tooth enamel from the Sandelzhausen fossil site, situated 3.5 km north (Fig. 6.1) of Mittersberg (Tütken & Vennemann, 2009). The Sr isotopic compositions of the UFM dolomite and fossil tooth were interpreted by Graup et al. (1981) and by Tütken & Vennemann (2009) as representative for Miocene surface sediments and waters. The $^{87}Sr/^{86}Sr$ of the Sr-poor groundwater calcites at the Zweikirchen deposit are, however, more radiogenic than the pedogenic dolomites from the same site (Fig. 6.10). This indicates that two distinct fluids were involved in the precipitation of the two carbonate minerals at this site reinforcing the conclusions from Sr and Mn trace element chemical data.

The dolomites and calcites also reveal co-varying $^{87}Sr/^{86}Sr$, Sr concentrations, and $\delta^{18}O$ values (Fig. 6.11). This emphasises contrasting Sr sources and also suggests two end-members: a generally Sr-rich brackish surface water with low $^{87}Sr/^{86}Sr$ similar to the ratios in palustrine dolomites (with a mean of ~ 0.71070 derived from Table 6.4) and a dilute groundwater with more radiogenic Sr and $^{87}Sr/^{86}Sr$ equal or higher than those of calcites (≥ 0.71150 derived from the values Table 6.4).

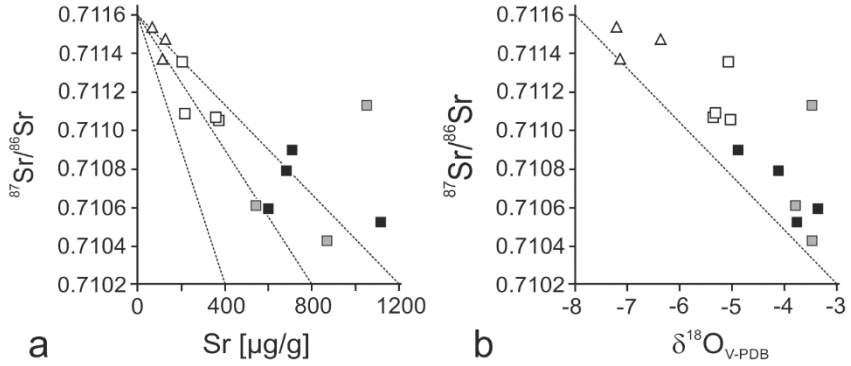

Fig. 6.11: Covariance of $^{87}Sr/^{86}Sr$ with a) Sr concentration and b) $\delta^{18}O$ values (from Köster & Gilg, 2015). Triangles (white): calcite, Squares: pedogenic (white) and palustrine dolomite (grey and black). Reproduced with the permission of the Mineralogical Society of Great Britain & Ireland, from Köster et al. (2017).

The Sr isotope values of dolomites and calcites in bentonites are within the range of $^{87}Sr/^{86}Sr$ for sediments and ground waters of the UFM in the North Alpine Foreland Basin (0.708 – 0.713; Tütken et al., 2006; Eichinger et al., 2007; Voerkelius et al., 2010; Waber et al., 2014) and consistent with the high $^{87}Sr/^{86}Sr$ (> 0.710) of sediments in the Eastern Molasse basin (Tütken & Vennemann, 2009). Here, the $^{87}Sr/^{86}Sr$ of waters in the UFM mirror the composition of the sediments, with Sr having high $^{87}Sr/^{86}Sr$ derived from silicate rocks of the Variscan basement (crystalline basement rocks of the Ries impact: 0.7100 – 0.7180 and 0.7216 – 0.7236 in Graup et al., 1981; Horn et al., 1985; plutonic rocks of the Bavarian Forest: 0.70881 – 0.74060; Siebel et al., 2005; Köhler et al., 2008) and Sr with low $^{87}Sr/^{86}Sr$ derived from lime- and dolostones of the Mesozoic cover both in Alps and the South German Block (0.70835 to 0.70965; McArthur et al., 2001; Zorlu, 2007; Geske et al., 2012).

High weathering rates of lime- and dolostones clasts in soils profoundly affect the Sr isotopic composition of water even in silicate-rich sediments (Blum et al., 1998) because of the prevailing release of Sr from carbonates (Clow et al., 1997). The wide-spread dissolution and precipitation of carbonates in sediments (Egger et al., 1983) and paleosols of the UFM (Schmid, 2002) is therefore responsible for both the formation of Ca-Mg-HCO_3 waters (Egger et al., 1983) and a disparate release of Sr from carbonate weathering in the UFM. The rapid weathering of dolomite in soils additionally is a major Mg source that can produce waters with high molar Mg/Ca (~ 2.0) in dolomite-bearing, mixed carbonate-siliciclastic sediments (Jin et al., 2008).

The low $^{87}Sr/^{86}Sr$ (~ 0.71070) in our dolomites therefore argue for Sr predominately but not exclusively derived from lime- and dolostones whereas the higher $^{87}Sr/^{86}Sr$ (~ 0.71150) of calcites point to more radiogenic Sr from silicate weathering, as confirmed by high Mn and Rb contents (Table 6.3; Table 6.4), and high Rb/Sr (Table 6.4). The latter point to Rb/Sr of groundwater in carbonate-free, siliciclastic sediments of the UFM (carbonate-free: 0.0266; carbonate-bearing: 0.0023 and 0.0025, Wagner et al., 2003; Kainzmaier et al., 2007).

6.5.4 Strontium isotope geochemistry of smectites and carbonates, and Rb-Sr dating

Although the Sr content in smectites (< 0.2 µm fractions) is mostly concentrated in the exchangeable interlayer and is much lower than in the associated carbonates, the $^{87}Sr/^{86}Sr$ are much higher (Fig 6.10; Table 6.4) than those of the soil and groundwater carbonates (Fig. 6.4a, c, d). This strongly suggests that the interlayer Sr in the smectites has partly or completely exchanged after carbonate formation with more radiogenic fluids than those involved in carbonate precipitation.

This post-formational interlayer exchange is corroborated by a comparison of the molar Mg/Ca (MB and GB: 0.59 ± 0.21; ZW: 1.15 ± 0.21) in the exchangeable interlayer site with the Mg/Ca (2 – 5) estimated for the dolomite precipitating fluid, assuming a cogenetic origin of dolomite and bentonite (Köster & Gilg, 2015). The molar Mg/Ca of the smectite leachates (< 0.2 µm fractions) are in equilibrium with a water having a molar Mg/Ca of 0.9 to 1.5. These values are lower than the Mg/Ca values (2 – 5) estimated for the fluid involved in dolomite formation even in consideration of preferential Ca uptake into the smectite interlayer (Laudelout et al., 1968; Sayles & Mangelsdorf, 1979), and are more similar to values (0.8 – 1.8) estimated for the water(s) that precipitated calcite. The chemical (Sr, Mg, Ca) and isotopic ($^{87}Sr/^{86}Sr$) compositions of smectite leachates are therefore not indicative of the fluids involved in bentonite formation, nor are they related to dolomite precipitation in bentonites.

This post-formational interlayer cation exchange with more radiogenic Sr has influence on the smectite leachate-residue model ages of the < 0.2 µm fractions yielding younger apparent ages. Nevertheless almost all < 0.2 µm fractions reveal smectite leachate–residue ages (35.5 – 17.5 Ma; Table 6.4) in excess of the depositional age of the volcanic ash (14.7 Ma ± 0.2 Ma, Aziz et al., 2010). Therefore, an illitic component consisting of discrete illite and/or R0 illite-smectite (Table 6.1 and 2; Fig. 6.5) is most likely responsible for the high Rb/Sr in the smectite residues (2.1 to 14.0; Table 6.4) and also the excess ages. Potential contaminants are detrital sedimentary clays in the UFM or fine-fractions of shales and limestones from the base of the Northern Calcareous Alps that have high $^{87}Sr/^{86}Sr_{14.7\ Ma}$ and Rb/Sr (Kralik, 1983; Horn et al., 1985).

However, a single bentonite sample (MB34) from the Mittersberg deposit (Fig. 6.1; Fig. 6.2) not containing detrital illitic components is characterised by the absence of discrete illite and a low interstratified illite (<10%) in smectite content (Table 6.2; Fig. 6.5). Both smectite leachate-residue (11.8 ± 1.5 Ma) and dolomite-residue models (14.7 ± 4.1 Ma) indicate an age (Fig. 6.9; Table 6.4) that postdates ash deposition.

This illite-poor illite-smectite in sample MB 34 and possibly also in samples containing older detrital illitic components could have been formed by illitisation of smectite during wetting and drying cycles in the palustrine environment (e.g., Eberl et al., 1986; Hugget & Cuadros, 2005) or even directly from the volcanic glass (Gilg et al., 2003). The syngenetic dolomite-smectite age model and the elevated Li concentrations in both the palustrine dolomites and the smectite residues (~ 20 µg/g; Table 6.3) indicate a cogenetic formation from Li-bearing evaporated fluids, and thus an onset of bentonitisation during dolomite formation. The Rb-Sr data (Fig. 6.9) also suggest that bentonitisation of the volcanic ash in the Landshut bentonites occurred not later than 4 m.y. after deposition.

6.6 Bentonite and carbonate formation

We propose two modes to explain dolomite and calcite formation in the Landshut bentonites, as well as the onset of bentonitisation (Fig. 6.12). Although these modes may resemble features of topographic "highs" and "lows" suggested by Ulbig (1994, 1999) they are based on the fluvial-lacustrine depositional environment of the anastomosing to braided river system and associated palaeosols of the UFM (Schmid, 2002; Maurer & Buchner, 2007). This circumvents the problematic preservation of unconsolidated volcanic ash on topographic "highs" (Ulbig, 1994) in a strongly seasonal climate and the inherent dryness of such topographic "highs" (Böhme et al., 2007) that contradicts the sedimentological evidence of moist soils and wetlands (Unger, 1996; Schmid, 2002; Maurer & Buchner, 2007; Aziz et al., 2010).

1) Palustrine deposits, such as Mittersberg and Gabelsberg, have a pronounced asymmetric character with tuff and/or dolomite in the upper part but bentonite with or without carbonates in the lower part above a clayey footwall (Fig. 6.12). Deep reaching root features in partially altered tuffs and bentonites, and modern rooting depths (Canadell et al., 1996) of sclerophyllous (5.2 ± 0.8m), tropical (7.3 ± 2.8m) and temperate deciduous forest and shrubland (2.9 ± 0.9m) resembling Miocene vegetation (Böhme et al., 2007) imply strict surface vicinity of the bentonite deposits during the onset of bentonite and carbonate formation. The elevated Li concentrations (~ 20 µg/g; Table 6.3) and Sr isotope data of smectite residue (especially MB34; Table 6.4; Fig. 6.9) and palustrine dolomites strongly suggest a cogenetic origin from the same evaporated Li-enriched fluid with low $^{87}Sr/^{86}Sr$ (~ 0.71070), and thus links smectite to dolomite formation. The formation of dolomite and bentonite in floodplains, ponds or wetlands therefore occurred in brackish evaporated surface waters with a molar Mg/Ca of 2 to 5, but a fluid with a more radiogenic Sr isotope composition (Fig. 6.10) was later involved in cation exchange reactions. A combination of insufficient leaching of K from the K_2O-rich glass (Ulbig, 1994) due to frequent wet-dry cycles (Eberl et al., 1986, 1993) and cyclic water-logging in palustrine deposits (Köster & Gilg, 2015) favouring a return to reducing conditions could have led to the incipient illitisation of smectite and formation of illite-poor R0 illite-smectite, similar to observations in calcareous palaeosols of the UFM (Stanjek & Marchel, 2008), though we cannot exclude the direct formation of illite-poor R0 illite-smectite from the K-rich glass. Bentonitisation was therefore limited to phreatic horizons permanently saturated with brackish, Sr-rich and Li-bearing water and probably isolated against dilute groundwater having more radiogenic Sr by the clayey footwalls (Fig. 6.2).

2) Pedogenic and groundwater (Fig. 6.12) dominated deposits, such as Zweikirchen, have the characteristic symmetry of bentonite – tuff – bentonite (Vogt, 1980) hosted by sand or gravel. We think that this is the result of its more protected alteration setting (Fig. 6.12) that has less evaporation and less risk of desiccation to dryness as the palustrine environments, indicated by lower $\delta^{13}C$ and $\delta^{18}O$ values (Fig. 6.7; and Köster & Gilg, 2015), lower Sr concentrations but higher Mn, Rb/Sr and $^{87}Sr/^{86}Sr$ (Table 6.3; Table 6.4; Fig. 6.10). Dolomite and calcite are abundant but calcites dominate the lower horizons. The lower parts of the deposits (Fig. 6.2; Fig. 6.12) were continuously below reducing groundwater levels while water levels fluctuated at the top (Köster & Gilg, 2015). Infiltration of surface water and significant evaporation (Fig. 6.12) were nevertheless essential for the precipitation of dolomite. In contrast, calcite formation and bentonitisation occurred in the predominantly saturated zone from waters similar to recent reducing groundwater in the UFM. Some Mn-poor calcites (Table 6.3) formed during later oxidation events in the now yellow bentonite, possibly from the same waters that were involved in post-formational cation exchange reactions with the smectite interlayer (Fig. 6.10).

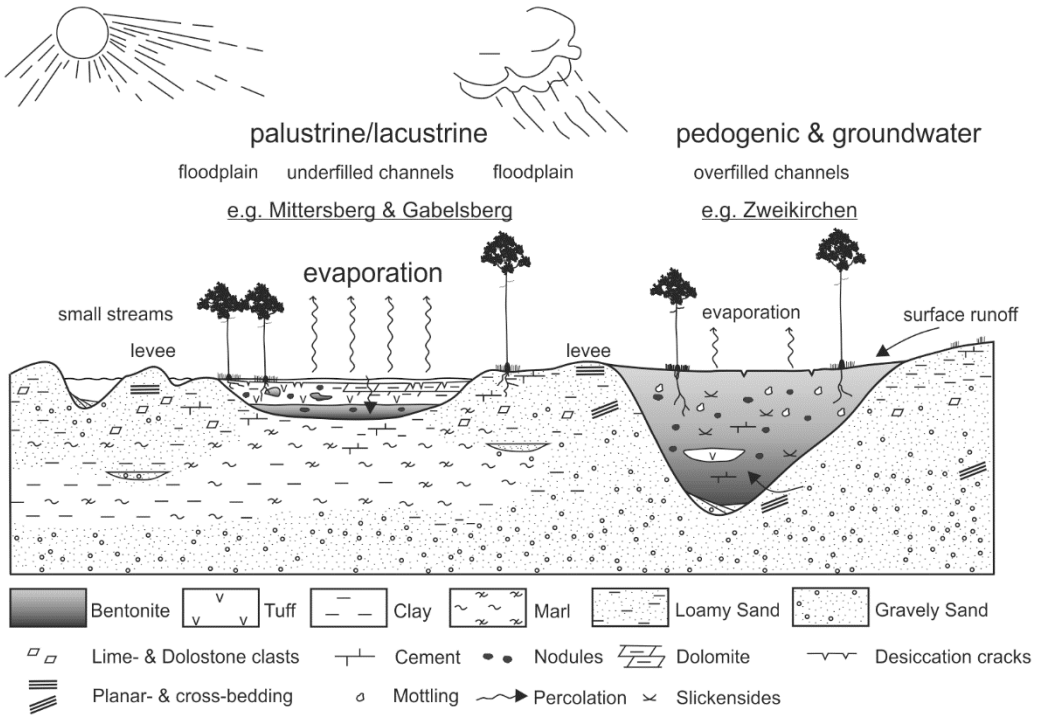

Fig. 6.12: Dolomite and calcite formation in bentonites in the alteration and depositional context of the fluviatile-lacustrine environment of the UFM. Not to scale! Reproduced with the permission of the Mineralogical Society of Great Britain & Ireland, from Köster et al. (2017).

6.7 Summary

The major and trace element geochemistry including Sr isotopes of carbonates and smectites from the terrestrial Landshut bentonites in Germany were systematically examined to explore fluid composition and cation provenance, and clearly reveal that two distinct fluids were involved in dolomite and calcite formation. Strontium, calcium and magnesium for carbonate and bentonite formation were re-mobilised by carbonate and silicate weathering in soils and from subsurface sediments in the North Alpine Foreland Basin. Dolomites precipitated from evaporated surface water with variable salinity and high molar Mg/Ca. Calcite formation was restricted to dilute, both oxidising and reducing ground- and soil waters with low molar Mg/Ca. Dolomite-rich palustrine environments received a larger contribution of Sr from lime- and dolostone weathering, whereas pedogenic and groundwater settings are characterised by more radiogenic Sr from silicate weathering. The original interlayer cation composition in all smectites appears not to be fully preserved and was at least in part replaced with cations from more radiogenic, younger groundwater. Most < 0.2 µm fractions separated from bentonites still contain detrital illitic components. However, a < 0.2 µm fraction of the bentonite (MB34) from Mittersberg that contains no detrital illitic material has been dated at 14.7 ± 4.1 Ma using the Rb-Sr method on the acid-leached < 0.2 µm fraction and cogenetic dolomites. The smectite-rich < 0.2 µm fraction of the Mittersberg bentonite contains some illitic components as an interstratified clay mineral that probably formed during pedogenesis in a palustrine environment, and/or directly from the alteration of a K-rich volcanic glass. The geochronological data show that the bentonitisation of volcanic ash in the terrestrial distal Landshut bentonites occurred within less than 4 million years. The Rb-Sr method therefore appears to be a new viable technique to date smectites and associated carbonates from terrestrial bentonites using acid-leach techniques, possibly even in combination with K-Ar dating.

Acknowledgements

This publication is part of the doctoral thesis of the first author at the Lehrstuhl für Ingenieurgeologie, Technische Universität München, Germany supervised by Prof. Dr. H. Albert Gilg. Dr. Stefan Hölzl is gratefully acknowledged for access to, help and advice with Sr isotope analyses in the ZERIN-lab at the Ries Crater Museum Nördlingen. Dr. Jürgen Bär at the Institut für Werkstoffkunde, Universität der Bundeswehr München, supported us with access to the field-emission scanning electron microscopy facility. The ICP-MS analyses of method B were determined by Dr. Klaus Simon at

the Institut für Geochemie, Georg-August-Universität Göttingen. We are also grateful for access to bentonite mines granted by Bernhard Ratzke, Süd-Chemie AG (now Clariant), and the cooperation of Ulrich Boehnke, S&B Industrial Minerals (now Imerys). We are very grateful for the efforts of the reviewers Javier Cuadros and Helge Stanjek whose comments improved the manuscript considerably and the useful remarks of the editor. The carbon, oxygen, and strontium isotope, and geochemical analyses were financially supported by a Society of Economic Geologists SEG Graduate Fellowship Award 2012.

Appendix Chapter 6

Appendix 6.1: Rare earth element and yttrium contents of dolomites, calcites, and purified smectites. All concentrations in µg/g. L = leachate, R = residue.

Name	La	Ce	Pr	Nd	Sm	Eu	Gd	Tb	Dy	Y	Ho	Er	Tm	Yb	ΣREEY
Dolomites															
ZW26	< 0.8	< 2	< 0.2	< 0.8	< 0.2	< 0.2	< 0.2	< 0.2	< 0.6	0.6	< 0.4	< 0.2	< 0.2	< 0.2	0.6
ZW25	1.0	2.0	0.2	1.0	0.2	< 0.2	1.0	< 0.2	< 0.6	1.3	< 0.4	< 0.2	< 0.2	< 0.2	6.7
ZW23	3.7	12.0	1.0	4.6	1.7	0.5	1.8	0.4	3.0	15.4	0.7	2.2	0.4	2.5	49.9
ZW20	5.7	12.0	1.3	5.4	1.6	0.4	1.5	0.3	2.0	15.3	0.5	1.5	0.2	1.5	49.2
MB28	6.6	12.0	1.8	7.8	2.4	0.4	2.8	0.6	4.5	27.7	1.0	3.6	0.6	4.0	75.8
MB27	8.2	15.0	2.2	9.2	2.8	0.5	2.8	0.6	4.3	24.9	1.0	3.4	0.6	4.1	79.6
MB18	8.5	18.0	2.1	8.7	2.6	0.5	2.5	0.6	4.1	23.5	0.9	3.2	0.5	3.8	79.5
MB12	8.4	14.0	2.3	9.4	3.0	0.5	3.1	0.8	5.4	29.7	1.2	4.3	0.7	5.0	87.8
GB07	18.0	34.0	4.0	14.9	3.6	0.5	3.2	0.6	3.6	16.7	0.7	2.2	0.4	2.4	104.8
GB08	7.7	14.0	2.0	8.6	2.8	0.4	2.6	0.6	4.6	23.9	1.0	3.7	0.7	5.1	77.7
GB10	8.5	16.0	2.2	8.9	2.3	0.4	2.2	0.4	2.8	19.1	0.6	2.1	0.3	2.2	68.0
Calcites															
ZW16	11.2	25.0	2.5	9.6	2.6	0.5	2.6	0.5	3.2	19.8	0.7	2.2	0.3	2.2	82.9
ZW17	9.9	16.0	1.6	6.2	1.5	0.3	1.6	0.3	1.8	17.5	0.4	1.4	0.2	1.4	60.1
ZW18	14.9	24.0	2.7	10.0	2.2	0.4	2.3	0.4	2.3	19.5	0.5	1.6	0.2	1.5	82.5
Smectites															
ZW39 L	2.8	6.0	0.6	2.1	0.5	< 0.2	0.5	< 0.2	< 0.6	2.2	< 0.4	0.2	< 0.2	0.2	15.1
ZW48 L	5.6	11.0	1.2	4.7	1.1	< 0.2	1.1	< 0.2	0.8	4.7	< 0.4	0.4	< 0.2	0.4	31.0
ZW50 L	5.6	14.0	1.3	5.0	1.1	< 0.2	1.1	< 0.2	0.8	4.4	< 0.4	0.4	< 0.2	0.4	34.1
GB35A L	< 0.8	< 2	< 0.2	< 0.8	< 0.2	< 0.2	< 0.2	< 0.2	< 0.6	0.5	< 0.4	< 0.2	< 0.2	< 0.2	0.5
GB37B L	4.6	9.0	1.1	4.0	0.9	< 0.2	0.9	< 0.2	0.6	3.4	< 0.4	0.3	< 0.2	0.3	25.1
GB41 L	7.6	14.0	1.8	6.8	1.4	0.2	1.6	0.2	1.3	6.3	< 0.4	0.6	< 0.2	0.5	42.3
MB34 L	3.6	8.0	0.9	3.5	0.7	< 0.2	0.7	< 0.2	< 0.6	2.3	< 0.4	0.2	< 0.2	0.2	20.1
MB38 L	3.4	7.0	0.9	3.3	0.7	< 0.2	0.7	< 0.2	< 0.6	2.7	< 0.4	0.3	< 0.2	0.2	19.2
ZW39 R	9.0	19.0	2.0	7.0	1.4	< 0.4	1.1	< 0.4	< 1	3.8	< 0.8	< 0.4	< 0.4	0.4	43.7
ZW48 R	7.0	14.0	1.7	6.0	1.4	< 0.4	1.2	< 0.4	1.0	8.9	< 0.8	0.9	< 0.4	1.0	43.1
ZW50 R	7.0	15.0	1.6	6.0	1.2	< 0.4	1.2	< 0.4	< 1	4.4	< 0.8	0.4	< 0.4	0.4	37.2
MB34 R	10.0	22.0	2.5	10.0	1.9	< 0.4	1.9	< 0.4	1.0	5.5	< 0.8	0.6	< 0.4	0.6	56.0
MB38 R	5.0	11.0	1.2	4.0	0.9	< 0.4	0.8	< 0.4	< 1	3.4	< 0.8	< 0.4	< 0.4	< 0.4	26.3
GB37B R	8.0	17.0	1.9	7.0	1.6	< 0.4	1.3	< 0.4	< 1	5.5	< 0.8	0.5	< 0.4	0.5	43.3

Appendix 6.2: Handheld X-ray fluorescence results and background-corrected counts per second (cps) of bulk carbonate samples

Sample No	Material	Facies	CaO	Mn	Sr	Ca	Mn	Sr
			wt%	µg/g	µg/g	cps 30s	cps 30s	cps 30s
M29	Dol	pal	23.2	318	659	63481	915	55215
M28	Dol	pal	25.2	459	678	68999	1321	56758
M27	Dol	pal	25.2	543	569	68796	1562	47649
M24	Dol	pal	32.3	1239	452	88300	3566	37863
M23	Dol	pal	27.9	606	518	76145	1745	43421
M18	Dol	pal	18.3	435	598	50146	1253	50115
M14	Dol	pal	19.0	678	1112	52045	1952	93100
M12b-Mn	Dol	pal	14.4	13592	1075	39365	39134	90036
M12	Dol	pal	20.2	623	1382	55129	1793	115738
M11	Dol	pal	19.3	1280	418	52667	3685	34979
M09B	Dol	pal	17.6	502	421	48216	1445	35254
M09	Dol	pal	8.6	1041	275	23464	2997	23041
M09	Dol	pal	17.5	484	415	47930	1393	34764
M07B	Dol	pal	20.6	567	453	56421	1632	37938
M07	Dol	pal	20.6	567	453	56421	1632	37938
M05	Dol	pal	28.1	879	530	76870	2532	44350
M04	Dol	pal	17.9	984	424	49022	2834	35489
GB10	Dol	pal	24.5	513	436	67113	1477	36543
GB08Blightrim	Dol	pal	20.3	486	576	55611	1398	48228
GB08Adarkcore	Dol	pal	24.1	436	777	65873	1254	65040
GB01	Dol	pal	30.5	655	443	83319	1885	37135
GB06	Cal	gw	0.9	455	62	2588	1310	5198
GB04core	Both	gw	32.2	311	143	87909	896	11960
GB03core	Dol	gw	26.8	1624	241	73171	4676	20184
GB17	Cal	gw	54.4	125	48	148744	361	4028
H01	Dol	ped	18.6	282	762	50796	811	63805
H16	Cal	gw	74.9	37	17	204798	106	1450
H08	Cal	gw	79.6	37	11	217564	106	903
H05	Cal	?	78.8	31	13	215334	89	1071
HF07	Dol	pal	19.9	1139	101	54435	3279	8493
HF06	Dol	pal	70.7	163	24	193218	470	1982
HF05b	Dol	pal	67.2	2078	42	183818	5982	3528
HF05a	Dol	pal	56.8	3512	43	155253	10111	3605
HF04b	Dol	pal	18.1	246	579	49597	707	48522
HF04a	Dol	pal	18.6	534	686	50809	1537	57413
HF03b	Dol	pal	1.1	345	46	2965	992	3856
HF03a	Dol	pal	16.3	13012	467	44627	37462	39071
HF02	Dol	pal	19.1	2178	485	52279	6270	40577
HF01	Dol	pal	22.5	1268	938	61572	3652	78546
LD05	Cal	ped	78.4	84	34	214341	241	2816

Appendix 6.2: Continued.

Sample No	Material	Facies	CaO	Mn	Sr	Ca	Mn	Sr
			wt%	µg/g	µg/g	cps 30s	cps 30s	cps 30s
LD04	Cal	ped	78.6	127	40	214853	365	3326
LD03	Cal	ped	58.0	407	33	158563	1172	2767
LD02	Cal	gw	71.2	466	104	194720	1341	8675
LD01	Cal	ped	40.3	1781	80	110189	5129	6720
RB04	Cal	ped	76.0	210	37	207714	605	3087
RB02	Dol	pal	20.5	298	1093	56140	858	91549
UZ05	Cal	gw	22.4	721	1115	61267	2077	93420
UZ04	Dol	gw	61.9	195	29	169268	561	2422
UZ03	Cal	?	22.9	729	1078	62505	2098	90251
UZ01	Dol	gw	27.2	762	652	74265	2194	54581
ZW29	Dol	ped	32.3	1411	262	88200	4061	21928
ZW02	Dol	ped	27.0	1430	356	73788	4118	29852
ZW26	Dol	ped	33.0	441	224	90111	1269	18773
ZW25	Dol	ped	40.1	332	278	109693	956	23324
ZW24	Cal	ped	51.9	7413	55	141871	21343	4636
ZW23	Dol	ped	27.8	1123	233	76123	3233	19483
ZW05	Dol	ped	11.6	1204	189	31769	3467	15870
ZW03	Dol	ped	49.9	4369	61	136341	12579	5084
ZW04	Cal	gw	53.7	4839	70	146787	13932	5843
ZW21	Cal	ped	52.2	4103	103	142727	11814	8585
ZW20	Dol	ped	27.0	1928	314	73894	5550	26328
ZW18	Cal	gw	36.8	3701	129	100707	10655	10810
ZW17	Cal	gw	44.5	1568	93	121781	4513	7795
ZW16	Cal	gw	38.3	4328	101	104778	12462	8480
ZW15	Cal	ped	43.5	1452	87	118911	4180	7273
ZW14	Cal	ped	45.6	3308	78	124633	9525	6573
ZW01	Cal	gw	72.0	158	13	196931	455	1105

CHAPTER SEVEN

7. Boron isotope geochemistry of smectites from sodium, magnesium and calcium bentonite deposits

This is an extended draft of a manuscript soon to be submitted to Geochimica et Cosmochimica Acta.

This research project was designed by Mathias H. Köster with input from H. Albert Gilg (Technische Universität München). Mathias H. Köster performed the sample processing, the X-ray diffraction measurements and analysis. PGAA and SIMS samples were also processes by Mathias H. Köster. After instruction by Lynda B. Williams Mathias H. Köster conducted the SIMS measurements. Some samples were ad-hoc measured for boron isotope values by Lynda B. Williams (Arizona State University). The SIMS interpretation was done by Mathias H. Köster. The PGAA measurements were conducted by Petra Kudejova and Zsolt Revay (FRM II research neutron source), with final sample analysis and refinement by Mathias H. Köster. The carbonate content for isotope analysis of carbonates was determined by Mathias H. Köster. Sample weighing and processing for carbon and oxygen stable isotope analysis was done by Mathias H. Köster, the stable isotope measurements were performed by Christoph Mayr (Ludwig-Maximilians Universität München & Friedrich-Alexander-Universität Erlangen-Nürnberg). Mathias H. Köster drafted and wrote the manuscript, with editing and data verification by H. Albert Gilg, Lynda B. Williams and Petra Kudejova. Mathias H. Köster brought the manuscript into its final shape.

Abstract

The mineralogical, chemical and isotopic analyses of smectites from bentonite deposits with variable interlayer cation occupancies and from various depositional and formational environments reveal new insights into the boron sources and the fluids involved in bentonitization in marine and non-marine environments.

Smectites from bentonites have fixed, i.e. non-exchangeable, boron concentrations of 0.2 to 196 µg/g, with smectites from sodium bentonites having higher boron concentrations (> 30 µg/g) than those from magnesium or calcium bentonites. The examined smectites all have a small interstratified illitic component that has a major influence on boron concentrations, requiring the use of modified fluid-mineral boron partitioning coefficients. The modified fluid-mineral boron partitioning coefficients

indicate that bentonites formed from fluids of highly variable boron concentrations of < 0.1 mg/L B to more than 100 mg/L B, and at a chlorinity of 76.4 to more than 59,076 mg/L. The sodium bentonites formed from boron-rich saline fluids or brines whereas fluids involved in calcium and magnesium bentonite formation have a more variable composition.

The $\delta^{11}B$ values of the fixed boron in smectites reveal a range of -30.2 ‰ to +17.1 ‰. The smectites from terrestrial depositional settings have $\delta^{11}B$ values of about 0 ‰ to -30.2 ‰, whereas smectites from marine depositional settings have negative as well as positive $\delta^{11}B$ values. The boron isotope values indicate that all examined bentonites from terrestrial depositional settings but also many bentonites from marine depositional environments formed from basinal fluids or (hydrothermal) brines that experienced strong water-rock interaction, but not from unmodified seawater.

The boron isotope geochemistry of smectites is demonstrated to be a strong tool for elucidating the fluids involved in the formation of clay minerals deposits. It also has great potential for tracing fluids in other settings involving authigenic clay minerals such as sedimentary basins and crystalline rocks close to the surface, as well as man-made applications such as barriers in disposal sites for highly active nuclear waste.

7.1 Introduction

Bentonites are clay rocks predominantly comprised of smectites that generally form by the alteration of volcanic ash and pyroclastic rocks in marine, terrestrial, hydrothermal or diagenetic settings (Grim & Güven, 1978; Christidis & Huff, 2009). The smectites in bentonites have a distinct and exchangeable interlayer cation occupancy (Fig. 7.1) that can be used to classify bentonites as fully expandable Na-bentonites or the more common Ca- and Mg-bentonites that require acid or soda activation for use in specific applications (Grim & Güven, 1978; Odom, 1984; Murray, 2007). Fluid chemistry during bentonite formation and later, natural cation exchange reactions (Odom, 1984) are the likely cause for the characteristic interlayer cation occupancies – but the composition and types of waters involved in the formation of bentonites, e.g. seawater, freshwater, brines or hydrothermal fluids (Grim & Güven, 1978; Elzea & Murray 1990; Cadrin et al. 1995; Christidis & Huff, 2009), are only vaguely known.

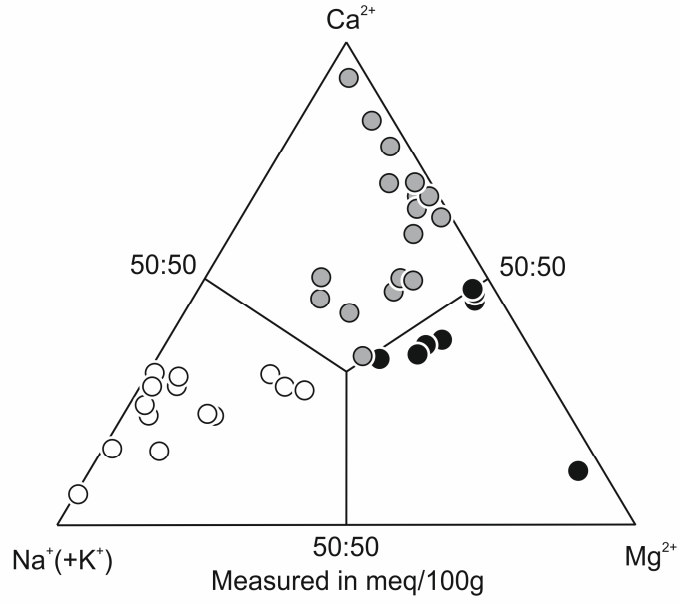

Fig. 7.1: Exchangeable cations in bentonites examined in consideration for use in the isolation of nuclear waste. Data from Kaufhold & Dohrmann (2008) and Dohrmann & Kaufhold (2010). Light grey: Na-bentonites: black: Mg-bentonites; and dark grey: Ca-bentonites.

Seawater is often cited as the main alteration fluid for many bentonite deposits (Grim & Güven, 1978), especially for deposits in marine depositional sequences and derived from Mg-poor, acidic parent material (Christidis, 1998; Berry, 1999; Christidis, 2008). However, stable H-O isotope data of smectites from many Na-bentonites in Cretaceous marine sedimentary rocks of Wyoming/Montana in the United States reflect the involvement of meteoric waters (Savin & Epstein, 1970; Taieb, 1990; Cadrin et al., 1995; Menegatti et al., 1999), whereas both seawater and meteoric fluids were probably involved in the formation of some Ca- and Mg-bentonite deposits on Milos Island in Greece (Christidis et al., 1995; Decher et al., 1996) and Cabo de Gata in Spain (Leone et al., 1983; Delgado, 1993; Caballero et al., 2005) that are located in the vicinity of the Mediterranean Sea. The Ca-(Mg)-bentonites in Southern Germany formed in a strictly terrestrial setting, consistent with their chemical composition as well as stable and radiogenic isotope values (Unger & Niemeyer, 1985a, b; Unger, 1999; Gilg, 2005; Aziz et al., 2010; Köster & Gilg, 2015; Bauer et al., 2016; Köster et al., 2017).

The existing stable H-O isotope data therefore seem to contradict geological and sedimentological evidence for some important bentonite deposits but are consistent for others. A satisfying model for the formation of Na-, Mg- and Ca-bentonites is therefore missing.

7.1.1 Boron isotope geochemistry

Boron is a highly mobile, conservative trace element that readily enters the fluid phase (Ellis & Mahon, 1964, 1967; Levinson, 1980) and broadly correlates with the salinity of the fluid (Vengosh et al., 1992; Lemarchand et al., 2015). Boron is therefore widely used for investigating water-rock interactions, weathering, evaporation processes, fluid origin, and mixing in low- or high-temperature geological settings (Spivack, 1986; Spivack et al., 1987; Vengosh et al., 1991; Barth, 1993; Morell et al., 2008; Williams et al., 2001a, b, c; Xiao et al., 2013).

In low-temperature environments boron is removed from the fluid by the preferential incorporation into clay minerals (Goldschmidt & Peters, 1932; Goldberg & Arrhenius, 1958). Clay minerals therefore have higher boron concentrations compared to other authigenic minerals formed in low-temperature environments such as quartz, carbonates, or feldspars (Harder, 1970). Illite and illite-smectite usually are the clay minerals with the highest boron concentrations (100 to 2000 µg/g B). Boron concentrations decrease from smectite (5 to 300 µg/g B), via chlorite (~ 50 µg/g B) to kaolinite (10 to 30 µg/g B) (Harder, 1959, 1970; Couch, 1971; Keren & Muzeman, 1981; Keren & O'Connor, 1982; Palmer et al., 1987). Although the uptake of boron into clay minerals correlates with the boron concentration of the fluid (Frederickson & Reynolds, 1960; Couch & Grim, 1968; Brockamp, 1973; Keren & Muzeman, 1981; Keren & O'Connor, 1982; Zeibig et al., 1989); it is often strongly modified by temperature, pH, and the potassium content of the clay minerals (Couch, 1971; Palmer et al., 1987; Spivack et al., 1987; You et al., 1995, 1996).

Boron is incorporated into clay minerals as adsorbed boron, tetrahedral boron substituting for silicon in the silica tetrahedra and very small amounts of interlayer boron. Tetrahedrally coordinated boron from the solution is adsorbed onto mineral surfaces (although this lacks a good explanation due to the negative charge of the clay surfaces and the neutral or negative charge of the boron species) and edge sites (Couch & Grim, 1968; Schwarcz et al., 1969; Palmer et al., 1987). The adsorption of boron is controlled by the temperature and pH value of the fluid (Schwarzc et al., 1969; Keren & Muzeman, 1981; Keren & O'Connor, 1982; Palmer et al., 1987; You et al., 1995, 1996) and decreases to zero with increasing temperature (~120°C; You et al., 1996). Fluid pH is therefore the main control on boron adsorption at low temperature (Keren & Muzeman, 1981; Keren & O'Connor, 1982; You et al., 1995, 1996). Boron adsorption on smectite and illite therefore does not follow a simple, linear relationship with the concentration of boron in the solution (Keren & Muzeman, 1981; Keren & O'Connor, 1982). Boron adsorption coefficients of 1.54 (Spivack et al., 1987) as well as 1 to 5 have been proposed (Palmer et al., 1987). You et al. (1996) used empirical and experimental methods on bulk

sediments in the development of a boron adsorption coefficient that includes both temperature and pH, with a K_D = -3.84-0.020*T+0.88*pH (T < 120°C) for pelagic clays and a K_D = -1.38-0.008*T+0.59*pH (T < 120°C) for advanced degrees of diagenesis. Boron adsorption on clays in unmodified seawater (4.7 – 5.3 mg/L B; Vengosh et al., 1991) therefore produces clays with ~15 to ~20 µg/g of adsorbed boron, plus the inherited boron in detrital clay minerals.

Boron can also be trapped in the clay mineral interlayer during (re-)-crystallization (Williams et al., 2001a, b) in an unknown molecular form that includes tetrahedral and trigonal boron species (Williams & Hervig, 2002) – or sample processing in the laboratory. Little information is available on the fluid-interlayer boron exchange. Experimentally formed and natural illite-smectites have interlayer boron concentrations of 8 to 70 µg/g, compared to total boron concentrations of 55 to 210 µg/g (Williams & Hervig, 2002). Both the adsorbed and interlayer boron are very easily exchangeable (Schwarcz et al., 1969; Keren & Mezumen, 1981; Spivack, 1986; Palmer et al., 1987) and are not necessarily indicative of the fluids primarily involved in clay mineral formation (Williams et al., 2001a, b), but can be related to later overprints.

In contrast to the exchangeable boron, the tetrahedrally coordinated boron in the silica tetrahedra of clay minerals is firmly fixed by substituting for silicon (Williams et al., 2001a; Williams & Hervig, 2005) during crystal growth and crystallization (Couch & Grim, 1968; Palmer et al., 1987; Palmer & Swihart, 1996). The fixed boron either originates as adsorbed boron that slowly diffuses into tetrahedral sites during late diagenetic (T > 60°C) potassium uptake and illitization (Perry, 1972; Spivack et al., 1987) or boron that is directly incorporated during precipitation of authigenic clay minerals (Couch & Grim, 1968; Spivack & Edmond, 1987; Spivack et al., 1987; Palmer et al., 1987; Palmer & Swihart, 1996; Williams et al., 2001a). The fixed boron is not substantially changed by low-temperature geological processes (Frederickson & Reynolds, 1960; Adams et al., 1965); though can be affected by recrystallization and the formation of ordered R1 and R3 illite-smectite (Williams et al., 2001a, b). Partition coefficients for the non-exchangeable, fixed boron in clay mineral tetrahedra have not yet been experimentally determined (Simon et al., 2006). However, Spivack & Edmond (1987) used boron and $\delta^{18}O$ data of ocean basalts altered to smectite from Donelly et al. (1979) and Muehlenbach (1979) to determine fluid to smectite-rich bulk sediment boron distribution coefficients (33 at 1°C and 11 at 100°C in Smith et al., 1995). If the boron partition coefficients of Spivack & Edmond (1987) or You et al. (1996) can be applied to purified authigenic clay minerals has not yet been tested.

Despite the complex nature of boron uptake, boron content and isotopes in bulk rocks (Potter et al., 1963; Couch & Grim, 1968; Brockamp, 1973; Spivack & Edmond, 1987; Zeibig et al., 1989) and in clay minerals are a useful tool to trace fluids (e.g. boron content, salinity) during mineral neoformation,

illitization, or recrystallization (Harder, 1970; Williams et al., 2001a, b, c; Kopf et al., 2003; Xiao et al., 2013). The boron contents of bulk sediments dominated by detrital kaolinite with some smectite and illite (< 10 µg/g B; Zeibig et al., 1989), mineralogically unconstrained clayey sediments (< 40 µg/g B; Potter et al., 1963), and illite-rich shales (< 50 µg/g B; Shaw & Bugry, 1966) have been used to define freshwater versus saline water depositional environments. Studies on the boron uptake in authigenic marine smectites formed from aforementioned oceanic basalt (Sayles et al., 1975; Donnelly et al., 1979; Spivack et al., 1987) have also shown that boron is firmly incorporated from the fluid into silica tetrahedra during precipitation. These marine smectites have boron concentrations of 110 to 150 µg/g (Donelly et al., 1979; Spivack et al., 1987; Ishikawa & Nakamura, 1993; Smith et al., 1995), but it is unclear if this includes boron trapped in pore water, surface adsorbed, or inherited boron. Newly formed illitic layers in experimentally-formed illite-smectite have also been shown to fix boron from the fluid into silica tetrahedra (Williams et al., 2001a, b).

Bentonites consist of authigenic smectites and/or illite-smectites with, usually, few detrital minerals and a low discrete illite content (Grim & Güven, 1978). The boron content of bentonite-associated magmatic minerals such as biotite (1 to 53 µg/g B; Chris & Harder, 1969) and volcanic rocks (< 53 µg/g B; Leeman & Sisson, 1996) such as in the Los Trancos bentonite deposit (< 2 µg/g B, Linares et al., 1987) or the Idaho batholith (< 15 µg/g B; Leeman et al., 1992) is low compared to illite and smectite (Harder, 1959, 1970). Boron is easily mobilized from volcanic rocks by low-temperature chemical weathering (Spivack et al., 1987), with higher temperatures drastically enhancing mobilization (Ellis & Mahon, 1964, 1967; Reyes & Trompetter, 2012). Boron is also the most mobile trace element in bentonite deposits of Cabo de Gata in Spain. Here, only small amounts (3 to 34 %) of boron from the volcanic parent material were retained during bentonitization (Caballero et al., 1992, 2005). The high water-rock ratios of 6 to 13 for Milos (Christidis, 1998) and ~2300 for Cabo de Gata (Caballero et al., 1992, 2005) required for bentonitization strongly suggest that most of the boron in authigenic smectites from bentonites is sourced from the fluid, consistent with aforementioned marine smectites being in boron isotope equilibrium with seawater and not oceanic crust (Donelly et al., 1979; Spivack et al., 1987; Ishikawa & Nakamura, 1993). Authigenic smectite and illite-smectite therefore are the major sink of boron also in bentonites (Couch & Grim, 1968; Palmer et al., 1987; Williams et al. 2001a). Boron in smectites thus could be a good indicator of fluid chemistry, especially in combination with boron isotope values.

A large relative mass difference between ^{10}B and ^{11}B (Vengosh et al., 1991) and the coordination change of dissolved boron from dominantly trigonal in the solution (pH > 7) to tetrahedral in silicates is the reason for the preferential incorporation of ^{10}B into clay minerals and a large boron isotope

fractionation (Kakihana & Kotaka, 1977; Palmer et al., 1987). Natural minerals and fluids therefore show a large variation of $\delta^{11}B$ values from -70 ‰ (Williams & Hervig, 2004) to +75 ‰ (Hogan & Blum, 2003). The large differences in $\delta^{11}B$ values between fluids and rocks, e.g. seawater (+39.5 ‰; Spivack, 1986) and continental crust (~ 0 ‰, Schwarzc et al., 1969; about -7‰, Chaussidon & Albarede, 1992), and the redox inactive (Palmer et al., 1987; Tomascak, 2004) though pH susceptible fluid-mineral isotope fractionation (Kakihana & Kotaka, 1977; Palmer et al., 1987) make boron isotopes an interesting tracer of boron origin, especially because materials with similar boron content can have different boron sources (Spivack, 1986; Spivack et al., 1987; Vengosh et al., 1991; Williams et al., 2001a, b; Williams & Hervig, 2002; Hervig et al., 2002; Deyhle & Kopf, 2005; Pennisi et al., 2009).

A temperature dependent (1/T) fluid-mineral boron isotope fractionation was empirically evaluated by Williams (2000), Williams et al. (2001a, b) and Williams et al. (2007) based on boron substitution for silicon during the illitization of smectite, and assuming a trigonal (fluid) to tetrahedral (mineral) coordination change. The boron isotope fractionation was anchored at low temperature (Williams, 2000; Williams et al., 2001a, b) using the fluid-adsorbed boron isotope fractionation of Palmer et al. (1987) because boron isotope fractionation during the fixation of adsorbed boron into the silica tetrahedra is very small with only a few per mil points (Palmer et al., 1992; Williams & Hervig, 2002).

This fluid-mineral boron isotope fractionation can be applied to silicates that involve a coordination change from trigonal boron acid in a near-neutral fluid to the tetrahedrally fixed boron in the mineral. The $\delta^{11}B$ values of clay minerals can therefore be used to estimate the $\delta^{11}B$ value of fluids that clay minerals precipitated from or interacted with (Palmer et al., 1987; Williams et al. 2001a, b) below the dissociation point of boric acid (pKa: 9.2 for pure water; 8.6 for seawater; Hershey et al., 1986; Bassett, 1977). However, in alkaline fluids boron speciation changes from the dominant trigonal boric acid to the tetrahedral borate ion. This reduces the fluid-mineral isotope fractionation because there is no coordination change between the dissolved tetrahedral coordinated boron and tetrahedral fixed boron in silicates (Palmer et al. 1987; Hervig et al., 2002). As a consequence, the fluid-mineral boron fractionation decreases from ~32 ‰ at 25°C (Williams, 2000; Williams et al., 2001a, b; Williams et al., 2007) to a value between 18 ‰ and 0 ‰ for fluids dominated by tetrahedrally coordinated boron at strongly alkaline conditions (pH > 10) (Kakihana & Kotaka, 1977; Palmer et al., 1987; Palmer et al., 1992; Liu & Tossell, 2005). A simplified two end-member model for the fractionation of the two boron species yields a boron isotope fractionation of $\Delta^{11}B_{fluid\text{-}mineral} = (X_{B3}*1000\ln\alpha_3) + (X_{B4}*1000\ln\alpha_4)$, with the mole fractions of the two boron species depending on pH, temperature, and the pKa (Hershey et al., 1986; Dickson, 1990; Liu & Tossell, 2005; Zeebe, 2005).

7.1.2 Boron in natural fluids

The boron content of most natural fluids correlates with chlorinity (Fig. 7.2) and sodium content because of the relatively high solubility of these elements from the surrounding rocks (Ellis & Mahon, 1964, 1967; Palmer & Sturchio, 1990; Boschetti et al., 2014). Boron concentrations are additionally influenced by temperature, weathering, evaporation, and mixing of seawater or brines (Vengosh et al., 1991; Morell et al., 2008). Exceptions to the boron-chlorine relationship are steam-dominated geothermal systems (D'Amore et al., 1977; D'Amore & Truesdell, 1979; Arnórsson & Andresdottir, 1995; Bernard et al., 2011), salt dissolution brines (Kloppmann et al., 2001), and pervasive boron adsorption on clays (Schwarcz et al., 1969; Vengosh et al., 1991; Vengosh & Hendry, 2001).

Fluids such as seawater, groundwater, lake water, brines, or geothermal waters of a given geological setting thus have distinct boron concentrations (Fig. 7.2), as well as $\delta^{11}B$ values (Barth, 1993; Xiao et al., 2013) that can be used to investigate fluid composition and boron sources (Spivack, 1986; Spivack et al., 1987; Palmer & Sturchio, 1990; Vengosh et al., 1991; Vengosh & Hendry, 2001; Boschetti et al., 2014). Many of the aforementioned fluids are also potential alteration fluids involved in bentonite formation, and later cation exchange reactions (Grim & Güven, 1978; Christidis & Huff, 2009) and therefore of special interest to our study.

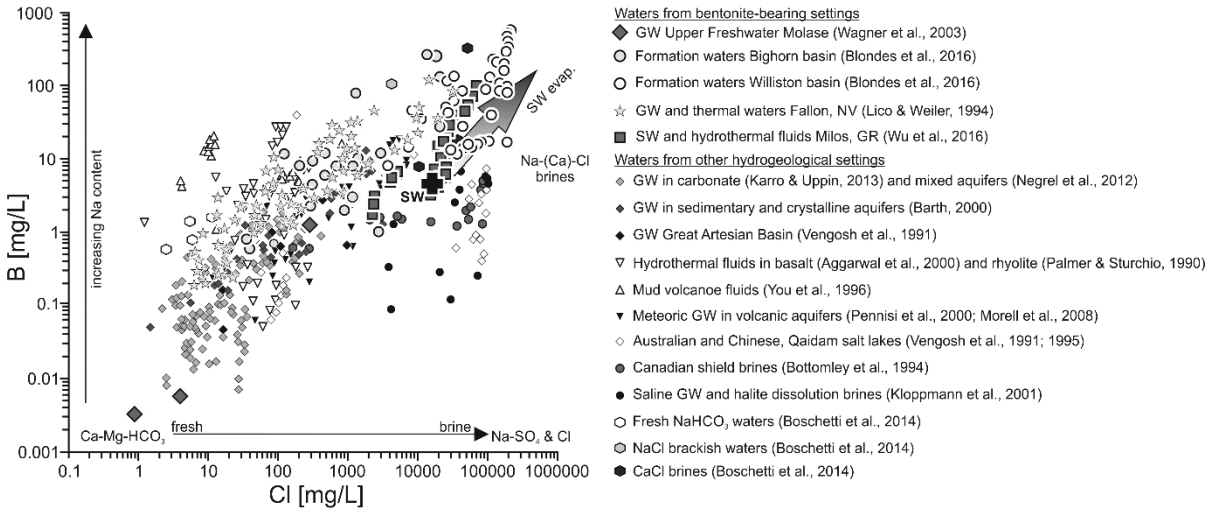

Fig. 7.2: The boron and chlorine concentrations of fluids from various hydrogeological settings. GW = groundwater, SW = seawater. SW values according to Vengosh et al. (1992) and Foster et al. (2010).

7.1.3 Aim and motivation

In this study we aim to use boron as a tool for elucidating the formation of bentonite deposits. We use smectite separates (< 0.2 µm fractions) of bentonites to trace a) the boron content and chlorinity/salinity of the bentonite-forming fluids (fixed boron content), b) the origin of the fluids ($\delta^{11}B$), and c) later diagenetic modifications (exchangeable boron and $\delta^{11}B$) in order to trace the fluids involved in bentonitization.

7.2 Bentonite deposits in this study

Bentonite samples are from Europe, the Caucasus region, North and South America, and were chosen because they originate from contrasting depositional and formational environments. Bentonite samples from Southern Germany (ZW48, ZW50, and MB34) were part of studies by Köster & Gilg (2015) and Köster et al. (2017). The Georgian (B17), Argentinian (B23), Armenian (B31) and Nevada (B51) bentonite samples have previously been studied by the Federal Institute for Geosciences and Natural Resources in Germany (Kaufhold & Dohrmann, 2008; Dohrmann & Kaufhold, 2010). Warr et al. (2016) supplied the Lago Pellegrini samples. Descriptions of bentonite deposits and, where available, the boron content and isotope values of host or parent rocks and local fluids are presented in Table 7.1 and Figure 7.3.

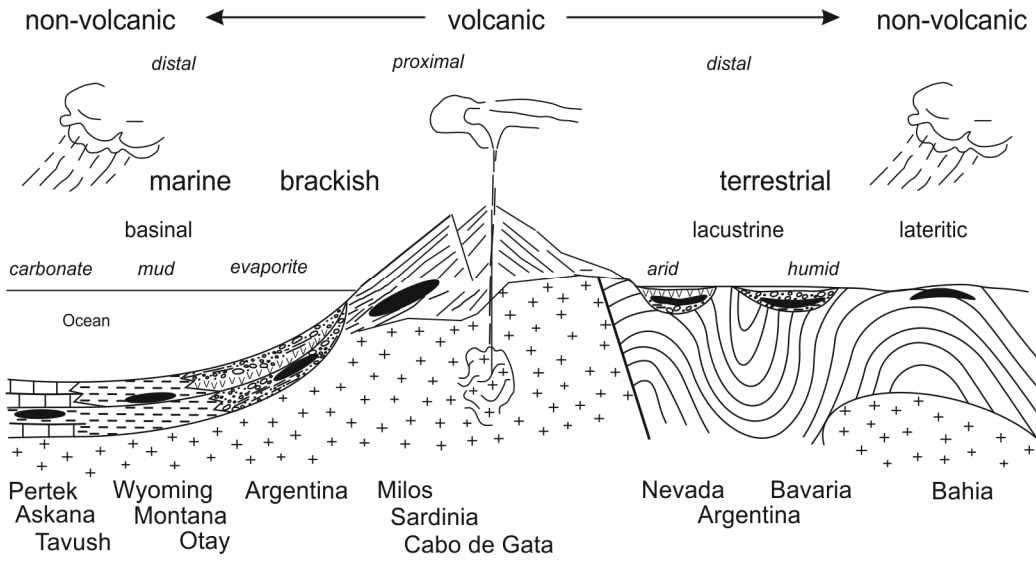

Fig. 7.3: Geological sketch of the depositional and formational environments encountered in the various bentonite deposits as described in the literature used for Table 7.1.

Table 7.1: Geological, mineralogical, and chemical information on the examined bentonite deposits. n.a. = no information available

Deposit	Location	Cations	Host lithology	Parent material	Depositional environment	Alteration environment
Dominantly marine depositional settings						
Angeria & Zoulias	Milos, GR	Ca, Mg	andesitic to dacitic pyroclastics	andesitic to dacitic	proximal, marine volcano-sedimentary	hydrothermal and/or seawater
Askana	Rep. of. Georgia	Na, Ca	pyroclastics, marls, shales	andesitic to trachytic pyroclastics	proximal (?), marine volcano-sedimentary	submarine hydrothermal
Glasgow	Montana, USA	Na, Ca	shale, mudstone, sandstone	likely rhyolitic; or andesitic, dacitic	distal, offshore marine	diagenetic or seawater
Lowell	Wyoming, USA	Na	shale, mudstone, sandstone	likely rhyolitic; or andesitic to dacitic	distal, brackish prodelta to offshore marine	diagenetic or seawater
Otay	California, USA	Mg, Ca	sandstone, mudstone	rhyodacitic to trachytic	distal, deltaic, shallow coastal lagoon	marine to brackish mixing
Pertek	Tunceli, TR	Na	limestone, marls	acidic to intermediate volcanics	distal, marine, carbonate platform	hydrothermal and/or seawater
Tavush	Armenia	Na, Ca, Mg	pyroclastics, sand- & limestone, marl	rhyodacitic, dacitic, trachyandesitic tuff	proximal (?), marine volcano-sedimentary	diagenetic or hydrothermal
Los Trancos	Almeria, ES	Mg, Ca	pyroclastic rocks	rhyolitic tuff	proximal, marine volcano-sedimentary	hydrothermal
Dominantly terrestrial depositional settings						
Bavaria	Germany, DE	Ca, Mg	Marls, Sand, Gravel marine and	rhyolitic ash	distal, fresh to brackish fluviatile-lacustrine	soil, wetland, groundwater
Bussu/S'Aliderru	Sardinia, IT	Mg, Ca	lacustrine limestone, gravels	rhyodacitic to rhyolitic	distal, lacustrine	lacustrine or saline groundwater
Fallon	Nevada, USA	Na	clastic, marly, pyroclastics	rhyolitic to dacitic	distal (?), saline-alkaline playa	hydrothermal, brine, lake water
Lago Pellegrini	Neuquén, AR	Na, Ca, Mg	pyroclastics, mudstones	rhyolitic to dacitic	distal, littoral marine, supratidal to terrestrial	lagoons, brines, brackish meteoric, seawater
La Tranquera	San Juan, AR	Na, Mg	mud- & sandstones, conglomerates	acidic to intermediate volcanics	distal, limnic to fluviatile playa	playa, incipient soils
Terrestrial Laterite						
Vitoria da Conquista	Bahia, BR	Mg, Ca	Granite, Gneiss, Amphibolite	Granite, Gneiss, Amphibolite	Laterite	soil or groundwater

Table 7.1: Continued. GW = groundwater, SW = seawater.

Deposit	Temperature	fluid chemistry	available B data	Depositional/eruption age	Dominant minerals
Dominantly marine depositional settings					
Angeria & Zoulias	30 to 90°C	Ca-Mg-HCO3, Na-Cl, or Na-Mg-Cl	Fluids: 3 to 99 mg/L, $\delta^{11}B$ < 10.3 ‰ & $\delta^{11}B$ 10.3–17.4 ‰; seawater	Pliocene - Pleistocene (3.5 to 0.09 Ma)	Sme, Qz, Ilt, kln, Opl-CT, Alu, Zeo, Fsp, Gp, Py
Askana	unknown	unknown	n.a.	Eocene	Mg-rich Sme, Ab, Crs, Ms, Mixed-layer minerals
Glasgow	not well constrained	Na-Cl-SO4	Bentonite: 70 µg/g; GW: <0.1 to 5.16 mg/L; Deep GW: 9.27 to 564 mg/L	Late Campanian - Maastrichtian (69 to 74.5 Ma)	Sme, Ilt, Qz, Cal, Gp, Zeo
Lowell	not well constrained	Na-Cl or Na-SO4	Sme: 6 to 12 µg/g; GW 0.12 - 1.3 mg/L; Deep GW: 0.03 - 262 mg/L	Albian - Lower Cenomanian	Sme, Ilt, Qz, Fsp, Zeo, Gp, Cal
Otay	unknown, low (<40°C?)	Seawater, river water	seawater	Eocene - Oligocene	Mg-rich Sme, Qz, Sa, Cal, Ms, Bt
Pertek	unknown	unknown	n.a.	Upper Eocene - Oligocene	Sme, Cal, Fsp, Qz, Zeo
Tavush	unknown	bicarbonate-rich	n.a.	Upper Santonian - Lower Campanian	Sme, Cel, Ilt/Sme
Los Trancos	40 to 100°C	Ca-Mg-HCO3	Parent rock: 0.66 to 1.71 µg/g; Sme: 4.12 µg/g; seawater	Langhian - Messinian (15-7 Ma)	Sme, Plg, Ilt/Sme, Qz, Cal, Dol
Dominantly terrestrial depositional settings					
Bavaria	15 to 40°C	Ca-Mg-HCO3	GW: 0.003 to 1.28 mg/L; Rain $\delta^{11}B$ ~13 ‰; Ries water $\delta^{11}B$ +7.5 ± 1.6 ‰	Mid-Miocene (14.77 ± 0.03 Ma)	Sme, Ilt/Sme, Ilt, Qz, Fsp, Dol, Cal
Bussu	unknown	Ca-HCO3 & saline (Na) water	n.a.	Oligocene-Miocene	Mg-rich Sme, Qz, Fsp
Fallon	possibly 20 to 80°C	Na-K-Cl	GW and brines: 14 to 120 mg/L	Miocene (to Pleistocene)	Ilt/Sme, Qz, Fsp, Cal, Dol, rock fragments
Lago Pellegrini	low (<40°C?)	Na-Cl or Na-SO4? Groundwater?	SW: 3.5 to 5.3 mg/L	Campanian to Lower Maastrichtian(80.3 - 76.2 Ma)	Sme, Plg, Ms, Bt
La Tranquera	unknown, ambient?	Na-Mg-Cl?	n.a.	Hettangian-Toarcian	Sme, Plg
Terrestrial Laterite					
Vitoria da Conquista	<40°C	meteoric	n.a.	Miocene - Pleistocene	Fe-/Mg-rich Sme, Vrm, Kln, Ilt, Bs, Opx/Cpx, Amp, rock fragments

7.2.1 La Tranquera, San Juan Province, Cuyo region, Argentina (B23)

The Tranquera Na-Mg-bentonite is part of the Canyon de Colorado Formation at the south-eastern Sierra de Mogna. The tuffs in bentonite deposits have been allocated to the Miocene (Hevia, 1989; Argiel, 1992) but the discovery of dinosaur tracks clearly indicates a Mesozoic, probably Lower Jurassic age (Hettangian-Toarcian) (Martínez, 1999; Martínez & Colombi, 2011). The single white bentonite bed is less than 2 m thick (B23). The pyroclastic material was deposited in distal, limnic to fluviatile playa environments, and is part of a succession of mudstones, sandstones and conglomerates (Hevia, 1989; Martinez & Colombi, 2011). The chemistry of the tuffs is unknown but Ti-Al and Fe-Al ratios of bulk bentonites (Gilg, 2018) indicate a parent material with a high to intermediate silica content (Hevia, 1989; Argiel, 1992). Montmorillonite and plagioclase are the only major phases in the clay (Hevia, 1989). Bentonites in the Cuyo region have been affected by incipient palaeosol development (Martinez & Colombi, 2011). High Sr concentrations (216 to 575 µg/g Sr) in other bentonites from the Cuyo region indicate a strongly evaporation-affected setting (Argiel, 1992) consistent with a playa environment.

7.2.2 Lago Pellegrini, Rio Negro Province, Argentina (Arg1, Arg5, Arg11)

The less than one meter thick but laterally extensive Na-bentonite (Argiel, 1992; Lombardi et al., 2002; Iborra et al., 2006) horizon is located at the south-eastern shoreline of Lake Pellegrini. The sampled bentonite is a part of the middle section of the Upper Cretaceous Allen Formation at the base of the Malargüe group (Vallés et al., 1989; Argiel, 1992; Impiccini, 1995; Vallés & Giusiano 2001; Warr et al., 2016). The bentonite itself is found at the base of a mudstone-pyroclastic section and is mainly comprised of montmorillonite, plagioclase and micas (Warr et al., 2016). The sedimentary infill of the Neuquén basin also includes several other Upper Cretaceous to Tertiary bentonite horizons (Lombardi et al., 2002).

Paleontological evidence indicates that the volcanic ash and mudstones were deposited during the Campanian to Lower Maastrichtian in a transitional littoral marine environment (Vallés et al., 1989; Impiccini 1995; Vallés & Giusiano 2001; Impiccini & Valles, 2011). However, there is substantial sedimentological evidence in the form of Aeolian dune sediments and horizontal sedimentation indicating flash-floods in the Allen Formation, and thus a predominantly non-marine depositional environment (Armas & Sánchez, 2013) consistent with previous studies on Patagonian bentonites by Andreis & Zalba (2001) who suggested glass alteration in lacustrine settings and lagoons. The new geological map quadrangles of the Neuquén and Rio Negro provinces also documents abundant non-

marine sedimentary intervals in the Allen Formation (Rodríguez et al., 2007; and sources therein). Sedimentological evidence thus suggest a sub-aerial, low-relief, playa- to sabkha-like depositional environment of the volcanic ash affected by occasional and short-lived marine transgressions, coherent with non-marine depositional environments at the base of the Malargüe group in other locations (Aguirre-Urreta et al., 2010).

7.2.3 Tavush region, Republic of Armenia (B17)

The Na-dominated bentonites (with some exchangeable Ca and Mg) of the Tavush region are part of Upper Santonian to Lower Campanian formations in the Chetyldag-Kechaldag anticline. Bentonite deposits (and zeolite deposits) formed from pyroclastic material of rhyodacitic, dacitic and/or trachyandesitic composition hosted in marine volcano-sedimentary sequences (Petrosov & Tsameryan, 1964; Rateyev et al., 1975). The deposits are stratiform to lenticular smectite-rich bodies located in tuff, ignimbrite, tuffaceous sandstone, limestone and marl. The dominant clay mineral is montmorillonite together with traces of celadonite and mixed-layer minerals (Rateyev et al., 1975). The bentonites formed by diagenetic and/or hydrothermal alteration (Petrosov, 1970) of the pyroclastic material along tectonic fracture zones (Rateyev et al., 1975) and the involvement of thermal, bicarbonate-rich fluids (Petrosov, 1970).

7.2.4 Vitória de Conquista, Bahia, Brazil (D15, KOP2, Furo)

The Mg-Ca-bentonite deposit occurs in the lower parts of a Miocene to Pleistocene laterite profile that formed from igneous and metamorphic rocks of the San Francisco Craton (Moreira, 1984; Albrecht, 2011). The San Francisco Craton forms a flat plateau with an elevation of 900 to 1000 m above sea level characterized by Archaic and Proterozoic amphibolite, gneiss, mica schist and quartzite that have been subject to continental weathering at least since the Cretaceous, and certainly during the Tertiary (Tardy et al., 1991). The bentonite contains residual fragments of crystalline rocks and shows excellent fabric preservation, e.g. foliation (Albrecht, 2011). It is characterized by a Fe- and Mg-rich montmorillonite (7.05 to 12.55 wt% Fe_2O_3 and 1.77 to 3.58 wt% MgO) and very rare nontronite, as well as traces of vermiculite, kaolinite, and illite (Moreira, 1984). Samples are from three drill cores (D, F and K) intersecting the bentonitic zone of the laterite horizon. The bentonite formed by the weathering of mafic minerals (i.e. amphiboles, mica, feldspar, and chlorite) in amphibolite, gneiss and mica schist during periods of poor drainage and arid climate (Moreira, 1984; Albrecht, 2011). A second

stage of weathering leached alkali and alkali earth elements, and promoted the transformation of montmorillonite to kaolinite and iron-hydroxides either because of better drainage or higher humidity during a sub-tropical climate period. The bentonite thus represents an intermediate weathering stage (Moreira, 1984). Albrecht (2011) described a 1-stage model invoking inhibited drainage and a semi-arid, tropical climate. The formation of the bentonite is therefore identical to the formation of smectite-rich bodies in the lower parts of laterites in Bahia and north-eastern Brazil (Trescases et al., 1981; de Oliveira et al., 1992).

7.2.5 Askana, Republic of Georgia (B31)

The Na-Ca-bentonites are found in tuff and breccia that are part of an Eocene sequence of marine marls and shales close (~30 km) to the modern-day Black Sea coast (Belyankin & Petrov, 1950; Dsotsenidze & Matchabely 1963). The bentonites formed from pumice-like andesitic to trachytic pyroclastic rocks by in-situ weathering (Belyankin & Petrov, 1950), submarine volcanism (Manuilova et al., 1965) and/or alteration by hydrothermal fluids (Rateyev, 1968). The latter two are considered as more likely by Rateyev & Gradusov (1970) in light of the close vicinity of the bentonite to zones of sulfide mineralization. Although a Ca-dominated bentonite is found in the upper parts, Na-dominated bentonite is found in the lower part of the deposit. The sample (B31) is from this Na-dominated bentonite bed. Dsotsenidze & Matchabely (1963) argue that the Na-variety formed by hydrothermal alteration from the parent rock and that the Ca-bentonite is a result of the weathering of the original Na-bentonite (Chukhrov, 1968). The clay is comprised of Mg-rich (4.6 wt% MgO) montmorillonite with a low Fe content (Grim & Güven, 1978) and various admixtures of albite, cristobalite, mica and mixed-layer minerals described as a celadonite-montmorillonite (Dsotsenidze & Matchabely, 1963; Rateyev & Gradusov, 1970).

7.2.6 Milos, Aegean Sea, Greece (ANG, ZO)

Large Ca- and Mg-bentonite deposits are located in the eastern half of the Island of Milos (Wetzenstein, 1972). Pliocene to Pleistocene volcanic rocks erupted from two or three volcanic centers have been identified as the parent material of bentonites (Christidis & Dunham, 1993, 1997; Christidis et al., 1995) and were derived from arc volcanism 3.5 to 0.09 Ma ago (Fyticas et al., 1986). The Angeria (ANG) and Zoulias (ZO) bentonite deposits formed from rocks of andesitic to dacitic composition (Wetzenstein, 1972; Christidis & Dunham, 1993) deposited in a marine setting and altered in-situ

(Wetzenstein, 1972; Christidis & Dunham, 1993; Christidis et al., 1995). It is, however, not entirely clear whether the alteration occurred in marine conditions, i.e. in contact with seawater (Wetzenstein, 1972; Christidis, 1998), hydrothermal fluids (Fyticas, 1977) or a combination of both seawater and hydrothermal fluids (Wetzenstein, 1972; Luttig & Wiedenbein, 1990). Temperatures of 30 to 90°C estimated using the oxygen and carbon stable isotope values of smectite and calcite are more consistent with a hydrothermal alteration (Decher et al., 1996). However, bentonite deposits have also been affected by later hydrothermal alteration and illitization of smectite (Christidis et al., 1995). The Zoulias and Angeria bentonites contain variable amounts of montmorillonite, quartz, illite, kaolinite, opal-CT, alunite, zeolites, feldspars, sulfates and sulfide minerals (Wetzenstein, 1972; Christidis & Dunham, 1993; Christidis et al., 1995; Decher et al., 1996).

Milos is an active geothermal field where cold Ca-Mg-type surface waters mix with deep-seated geothermal fluids (Liakopoulos et al., 1991). Seawater has, however, been identified as the main source of Na and Cl based on the Sr isotope ratios and $\delta^{18}O$ values of fluids involved in the formation of epithermal ore deposits (Naden et al., 2005). Na-Mg-dominated hydrothermal fluids have been found in submarine vents and caves around Milos (Varnavas & Cronan, 2005). Low to neutral pH Na-Mg-Cl brine and fluid reservoirs exist at depth in Milos (Valsami-Jones et al., 2005). Wu et al. (2016) identified low $\delta^{11}B$ (< 10.3 ‰) and high $\delta^{11}B$ (10.3–17.4 ‰) fluids with various boron concentrations that suggest the presence of two or more fluid sources (e.g. magmatic, seawater or meteoric).

7.2.7 Bavaria, Germany (MB34, ZW48, ZW50)

The Landshut bentonites are located in a tectonic block in the North Alpine Foreland Basin bordered by NW-SE striking fault zones of a basement high (Unger, 1981, 1999; Aziz et al., 2010; Gilg & Ulbig, 2017). The deposits are limited to the 14.77 ± 0.03 Ma old main bentonite horizon (Rocholl et al., 2017) in the upper part of the fluviatile *Nördlicher Vollschotter* (NV) sand and gravel unit and floodplain sediments of the *Sand-Mergel-Decke* (SMD) of the Upper Freshwater Molasse (UFM) (Vogt, 1980; Unger & Niemeyer, 1985a, b; Unger et al., 1990; Ulbig, 1999). Bentonites formed from Mg- and Ca-poor, rhyolitic volcanic ashes in a fluvial-lacustrine depositional environment (Ulbig, 1999; Gilg, 2005; Aziz et al., 2010). Topographic “highs” and “lows” were used by Ulbig (1999) to explain sedimentological and depositional differences between deposits; “highs” are underlain by marl or clayey sand and associated with abundant dolomite and calcite, whereas “lows” are characterized by sandy to gravely footwalls and a lower carbonate content (Ulbig, 1999). The “high” and “lows” correspond to various depositional and formation environments within the anastomosing to braided

river system of the UFM (Schmid, 2002; Maurer & Buchner, 2007). Dolomite and bentonite formation in palustrine, pedogenic and ground water environments occurred in close spatial and timely association, and was in part cogenetic (Köster & Gilg, 2015). Pedogenic and palustrine bentonite deposits were subject to strong evaporation, as indicated by high Sr concentrations in bentonite-associated dolomites (up to 1382 µg/g Sr; Köster et al., 2017). Blue (ZW50) and yellow (ZW48) bentonites are from the lower half of the Zweikirchen deposit that is characterized by pedogenic and groundwater carbonates, and from the lower green bentonite bed underneath the an upper tuff bed of the Mittersberg deposit (MB34) that formed in a palustrine environment with abundant dolomite (Köster & Gilg, 2015). The water chemistry in aquifers of the UFM is dominated by Ca^{2+}, Mg^{2+}, and HCO_3^- (Egger et al., 1983; Wagner et al., 2003). The boron concentrations of the fresh Ca-Mg-HCO_3^- water range from 3.25 to 1282 µg/L boron, with a median of 5.68 µg/L (Wagner et al., 2003). Modern rainfall in Bavaria has a $\delta^{11}B$ value of about +13 ‰ (Eisenhut & Heumann, 1997). The $\delta^{11}B$ value of meteoric waters involved in smectite formation in the Middle Miocene Ries impact were estimated at +7.5 ‰ ± 1.6 ‰ (Muttik et al., 2011). The $\delta^{11}B$ values for groundwater in Quaternary sediments overlying the UFM in south-east Bavaria range from -20 ‰ to +46.6 ‰ (Eisenhut & Heumann, 1997).

7.2.8 Bussu (S'Aliderru), Sardinia, Italy (BU)

The Mg-Ca-bentonite deposit (Ginesu & Pietracaprina, 1985; Palomba et al., 2006) belongs to the type II deposits, i.e. it formed from distal fall-out material (Maccioni et al., 1995, 1998) but has been defined as a type I deposit formed by in-situ alteration of volcanic rocks by Palomba et al. (2006). Both deposit types are found in the uppermost parts of the Oligocene-Miocene volcanic complex with rocks of mainly rhyodacitic–rhyolitic compositions (Maccioni et al. 1995, 1998; Palomba et al., 2006). The white bentonite has a rather high amount of Mg in the octahedral site, and is largely composed of smectite with only minor traces of quartz and feldspar (Pietracaprina et al., 1987).

The deposit formed from acidic volcanic ash (Maccioni et al., 1995, 1998), lapilli and bombs deposited during the Oligocene to Miocene on a karstified paleo-surface on Mesozoic limestones. The bentonite is erosionally truncated by Plio-Pleistocene lacustrine carbonates, travertine, and gravels. Bentonitization occurred in the Miocene and/or Pliocene and is most complete at the contact with the Mesozoic limestones (Ginesu & Pietracaprina, 1985; Pietracaprina et al., 1987). Bentonite formation occurred by interaction with Ca- and bicarbonate-rich water percolating through the ash-fall. There is, however, bentonite with some exchangeable sodium probably derived from highly saline waters found

in the chalky aquifers in underlying Triassic rocks (Pietracaprina et al., 1987). Our sample was taken in close vicinity of a fault and thus could be affected by the more deep-rooted fluids.

7.2.9 Los Trancos, Cabo de Gata, Spain (TR)

The Mg-Ca-bentonite deposit is located in the northern the Sierra de Cabo de Gata at the margin of the Serrata de Nijar (Linares, 1963; Martin Vivaldi & Linares, 1968; Caballero et al., 1985). The volcanic-sedimentary sequence hosting the deposit is mainly comprised of pyroclastic rocks and ignimbrites (Fernández Soler, 1992) intruded by dacitic to andesitic domes. The parent materials of the bentonites are of dacitic to rhyodacitic composition (Martin-Vivaldi & Linares, 1968; Reyes et al., 1979). Los Trancos is located at the margin of a dome in the form of a band of altered tuff that has a rhyolitic composition (Linares et al., 1987; Delgado, 1993). The deposit was subaerially exposed and affected by soil formation (Delgado, 1993) and marine transgression during the Tortonian to Messinian (Dabrio & Martin, 1978). Deformation, brecciation and the associated thermal effect on the tuff during dome emplacement played an important role in the formation of the bentonite (Delgado, 1993). The deposit shows calcite-filled fractures as well as calcite nodules that indicate the involvement of bicarbonate water in bentonitization (Delgado, 1993; Delgado et al., 1993) concurring with a diluted, Ca-Mg-HCO_3-dominated water chemistry inferred on the basis of water-soluble ions (Caballero et al., 1985, 2005). The oxygen isotopic composition of quartz, smectite and the calcite fillings indicate slightly higher than ambient equilibrium temperatures of 40 to 100°C (Leone et al., 1983; Delgado, 1993; Delgado & Reyes, 1993).

Boron has been recognized as one of the most mobile elements during bentonite formation in the Cabo de Gata. Low boron concentrations are characteristic for the acidic parent rocks of Los Trancos (0.66 to 1.71 µg/g B; Linares et al., 1987) and bentonites show statistically calculated – but not directly measured - boron concentrations of 0.95 µg/g in Los Trancos to 3.73 µg/g in other deposits. Smectites were calculated by Linares et al. (1987) to contain an average of 4.12 µg/g boron.

7.2.10 Pertek, Tunceli province, Turkey (PE)

The Na-bentonite deposit is located east of the Keban dam lake about 5 km NW of Pertek close to the city of Elazig, Turkey. Although the exact stratigraphic position of the deposit is unknown, marls and nummulite-rich limestones in the hanging- and footwall sections of the deposit (oral communication Dr. Werneck, Clariant) indicate that it is part of the Upper Eocene to Oligocene

Kirkgecit Formation composed of shallow shelf sediments (Afshar, 1965; Aksoy et al., 2005). The sediments are argillaceous at the base and grade into pure limestones towards the top, with several interbedded andesitic flows, as well as pyroclastic tuffs and agglomerates (Afshar, 1965). The Kirkgecit Fm. rests unconformable on Upper Cretaceous granitoids and the Keban metamorphics (Afshar, 1965; Kürum et al., 2011; Herece & Acar, 2016). All rock formations in the Pertek area are cut by a NNW-SSE trending fracture zone, the Pertek fault (Savci, 1983; Kürum et al., 2011) which could be a source of bentonite-forming fluids due to its vicinity (less than 5 km) to the Pertek deposit. In the vicinity of Pertek, clayey, smectite-rich dolomitic and zeolite-bearing marls and limestones with volcanic material are described south of the Keban lake in the lacustrine-fluviatile Upper Miocene-Pliocene Caybagi Fm. (Akkoca & Sagiroglu, 2005) and close to Elazig in the Upper Cretaceous to Middle Eocene marine Gehroz Fm. (Akkoca et al., 2013). These sediments, including the Kirkgecit Fm., are part of a belt of marine sediments (Akkoca & Sagiroglu, 2005; Akkoca et al., 2013) rich in volcanogenic smectite along the margin of the Neotethys (Shoval, 2004). The area east of Pertek is the target of epithermal low sulfidation vein- and stockwork-style gold and copper exploration projects with an unknown age of mineralization (Royal & Branch, 2014; Royal et al., 2015).

7.2.11 Lowell, Wyoming, USA (MOFO, MOFR, MOHO)

Na-bentonite deposits in the northern Bighorn basin are part of Lower Cretaceous to lowermost Upper Cretaceous (Albian to early Cenomanian) sedimentary successions (Knechtel & Patterson, 1956, 1962; Slaughter & Early, 1965; Cobban & Kennedy, 1989). Our samples originate from the F and H beds located slightly above the Clay Spur bed in the upper Mowry Shale (Knechtel & Patterson, 1956, 1962; Slaughter & Early, 1965). The Mowry shale was deposited in brackish and dysaerobic prodeltas to offshore marine settings that became increasingly saline and anaerobic towards the southeast (Davis, 1970; Byers & Larson, 1979; Davis et al., 1989).

The volcanic ash probably originated in western Wyoming and Idaho in association with the Idaho batholith. The ash was mostly rhyolitic in composition (Elzea, 1990; Elzea & Murray, 1990), although a variety of compositions from andesitic, latitic, trachytic, dacitic to rhyolitic have been documented (Slaughter & Earley, 1965). The volcanic ash was altered to bentonite in brackish water to seawater, based on the trace element content of smectites (Elzea, 1990; Elzea & Murray, 1990). Cadrin et al. (1995) showed that the δD and $\delta^{18}O$ values of some bentonites (i.e. Clay Spur bed) in Wyoming are compatible with waters of the Greenhorn Sea during the Middle Cenomanian, whereas δD and $\delta^{18}O$ values of other bentonites are inconsistent with a formation from seawater. The formation conditions

and fluids of the Wyoming and Montana bentonites in general are therefore not fully resolved (Smellie, 2001). The Mowry Shale and other sedimentary rocks of the Bighorn Basin have been identified as source rocks for hydrocarbons (Warner, 1982; Finn, 2010), the maturation of which has a major influence on smectite and illite composition in the Mowry Shale (Burtner & Warner, 1986). Blue and yellow bulk Clay Spur bentonite was reported to have boron concentrations of 6 to 7 µg/g (Knechtel & Patterson, 1962) which is slightly lower than K-saturated smectites from Wyoming bentonites (10 to 12 µg/g B; Williams & Hervig, 2002, 2005). Modern-day water in the Mowry confining unit and directly under- and overlying formations is Na-SO_4 dominated and has boron concentration of 0.12 to 1.3 mg/L (Taucher et al., 2012).

7.2.12 Glasgow bentonite, Valley County, Montana, USA (SB01, SB02)

The Na-Ca-bentonite deposit is situated in the Malta-Glasgow district about 33 km west-southwest of Glasgow, Montana (Berg, 1969; Hosterman & Patterson, 1992; Department of the Interior - Bureau of Land Management, 2015). The bentonite is part of the Upper Cretaceous (Late Campanian to Maastrichtian) Bearpaw Shale. The Bearpaw Shale was deposited in an offshore marine environment of the western-most margin, i.e. the "western facies belt" of Tourtelot (1962), of the Williston Basin (Jensen & Varnes, 1963; Anna et al., 2007) and is the stratigraphic equivalent of the Upper Pierre Shale (Tourtelot, 1962). The Bearpaw Shale in north-central Montana rest conformably on the terrestrial sandstones of the Judith River Formation and is itself conformably overlain by the terrestrial Fox Hill sandstone. The Bearpaw Shale Fm. is host to many sediments rich in volcanic ash, just as the Pierre Shale (Berg, 1969, 1970; Schultz et al., 1980). Formations younger than the Bearpaw Shale in north-central Montana have been eroded by the last glaciation (Jensen & Varnes, 1963; Berg, 1970). The Malta-Glasgow district is bordered by the Bearpaw Mountains in the west (Bearpaw uplift) and is situated directly on the Bowdoin dome, both are host to Upper Cretaceous biogenic gas plays (Rice, 1981; Perry et al., 1983). Several gypsiferous bentonite beds are found in the Bearpaw Shale. The origin of the gypsum, i.e. primary versus secondary, is not known. The two most economically important X and Y beds occur in the middle of the Bearpaw Shale (Jensen & Varnes, 1963). The upper X bed (sample SB01) is light yellowish grey to cream colored, and the Y bed (sample SB02) 4.5 m below the X bed has a medium-grey color (Berg, 1969, 1970; Hosterman & Patterson, 1992). The Glasgow bentonite has not been dated, but a combination of Baculites ammonite zones and K-Ar data of sanidine and biotite from bentonites of the "western facies belt" in the Bearpaw Shale of the South Saskatchewan River Valley in Canada suggest an age of 69 to 74.5 Ma (Folinsbee et al., 1961, 1965; Caldwell, 1968). The

composition of the volcanic ash in the Glasgow area is unknown. Andesitic, dacitic and rhyolitic ash beds have been documented in the Upper Campanian of the late Western Interior Seaway (Armstrong & Ward, 1993; Bertog et al., 2007). Braun (1983) suggested that the source for volcanic material in the Judith River Fm. and the overlying Bearpaw Shale was mainly Campanian volcanic rocks from the Elkhorn Mountains (Smedes, 1966). The Elkhorn Mountains were the only explosive volcanic center in the vicinity of the Malta-Glasgow district during the timeframe defined by K-Ar ages (Folinsbee et al., 1961, 1965; Armstrong & Ward, 1993). The Bearpaw Mountain volcanics are much closer to the Malta-Glasgow district, but their Eocene emplacement age (Bearpaw uplift) excludes them as a source (Schmidt et al., 1964). Bulk sediment of the Pierre Shale has boron concentrations ranging from 20 to 180 μg/g, with the higher values being more frequent in the eastern facies belts and towards the center of the Willison basin (Tourtelot et al., 1961; Tourtelot, 1962; Schultz et al., 1980). A single bulk claystone from the Bearpaw Shale in Valley County was shown to have a boron content of 70 μg/g (Tourtelot, 1962). Modern-day Na-Cl-SO_4 dominated groundwater in the underlying Judith River Fm. of north-central Montana has boron concentrations of 4.65 to 5.16 μg/g (Durum, 1955), whereas more recent data shows a more variable boron content of <0.1 to 4.0 μg/g in groundwater (Lawlor, 2000).

7.2.13 Fallon, Nevada, USA (B51, B52)

The Fallon Na-bentonite bentonite is located at the eastern end of Wyemaha Valley in the Lahontan Mountains in Nevada. The deposit is found in Miocene claystone associated with hydrothermally altered rhyolite and andesite (Post, 1996, 1997). Samples are from 3 and 4 m below the surface. Sediments of the late Pleistocene Sehoo Formation (Lake Sehoo) cover most of Wyemaha Valley (Post, 1996, 1997; LaPointe et al., 2011; Davis, 2014) and were previously assigned to the Miocene Bunejug Formation (Morrison, 1964). Recent mapping shows that this is inconsistent with the abundance of basalt flows in the Bunejug Mountains (Bell et al., 2010). The Tertiary to Pliocene sediments of Wyemaha Valley comprise siltstone, sandstone, conglomerate, tuffaceous sandstone, lithic tuff, pumice, interbedded olivine basalt, rhyolitic pyroclastic agglomerates, diatomite, and minor limestone. The Sehoo Formation and Tertiary sediments contain multiple tephra layers of rhyolitic to basaltic composition (Morrison, 1964; Bell et al., 2010). The Tertiary sediments are underlain by either or both the Tertiary dacite of Rainbow Mountain and/or the rhyolite of Eagle House (Bell et al., 2010). The dacitic volcanic flow grades from a quartz latite to rhyolite in composition (Morrison, 1964; Bell et al., 2010). Wyemaha Valley shows signs of past hydrothermal activity such as silified and celadonite-altered Miocene pumice and conglomerate (LaPointe et al., 2011), altered dacite and altered

sediments (Bell et al., 2010). Hydrothermal hot springs (~45 to ~75°C) and vents in Salt Wells playa and marshes five km south of the Fallon deposit are associated with silified sediments, siliceous sinters, and zone of argillic alteration (Morrison, 1964; Coolbaugh et al., 2006). Whether the recent hydrothermal systems are related to bentonitisation is unknown. However, shallow to thermal groundwater of the area (Lico & Seiler, 1994), as well as groundwater in the Fallon basalt aquifer (12°C to 21°C) to the west (Lico & Seiler, 1994; Maurer & Welch, 2001), have high boron (14000 to 120000 µg/L in the proximity of Rainbow Mountains) and lithium concentrations (up to 8200 µg/L) that suggest high B and Li concentrations in authigenic clay minerals formed from them. The Na-K-Cl-dominated water chemistry (Lico & Seiler, 1994; Maurer & Welch, 2001; Coolbaugh et al., 2006) would be consistent with Na-bentonite formation (Post, 1996, 1997; Davis, 2014).

7.2.14 Otay, San Diego area, California, USA (OT)

The Mg-bentonites are a part of the sandstone-mudstone member of the Oligocene to Miocene Upper Otay Formation (Berry, 1991, 1999; Walsh & Demere, 1991; Tan & Kennedy, 2002), previously assigned to the Pliocene San Diego Formation (Cleveland, 1960). Although bentonites are present in most Eocene to Miocene sediments of the region (Berry, 1991, 1999). The continental, deltaic, and shallow coastal lagoon deposits of the Otay formation are comprised of sandstone, siltstone and claystone with six interbedded layers or lenses of bentonite (Cleveland, 1960; Berry, 1991, 1999; Walsh & Demere, 1991; Tan & Kenney, 2002). Sanidine crystals from the Otay waxy bentonite reveal an Oligocene age ($^{40}Ar/^{39}Ar$ age: 28.86 Ma, no error given) whereas sanidine from the Mission Valley Formation have an Eocene age ($^{40}Ar/^{39}Ar$ age: 42.18 Ma, no error given; Berry, 1991, 1999). The Zr/TiO_2 and Nb/Y of bulk bentonites suggest a rhyodacitic to trachytic composition (Berry, 1999). Eocene and Oligocene primary and secondary waxy bentonites were interpreted as primary ash-fall deposits in marine but shallow, near-shore environments or as re-deposited ash mixed with fluvial detritus (Cleveland, 1960; Berry, 1999). This is consistent with a more riverine environment in the eastern Otay Formation (Walsh & Demere, 1991) and $\delta^{18}O$ and δD values of altered volcanic glass and bentonite in the Miocene Monterrey Formation in equilibrium with slightly modified seawater (Compton et al., 1999). This is in turn consistent with marine-fresh water mixing in recent groundwater of the Otay region (Hanson et al., 2009).

7.3 Methods

7.3.1 Size separation

Illite, mica, tourmaline, and other accessory minerals may contain significant amounts of boron (Frederickson & Reynolds, 1960; Harder, 1970). We therefore separated the < 0.2 µm fractions of bentonites to produce "pure" smectite separates. No dispersion aids were used during sample processing to avoid contamination by trace elements. The equipment used for size separation and in direct contact with our samples was triple-rinsed with a 1.82 % mannitol solution to remove adsorbed and water-soluble boron.

The < 0.2 µm fractions were separated from dried (18 hours at 40°C) but otherwise untreated whole-rock bentonites that were dispersed in distilled water (EC < 0.9 µS/cm) using PE bottles. The suspensions were shaken and soaked in an ultrasound bath for 15 minutes, divided into three blocks to prevent excessive heating. After 24 hours the < 0.2 µm fractions were separated by centrifugation and the supernatant decanted into PE foil lined PE bowls. The supernatant was evaporated in a drying cabinet at 40°C. These size separates constitute the untreated (U) sub-samples. The < 2.0 µm fraction of the Clay Minerals Society standard Imt-1 illite was used as a reference material. The Imt-1 was dispersed in distilled water and separated in triple mannitol-washed Atterberg cylinders.

7.3.2 Dialysis, cation exchange and acid ammonium oxalate treatment

Our size separation method can result in the accumulation of water-soluble phases and/or boron in the < 0.2 µm fractions. We dialyzed the size separates using three different solutions. Splits of untreated separates (U) were dispersed in distilled water (D), an aqueous 1.82% mannitol (M) solution, and a 1 M ammonium acetate (A) solution followed by a 1.82% mannitol solution to remove water-soluble phases, adsorbed, and interlayer boron. Mannitol is a polyhydric sugar alcohol that bonds boron to hydroxyl groups and can remove adsorbed boron from clay surfaces (Hingston, 1964). The ammonium exchange re-expands the smectites and removes (some) interlayer boron (Zhang et al., 1998). The combined ammonium exchange and mannitol treatment therefore can remove both interlayer and adsorbed boron (e.g. Williams et al., 2001a; Williams & Hervig, 2005, 2006).

Selected sub-samples were treated with a 0.1 M acid ammonium oxalate (AAO) solution to remove Fe-hydroxides (Schwertmann, 1964). Ammonium oxalate and oxalic acid were mixed immediately before sample treatment. The 0.1 M solution is less effective (i.e. slower) than the original 1 M solution

by Schwertmann (1964) but its pH value (4 instead of 3) is less damaging to the clay minerals. The AAO treatment was followed by dialysis and mannitol treatment identical to the other sub-samples.

For all treatments ~ 300 mg of the dry < 0.2 µm fraction was weighed into 50 ml Nalgene bottles. 25 ml of the respective solution was added to the sample, shaken, and soaked in an ultrasound bath for 15 minutes, and left soaking for 24 hours. The large fluid volumes were necessary to prevent the formation of smectite gels and made it easier to handle the suspensions. The suspension was shortly shaken before introducing it into the flexible dialysis tubes which were in turn placed into transparent PE boxes with distilled water (EC < 0.9 µS/cm) as buffer solution. The distilled water was replaced daily until its EC remained constant at 0.9 to 1.0 µS/cm. The < 0.2 µm fractions were then dried at 40°C. The < 2.0 µm fraction of the Imt-1 was treated identical to the mannitol-washed sub-samples.

7.3.3 X-ray diffraction analysis (XRD)

The mineral compositions were determined by X-ray diffraction analysis from 2 to 70°2θ (Phillips PW 1800, Cu Kα) using random powder mounts as well as air-dried (AD) and ethylene-glycolated (EG) orientated mounts of the < 0.2 µm fractions (and the < 2.0 µm of the Imt-1). Random powder mounts were quantified by full-pattern Rietveld refinement using BGMNwin 1.8.6. (Bergmann et al., 1998). Smectite was identified in oriented mounts based on the migration of the d_{001} reflection from roughly 12.0 Å (mostly interlayer Na) and 14.5 Å (mostly interlayer Ca) in AD samples to 16.5 Å to 17.5 Å in EG-solvated samples.

The interstratified illite in smectite content was determined according to Środoń (1980) using the peak migration method (26° - 28° 2θ and 15° - 18° 2θ). As discrete illite can interfere with the identification of the peak positions (Środoń, 1980), the percentage of interstratified illite in smectite was also estimated by comparing the differences of the 001/002 and 002/003 positions (Moore & Reynolds, 1997). Both methods yield roughly similar but not identical results. However, these methods can produce errors of up to 30 % for the illite content because of variable humidity, interlayer composition and/or layer charge (Środoń, 1980).

7.3.4 Prompt Gamma Neutron Activation Analysis (PGAA)

Prompt gamma neutron activation analysis is a non-destructive techniques that offers very low detection limits (< 0.05 µg/g) for boron determination because of its high neutron capture cross section (Robertson & Dyar, 1996). The boron concentrations and chemical compositions of the < 0.2 µm

fractions were determined at the research neutron source at the FRM II/Heinz Maier-Leibnitz Centre, Garching, Germany. About 50 to 300 mg of untreated (U), distilled water-washed (D), mannitol-washed (M), and ammonium exchanged plus mannitol-washed (A) sub-samples, as well as AAO-treated (F) material were sealed into 25 µm thick PTFE foil. The PTFE bags were irradiated with cold (25 K) neutrons for 1 to 2.5 hours in a vacuum (0.3 mbar) with a flux of $3.8*10^8$ to $2.0*10^{10}$ neutrons per cm^2/s. The gamma spectra were detected by a Compton-suppressed spectrometer using a 60% high-purity germanium (HPGe) detector coupled with a bismuth-germanate-oxide (BGO) scintillator. The PGAA data were processed and quantified using the Hypermet PC software. The elemental compositions were determined using the Excel macro and Excel sheet package ProSpeRo. The high neutron cross section of hydrogen makes it possible to reliably determine the hydrogen content (i.e. adsorbed and interlayer water, and hydroxyl groups in the octahedral sheet) and normalize samples to a H_2O-free composition, thus making a systematic comparison of boron concentrations feasible. The ammonium content in ammonium exchanged samples was determined by allocating the corresponding amount of hydrogen atoms to the measured nitrogen concentration. The PTFE foil, PE foil, mannitol powder, ammonium acetate powder, and distilled water samples used in sample processing were also irradiated to verify their boron content (Table 7.2).

Table 7.2: Boron content and other trace elements in equipment and chemicals, in µg/g

Material	Al_2O_3	Cl^-	Pb	B
PTFE foil	0.16	0.29	7000	0.39
PE foil	0.12	-	12000	0.19
Mannitol powder	0.13	7.00	13000	0.25
Ammonium acetate	0.21	-	4.10	0.79
water stored in old PE bottle	-	0.70	-	0.52
water stored in new PE bottle	-	0.70	-	0.61

7.3.5 Secondary Ion Mass Spectrometry (SIMS)

Boron isotope analysis was carried out at the SIMS lab of the Arizona State University, Tempe, AZ using a CAMECA IMS 6f with a defocused oxygen ion beam and a spot size of 30 µm for a more homogenous sputtering of the sample surface. The SIMS mass resolution (nominal mass/D mass with interfering m/z) was set to 1000 to eliminate molecular interferences (e.g. ^{10}BH from ^{11}B) (Williams, 2000). Mannitol-washed and ammonium exchanged sub-samples were dispersed in boron-free (Amberlite resin filtered: Tonarini et al., 1997) distilled water and pipetted onto boron-free glass slides. The Imt-1 standard of the Clay Minerals Society was pipetted onto the center of the slide and was used

as a reference with an average $\delta^{11}B$ value of -9.0 ‰ ± 0.6 (n=5) relative to NBS SRM 951 (Williams, 2000). The instrumental mass fractionation (IMF) was determined on the Imt-1 (Fig. 7.4) before and after each sub-sample and varied from -29.1 ‰ to -46.0 ‰ (excluding outliers caused by electronic instability, charging or non-flat samples were manually removed). Blocks of stable IMF were defined to calculate the $\delta^{11}B$ value of the smectite separates, reported as $\delta^{11}B = [((^{11}B/^{10}B_{sample}) / (^{11}B/^{10}B_{standard}) - 1) * 1000] - IMF$. A table of IMF values used in each sample is shown in Appendix 7.1. Although SIMS cannot provide the high precision results as TIMS (Tonarini et al., 1997) it has a much better spatial resolution. It is therefore possible to assess the variation in boron isotope values at different spot locations on the same sample (Williams, 2000; Chaussidon et al., 1997). The lower precision is in part compensated for by the very large boron isotope variation in natural fluids and minerals (-70 to +75 $\delta^{11}B$; Vengosh et al., 1992; Swihart et al., 1986; Hogan & Blum, 2003; Williams & Hervig, 2004).

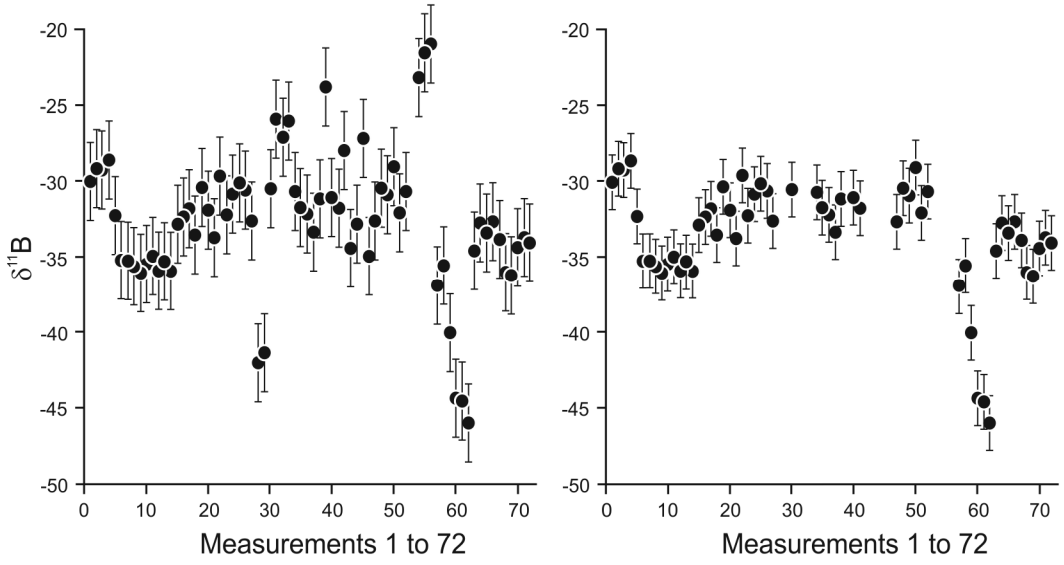

Fig. 7.4: Variation in instrumental mass fractionation (IMF) in the clay mineral standard Imt-1. Left: IMF uncorrected for fluctuations in current, manual errors, or instrumental drift. Right: The IMF used for defining areas of stable IMF for boron isotope analysis. Outliers were manually removed.

7.3.6 Exchangeable cations and cation exchange capacities

The exchangeable cations and cation exchange capacity of dialyzed < 0.2 µm fractions were double determined on 0.2g (a) and 0.3g (b) sub-samples at the Federal Institute for Geosciences and Natural Resources (BGR), Germany. The material was dried at 105°C to determine the water content and then dispersed in a three times calcite oversaturated Copper-triethylenetetramine ("Cu-trien") solution. The sodium, potassium, magnesium and calcium content of the exchange solution was determined by

inductively coupled plasma mass spectrometry. The exchangeable cations, as well as sulfate and chloride content, of samples B17, B23, B31 and B51 had previously been determined on 0.5 g of material at the Federal Institute for Geosciences and Natural Resources, Germany (Kaufhold & Dohrmann, 2008; Dohrmann & Kaufhold, 2010).

7.3.7 Carbon and oxygen stable isotope

The $\delta^{18}O$ and $\delta^{13}C$ values of disseminated carbonates in bentonites were determined with a Con-Flow DeltaPlus (Thermo Scientific) isotopic-ratio mass spectrometer linked to a Gasbench II (GeoBio-Center LMU, Munich, Germany). Isotope ratios are reported as δ-values in ‰ relative to V-PDB with an estimated accuracy and precision of ± 0.1 ‰. Standards NBS18 and NBS19 and an internal laboratory standard (Solnhofen Plattenkalk: $\delta^{18}O_{V\text{-}PDB}$ of -4.84 ‰ and $\delta^{13}C_{V\text{-}PDB}$ of 0.47 ‰) were included in the isotope measurements. The $\delta^{18}O$ values of dolomite were corrected using a phosphoric acid fractionation factor of 1.00986 at 72°C (Rosenbaum & Sheppard, 1986).

7.4 Results

7.4.1 Mineralogical composition

The mineralogical composition of whole-rock bentonites (Table 7.3) is dominated by dioctahedral smectites (d_{060}; 1.505 to 1.497 Å). Many whole-rock bentonites also contain illite or micas, quartz, feldspar, and with decreasing frequency variable amounts of chlorite, calcite or dolomite, zeolites, kaolinite, sulfates, opal-CT as well as traces of halite, pyrite, goethite, or hematite. Talc, serpentine, pyroxene, amphibole, as well as traces of sepiolite were found in laterite-hosted bentonites from Bahia, Brazil (Table 7.3). The untreated, orientated and air-dried < 0.2 µm fractions expand upon EG-treatment from roughly 12.0 ± 0.2 Å or 14.5 ± 0.2 Å (for mono- or divalent interlayer cations) to about 16.5 to 17.5 Å after ethylene-glycol solvation. Most smectite separates are characterized by small amounts of an interstratified illitic component (Fig. 7.5). The peak migration method of Środoń (1980) and the comparison of the differences of the 001/002 and 002/003 positions of Moore & Reynolds (1997) reveal up to ~20 % respective ~26 % interstratified illite in smectite. Most samples have ≤ 10 % interstratified illite (Fig. 7.5). Small amounts (< 5 wt%) of other phases were detected in smectite separates (< 0.2 µm fractions), including discrete illite, quartz, kaolinite, carbonates, and traces of chlorite, sulfates, halides, feldspar, opal-CT, talc, serpentine, or hematite (Table 7.4).

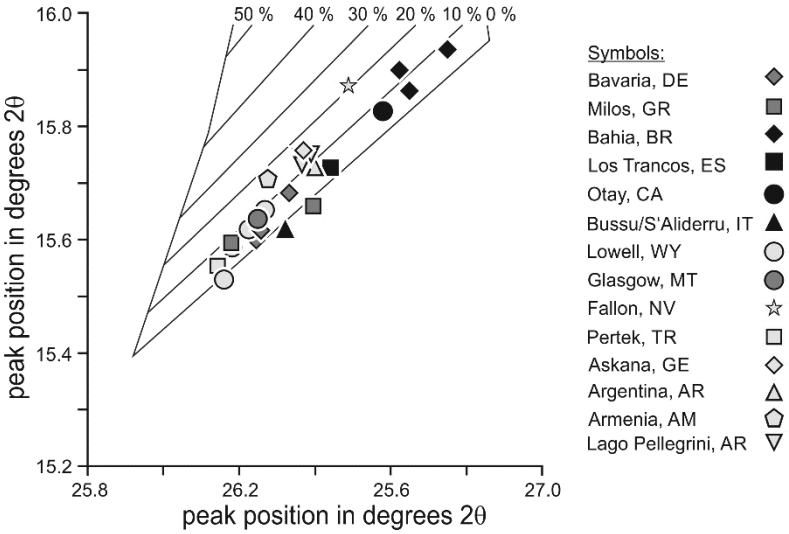

Fig. 7.5: The interstratified illite in smectite content of the < 0.2 µm separates. Black: Mg-bentonites; dark grey: Ca-bentonites, and light grey: Na-bentonites.

Table 7.3: Mineralogical composition of bulk bentonites as determined by X-ray diffraction. Arg1, 5, 11 from Warr et al. (2016). Px : Pyroxenes.

Sample	Sme	Ilt/Ms	Chl	Kln	Zeo	Qz	Opl-CT	Dol	Cal	Fsp	Gp	Hl	Py	Hem	Px/Amp	Sep	Tlc	Ap	Cel
ZW50	76	8	3			6		0		6			T						
ZW48	79	9	3			6		0		4									
MB34	83	4	6			3		T		4									
Pertek	60	2			14	1	18		2	3									
Zoulias	67					2	6		4	22		T							
Angeria	92	2				1					1		4						
Trancos	90		1			3				6									
Bussu	90	2				1				7									
MOFOA	70	1			10	10			T	9									
MOFOR	77	2			T	10			1	12									
MOHO	54	12			1	20			1	12									
Otay	82	3	1			5				10				T					
D15	81		6	1	1	T				T					6	3	3	1	
KOP2	90	3				2	1			4					1				
Furo	73		3			T				21					T	3			
SB01	85					6			3	4	2								
SB02	76	4				3			2	12	2	1							
B17	84	5				T		2	2	6		0							
B23	77					8				15		0							
B31	65					3	8			9									15
B51	49					41		T		8		1		1					
Arg1	93	6								T									
Arg5	97	2								T									
Arg11	97	2								T									

Table 7.4: The mineralogical composition of the < 0.2 µm fractions. XXX > 95 wt%, X < 5 wt%, T << 1 wt%.

Deposit	Sample	Sme	Ilt/Ms	Chl	Kln	Qz	Opl-CT	Dol	Cal	Fsp	Gp	Hl	Tlc	Sep	Hem
Angeria	ANG	XXX		T		X		T	T		XX				
Zoulias	ZO	XXX	T				X		T	T					
Askana	B17	XXX	T						T	T					
Glasgow	SB01	XXX				T									
Glasgow	SB02	XXX							X						
Mowry, oxi.	MOFO	XXX				X				T					
Mowry, red.	MOFR	XXX				X				T					
Beaver, oxi	MOHO	XXX				X	X				XX	T			
Otay	OT	XXX	T									XX			
Pertek	PE	XXX	T				X		X			T			
Tavush	B31	XXX					X		X						
Los Trancos	TR	XXX	T												
Zweikirchen	ZW50	XXX	T					X	T						
Zweikirchen	ZW48	XXX				X		X		T					
Mittersberg	MB34	XXX	X	T		X		T							
Bussu (S'Aliderru)	BU	XXX	T									T			
La Tranquera	B23	XXX													T
Lago Pellegrini	Arg1	XXX													
Lago Pellegrini	Arg5	XXX				T									
Lago Pellegrini	Arg11	XXX				T									
Fallon	B51	XXX								T					
Vitoria da Conquista	D15	XXX	T		X	T				T			X	X	
Vitoria da Conquista	KOP2	XXX	T		T	T									
Vitoria da Conquista	Furo	XXX	T	T	T										

7.4.2 Exchangeable cations

The exchangeable cation occupancy of the smectite separates (Table 7.5) is illustrated in Figure 7.6. The Milos and Bavarian bentonites, and one Montana bentonite (Glasgow), have calcium as the dominant interlayer cation; whereas bentonites from Sardinia, Otay, Cabo de Gata, and Bahia reveal magnesium as the dominant cation. Magnesium ions, however, never comprise more than 56 % of the exchangeable cations. Although sodium is the main exchangeable cation in Na-bentonites, some calcium and/or magnesium ions are always present (Fig. 7.6). The exchangeable cation composition of bentonites from Bavaria, Milos, Otay and Wyoming is consistent with previous results (Grim & Güven, 1978; Ulbig, 1994). Only the Otay smectite separate (Fig. 7.6) shows a cation occupancy possibly consistent with a smectite interlayer in equilibrium with modern-day seawater (Sayles & Mangelsdorf, 1977). The interlayer sodicity (mol-% Na) of the Glasgow (Montana) and Pertek (Turkey) bentonites suggests that they are in equilibrium with a fluid having a sodicity (Fig. 7.10) corresponding to that of seawater (Sayles & Mangelsdorf, 1977). Too little material was left of the Lago Pellegrini bentonites supplied by Warr et al. (2016) to determine the exchangeable cations, we therefore cite results by Iborra et al. (2006) of on average of 76.2 mol-% exchangeable sodium, and some exchangeable magnesium (15.6 mol-%) and calcium (7.7 mol-%).

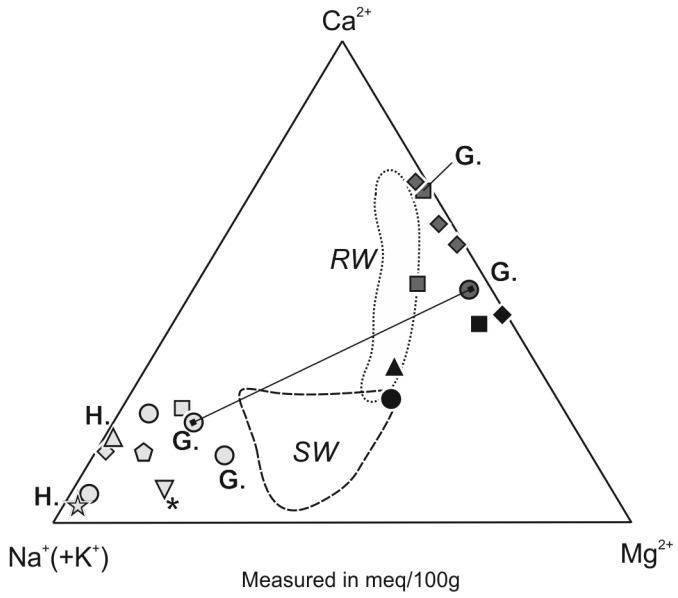

Fig. 7.6: The exchangeable cation compositions, and smectite interlayer occupancies in equilibrium with river (RW) and modern seawater (SW) from Sayles & Mangelsdorf (1977). Black: Mg-bentonites; dark grey: Ca-bentonites, and light grey: Na-bentonites. H. = halite, G. = gypsum, the solid line connects oxidized and reduced bentonites from the Glasgow deposit. Average interlayer occupancy of Lago Pellegrini bentonites (Iborra et al., 2006) is marked with an asterisks.

Table 7.5: The double-determined exchangeable cations (in meq/100g) in the smectite interlayer and cation exchange capacities. Data for B17, 23, 31 and 51 kindly provided by the Federal Institute for Geosciences and Natural Resources.

Sample	Mass (g)	Na^+	K^+	Mg^{2+}	Ca^{2+}	Sum cations	CEC	Remarks
ZW48a	0.2009	0.0	0.6	45.1	63.0	108.6	95.8	trace sulphate
ZW48b	0.2999	0.0	0.7	44.2	58.0	102.8	94.6	
ZW50a	0.2007	0.0	1.2	41.0	70.8	113.1	95.7	
ZW50b	0.3003	0.0	1.2	40.0	65.1	106.3	94.2	
MB34a	0.2003	0.0	1.0	33.4	84.5	118.9	105.9	
MB34b	0.3012	0.0	0.3	32.7	80.1	113.2	103.3	
KOP2a	0.2003	0.0	0.4	65.9	54.4	120.7	108.6	trace sulphate
KOP2b	0.3009	0.0	0.3	64.5	48.9	113.8	107.3	
BUa	0.2005	13.8	1.5	51.0	39.3	105.6	113.6	trace sulphate
BUb	0.3004	13.9	1.4	50.0	39.7	105.0	110.6	
ZOa	0.2011	5.3	1.6	42.2	54.9	104.0	105.1	
ZOb	0.2999	4.8	1.1	41.4	55.5	102.7	103.1	
ANGa	0.2021	0.0	0.8	29.9	70.0	100.7	103.0	
ANGb	0.3012	0.0	1.0	29.7	69.7	100.3	100.8	
TRa	0.2015	2.6	0.8	61.6	47.7	112.7	120.0	
TRb	0.3006	3.0	1.1	59.5	47.4	111.1	116.9	
MOFOa	0.2003	49.6	0.7	7.4	30.9	88.6	98.5	
MOFOb	0.3018	50.3	0.7	7.2	31.0	89.2	96.8	
MOFRa	0.2016	79.0	0.9	6.1	9.0	94.9	101.5	
MOFRb	0.3005	81.6	1.1	5.9	8.9	97.4	99.2	
MOHOa	0.2008	39.9	0.7	29.1	18.1	87.8	93.5	
MOHOb	0.3011	39.4	0.6	29.0	18.4	87.4	92.5	
PEa	0.2004	39.6	1.8	13.6	30.1	85.2	92.9	
PEb	0.3013	39.6	1.9	13.5	30.2	85.2	91.6	
OTa	0.2005	17.9	0.9	59.0	32.6	110.5	115.9	
OTb	0.3000	17.7	0.8	57.3	32.3	108.0	114.8	
SB01a	0.2017	0.9	0.5	47.2	46.8	95.4	94.6	
SB01b	0.3009	1.1	0.6	45.9	46.1	93.6	93.1	
SB02a	0.2007	43.1	0.6	18.8	26.9	89.3	93.3	
SB02b	0.3016	42.4	0.7	18.4	26.5	88.1	91.4	
B17	-	65.5	4.8	2.7	23.6	96.6	96.1	
B23	-	62.6	1.2	1.1	29.3	94.5	96.0	
B31	-	52.4	1.5	12.5	19.4	85.8	82.4	
B51	-	60.7	2.0	2.6	3.3	68.6	57.4	
Clay standard RV6a	0.5011	0.0	0.7	6.4	22.9	30.0	30.7	
Clay standard RV6b	0.9998	0.1	0.7	6.2	22.0	28.9	29.3	
Clay standard SP-4a	0.2021	24.7	1.8	51.3	38.1	116.0	111.3	
Clay standard SP-4b	0.3014	24.6	1.5	50.2	37.6	113.9	109.9	

7.4.3 Chemical composition of smectite separates

The elemental compositions (Table 7.6) of H_2O-free normalized smectite separates (D, M and A sub-samples) are consistent with values expected for clay fractions comprised of dioctahedral smectites (Weaver & Pollard, 1973, Grim & Güven, 1978) as well as previous results for the respective bentonite deposits (Grim & Güven, 1978; Vogt & Köster, 1978; Christidis & Dunham, 1993; Delgado, 1993; Ulbig, 1994).

The various sample processing methods resulted in the removal of water-soluble, absorbed and exchangeable elements; mostly boron, lithium and sodium. Untreated sub-samples (Table 7.6) have elevated, boron, lithium, sodium chlorine and sulphur concentrations, probably concentrated by our size separation method. Water-soluble elements concentrated by processing were removed using distilled water or 1.52% aqueous mannitol-solution, and subsequent dialysis (Table 7.6). The cation exchange resulted in an additional reduction in sodium, calcium, and magnesium concentrations (Table 7.6), as expected for elements located in the smectite interlayer, but had only a small effect on B concentrations (Fig. 7.8), indicating that B is mostly (but not exclusively) fixed in tetrahedral positions. The removal of ancillary Fe-hydroxides using the AAO method had no notable influence on B contents (Fig. 7.9).

The < 0.2 μm fractions of bentonites from Bahia, Brazil and Fallon, Nevada have the most unusual compositions. The < 0.2 μm fractions from Bahia are characterised by low SiO_2 and Al_2O_3 concentrations but by the highest Fe_2O_3 (12.5 to 16.9 wt%), TiO_2 (up to 0.77 wt%) and Cr_2O_5 (up to 0.9 wt%) concentrations (Table 7.6). The < 0.2 μm fraction of the Fallon bentonite is characterised by the lowest SiO_2 and the highest Al_2O_3 concentrations of our samples. About 1.9 wt% of Li_2O was detected in the untreated Fallon sub-sample, indicating the presence of a soluble lithium phase that was completely removed by dialysis. The < 0.2 μm fraction from Fallon also has the highest K_2O concentration (2.7 wt%; Table 7.6), confirming XRD results indicating an illite-rich, R0 illite-smectite.

The boron concentrations in smectites from Bavaria are consistent with smectites formed in meteoric water in Miocene Ries impact crater (Muttik et al., 2011); whereas the boron content of our Wyoming bentonites does not match the bulk B content of the Pierre Shale in Montana (Tourtelot et al., 1961) nor the low B content (< 10 μg/g) of K-exchanged Wyoming bentonite (Swy-1; Williams et al., 2001a; Williams & Hervig, 2005), probably because of the differences in sample composition (bulk versus < 0.2 μm fractions), processing (treatment with mannitol and cation exchange with ammonium acetate), and/or depositional environments of the bentonites.

The tetrahedral fixed B concentrations of the NH_4^+-exchanged < 0.2 µm fractions range from 0.2 to 196 µg/g, whereas untreated sub-samples have much higher values (9.4 to 429 µg/g B; Table 7.6). The < 0.2 µm fractions of Ca- and Mg-bentonites have lower B concentrations of up to 30 µg/g, with the lowest values (~ 0.2 µg/g) in lateritic bentonite from Bahia, Brazil. The < 0.2 µm fractions of Na-bentonites have higher but more variable B concentrations of up to 160 µg/g in the K_2O-and illite-poor smectite from Pertek, Turkey and up to 196 µg/g of B in the K_2O-rich, R0 illite-smectite from Fallon, Nevada (Table 7.6; Fig. 7.7). The K_2O and B concentrations reveal two groups when plotted against each other. One group shows little covariation in K_2O and B content, whereas the other group shows an increase in B content with increasing K_2O content (Fig. 7.7). The covariation of B and K_2O is consistent with the covariation of B and interstratified illite content (Fig. 7.7). There is no systematic variation of the $\delta^{11}B$ values with the K_2O content.

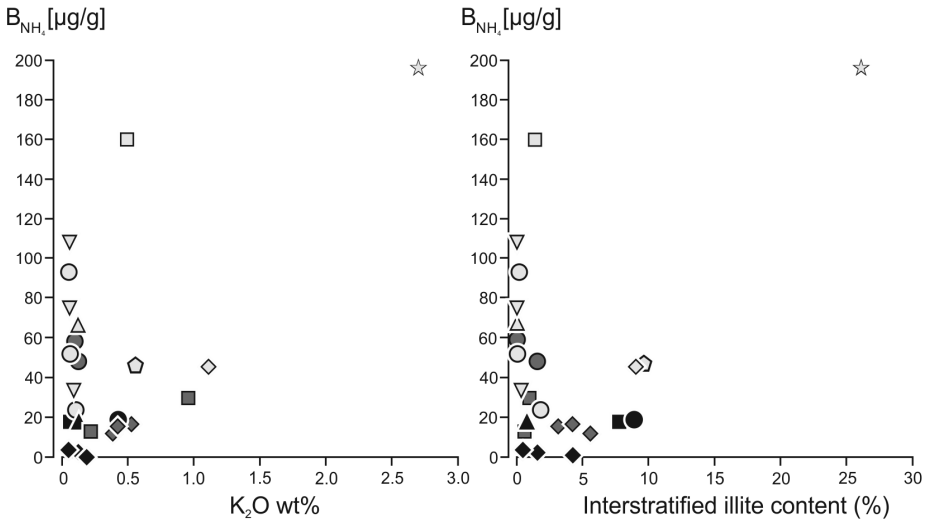

Fig. 7.7: Variation in boron concentration with K_2O and the interstratified illite content of ammonium exchanged < 0.2 µm fractions. Black: Mg-bentonites; dark grey: Ca-bentonites, and light grey: Na-bentonites

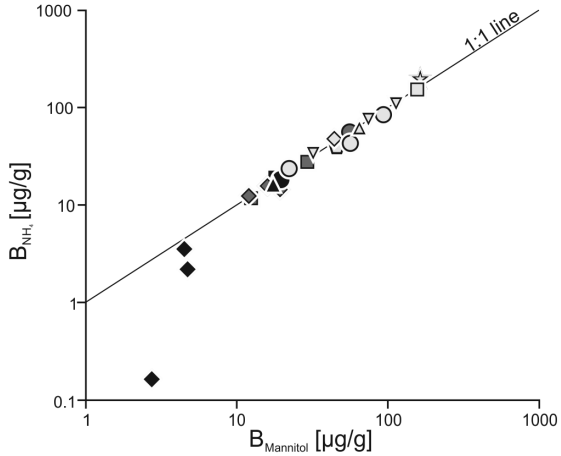

Fig. 7.8: Comparison of the boron content in mannitol treated and ammonium exchanged smectite separates. Symbols: Fig. 7.5.

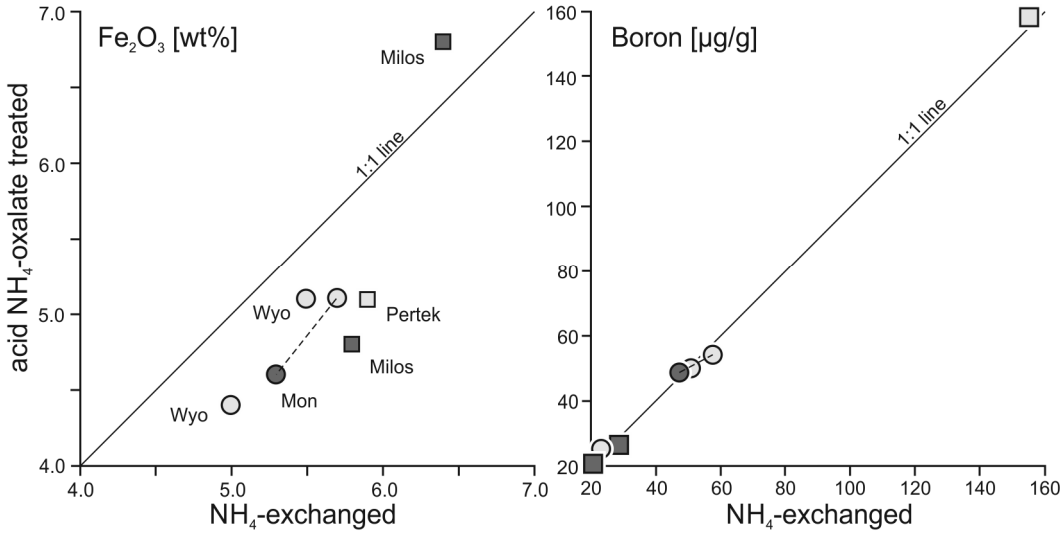

Fig. 7.9: The effect of AAO treatment on the soluble iron phases (left) and the boron content (right) of smectite separates determined using PGAA. Dark grey: Ca-bentonites, and light grey: Na-bentonites.

Table 7.6 - Part 1: Geochemical compositions of untreated (U), distilled water (D), mannitol (M), and ammonium exchanged - mannitol (A) treated, as well as acid ammonium oxalate (F) treated < 0.2 µm fractions. **Part 2** includes the estimated boron concentrations in the fluids, based on Spivack & Edmond (1987) and You et al. (1995, 1996). See text for further explanation.

	Element	SiO_2	Al_2O_3	Fe_2O_3	TiO_2	MnO	CaO	MgO	Na_2O	K_2O	Li_2O	SO_3^-	PO_4	Cl^-	NH_4^-	Cr_2O_5	VO_3	CoO	Sm_2O_3	Gd_2O_3	B
	unit	wt%	wt%	wt%	wt%	µg/g	wt%	wt%	wt%	wt%	wt%	wt%	wt%	µg/g	wt%	wt%	µg/g	µg/g	µg/g	µg/g	µg/g
	unc %	<1.4	<2.6	<3.8	<7.0	<8.0	<19.0	<7.0	<11.0	<12.0	8.0	<9.0	<9.0	<25.0	<5.0	<7.0	7.0	7.0	<16.0	<17.0	<5.0
Dominantly marine depositional environments																					
Milos, GR																					
Angeria	ANG-U	59.0	24.0	5.6	0.49		2.1	3.4	2.4	1.2		1.3		310				160	1.0	1.1	31.8
	ANG-D	63.0	22.8	5.2	0.51		1.8	4.9	0.9	0.8		0.2		30			T	T	0.7	0.6	22.3
	ANG-M	62.0	24.0	5.6	0.57		2.2	4.3	0.1	1.0		T		40			690	260	0.9	0.0	28.8
	ANG-A	64.0	22.3	5.8	0.56	230	0.2	3.9	0.4	0.9				16	1.7		650		0.8	0.8	29.1
	ANG-F	65.0	23.6	4.8	0.67			3.2		0.7				32	1.1		650		0.7	0.7	26.3
Zoulias	ZO-U	63.0	19.0	6.2	0.52	500	2.0	5.5	2.2	0.3				490				240	2.5	3.0	13.9
	ZO-M	63.0	22.0	6.9	0.57	570	1.8	5.9	0.2	0.2				20				180	2.7	3.0	12.6
	ZO-A	65.0	20.7	6.4	0.57	230	0.4	4.7	0.1	0.2				70	1.9				1.9	2.2	13.0
	ZO-F	65.0	19.5	6.8	0.64	410	1.9	4.1		0.2				20	1.0				2.3	2.6	17.1
Georgia, Rep. of																					
Askana	B17-U	63.0	21.5	3.9	0.18	650	0.9	5.0	3.8	1.2		0.7		600					0.5	0.4	58.4
	B17-M	65.0	21.7	4.0	0.19	470	0.9	5.0	1.5	1.1		0.1		40					0.5	0.5	45.7
	B17-A	64.0	22.0	4.1	0.20	520	0.1	5.8	0.5	0.9				20	1.8				0.4	0.4	45.4
	B17-BGR	65.7	21.2	3.7	0.39		0.1	4.8	3.2	0.8		0.0	0.04								
Montana, USA																					
Glasgow	SB01-U	61.0	22.0	4.2	0.14	180	1.3	4.5	4.5	0.3		2.0		149					1.7	2.8	45.4
	SB01-M	65.0	23.0	5.0	0.13	410	1.3	4.4		0.2		0.3		60					2.7	3.3	48.8
	SB01-A	64.0	24.0	5.3	0.14	540	0.2	3.9		0.1		0.2		50	1.6				1.9	2.9	47.7
	SB01-F	66.0	23.0	4.6	0.12	159	1.6	3.4		0.2		0.1		T	1.2				2.1	3.0	48.8
	SB02-U	61.0	22.0	5.0	0.18	260	0.7	3.6	4.8	0.2		2.2		40					2.7	3.2	61.5
	SB02-M	65.0	23.5	5.3	0.20	340	0.8	3.4	1.2	0.1		0.2		40					0.0	0.0	57.1
	SB02-A	64.0	24.0	5.7	0.24	290	0.2	3.4	0.5	0.1		T		80	1.6				2.6	3.2	57.8
	SB02-F	66.0	23.4	5.1	0.21	160	0.9	3.2		0.1		0.1			1.2				2.0	2.0	54.0
Wyoming, USA																					
Mowry, oxi.	MOFO-U	63.0	24.0	5.5	0.14	240	0.9	2.8	3.5	0.1				50					0.9	0.0	49.1
	MOFO-D	63.0	25.0	5.8	0.15	250	1.0	2.8	2.1	0.1		0.1		28					0.9	0.8	50.9
	MOFO-M	62.0	25.2	6.1	0.16	260	1.0	3.3	2.1	0.1				18					1.1	1.0	54.3
	MOFO-A	65.0	23.9	5.5	0.16	280	0.2	3.0	0.3	0.1				32	1.7				0.7	0.8	51.2
	MOFO-F	65.0	24.0	5.1	0.15	160	1.0	2.6	0.3	0.0					1.23			210	0.6	0.5	50.0

Table 7.6 - Part 1: Continued.

	Element	SiO_2	Al_2O_3	Fe_2O_3	TiO_2	MnO	CaO	MgO	Na_2O	K_2O	Li_2O	SO_3^-	PO_4	Cl^-	NH_4^-	Cr_2O_5	VO_3	CoO	Sm_2O_3	Gd_2O_3	B
	unit	wt%	wt%	wt%	wt%	µg/g	wt%	wt%	wt%	wt%	wt%	wt%	wt%	µg/g	wt%	wt%	µg/g	µg/g	µg/g	µg/g	µg/g
	unc %	<1.4	<2.6	<3.8	<7.0	<8.0	<19.0	<7.0	<11.0	<12.0	8.0	<9.0	<9.0	<25.0	<5.0	<7.0	7.0	7.0	<16.0	<17.0	<5.0
Dominantly marine depositional environments																					
Mowry, red.	MOFR-U	62.0	24.0	4.6	0.14		0.2	2.8	5.6	0.1		0.5	0.50						0.0	1.5	33.7
	MOFR-D	64.0	24.1	4.9	0.16	230	0.2	3.1	3.4	0.1		0.3							2.4	2.2	22.2
	MOFR-M	61.0	26.0	5.0	0.15	150	0.4	3.5	3.2	0.1		0.2							2.0	1.7	22.2
	MOFR-A	66.0	23.8	5.0	0.15	120		3.1	0.1	0.1				40	1.7				1.6	1.4	23.4
	MOFR-F	66.0	24.6	4.4	0.16	150	0.4	3.1		0.1				90	1.7				0.5	0.5	25.3
Beaver, oxi	MOHO-U	64.0	22.5	5.0	0.10	300	0.6	3.6	3.0	0.1		0.6							1.5	1.5	87.6
	MOHO-M	62.0	24.8	5.7	0.12	210	0.6	3.9	2.0	0.0		0.3		22					1.7	1.7	93.2
	MOHO-A	64.0	24.5	5.7	0.12	290	0.1	3.2	0.3	0.0				12	1.9				1.3	1.4	83.9
Otay, USA																					
Otay	OT-U	61.0	17.0	2.8	0.10	600	1.2	8.3	5.6	0.4				33000					0.1	2.2	154.4
	OT-M	64.0	19.3	3.1	0.16	540	1.1	9.7	0.7	0.4				20		0.7			2.8	2.8	19.8
	OT-A	65.0	19.9	3.3	0.21	240	0.2	8.5	0.5	0.3				12	2.0				1.8	1.7	19.0
Tunceli, TR																					
Pertek	PE-U	60.0	24.0	5.8	0.20	520	1.0	3.5	4.4	0.5				40					3.4	0.0	169.9
	PE-D	63.0	24.0	6.0	0.19	520	1.1	3.4	1.8	0.4				60					0.7	0.8	164.9
	PE-M	63.0	24.0	5.9	0.22	590	1.4	3.5	1.7	0.5				62					2.8	1.5	161.2
	PE-A	64.0	24.0	5.9	0.18	250	0.1	3.5	0.6	0.3				40	1.6					0.5	155.3
	PE-F	67.0	21.6	5.1	0.34	?	1.5	2.6	0.1	0.4					1.4				0.8	0.8	158.1
Armenia																					
Tavush	B31-U	65.0	16.8	7.1	0.28	230	1.1	4.8	3.8	0.6		0.5		510					0.3	0.5	53.7
	B31-M	67.0	18.7	6.7	0.29	290	0.8	4.8	1.3	0.5		0.2		50					0.4	0.4	45.3
	B31-A	66.0	19.2	6.9	0.30	210	0.1	5.2	0.7	0.5					1.7				0.3	0.4	46.8
	B31-BGR	69.7	16.3	5.6	0.77		0.4	3.7	2.8	0.6			0.11								
Cabo de Gata, ES																					
Los Trancos	TR-U	63.0	23.8	2.7	0.14	880	1.5	7.1	0.9	0.2				820					1.6	1.5	61.8
	TR-M	66.0	22.0	2.6	0.15	950	1.5	6.9		0.1				40					1.3	1.5	18.9
	TR-A	67.0	22.3	3.0	0.16	310	0.2	5.5	0.5	0.1				24	1.7				0.5	0.8	17.9

Table 7.6 - Part 1: Continued.

	Element	SiO_2	Al_2O_3	Fe_2O_3	TiO_2	MnO	CaO	MgO	Na_2O	K_2O	Li_2O	SO_3^-	PO_4	Cl^-	NH_4^-	Cr_2O_5	VO_3	CoO	Sm_2O_3	Gd_2O_3	B
	unit	wt%	wt%	wt%	wt%	µg/g	wt%	wt%	wt%	wt%	wt%	wt%	wt%	µg/g	wt%	wt%	µg/g	µg/g	µg/g	µg/g	µg/g
	unc %	<1.4	<2.6	<3.8	<7.0	<8.0	<19.0	<7.0	<11.0	<12.0	8.0	<9.0	<9.0	<25.0	<5.0	<7.0	7.0	7.0	<16.0	<17.0	<5.0
Dominantly terrestrial depositional environments																					
Bavaria, DE																					
Zweikirchen	ZW50-U	63.0	19.0	8.3	0.19	180	2.3	5.5	0.3	0.9		0.2		30				60	6.3	7.0	18.3
	ZW50-M	64.0	19.8	7.8	0.19		1.7	5.5	0.9	0.6									7.0	8.3	16.3
	ZW50-A	64.0	20.0	8.1	0.20		0.3	5.3	0.7	0.5				80	1.4				4.2	5.0	16.0
	ZW48-U	65.0	19.5	7.1	0.20	180	1.7	5.5		0.6				40					7.6	9.0	16.1
	ZW48-D	64.0	21.4	7.4	0.22	200	1.6	5.0	0.2	0.5				48				290	7.7	10.0	17.2
	ZW48-M	62.0	23.0	6.4	0.21	350	1.8	5.7		0.5				100					8.0	10.0	19.4
	ZW48-A	65.0	20.9	7.0	0.20		0.2	4.9	0.1	0.4				50	1.5			60	0.1	5.0	15.2
Mittersberg	MB34-U	63.0	20.0	5.1	0.21	230	2.5	7.4	0.5	0.5				130					10.3	13.0	12.2
	MB34-M	64.0	21.0	5.0	0.21	290	2.6	7.1		0.4				34					10.7	13.0	12.0
	MB34-A																				
Sardinia, IT																					
Bussu/S'Aliderru	BU-U	66.0	22.0	3.3	0.21	1230	1.2	5.9	1.3	0.1				1450					1.0	1.4	23.3
	BU-M	64.0	23.6	3.5	0.20	1050	1.3	6.1	0.6	0.1				23					0.3	0.5	18.1
	BU-A	66.0	23.0	3.5	0.20	280	0.1	5.5	0.5	0.1				40	1.9				0.004	0.006	18.3
Rio Negro, AR																					
Lago Pellegrini	Arg1-M	64.0	23.0	6.3	0.72	100	0.2	3.6	2.1	0.14				180					2.6	2.4	32.1
	Arg-A	64.0	23.4	6.2	0.72	140	0.2	3.9	0.2	0.08					1.3				2.6	2.7	33.5
	Arg5-M	65.0	23.0	5.7	0.16	160	0.1	3.5	2.2	0.05		0.1							1.5	1.3	74.5
	Arg5-A	65.0	23.0	6.0	0.17	190	0.1	3.6	0.2	0.05					1.6				1.5	1.4	76.1
	Arg11-M	66.0	22.5	5.2	0.16	220	0.8	3.9	1.5	0.05									1.0	1.1	113.0
	Arg11-A	67.0	22.2	5.1	0.15	230	0.5	3.8	0.1	0.05					1.5				1.0	1.5	109.6
Nevada, USA																					
Fallon	B51-U	57.0	21.6	6.1	0.61	300	0.7	3.8	3.9	2.7	1.9	0.6		5400					1.8	1.9	429.2
	B51-M																				165.0
	B51-A	59.0	25.0	6.7	0.60	310	0.1	3.3	0.1	2.7				20	1.5				1.7	2.3	196.0
San Juan, AR																					
La Tranquera	B23-U	65.0	22.0	2.0	0.11		1.1	5.2	3.4	0.1		0.2		590					0.8	1.2	75.5
	B23-M	67.0	22.6	2.0	0.12		1.1	5.1	2.2	0.1				50					1.1	1.2	65.2
	B23-A	66.0	24.0	2.1	0.12	150	0.1	5.2	0.3	0.05				30	2.3				0.7	1.0	58.7
	B23-BGR	69.7	20.6	1.3	0.26		0.3	3.8	3.6	0.4			0.04								

R

Table 7.6 - Part 1: Continued.

	Element	SiO_2	Al_2O_3	Fe_2O_3	TiO_2	MnO	CaO	MgO	Na_2O	K_2O	Li_2O	SO_3^-	PO_4	Cl^-	NH_4^-	Cr_2O_5	VO_3	CoO	Sm_2O_3	Gd_2O_3	B
	unit	wt%	wt%	wt%	wt%	µg/g	wt%	wt%	wt%	wt%	wt%	wt%	wt%	µg/g	wt%	wt%	µg/g	µg/g	µg/g	µg/g	µg/g
	unc %	<1.4	<2.6	<3.8	<7.0	<8.0	<19.0	<7.0	<11.0	<12.0	8.0	<9.0	<9.0	<25.0	<5.0	<7.0	7.0	7.0	<16.0	<17.0	<5.0
Terrestrial Laterite																					
Bahia, BR Vitoria da Conquista	D15-U	58.0	16.5	13.5	0.10		4.1	5.0	0.6	0.5				11000					0.7	0.0	14.6
	D15-M	61.0	17.6	13.8	0.16	240	2.3	5.1	0.3	0.1				51		0.0			0.8	1.4	4.8
	D15-A	61.0	18.0	14.2	0.17	260	0.2	4.0	0.4	0.1				80	2.2				0.5	0.5	2.1
	KOP2-U	61.0	19.3	12.5	0.38		1.2	4.4	0.4	0.2				700		0.8	500		11.0	T	9.4
	KOP2-M	61.0	18.8	12.8	0.48		1.2	4.4	0.7	0.1				180		0.8	550		0.1	0.3	4.6
	KOP2-A	62.0	19.0	12.9	0.47	90	0.1	3.7	0.2	0.1					1.9	0.9			9.0	0.2	3.4
	Furo-U	60.0	14.9	16.9	0.44		1.7	4.9	0.6	0.3				1000		0.1		110	0.5	1.2	28.3
	Furo-M	60.0	14.9	16.8	0.77	840	1.6	5.5	0.2	0.1				25		0.1	340		1.4	3.5	2.7
	Furo-A	62.0	15.1	16.5	0.69	220	0.2	3.5	0.4	0.2				30	1.8	0.1		80	0.8	2.1	0.2

Table 7.6 - Part 2: The estimated boron concentrations in the fluids, based on Spivack & Edmond (1987) and You et al. (1995, 1996). See text for further explanation.

	Sample	B_{K2O} µg/g	B_{uptake} µg/g	B_{fluid} K-corrected in mg/L K_D after You et al. (1996)					B_{fluid} not K-corrected in mg/L					B_{fluid} K-corrected in mg/L K_D after Spivack & Edmond (1987)				B_{fluid} not K-corrected in mg/L			
				5.0 high pH	4.0	3.0	2.0	1.0 high Temp.	5.0 high pH	4.0	3.0	2.0	1.0 high Temp.	33 1°C	29 25°C	21 40°C	11 100°C	33 1°C	29 25°C	21 40°C	11 100°C
Dominantly marine depositional environments																					
Milos, GR																					
Angeria	ANG-M	28.1	0.8	0.2	0.2	0.3	0.4	0.8	5.8	7.2	9.6	14.4	28.8	0.02	0.03	0.04	0.1	0.9	1.0	1.4	2.6
	ANG-A	24.3	4.8	1.0	1.2	1.6	2.4	4.8	5.8	7.3	9.7	14.5	29.1	0.1	0.2	0.2	0.4	0.9	1.0	1.4	2.6
Zoulias	ZO-M	6.5	6.1	1.2	1.5	2.0	3.0	6.1	2.5	3.2	4.2	6.3	12.6	0.2	0.2	0.3	0.6	0.4	0.4	0.6	1.1
	ZO-A	4.9	8.1	1.6	2.0	2.7	4.1	8.1	2.6	3.3	4.3	6.5	13.0	0.2	0.3	0.4	0.7	0.4	0.4	0.6	1.2
Georgia, Rep. of	B17-M	30.0	15.7	3.1	3.9	5.2	7.9	15.7	9.1	11.4	15.2	22.9	45.7	0.5	0.5	0.7	1.4	1.4	1.6	2.2	4.2
Askana	B17-A	23.7	21.6	4.3	5.4	7.2	10.8	21.6	9.1	11.3	15.1	22.7	45.4	0.7	0.7	1.0	2.0	1.4	1.6	2.2	4.1
Montana, USA	SB01-M	4.1	44.7	8.9	11.2	14.9	22.3	44.7	9.8	12.2	16.3	24.4	48.8	1.4	1.5	2.1	4.1	1.5	1.7	2.3	4.4
Glasgow	SB01-A	3.0	44.7	8.9	11.2	14.9	22.3	44.7	9.5	11.9	15.9	23.8	47.7	1.4	1.5	2.1	4.1	1.4	1.6	2.3	4.3
	SB02-M	3.3	53.9	10.8	13.5	18.0	26.9	53.9	11.4	14.3	19.0	28.6	57.1	1.6	1.9	2.6	4.9	1.7	2.0	2.7	5.2
	SB02-A	2.2	55.6	11.1	13.9	18.5	27.8	55.6	11.6	14.4	19.3	28.9	57.8	1.7	1.9	2.6	5.1	1.8	2.0	2.8	5.3
Wyoming, USA	MOFO-M	2.2	52.2	10.4	13.0	17.4	26.1	52.2	10.9	13.6	18.1	27.2	54.3	1.6	1.8	2.5	4.7	1.6	1.9	2.6	4.9
Mowry, oxi.	MOFO-A	2.2	49.1	9.8	12.3	16.4	24.5	49.1	10.2	12.8	17.1	25.6	51.2	1.5	1.7	2.3	4.5	1.6	1.8	2.4	4.7
	MOFR-M	3.0	19.2	3.8	4.8	6.4	9.6	19.2	4.4	5.5	7.4	11.1	22.2	0.6	0.7	0.9	1.7	0.7	0.8	1.1	2.0
Mowry, red.	MOFR-A	3.0	20.4	4.1	5.1	6.8	10.2	20.4	4.7	5.8	7.8	11.7	23.4	0.6	0.7	1.0	1.9	0.7	0.8	1.1	2.1
	MOHO-M	1.3	91.9	18.4	23.0	30.6	45.9	91.9	18.6	23.3	31.1	46.6	93.2	2.8	3.2	4.4	8.4	2.8	3.2	4.4	8.5
Beaver, oxi	MOHO-A	1.3	82.5	16.5	20.6	27.5	41.3	82.5	16.8	21.0	28.0	41.9	83.9	2.5	2.8	3.9	7.5	2.5	2.9	4.0	7.6
Otay, USA	OT-M	12.0	7.8	1.6	2.0	2.6	3.9	7.8	4.0	5.0	6.6	9.9	19.8	0.2	0.3	0.4	0.7	0.6	0.7	0.9	1.8
Otay	OT-A	9.0	10.0	2.0	2.5	3.3	5.0	10.0	3.8	4.8	6.3	9.5	19.0	0.3	0.3	0.5	0.9	0.6	0.7	0.9	1.7
Tunceli, TR	PE-M	13.6	147.5	29.5	36.9	49.2	73.8	147.5	32.2	40.3	53.7	80.6	161.2	4.5	5.1	7.0	13.4	4.9	5.6	7.7	14.7
Pertek	PE-A	7.1	148.2	29.6	37.0	49.4	74.1	148.2	31.1	38.8	51.8	77.6	155.3	4.5	5.1	7.1	13.5	4.7	5.4	7.4	14.1
Armenia	B31-M	14.7	30.5	6.1	7.6	10.2	15.3	30.5	9.1	11.3	15.1	22.6	45.3	0.9	1.1	1.5	2.8	1.4	1.6	2.2	4.1
Tavush	B31-A	13.9	32.9	6.6	8.2	11.0	16.4	32.9	9.4	11.7	15.6	23.4	46.8	1.0	1.1	1.6	3.0	1.4	1.6	2.2	4.3
Cabo de Gata, ES	TR-M	2.7	16.1	3.2	4.0	5.4	8.1	16.1	3.8	4.7	6.3	9.4	18.9	0.5	0.6	0.8	1.5	0.6	0.7	0.9	1.7
Los Trancos	TR-A	1.8	16.0	3.2	4.0	5.3	8.0	16.0	3.6	4.5	6.0	8.9	17.9	0.5	0.6	0.8	1.5	0.5	0.6	0.9	1.6

Table 7.6 - Part 2: Continued.

	Sample	B_{K2O} µg/g	B_{uptake} µg/g	B_{fluid} K-corrected in mg/L K_D after You et al. (1996)					B_{fluid} not K-corrected in mg/L					B_{fluid} K-corrected in mg/L K_D after Spivack & Edmond (1987)				B_{fluid} not K-corrected in mg/L			
				5.0 high pH	4.0	3.0	2.0	1.0 high Temp.	5.0 high pH	4.0	3.0	2.0	1.0 high Temp.	33 1°C	29 25°C	21 40°C	11 100°C	33 1°C	29 25°C	21 40°C	11 100°C
Dominantly terrestrial depositional environments																					
Bavaria, DE	ZW50-M	15.0	1.3	0.3	0.3	0.4	0.6	1.3	3.3	4.1	5.4	8.2	16.3	0.04	0.04	0.06	0.12	0.49	0.56	0.78	1.48
Zweikirchen	ZW50-A	13.1	2.9	0.6	0.7	1.0	1.5	2.9	3.2	4.0	5.3	8.0	16.0	0.09	0.10	0.14	0.26	0.48	0.55	0.76	1.45
	ZW48-M	12.8	6.6	1.3	1.6	2.2	3.3	6.6	3.9	4.8	6.5	9.7	19.4	0.20	0.23	0.31	0.60	0.59	0.67	0.92	1.76
	ZW48-A	11.2	4.0	0.8	1.0	1.3	2.0	4.0	3.0	3.8	5.1	7.6	15.2	0.12	0.14	0.19	0.37	0.46	0.52	0.72	1.38
Mittersberg	MB34-M	10.6	1.4	0.3	0.3	0.5	0.7	1.4	2.4	3.0	4.0	6.0	12.0	0.04	0.05	0.06	0.12	0.36	0.41	0.57	1.09
	MB34-A																				
Sardinia, IT	BU-M	3.5	14.5	2.9	3.6	4.8	7.3	14.5	3.6	4.5	6.0	9.0	18.1	0.4	0.5	0.7	1.3	0.5	0.6	0.9	1.6
Bussu/S'Aliderru	BU-A	3.5	14.8	3.0	3.7	4.9	7.4	14.8	3.7	4.6	6.1	9.2	18.3	0.4	0.5	0.7	1.3	0.6	0.6	0.9	1.7
Rio Negro, AR	Arg1-M	3.8	28.3	5.7	7.1	9.4	14.2	28.3	6.4	8.0	10.7	16.1	32.1	0.9	1.0	1.3	2.6	1.0	1.1	1.5	2.9
Lago Pellegrini	Arg-A	2.2	31.4	6.3	7.8	10.5	15.7	31.4	6.7	8.4	11.2	16.8	33.5	1.0	1.1	1.5	2.9	1.0	1.2	1.6	3.0
	Arg5-M	1.4	73.2	14.6	18.3	24.4	36.6	73.2	14.9	18.6	24.8	37.3	74.5	2.2	2.5	3.5	6.7	2.3	2.6	3.5	6.8
	Arg5-A	1.4	74.7	14.9	18.7	24.9	37.4	74.7	15.2	19.0	25.4	38.0	76.1	2.3	2.6	3.6	6.8	2.3	2.6	3.6	6.9
	Arg11-M	1.4	111.7	22.3	27.9	37.2	55.8	111.7	22.6	28.3	37.7	56.5	113.0	3.4	3.9	5.3	10.2	3.4	3.9	5.4	10.3
	Arg11-A	1.4	108.3	21.7	27.1	36.1	54.1	108.3	21.9	27.4	36.5	54.8	109.6	3.3	3.7	5.2	9.8	3.3	3.8	5.2	10.0
Nevada, USA	B51-M																				
Fallon	B51-A	73.6	122.3	24.5	30.6	40.8	61.2	122.3	39.2	49.0	65.3	98.0	196.0	3.7	4.2	5.8	11.1	5.9	6.8	9.3	17.8
San Juan, AR	B23-M	3.3	61.9	12.4	15.5	20.6	31.0	61.9	13.0	16.3	21.7	32.6	65.2	1.9	2.1	2.9	5.6	2.0	2.2	3.1	5.9
La Tranquera	B23-A	1.3	57.4	11.5	14.3	19.1	28.7	57.4	11.7	14.7	19.6	29.3	58.7	1.7	2.0	2.7	5.2	1.8	2.0	2.8	5.3
Terrestrial Laterite																					
Bahia, BR	D15-M	1.9	2.9	0.6	0.7	1.0	1.5	2.9	1.0	1.2	1.6	2.4	4.8	0.1	0.1	0.1	0.3	0.1	0.2	0.2	0.4
Vitoria da Conquista	D15-A	3.5	-1.4	-0.3	-0.3	-0.5	-0.7	-1.4	0.4	0.5	0.7	1.1	2.1	0.0	0.0	-0.1	-0.1	0.1	0.1	0.1	0.2
	KOP2-M	1.5	3.0	0.6	0.8	1.0	1.5	3.0	0.9	1.1	1.5	2.3	4.6	0.1	0.1	0.1	0.3	0.1	0.2	0.2	0.4
	KOP2-A	1.4	2.0	0.4	0.5	0.7	1.0	2.0	0.7	0.9	1.1	1.7	3.4	0.1	0.1	0.1	0.2	0.1	0.1	0.2	0.3
	Furo-M	1.4	1.4	0.3	0.3	0.5	0.7	1.4	0.5	0.7	0.9	1.4	2.7	0.0	0.0	0.1	0.1	0.1	0.1	0.1	0.2
	Furo-A	5.2	-5.0	-1.0	-1.3	-1.7	-2.5	-5.0	0.0	0.0	0.1	0.1	0.2	-0.2	-0.2	-0.2	-0.5	0.005	0.01	0.01	0.01

7.4.4 Boron isotope values (SIMS)

Mannitol-treated and cation exchanged smectites (< 0.2 µm fractions) show different ranges of $\delta^{11}B$ values of -22.0 ‰ to +27.2 ‰ respective -30.2 ‰ to +17.2 ‰ relative to NBS SRM 951 (Table 7.7). Although the cation exchange with ammonium had only a minor effect on the B concentrations it can influence the $\delta^{11}B$ values (Tables 7.6 and 7.7), with the $\delta^{11}B$ values of the Glasgow and the La Tranquera bentonites being the most drastically influenced (Table 7.7; Fig. 7.10 and 7.11). Other bentonites show only a small or almost no change in $\delta^{11}B$ values after cation exchange (Table 7.7; Fig. 7.10 and 7.11), indicating the presence of a very small exchangeable boron component with only slightly different $\delta^{11}B$ values. The smectites from bentonites deposited in a purely terrestrial environments exhibit negative $\delta^{11}B$ values, whereas Na-bentonites from marine depositional settings reveal highly variable boron isotope values (Table 7.7). It must finally be noted that the small concentrations of interlayer boron - comparing mannitol-treated and cation exchanged smectites - make the calculation of interlayer $\delta^{11}B$ unreliable due to a high propagated error.

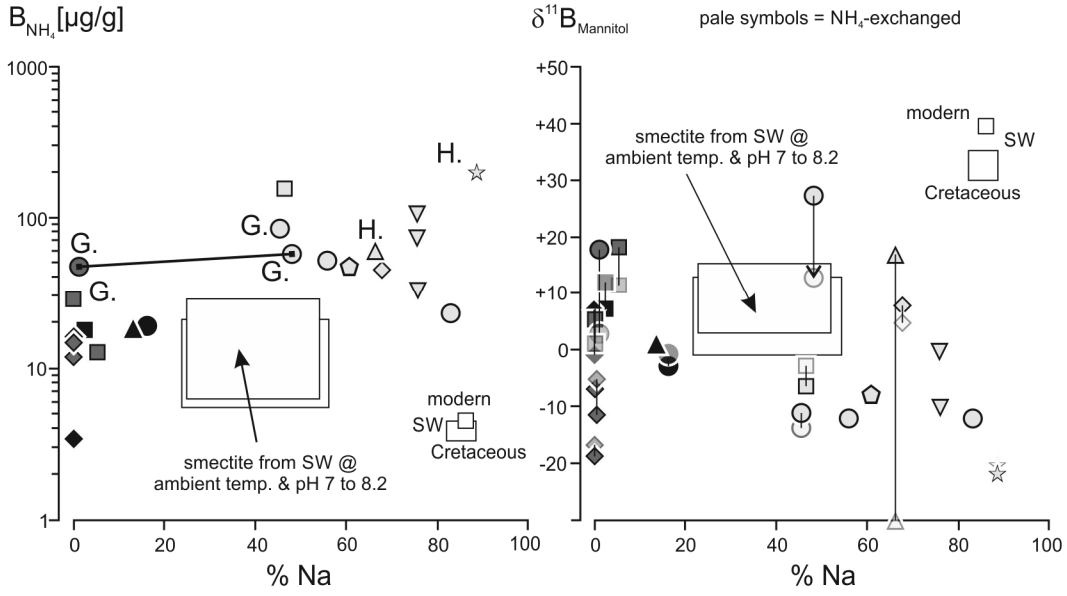

Fig. 7.10: The fixed boron content (left), $\delta^{11}B$ values (right) and sodicity of the smectite interlayer, and estimated interlayer compositions in equilibrium with seawater at variable B concentrations and pH values. Black: Mg-bentonites; dark grey: Ca-bentonites, and light grey: Na-bentonites. H. = halite, G. = gypsum, the thick solid line connects oxidised and reduced bentonites from a deposit at Glasgow, Montana. The average exchangeable sodium content for Lago Pellegrini was taken from Iborra et al. (2006). Boron partition factors: Palmer et al., 1987; and Spivack et al., 1987; You et al., 1996. Boron isotope fractionation: Williams, 2000; Williams et al., 2001a. Sodium content of smectites in equilibrium with seawater: Sayles & Mangelsdorf, 1977; Modern and Cretaceous SW: Vengosh et al., 1991; Lemarchand et al., 2002; Timofeeff et al., 2006; Paris et al., 2010.

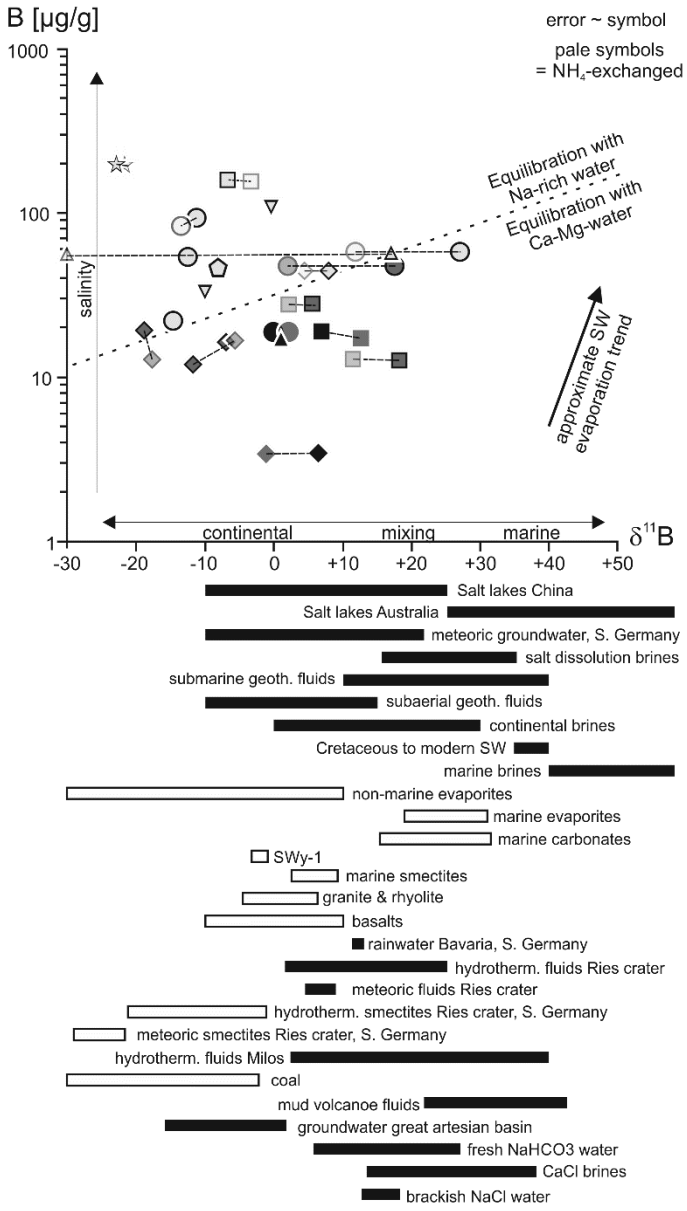

Fig. 7.11: Boron concentrations and $\delta^{11}B$ values of smectites from bentonites, as well as $\delta^{11}B$ values of various fluids (black boxes), rocks and smectites (white boxes). Black: Mg-bentonites; dark grey: Ca-bentonites; light grey: Na-bentonites. Dashed lines connect differently treated sub-samples. (Data from: Swihart et al., 1986; Spivack et al., 1987; Palmer et al., 1987; Palmer, 1991; Vengosh et al., 1991; Barth, 1993; Ishikawa & Nakamura, 1993; Vengosh et al., 1995; You et al., 1995, 1996; Leeman & Sisson, 1996; Palmer & Swihart, 1996; Eisenhut & Heumann, 1997; Barth, 2000; Williams, 2000; Williams et al., 2001a; Lemarchand et al., 2002; Paris et al., 2010; Muttik et al., 2011; Xiao et al., 2013; Boschetti et al., 2014).

Table 7.7: SIMS boron content and $\delta^{11}B$ values of smectites, and estimated $\delta^{11}B$ values of the fluid at 25° and 90°C. B3: 3-coordinated dissolved boron, B4: 4-coordinated dissolved boron, M: Mannitol-treated samples, and A: Ammonium-exchanged plus mannitol-treated samples.

Location & Deposit	**Sample**	**B**	**Mean**	**±**	**Min.**	**Max.**	**100 % B3**	**80% B3**	**70% B4**	**100% B4**	**100 % B3**	**80% B3**	**70% B4**	**100% B4**
		µg/g	$\delta^{11}B_{NBS\ SRM\ 951}$	2 SD			298K	298K	298K	298K	363K	363K	363K	363K
Dominantly marine depositional settings														
Milos, GR														
Angeria	ANG-M	25.1	5.6	2.0	1.4	13.0	37.1	33.5	24.6	19.2	30.8	27.9	20.7	16.3
	ANG-A	26.5	2.7	1.2	-0.3	3.1	34.1	30.6	21.6	16.3	27.9	25.0	17.7	13.4
Zoulias	ZO-M	26.2	18.4	2.5	16.8	20.9	49.8	46.2	37.3	32.0	43.6	40.7	33.4	29.1
	ZO-A	14.6	11.7	4.6	9.4	14.0	43.1	39.6	30.7	25.3	36.9	34.0	26.8	22.4
Georgia, Rep. Of														
Askana	B17-M	47.6	8.1	1.7	6.4	9.2	39.5	35.9	27.0	21.7	33.3	30.4	23.1	18.8
	B17-A	38.8	4.5	1.4	2.4	6.3	35.9	32.4	23.4	18.1	29.7	26.8	19.5	15.2
Montana, USA														
Glasgow	SB01-M	64.3	17.6	1.6	16.6	19.3	49.1	45.5	36.6	31.2	42.9	40.0	32.7	28.3
	SB01-A	36.6	2.3	0.2	2.2	2.4	33.8	30.2	21.3	15.9	27.5	24.6	17.4	13.0
	SB02-M	49.1	27.2	2.4	24.8	28.4	58.6	55.1	46.1	40.8	52.4	49.5	42.2	37.9
	SB02-A	47.1	11.8	0.5	11.4	12.1	43.3	39.7	30.8	25.4	37.1	34.2	26.9	22.5
Wyoming, USA														
Lowell	MOFO-M	42.4	-12.2	1.3	-13.0	-10.0	19.2	15.7	6.7	1.4	13.0	10.1	2.8	-1.5
	MOFR-M	19.0	-14.5	0.9	-15.4	-13.9	17.0	13.4	4.5	-0.9	10.8	7.8	0.6	-3.8
	MOHO-M	66.2	-11.2	1.5	-12.9	-9.3	20.3	16.7	7.8	2.4	14.1	11.2	3.9	-0.5
	MOHO-A	64.8	-13.3	0.9	-14.8	-12.4	18.1	14.6	5.6	0.3	11.9	9.0	1.7	-2.6
Otay, USA														
Otay	OT-M	17.5	-2.9	1.3	-4.7	-1.7	28.5	25.0	16.0	10.7	22.3	19.4	12.2	7.8
	OT-A	16.0	1.8	1.8	-2.0	4.6	33.2	29.6	20.7	15.4	27.0	24.1	16.8	12.5
Tunceli, TR														
Pertek	PE-M	125.0	-6.5	1.5	-8.2	-4.8	25.0	21.4	12.5	7.1	18.8	15.8	8.6	4.2
	PE-A	121.8	-3.3	0.3	-3.6	-3.0	28.2	24.6	15.7	10.3	21.9	19.0	11.8	7.4
Armenia														
Tavush	B31-M	55.3	-8.1	0.8	-8.8	-7.3	23.4	19.8	10.9	5.5	17.1	14.2	7.0	2.6
Cabo de Gata, ES														
Los Trancos	TR-M	17.6	7.1	1.0	6.2	8.0	38.6	35.0	26.1	20.7	32.3	29.4	22.2	17.8
	TR-A	23.7	12.2	0.9	11.7	12.9	43.7	40.1	31.2	25.8	37.5	34.5	27.3	22.9

Table 7.7: Continued.

Location & Deposit	Sample	B	Mean	±	Min.	Max.	100 % B3	80 % B3	70 % B4	100 % B4	100 % B3	80 % B3	70 % B4	100 % B4
		µg/g	$\delta^{11}B_{NBS\ SRM\ 951}$	SD			298K	298K	298K	298K	363K	363K	363K	363K
Dominantly terrestrial depositional settings														
Bavaria, DE														
Zweikirchen	ZW50-M	16.4	-6.8	1.4	-8.8	-3.9	24.6	21.1	12.1	6.8	18.4	15.5	8.3	3.9
	ZW48-M	12.4	-18.7	1.4	-22.8	-13.6	12.8	9.2	0.3	-5.1	6.5	3.6	-3.6	-8.0
	ZW48-A	12.7	-17.5	2.1	-18.6	-14.2	13.9	10.4	1.4	-3.9	7.7	4.8	-2.5	-6.8
Mittersberg	MB34-M	23.1	-11.6	2.5	-19.0	-4.1	19.9	16.3	7.4	2.0	13.7	10.8	3.5	-0.9
	MB34-A	16.7	-5.9	1.9	-6.9	-5.0	25.5	21.9	13.0	7.7	19.3	16.4	9.1	4.8
Sardinia, IT														
Bussu (S'Aliderru)	BU-A	13.85	0.6	1.8	-0.9	2.2	32.0	28.5	19.5	14.2	25.8	22.9	15.6	11.3
San Juan, AR														
La Tranquera	B23-M	41.3	17.1	4.0	13.3	20.0	48.6	45.0	36.1	30.7	42.4	39.5	32.2	27.8
	B23-A	39.7	-30.1	0.3	-30.3	-30.0	1.3	-2.2	-11.2	-16.5	-4.9	-7.8	-15.1	-19.4
Rio Negron, AR														
Lago Pellegrini	Arg1-A	27.3	-9.9	1.2	-11.1	-9.2	21.6	18.0	9.1	3.7	15.3	12.4	5.2	0.8
	Arg11-A	82.1	-0.2	0.7	-0.6	0.2	31.3	27.7	18.8	13.4	25.0	22.1	14.9	10.5
Nevada, USA														
Fallon	B51-M	145.9	-22.0	3.1	-32.1	-19.9	9.5	5.9	-3.0	-8.4	3.2	0.3	-6.9	-11.3
	B51-A	153.5	-21.5	1.1	-22.7	-20.8	9.9	6.4	-2.6	-7.9	3.7	0.8	-6.5	-10.8
Terrestrial Laterite														
Bahia, BR														
Vitoria da Conquista	KOP2-M	7.0	6.6	4.1	4.1	10.6	38.0	34.4	25.5	20.2	31.8	28.9	21.6	17.3
	KOP2-A	5.9	-1.0	0.7	-2.6	0.8	30.5	26.9	18.0	12.6	24.3	21.3	14.1	9.7

7.4.5 Calcite and dolomite in bentonites and their stable isotope values

The majority of bulk bentonites contain calcite as the only carbonate phase, with the exception of dolomite in a bentonite (MB34) from Southern Germany, and both dolomite and calcite in bentonites from Askana (B17) and Fallon (B51 and B52). The $\delta^{13}C_{V\text{-}PDB}$ and $\delta^{18}O_{V\text{-}PDB}$ values of the bentonite-associated calcite and dolomite have a range of -14.3 ‰ to +1.8 ‰ for carbon, and exclusively negative values for oxygen of -15.5 ‰ to -4.2 ‰ (Table 7.8; Fig. 7.12). There are no systematic differences in the $\delta^{13}C_{V\text{-}PDB}$ and $\delta^{18}O_{V\text{-}PDB}$ values of carbonates from Na-, Mg- or Ca-bentonites.

Table 7.8: $\delta^{13}C_{V\text{-}PDB}$ and $\delta^{18}O_{V\text{-}PDB}$ values of bentonite-associated carbonates. B.d.l. = below detection limit. Note: Samples with no carbonate are not shown.

Location & deposit	Sample	Material	$\delta^{13}C_{VPDB}$	$\delta^{18}O_{VPDB}$	Comments
Dominantly marine depositional settings					
Milos, GR					
Angeria	ANG	Calcite	1.82	-15.52	
Zoulias	ZO	Calcite	-2.10	-10.05	
Georgia, Rep. of					
Askana	B17	Dolomite/Calcite	0.48	-9.26	
Montana, USA					
Glasgow	SB01	Calcite	-7.97	-8.98	
Glasgow	SB02	Calcite	-14.28	-13.19	
Wyoming, USA					
Mowry, oxi.	MOFO	Calcite	-10.48	-13.96	
Mowry, red.	MOFR	Calcite	-12.20	-10.60	
Beaver, oxi	MOHO	Calcite	-6.76	-10.92	
Tunceli, TR					
Pertek	PE	Calcite	1.52	-9.00	
Armenia					
Tavush	B31	Calcite	-5.91	-8.07	
Cabo de Gata, ES					
Trancos	TR	Calcite/Dolomite	b.d.l	b.d.l	
Dominantly terrestrial depositional settings					
Bavaria, DE					
Zweikirchen	ZW50	Calcite	-8.91	-6.70	Köster & Gilg, 2015
Zweikirchen	ZW48	Calcite	-11.34	-8.42	Köster & Gilg, 2015
Mittersberg	MB34	Dolomite	-7.34	-4.17	Köster & Gilg, 2015
Sardinia, IT					
Bussu (S'Aliderru)	BU	Calcite	-12.7	-6.84	Concretion in bentonite
Bussu (S'Aliderru)	BU	Calcite	-6.25	-16.12	Travertine
Bussu (S'Aliderru)	BU	Calcite	-6.06	-7.61	Cement in conglomerate
Nevada, USA					
Fallon	B51	Calcite	b.d.l	b.d.l	Illite-smectite
Fallon	B52	Calcite	-2.77	-14.24	Traces of dolomite

7.5 Discussion

The analysis of the < 0.2 μm fractions ("smectites") from bentonites provides new insights into the fluids and boron sources during bentonitization. Our analyses show that smectites have fixed boron concentrations (0.2 to 196 μg/g B; Table 7.1) that encompass the entire range of known boron concentrations in montmorillonites (Harder, 1959, 1970), and that smectites from Na-bentonites can be distinguished (> 30 μg/g B) from smectites from Mg- and Ca-bentonites based on the boron concentration. However, the Pertek bentonite (155.3 μg/g B) and one Lago Pellegrini bentonite sample (Arg11: 109.6 μg/g B) are the only smectites from marine depositional settings with a boron content consistent with authigenic marine smectites formed from ocean basalts during the last 20 Ma (110 to 150 μg/g B; Donelly et al., 1979; Dymond, 1981; Spivack & Edmond, 1987; Ishikawa & Nakamura, 1993; Smith et al., 1995); whereas other smectites have lower boron concentrations. Smectites from bentonites in strictly terrestrial depositional settings (Table 7.1; Fig. 7.3) have the most variable boron concentrations (Table 7.6), including both the lowest (0.2 μg/g B) and the highest (196 μg/g B). Contrary to boron content the $\delta^{11}B$ values of mannitol-treated (fixed + interlayer boron; -22.0 ‰ to +27.2 ‰) and ammonium exchanged (fixed boron; -30.2 ‰ to +17.2 ‰; Table 7.7) smectites reveal no systematic relationship with the exchangeable cation occupancy (Fig. 7.10). Smectites from marine depositional environments have both positive $\delta^{11}B$ values similar to aforementioned marine smectites formed from ocean basalts (+2.8 to +9.3 ‰; Ishikawa & Nakamura, 1993) as well as $\delta^{11}B$ values inconsistent with those marine smectites (too high or too low) such as those from Wyoming, Montana, Lago Pellegrini or Pertek (Table 7.7), suggesting variable depositional or diagenetic influences during bentonitization. Smectites from strictly terrestrial depositional settings have $\delta^{11}B$ values ≤ 0 ‰ (Table 7.7) indicating terrestrial fluid sources, oil field waters or fluids interacting with fossil plants or coal.

7.5.1 Boron in Fe-hydroxides, detrital minerals, and the parent material

Amorphous Fe-hydroxides strongly adsorb boron and could be a source of additional boron related to later oxidation (Hara & Tamai, 1968; Goldberg & Glaubig, 1985). However, the removal of Fe-hydroxides of smectites from oxidized and reduced bentonites had no notable influence on boron concentrations (Fig. 7.9), indicating that boron content in Fe-hydroxides is negligible and does not affect our interpretation.

Detrital mica, illite and tourmaline are more problematic because they have higher boron concentrations than smectite (Harder, 1970; Brockamp, 1973; Zeibig et al., 1989). Size separation

produced < 0.2 µm fractions comprised largely of smectite, but there still are traces of illite, quartz, opal-CT, and/or carbonate, or other minerals (Table 7.4). However, average boron concentrations in quartz, opal-CT and carbonate are usually lower than in smectite, illite, mica or tourmaline (Harder, 1970; Leeman & Sisson, 1996; Henry & Dutrow, 1996) whereas discrete illite or mica (except Germany), nor high-B minerals such as tourmaline (Henry & Dutrow, 1996) have not been detected by XRD (Table 7.4). The low abundance of the problematic minerals therefore suggests that their effect on boron content is minor.

Bentonites usually form from volcanic rocks including acidic (rhyolite) to alkaline (basalt) parent materials (Grim & Güven, 1978; Christidis & Huff, 2009). These volcanic rocks have boron concentrations of 0.5 to 53 µg/g, with the silica-rich rhyolites (commonly 2 to 25 µg/g B; Shaw & Sturchio, 1992; Leeman & Sisson, 1996; Reyes & Trompetter, 2012) usually having higher boron concentrations than dacitic, andesitic or basaltic rocks (Ryan & Langmuir, 1963; Leeman & Sisson, 1996). Even higher boron concentrations have been described for fluorine-rich topaz rhyolites and Macusani glasses (100s to 1000s of µg/g B; Pichavant et al., 1987; Webster et al., 1989; Congdon & Nash, 1991; Leeman & Sisson, 1996), but these peraluminous glasses have not yet been documented from bentonite deposits.

The boron concentrations of the volcanic parent material of bentonite deposits are unfortunately unknown, except for the Los Trancos deposit in Spain and the Wyoming bentonites in the United States. Rhyolitic tuffs from the Los Trancos deposit contain < 2 µg/g B (Linares et al., 1987); whereas the silica-rich, granitic Idaho batholith and possible volcanic source of Wyoming bentonites (Slaughter & Earley, 1965; Elzea & Murray, 1990) has boron concentrations < 15 µg/g (Leeman et al., 1992). The volcanic parent materials therefore could be a source of a part of boron in smectites.

However, boron retention during argillic alteration (Reyes & Trompetter, 2012) and bentonitization (Caballero et al., 1992, 2005) shows drastic differences for the various volcanic rocks. Boron from andesite hydrothermally altered to smectite and illite-smectite in the Taupo volcanic field is largely retained (66 %; Reyes & Trompetter, 2012). In contrast, only 3 % (rhyolite) to 34 % (dacite) of boron in the rhyolitic and dacitic parent material of bentonites from Cabo de Gata in Spain is preserved, making boron the most mobile trace element in these deposits (Caballero et al., 1992, 2005). The rhyolitic composition of the parent materials in most of the examined bentonite deposits (Table 7.1) therefore indicates that boron from the volcanic parent material is lost during alteration. Boron in bentonites must therefore be derived from the bentonite-forming fluid, especially in consideration of the high water-rock ratios during bentonitization (6 to 13; Christidis, 1998; ~2300; Caballero et al., 1992, 2005).

7.5.2 Fluid-smectite boron partitioning

Our mineralogical (Table 7.4) and chemical analyses (Table 7.6) show that smectites contain traces of interstratified illite and traces of potassium (Fig. 7.5; Fig. 7.7). Plots of the interstratified illite or the potassium content against the boron content reveal two groups: One group shows a linear increase of boron with potassium and interstratified illite content, and another group that lacks such a relationship (Fig. 7.7), indicating that the boron content of K-rich samples is strongly affected by the interstratified illite content, as shown in previous studies (Couch, 1971; Palmer et al., 1987; Spivack et al., 1987; You et al., 1996; Williams et al., 2001a; Williams & Hervig, 2002).

There are, however, no experimentally determined fluid-mineral partition coefficients for the non-exchangeable, fixed tetrahedral boron in smectite or illite-smectite (Simon et al., 2006). We therefore use the temperature- and pH-dependent boron partition coefficients for boron adsorption on clay minerals (Palmer et al., 1987; You et al., 1995, 1996) and the temperature-dependent partition for boron incorporation into marine smectites formed from ocean basalts (Spivack & Edmond, 1987) as a basis for estimating the fluid-smectite boron partitioning and boron content in the fluids (Table 7.6).

We also apply a potassium correction factor relating the boron content to the potassium content based on ideas in earlier studies on boron as a paleosalinity indicator (Curtis, 1963; Potter et al., 1963; Walker & Price, 1963; Couch, 1971) because our smectites contain traces of potassium and interstratified illite (Fig. 7.7). We focus on the potassium content because the determination of the interstratified illite content can produce larger errors (~30 %; Środoń, 1980). Our potassium correction equals about 33 µg/g of boron for every weight percent of potassium based on data in Smith et al. (1995) instead of relying on the hard to define adjusted or equivalent boron content of illitic or kaolinitic sediments (Curtis, 1963; Potter et al., 1963; Walker & Price, 1963; Couch, 1971).

The total boron content in µg/g of K-bearing smectite is thus defined by $B_T = (K_C * F_K) + (B_F * K_D)$, with K_C = potassium content in wt%, F_K = uptake factor, K_D values according to You et al. (1996) or Spivack & Edmond (1987), B_F = boron content of the fluid in ppm. We decided to use the linear boron-potassium relationship of authigenic marine smectites (Fig. 2 in Smith et al., 1995) because they show a boron-potassium relationship similar to our smectites (Fig. 7.7). The marine smectites also formed from volcanic (though basaltic) parent material, from the same fluid (more or less seawater), and at low-temperatures (< 100°C; Donelly et al., 1979; Muehlenbach, 1979; Smith et al., 1995), and thus at conditions similar to bentonites in marine, volcano-sedimentary depositional environments (Grim & Güven, 1978; Christidis & Huff, 2009).

7.5.3 Boron concentration and chlorinity of the alteration fluids

As boron uptake into authigenic clay minerals broadly correlates with the boron and chlorine content of the solution (Frederickson & Reynolds, 1960; Couch & Grim, 1968; Brockamp, 1973; Zeibig et al., 1989), and assuming equilibrium, we can use the fixed boron content in smectite to estimate the boron content of the fluid (Table 7.6) using our modified and the original boron partition coefficients (Spivack & Edmond, 1987; You et al., 1996). The boron-chlorine relationship of various hydrogeological settings (Fig. 7.2) is subsequently used to estimate the chlorinity of some fluids involved in the formation of selected bentonite deposits.

The original and the K-corrected boron partitioning after Spivack & Edmond (1987) yield boron concentrations (< 5 mg/L) in the lower ranges of most natural fluids (Fig. 7.2; Table 7.6). The original and the K-corrected boron partitioning do yield boron concentrations (0.04 to 0.76 mg/L B, excluding high temperatures; Table 7.6) consistent with meteoric waters in mixed carbonate/clastic aquifers (Fig. 7.2) and local meteoric groundwater (0.003 to 1.2 mg/L B; Wagner et al., 2003) involved in terrestrial bentonite formation in Southern Germany (Vogt, 1980; Ulbig; 1999; Köster & Gilg, 2015). However, this is the only example where the original and the K-corrected boron partitioning after Spivack & Edmond (1987) yields boron concentrations consistent with local fluids.

In most other cases such as the hydrothermally-fed playa lakes in Fallon, Nevada (Coolbaugh et al., 2006), and environments very likely influenced by saline fluids such as seawater or brines with known boron-chlorine concentrations (Fig. 7.2; Table 7.1) such as in Wyoming, Montana (Blondes et al., 2016), and Milos (Wu et al., 2016) boron concentrations estimated using boron partitioning of Spivack & Edmond (1987) are too low, with a maximum concentration of 7.3 mg/L B (Table 7.6). The boron concentrations in fluids of bentonites from marginal marine (Otay) and marine influenced hydrothermal settings (Milos, Los Trancos, Askana) also are rather low with < 4.3 mg/L B even for the most extreme boundary condition (100°C, K_D=11; Table 7.6). Such a high temperature is not consistent with the roughly 40°C for Otay (Berry, 1999; Compton et al., 1999) and the temperature range for Los Trancos (rather 40°C than 100°C; Leone et al., 1983; Delgado, 1993; Delgado & Reyes, 1993) or Milos bentonites (30°C to 90°C; Decher et al., 1996).

The boron partitioning after Spivack & Edmond (1987) also yields very high fixed boron concentrations in smectites if applied to the present day fluids with known boron-chlorine data (Fig. 7.2) from Nevada (Coolbaugh et al., 2006), Wyoming, Montana (Blondes et al., 2016) or Milos (Wu et al., 2016). The D values of 33 at 1°C or 11 at 100°C (Spivack & Edmond, 1987) would result in smectites

with a boron concentration inconsistent with our samples, as well as exceed the documented boron concentrations of smectites (max. 200-300 µg/g B; Harder, 1970) by up to several thousand µg/g B.

In contrast, boron concentrations estimated according to the original and the K-corrected boron partition coefficients for boron adsorption (You et al., 1996) indicate boron concentrations in the fluids (0.3 to 122 mg/L B; Table 7.6) within the range of natural fluids (Fig. 7.2). Although at first sight the unmodified boron partitioning coefficient yields rather high boron concentrations for fluids involved in terrestrial bentonite formation in Southern Germany, the K-corrected boron concentrations are well within the range of the local meteoric groundwater (0.0003 to 1.2 mg/L B; Wagner et al., 2003), especially in consideration of the up to 20-fold evaporative concentration of these waters (Köster & Gilg, 2015; Köster et al., 2017). The K-corrected estimates of the boron concentrations in the fluids for Fallon, Wyoming, Montana, and Milos (Table 7.6) are also in the documented range of brackish to saline waters in playas, hydrothermal fluids, and brines, including the boron-chlorine data (Fig. 7.2) for these localities (Wagner et al., 2003; Coolbaugh et al., 2006; Blondes et al., 2016; Wu et al., 2016). The boron concentrations estimated using this method for Wyoming bentonites are furthermore consistent with high salinity (up to 25 wt% NaCl equivalent) fluid inclusions in quartz in the Bighorn Basin (Beaudoin et al., 2014) that suggest a higher salinity and/or boron content than e.g. in seawater. The higher boron concentration estimated for Lago Pellegrini after You et al. (1996) also are more consistent with its transitional marine-terrestrial (Table 7.1) and evaporation affected formational environment that certainly excludes formational temperatures of 100°C (Vallés et al., 1989).

Our K-corrected boron adsorption coefficients also yield boron concentrations (< 10 mg/L B; Table 7.6) close to seawater concentration for deposits that very likely did form by some involvement of seawater (4.7 to 5.3 mg/L B for modern SW, Vengosh et al., 1992; 3.5 mg/L B for Cretaceous SW, Lemarchand et al., 2002; 1 to 9 mg/L B for the last 50 Ma, Simon et al., 2006) such as Otay, Milos, Askana, and perhaps Los Trancos. The estimated boron content of the fluids for these deposits indicates brackish to saline waters (Fig. 7.2), consistent with seawater mixing with non-marine boron in marginal-marine lagoons (Otay) or marine-influenced hydrothermal settings (Los Trancos, Milos, Askana) – as described in Table 7.1.

A comparison of our boron estimates (Table 7.6) with the boron-chlorine data for waters in Bavaria, Fallon, Wyoming, Montana, and Milos – and the fluids in various other hydrogeological settings (Fig. 7.2) – finally indicates that the chlorinity of the fluids likely ranged from freshwater for Bavaria, to less than that of seawater for Fallon and Milos, and up to the chlorinity of dilute to concentrated brine in Wyoming and Montana (Table 7.9). It is therefore reasonable to assume that B-rich Na-smectites formed from saline water or brine with up to three times (Table 7.9) the chlorinity of seawater because

B-rich fluids in marine and terrestrial settings are often dominated by Na-Cl or Na-SO_4 (Fig. 7.2) (Palmer & Sturchio, 1990; Boschetti, 2011; Boschetti et al., 2014). The B-rich, but illite-poor Pertek Na-bentonite (Table 7.6) thus must have formed from a highly concentrated, probably hydrothermal, Na-rich brine.

Table 7.9: The chlorinity of the fluids for five deposits based on the lowest and highest estimated B content.

Deposit	B_{low} [mg/L]	Cl^- [mg/L]	B_{high} [mg/L]	Cl^- [mg/L]
Milos	1.0	1876.8	8.1	11950.7
Montana	8.9	7566.4	55.6	59076.0
Wyoming	4.1	383.5	82.5	23633.0
Bavaria	0.3	76.4	1.3	323.3
Fallon	11.5	1091.5	57.4	14323.5

The preceding discussion indicates that the K-corrected fluid-mineral boron partitioning based on You et al. (1995, 1996) provides realistic estimates for the boron concentration in the smectite-forming fluid.

1) You et al. (1995, 1996) consider both temperature and pH, 2) use empirical and experimental evidence, 3) include both pore water boron data and controlled fluid compositions from laboratory experiments, 4) Smectite-rich and illite/smectite-rich intervals of the Nankai Through sediments used by You et al. (1995, 1996) formed from volcanic ash of andesitic to rhyolitic composition (Underwood et al., 1993) and not basalt (Spivack & Edmond, 1987), 5) Boron adsorbed on early-formed authigenic smectite, as well as boron trapped in the interlayer, is fixed into the smectite lattice during crystal growth (Couch & Grim, 1968; Spivack et al., 1987; Palmer et al., 1987; Palmer & Swihart, 1996; Williams et al., 2001a) and, 6) K-corrected estimates after You et al. (1995, 1996) provide more realistic boron concentrations for a larger set of samples (Fig. 7.2; Table 7.6). The most likely reason for this is that boron analysis of altered ocean basalts was performed on bulk sediment samples involving complete digestion by pyrohydrolysis at 1400°C (Spivack & Edmond, 1987). The analyses therefore are likely to include boron from other materials than smectites.

7.5.4 The boron isotope composition and origin of the smectite-forming fluids

Most smectites from marine and terrestrial bentonites studied here (Fig. 7.11; Table 7.7) reveal negative or slightly positive $\delta^{11}B$ values identical to $\delta^{11}B$ values of the continental crust (Schwarzc et al., 1969; Chaussidon & Albarede, 1992), continental fluids (Barth, 1993; Xiao et al., 2013), or smectites formed from meteoric or hydrothermal fluids in the Miocene Ries crater in Southern Germany (Muttik

et al., 2011). Few smectites have $\delta^{11}B$ values similar or identical to marine smectites and sediments (~+2.8 ‰, Spivack et al., 1987; +2.3 ‰ to +9.8 ‰, Ishikawa & Nakamura, 1993).

The boron isotope fractionation of Williams et al. (2001a) is used to determine the $\delta^{11}B$ values of the smectite-forming fluid and to verify if smectites formed from fluids consistent with the depositional environment of the parent material (Table 7.1) using cation-exchanged smectites whose interlayer boron was removed, and where not available mannitol-treated smectites (Table 7.7; Fig. 7.11).

However, the exchangeable and fixed boron are not the only issue that has to be considered. The formation temperatures, pH, and ionic strengths of the fluids in many bentonite deposits (Table 7.1) are only vaguely known, but influence the pKa of boric acid, and therefore B isotope fractionation (Hershey et al., 1986; Dickson, 1990; Palmer et al., 1987). Brines up to a pH of ~ 9 can show a B isotope fractionation similar to near-neutral fluids (Williams et al., 2001a; Kharaka & Hanor, 2003) because of their high ionic strength lowering the pKa (4.77 at 25°C and 3.42 at 100°C; Kharaka et al., 1988; Kharaka & Hanor, 2003). But it is especially the pH and ionic strength during bentonite formation that are not well constrained to reliably determine boric acid (B_3) to borate (B_4) ratios. We therefore prefer to assume a B_3 and a B_4 dominated end-member, and various molar B_3-B_4 ratios, as well as temperatures of 25°C and 90°C consistent with most bentonite formation temperatures (Table 7.1). A fluid-mineral fractionation of 31.45 ‰ at 25°C (Williams et al., 2001a) is used for the boric acid end-member, and a fluid to mica-like fractionation of 13.46 ‰ at 25°C for the end-member dominated by borate ions (Liu & Tossell, 2005). The borate fluid-mineral fractionation of Liu & Tossell (2005) was extrapolated to 10.7 ‰ at 90°C. The $\delta^{11}B$ values of the fluids (Table 7.7) are therefore controlled by the molar B_3-B_4 ratio of the solution, and the temperature effect on the end-members of the fluid-mineral B isotope fractionation at neutral and highly alkaline conditions (Kakihana et al., 1977; Palmer et al., 1987; Williams et al., 2001a; Williams & Hervig, 2002; Liu & Tossell, 2005). As bentonite formation is usually associated with open hydrological systems (Caballero et al., 1992; Christidis, 2008) and large water-rock ratios (Christidis, 1998; Caballero et al., 1992, 2005) – even after the transformation of the volcanic ash to an aquitard there still is fluid-grain boundary diffusion of elements such as K during illitization – we assume that no or insignificant Rayleigh-type isotope fractionation occurred.

The $\delta^{11}B$ values of the B_3 or B_4 dominated end-members at 25°C range from 17.0 ‰ to 43.7 ‰ (B_4: -0.9‰ to 25.8‰) for bentonites from marine depositional settings, and 9.5 ‰ to 32.0 ‰ (B_4: -7.9 ‰ to 14.2 ‰) for bentonites from terrestrial depositional environments; and is 30.6 ‰ (B_4: 12.6 ‰) for the laterite-associated bentonite. The Lago Pellegrini bentonite shows B_3 dominated fluid $\delta^{11}B$ estimates of 21.6 ‰ to 31.3 ‰ (B_4: 3.7 ‰ to 13.4 ‰). A higher formation temperature of 90°C reduces

the respective $\delta^{11}B$ value of the fluid by 6 ‰ or less, temperature therefore has a smaller influence on boron isotope fractionation than the B_3-B_4 ratio.

The most striking observation of the $\delta^{11}B$ values for the bentonite-forming fluids is that, irrespective of depositional environment and boundary conditions (B_3-B_4 ratio, temperature), most results are below $\delta^{11}B$ values (Table 7.7; Fig. 7.11) expected for Cretaceous (36 ‰ to 40 ‰, Lemarchand et al., 2002; Simon et al., 2006), Mediterranean (37.7 ‰, Vengosh et al., 1992) or modern seawater (39.61 ‰, Foster et al., 2010). This does not change much even for a lower $\delta^{11}B$ value of 30 ‰ for Cretaceous and 35 ‰ for Neogene seawater as suggest by Paris et al. (2010).

However, the estimated $\delta^{11}B$ values of the fluid for Miocene to Pleistocene deposits on Milos and in Los Trancos, as well as the Eocene to Oligocene Askana and Otay bentonite deposits, are potentially consistent with aforementioned seawater $\delta^{11}B$ values, especially when compared to the lower $\delta^{11}B$ values of Paris et al. (2010). This is consistent with previous results indicating that seawater mixes with non-marine fluids in some deposits on Milos (Wetzenstein, 1972; Luttig & Wiedenbein, 1990; Christidis, 1998) and in Askana (Rateyev, 1968), and evaporated seawater mixing with continental input in marginal-marine lagoons of Otay (Berry, 1999; Compton et al., 1999). The reconstructed fluid $\delta^{11}B$ values for Milos are, in addition, similar to mixed seawater-meteoric hydrothermal vent fluids in Milos (Wu et al., 2016).

A seawater involvement, however, contradicts H-O stable isotope data of smectites indicating a largely non-marine hydrothermal fluid for Los Trancos (though might indicate seawater in other deposits of Cabo de Gata: Leone et al., 1983; Delgado, 1993; Delgado & Reyes, 1993) and on Milos (Decher et al., 1996). But our estimated boron concentrations in the fluids for Milos, Los Trancos, Askana, and Otay (3 to <10 mg/L B; Table 7.6) are compatible with seawater (4.7 to 5.3 mg/L B; Vengosh et al., 1992; 3.5 mg/L B; Lemarchand et al., 2002) as well as hydrothermal fluids (Fig. 7.2) such as in Milos (Wu et al., 2016), thus suggesting that the smectite-forming fluids were either the result of seawater mixing with another fluid (magmatic, hydrothermal, sedimentary, meteoric), or that fluids had a B source with B isotope values close to seawater, e.g. leached from marine sediments.

The Cretaceous seawater $\delta^{11}B$ value of 30 ‰ (Paris et al., 2010) might also be invoked to suggest a seawater B origin for the Glasgow bentonite because it is very close to our $\delta^{11}B$ values estimated for the fluids (Table 7.7). The high B concentrations in smectites, however, indicate the involvement of a fluid with a higher B content than seawater (Table 7.6). This could be a residual brine of evaporated seawater, but the allocation of B origin greatly depends on the B isotope composition of the unmodified Cretaceous seawater, i.e. 30 ‰ (Paris et al., 2010) versus 36 ‰ to 40‰ (Lemarchand et al., 2002; Simon et al., 2006), or seawater of earlier times as brines in the Williston basin date back to

the Paleozoic (Blondes et al., 2016). However, the $\delta^{11}B$ values of the fluids in Glasgow (Table 7.7) are identical to saline waters and salt dissolution brines formed from Permian salts (Fig. 7.11) (Kloppmann et al., 2001) consistent with the presence of Silurian to Jurassic evaporite intervals in the Williston basin (Maughan, 1966) and the Sr isotope ratios of brines (~0.707 to ~0.712; Blondes et al., 2016) indicative of a mixed fluid origin. A salt dissolution brine therefore is the most likely option.

The $\delta^{11}B$ values of the remaining smectites from both marine or terrestrial settings, and the corresponding $\delta^{11}B$ values for low- and high-temperature estimates of the fluids, are smaller ~33 ‰ (Table 7.7). These values thus reveal a non-marine boron source influenced by strong water-rock interaction (Palmer, 1991; Barth, 1993; Palmer & Swihart, 1996) not only for terrestrial deposits in Southern Germany (Vogt, 1980; Unger & Niemeyer, 1985a, b; Ulbig, 1999; Gilg, 2005; Köster & Gilg, 2015), Fallon in Nevada (Post, 1996, 1997; LaPointe et al., 2011), La Tranquera in Argentina (Hevia, 1989; Martínez & Colombi, 2011), and Bahia in Brazil (Moreira, 1984; Albrecht, 2011), but also for bentonite deposits in transitional marine settings such as for Lago Pellegrini and strictly marine depositional environments in Wyoming, Pertek, and Tavush (Fig. 7.3; Table 7.1).

The results for Wyoming and Lago Pellegrini are, however, problematic. For Wyoming, the $\delta^{11}B$ values and H-O stable isotope data of smectites are consistent with other Cretaceous bentonites that formed by the involvement of meteoric waters (Cadrin et al., 1995), but contradict the mostly "marine" trace element and H-O stable isotope values of the X bentonite (i.e. Clay Spur bentonite in Wyoming) from the Mowry shale (Elzea & Murray, 1990; Cadrin et al., 1995; Smellie, 2001) – where our samples are from. We still prefer the meteoric B isotope signal over the marine H-O stable isotope signal for two reasons. One, boron in the silica tetrahedra is less affected by low-temperature geological process (Frederickson & Reynolds, 1960; Adams et al., 1965) and only exchanges when Si-O bonds are broken (Williams et al., 2001a). Two, the trace elements in the western-most Clay Spur in the Big Horn basin indicate a rather brackish fluid (Elzea & Murray, 1990) and thus might be consistent with B isotope values that suggest a non-marine B source.

For Lago Pellegrini the transitional marine environment would suggest much higher $\delta^{11}B$ values in a smectite formed from seawater (Vengosh et al., 1992). An explanation for this seeming discrepancy is the transitional marine environment itself. The $\delta^{11}B$ values of fluids in transitional marine settings such as sabkhas in Kuwait range from about 21 ‰ to 39 ‰ due to continental run-off mixing with seawater (Duane & Zammel, 1999), and would probably be even lower when assuming a Cretaceous seawater composition (Paris et al., 2010). The B content and $\delta^{11}B$ values of the three Lago Pellegrini smectites thus could be interpreted to indicate the fractional evaporation of a mixed marine-meteoric brine.

7.5.5 The exchangeable cation occupancy

Bentonites have an easily exchangeable interlayer cation occupancy (Grim & Güven, 1978; Odom, 1984), often resulting in the preferentially exchange of sodium ions with calcium or magnesium ions (Laudelout et al., 1968). The post-formational cation exchange in bentonites is a very rapid process, as indicated by experiments testing bentonites for the isolation of nuclear waste that resulted in the complete rearrangement of exchangeable interlayer cations (Dohrmann et al., 2013; Dohrmann & Kaufhold, 2014; Dohrmann & Kaufhold, 2017) as well as contrasting exchangeable and fixed $^{87}Sr/^{86}Sr$ of Otay, Clay Spur (Chaudhuri & Brookins, 1979), and bentonites in Southern Germany (Köster et al., 2017). The presence of the easily exchangeable sodium ions (Fig. 7.6) might therefore indicate an original interlayer cation occupancy and thus the presence of original interlayer boron.

Two studies on the interlayer-water B isotope fractionation (Williams & Hervig, 2002; Williams et al., 2007) showed that the interlayer B of authigenic illite-smectite is isotopically heavier than the tetrahedrally fixed boron, suggesting that smectites that have lower $\delta^{11}B$ values after a cation exchange treatment might have preserve an original interlayer cation occupancy.

However, our smectites have $\delta^{11}B$ values (Fig. 7.11; Table 7.7) whose shift of $\delta^{11}B$ values after cation exchange can only be explained by the presence of interlayer boron with either higher $\delta^{11}B$ values or lower $\delta^{11}B$ values than the tetrahedrally fixed boron. If interlayer B originating from the same fluid as fixed B is indeed isotopically heavier, then smectites that show an increase in $\delta^{11}B$ values after cation exchange indicate that the interlayer has exchanged with another fluid. This would be consistent with the Sr isotope results of exchangeable and fixed Sr for Otay (Chauduri & Brookins, 1979) and Southern Germany (Köster et al., 2017).

We therefore interpret that the original exchangeable cation occupancy of Los Trancos, Otay, Bavaria in Southern Germany and Pertek samples (Fig. 7.10; Fig. 7.11) is not preserved because they show a shift to higher $\delta^{11}B$ values after cation exchange. This implicates that smectites that show a shift to lower $\delta^{11}B$ values after cation exchange treatment such as Wyoming, Montana, Milos, and Askana (Fig. 7.11; Table 7.7) might preserve the original interlayer cation occupancy, B and $\delta^{11}B$ value. But a change in $\delta^{11}B$ value of 47.2 ‰ after cation exchange as for La Tranquera is probably too drastic because it is much larger than the interlayer-water fractionation indicated by Williams & Hervig (2002) or Williams et al. (2007). The Wyoming, Montana, Milos, and Askana bentonites thus can tentatively be interpreted as primary sodium, calcium or magnesium bentonites, assuming that they have not interacted with fluids having similar $\delta^{11}B$ values as the original fluid involved in bentonite formation.

7.5.6 Laterite-hosted bentonite

The negative $\delta^{11}B$ value (-1.0 ‰ ± 0.7 ‰; Table 7.7) of one smectite from Bahia, Brazil is identical to the B isotope value of the continental crust (~0 ‰, Schwarzc et al., 1969; about -7 ‰, Chaussidon & Albarede, 1992) and its boron content is in the lower range of gneiss (1 to 20 µg/g B; Leeman & Sisson, 1996; Palmer & Swihart, 1996). As the weathering of continental rocks produces smectites with $\delta^{11}B$ values around 0‰ because of the tetrahedral coordination of boron in mica, pyroxene and amphibolite the smectite $\delta^{11}B$ value is probably similar to the (unknown) $\delta^{11}B$ value of the metamorphic parent material because, assuming that no boron was added by external fluids (Leeman & Sisson, 1996; Palmer & Swihart, 1996). The Cr_2O_5, VO_3 and CoO content (Table 7.6) of the smectites from Bahia indeed suggest that smectites formed by the replacement of minerals containing such elements such as mica, pyroxene or amphibole (Moreira, 1984; Albrecht, 2011). Leaching of mobile elements during the development of the laterite profile in Bahia, Brazil (Trescases et al., 1981; de Oliveira et al., 1992) might, however, be associated with a loss of boron and could be an explanation for the negative boron concentrations estimated in the fluids (Table 7.7).

7.5.7 Carbonates in bentonites

Disseminated carbonates in bentonite deposits (Knechtel & Patterson, 1956, 1962; Vogt, 1980; Delgado, 1993; Decher et al., 1996; Köster & Gilg, 2015) have a high potential as palaeoenvironmental indicators (Banner, 1995) also in bentonites (Köster & Gilg, 2015; Köster et al., 2017). All carbonates in bentonites have negative $\delta^{18}O_{VPDB}$ values and $\delta^{13}C_{VPDB}$ values smaller than +2 ‰ (Fig. 7.12), indicating carbonate formation both from non-marine and from some mixed (Milos, Pertek, Askana) fluids (Banner, 1995; Nelson & Smith, 1996), consistent with previous studies (Decher et al., 1996; Köster & Gilg, 2015). The low $\delta^{18}O_{VPDB}$ and rather high $\delta^{13}C_{VPDB}$ values for Milos, Pertek and Askana (Fig. 7.12) thus indicate a marine formational settings environment in part consistent (Milos, Askana) and contradicting (Pertek) the B isotope geochemical results for smectites. The timing of carbonate and smectite formation in Pertek can therefore not be identical.

The carbonates in the other carbonate-bearing deposits indicate carbonate precipitation from non-marine fluids (Banner, 1995; Nelson & Smith, 1996) indicating contemporaneous or later carbonate formation, consistent with the B isotope results.

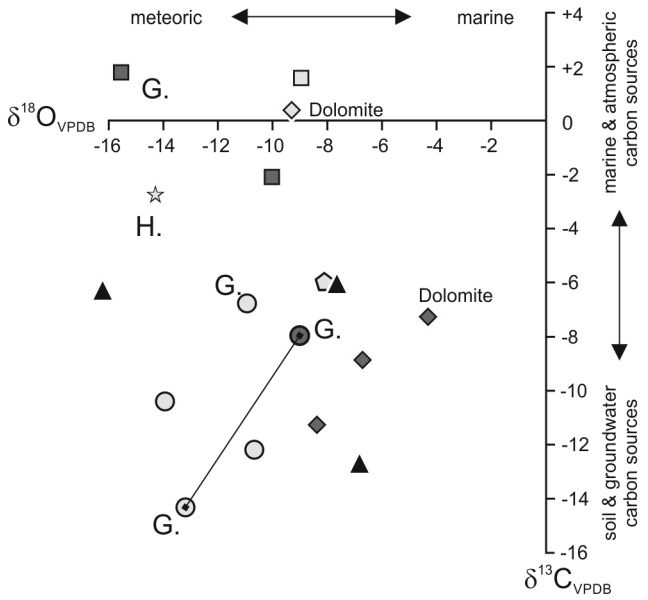

Fig. 7.12: The $\delta^{13}C_{V\text{-}PDB}$ and $\delta^{18}O_{V\text{-}PDB}$ values of bentonite-associated calcite and dolomite. The solid line connects the two samples from the Glasgow Ca- and Na-bentonite. H. = halite, G. = gypsum. Please note that bentonite samples not containing carbonates are not shown.

7.6 Conclusions

Smectites and bulk material of fourteen bentonite deposits from various depositional environments have been analyzed for boron content, B isotope values, as well as their overall chemical and mineral composition. Smectites have a wide range of fixed boron concentrations (0.2 to 196 µg/g B) and $\delta^{11}B$ values (-30.2 ‰ to +17.1 ‰), and contain up to 10 µg/g of interlayer boron. Almost all smectites contain small amounts of interstratified illite that has a notable effect on boron concentrations, indicating that boron uptake even in illite-poor (< 5% illite interstratified) smectites is strongly influenced by the illitic component. Sodium-bentonites have high B concentrations (> 30 µg/g B) whereas smectites from Mg- and Ca-bentonites have lower fixed boron concentrations of up to a few tens of ppm (< 30 µg/g B). The lowest B content (0.2 µg/g B) was found in smectites formed by lateritic weathering of igneous and metamorphic rocks in Bahia in Brazil.

The $\delta^{11}B$ values of smectites show no systematic link with their interlayer cation occupancy. The $\delta^{11}B$ values of smectites and the estimated B content of the fluids indicate that bentonite formation occurred in brackish to saline fluids, as well as brines with a strong continental component, confirmed by similarly “non-marine” carbon and oxygen isotope values of most bentonite-associated carbonates. However, the intermediate B concentrations and positive $\delta^{11}B$ values of some Mg- and Ca-bentonite deposits (Otay, Milos, Askana, Los Trancos) indicate that seawater mixing with other fluids was

probably involved in the formation of some bentonites. Nevertheless, unmodified seawater is unlikely to be a major factor in the formation of the valuable Na-bentonites, whereas B- and Na-rich formation waters, hydrothermal fluids, salt dissolution brines, or salt lake waters are involved for the formation of Na-bentonites. The sometimes highly contrasting $\delta^{11}B$ values of cation-exchanged and not cation-exchanged sub-samples (e.g. Glasgow, La Tranquera, and Bahia), together with the carbon and oxygen stable isotopes of carbonates, indicate that some bentonites experienced a substantial post-formational alteration. The exchangeable cation occupancy of smectites which shift to more positive values after cation exchange treatment, as well as those smectites that show strongly contrasting (> 10 ‰) $\delta^{11}B$ values before and after treatment, is unlikely to be related to the original bentonite-forming fluids.

Acknowledgements

This publication is part of the first author's doctoral research at the Lehrstuhl für Ingenieurgeologie, Technische Universität München, Germany, supervised by Prof. Dr. H. Albert Gilg. PD Dr. Christoph Mayr at the Institut für Geographie, Friedrich-Alexander-Universität Erlangen-Nürnberg, Germany kindly analyzed the carbon and oxygen stable isotopes of carbonates. We are grateful for access to bentonite mines in Southern Germany granted by Bernhard Ratzke, Süd-Chemie AG (now Clariant), and the cooperation of Ulrich Boehnke, S&B Industrial Minerals (now Imerys). The SIMS boron isotope analyses was financially supported by the Clay Minerals Society Student Research Grant 2014, and the carbon and oxygen stable isotope analysis by the Society of Economic Geologists SEG Graduate Fellowship Award 2012.

Appendix Chapter 7

Appendix 7.1: Instrumental mass fractionation used for boron isotope determination of each sample. Crossed-out values were not used.

Sample	11/10	S.E. ‰	PE ‰	$\delta^{11}B$	IMF	$\delta^{11}B$ corr.	Comments
IMt-1	3.8859	0.7	0.5	-39.0	-30.0	-9	
	3.8894	0.5	0.5	-38.2	-29.2	-9	
	3.8891	0.6	0.5	-38.2	-29.2	-9	
	3.8915	0.7	0.5	-37.6	-28.6	-9	
	3.8767	0.7	0.4	-41.3	-32.3	-9	
				Avg	-29.9		
				S.E.	0.6		
PE-M	3.8803	0.9	0.7	-40.4	-35.6	-4.8	50 cycles
	3.8763	0.4	0.2	-41.4	-35.6	-5.8	100 cycles
	3.8666	0.3	0.2	-43.8	-35.6	-8.2	
	~~3.8512~~	~~0.40~~	~~0.40~~	~~-47.61~~	-35.6	~~-12.01~~	possibly not flat
	3.8710	0.4	0.3	-42.7	-35.6	-7.1	
					Avg	-6.5	
					S.E.	0.7	
IMt-1	3.8633	0.5	0.4	-44.6	-35.6	-9	
ZW48-M	3.8259	1.4	1.3	-53.9	-35.6	-18.3	50 cycles
	3.8107	1.5	1.2	-57.6	-35.6	-22.0	
	3.8292	1.1	1	-53.0	-35.6	-17.4	
	3.8252	0.9	0.8	-54.0	-35.6	-18.4	
	3.8214	1	0.9	-55.0	-35.6	-19.4	
	3.8279	1	1.1	-53.4	-35.6	-17.8	
	3.8077	0.9	0.9	-58.4	-35.6	-22.8	
	3.8316	0.8	0.8	-52.5	-35.6	-16.9	
	3.8448	1	0.8	-49.2	-35.6	-13.6	
	3.8216	0.7	0.8	-54.9	-35.6	-19.3	
	3.8180	0.8	0.8	-55.8	-35.6	-20.2	
	3.8135	0.6	0.7	-56.9	-35.6	-21.3	
	3.8363	1	1	-51.3	-35.6	-15.7	
					Avg	-18.7	
					S.E.	0.7	
IMt-1	3.8647	0.5	0.4	-44.3	-35.3	-9	
	3.8632	0.9	0.4	-44.6	-35.6	-9	
	3.8614	0.8	0.4	-45.1	-36.1	-9	
	3.8639	0.7	0.4	-44.5	-35.5	-9	
				Avg	-35.6		
				S.E.	0.2		
ZW48-A	3.8424	0.9	0.7	-49.8	-35.6	-14.2	100 cycles, cps dropping

	3.8331	0.9	0.7	-52.1	-35.6	-16.5	
	3.8247	0.9	0.7	-54.2	-35.6	-18.6	
					Avg	-17.5	
					S.E.	1.0	
PE-A	3.8866	0.7	0.3	-38.9	-35.6	-3.3	50 cycles
	3.8851	0.6	0.3	-39.2	-35.6	-3.6	50 cycles
	3.8876	0.7	0.3	-38.6	-35.6	-3.0	
					Avg	-3.3	
					S.E.	0.2	
IMt-1	3.8658	0.6	0.4	-44.0	-35.0	-9	
	3.8620	0.7	0.4	-44.9	-35.9	-9	
	3.8644	1	0.3	-44.3	-35.3	-9	15nA!
MOHO-M	3.8621	0.9	0.5	-44.9	-35.6	-9.3	
	3.8562	0.7	0.5	-46.4	-35.6	-10.8	
	3.8475	0.7	0.5	-48.5	-35.6	-12.9	
	3.8528	0.7	0.5	-47.2	-35.6	-11.6	
					Avg	-11.2	
					S.E.	0.8	
IMt-1	3.8619	0.7	0.4	-44.9	-35.9	-9	15nA!
KOP2-A	3.8948	0.8	0.7	-36.8	-35.6	-1.2	
	3.9031	1.0	0.7	-34.8	-35.6	0.8	
	3.8990	0.9	0.8	-35.8	-35.6	-0.2	
	3.8997	0.9	0.8	-35.6	-35.6	0.0	
	3.8929	0.8	0.7	-37.3	-35.6	-1.7	
	3.8961	1.0	0.8	-36.5	-35.6	-0.9	
	3.8917	1.0	0.8	-37.6	-35.6	-2.0	
	3.8953	1.0	0.8	-36.7	-35.6	-1.1	
	3.8894	0.9	0.8	-38.2	-35.6	-2.6	
					Avg	-1.0	
					S.E.	0.4	
IMt-1	3.8744	0.5	0.4	-41.9	-32.9	-9	5nA!
	3.8764	0.5	0.4	-41.4	-32.4	-9	5nA!
	3.8787	0.6	0.4	-40.8	-31.8	-9	
	3.8716	0.5	0.4	-42.6	-33.6	-9	
	3.8845	0.4	0.4	-39.4	-30.4	-9	
				Avg	-32.2		
				S.E.	0.5		
MOHO-A	3.8632	0.8	0.8	-44.6	-31.5	-13.1	4.5nA 50 cycl
	3.8563	1.0	0.8	-46.3	-31.5	-14.8	50 cyl for B content
	3.8664	0.9	0.8	-43.9	-31.5	-12.4	
	3.8613	0.8	0.8	-45.1	-31.5	-13.6	
	3.8651	0.9	0.8	-44.2	-31.5	-12.7	
					Avg	-13.3	

					S.E.	0.5	
IMt-1	3.8782	0.6	0.4	-40.9	-31.9	-9	5nA!
KOP2-M	3.9364	1.7	1.6	-26.5	-31.5	5.0	107 cycl
	3.9329	1.4	1.5	-27.4	-31.5	4.1	130 cycl
	3.9592	1.6	1.4	-20.9	-31.5	10.6	150 cycl
					Avg	6.6	
					S.E.	2.0	
IMt-1	3.8708	0.5	0.4	-42.8	-33.8	-9	
	3.8877	0.9	0.4	-38.6	-29.6	-9	
	3.8769	0.7	0.4	-41.2	-32.2	-9	
					Avg	-30.9	
					S.E.	1.3	
B51-A	3.8247	0.7	0.5	-54.2	-31.5	-22.7	5nA
	3.8321	0.8	0.6	-52.3	-31.5	-20.8	hung-up, no data file stored
	3.8311	0.8	0.6	-52.6	-31.5	-21.1	
					Avg	-21.5	
					S.E.	0.6	
IMt-1	3.8826	0.4	0.3	-39.8	-30.8	-9	apperture 1
	3.8855	0.4	0.4	-39.1	-30.1	-9	apperture 2
	3.8835	0.7	0.4	-39.6	-30.6	-9	
					Avg	-30.5	
					S.E.	0.2	
B51-M	3.7864	0.6	0.6	-63.6	-31.5	-32.1	bad sample, only few flakes
	3.8150	0.7	0.5	-56.5	-31.5	-25.0	bad sample, only few flakes
	3.8360	0.8	0.8	-51.4	-31.5	-19.9	bad sample, only few flakes
	3.8313	1	0.7	-52.5	-31.5	-21.0	bad sample, only few flakes
					Avg	-22.0	
					S.E.	1.6	
IMt-1	3.8754	0.4	0.4	-41.6	-32.6	-9	
OT-A	3.9082	1	0.9	-33.5	-31.5	-2	
	3.9327	0.5	0.4	-27.5	-31.5	4	chain 1
	3.9147	0.6	0.4	-31.9	-31.5	0	2
	3.9223	0.9	0.5	-30.0	-31.5	1	3
	3.9276	0.7	0.5	-28.7	-31.5	3	
	3.9341	1	0.5	-27.1	-31.5	4	
	3.9351	1	0.5	-26.9	-31.5	5	
	3.9132	0.3	0.5	-32.3	-31.5	-1	instrument shut-off: arc.
					Avg	1.8	
					S.E.	0.9	
IMt-1	3.8839	0.4	0.4	-39.5	-30.5	-9	imt3, reset to 2150.
OT-M	3.8971	2.2	1.6	-36.2	-31.5	-5	current dropped
	3.9061	2.3	2	-34.0	-31.5	-3	current dropped
	3.9096	0.7	0.6	-33.2	-31.5	-2	
	3.9055	0.7	0.6	-34.2	-31.5	-3	

	~~3.8826~~	~~1~~	~~0.8~~	~~-39.8~~	-31.5	~~-8~~	50 cycl
					Avg	-2.9	
					S.E.	0.7	
IMt-1	~~3.9025~~	~~0.7~~	~~0.2~~	~~-34.9~~	~~-25.9~~	~~-9~~	15nA!!!
	~~3.8975~~	~~0.5~~	~~0.4~~	~~-36.2~~	~~-27.2~~	~~-9~~	15nA!!!
	~~3.9020~~	~~0.7~~	~~0.4~~	~~-35.0~~	~~-26.0~~	~~-9~~	sample height difference
	3.8831	0.8	0.4	-39.7	-30.7	-9	
	3.8790	1.0	0.3	-40.7	-31.7	-9	5nA
	3.8771	0.6	0.3	-41.2	-32.2	-9	
	3.8723	0.7	0.3	-42.4	-33.4	-9	
	3.8812	0.8	0.4	-40.2	-31.2	-9	
				Avg	-32.1		
				S.E.	0.7		
MOFR-M	3.8602	1.4	1.5	-45.4	-31.5	-13.9	dropped to 5nA
	~~3.8582~~	~~2.1~~	~~2.6~~	~~-45.9~~	~~-31.5~~	~~-14.4~~	aborted after 13 cycles bc below 5nA
	3.8592	1	1	-45.6	-31.5	-14.1	
	3.8540	1.2	0.9	-46.9	-31.5	-15.4	
					Avg	-14.5	
					S.E.	0.5	
IMt-1	~~3.9110~~	~~0.5~~	~~0.4~~	~~-32.8~~	~~-23.8~~	~~-9~~	Below 5nA
	3.8817	0.9	0.4	-40.1	-31.1	-9	
MOFO-M	~~3.8947~~			~~-36.8~~	~~-31.5~~	~~-5.3~~	current not stable
	~~3.8746~~	~~0.8~~	~~0.6~~	~~-41.8~~	~~-31.5~~	~~-10.3~~	
	3.8757	0.8	0.6	-41.5	-31.5	-10.0	
	~~3.8834~~	~~0.7~~	~~0.7~~	~~-39.6~~	~~-31.5~~	~~-8.1~~	sample too thin
	3.8721	1.1	0.7	-42.4	-31.5	-10.9	
	3.8649	0.7	0.7	-44.2	-31.5	-12.7	
	3.8636	0.7	0.7	-44.5	-31.5	-13.0	
					Avg	-12.2	
					S.E.	0.7	
IMt-1	3.8789			-40.8	-31.8	-9	
ANG-M	3.9251	1.4	1.2	-29.3	-31.5	2.2	
	3.9237	0.5	0.4	-29.7	-31.5	1.8	
	3.9242	0.7	0.4	-29.6	-31.5	1.9	
	3.9422	0.6	0.3	-25.1	-31.5	6.4	
	3.9363	0.6	0.3	-26.6	-31.5	4.9	
	3.9485	0.6	0.4	-23.5	-31.5	8.0	
	3.9376	0.5	0.4	-26.2	-31.5	5.3	
	3.9543	0.5	0.4	-22.1	-31.5	9.4	
	3.9221	0.7	0.4	-30.1	-31.5	1.4	
	3.9471	1.7	0.4	-23.9	-31.5	7.6	
	3.9688	1.5	0.6	-18.5	-31.5	13.0	
	3.9382	1.1	0.3	-26.1	-31.5	5.4	
					Avg	5.6	

					S.E.	1.0	
IMt-1	3.8940	2.5	4.4	-37.0	-28.0	-9	5nA
	3.8678	1.5	1.3	-43.5	-34.5	-9	
	3.8745			-41.9	-32.9	-9	
	3.8973			-36.2	-27.2	-9	
	~~3.8660~~			~~-43.9~~	~~-34.9~~	~~-9~~	aborted
	3.8753	0.5	0.4	-41.6	-32.6	-9	
				Avg	-31.7		
				S.E.	1.3		
ZW50-M	3.8896	1.2	1.1	-38.1	-31.5	-6.6	current with bumps
	3.8908	0.9	0.9	-37.8	-31.5	-6.3	current dropping lightly
	3.8806	0.7	0.7	-40.3	-31.5	-8.8	75 cycl
	3.8861	1.4	0.6	-39.0	-31.5	-7.5	
	3.9005	1.3	0.8	-35.4	-31.5	-3.9	
	3.8852	1.3	0.6	-39.2	-31.5	-7.7	
					Avg	-6.8	
					S.E.	0.7	
IMt-1	3.8841	0.5	0.4	-39.5	-30.5	-9	very nice one! Use!
	3.8822	0.5	0.4	-39.9	-30.9	-9	very nice one! Use!
B17-M	3.9534	1.0	0.7	-22.3	-31.5	9.2	15nA
	3.9423	1.0	0.7	-25.1	-31.5	6.4	
	3.9510	0.8	0.5	-22.9	-31.5	8.6	
					Avg	8.1	
					S.E.	0.8	
IMt-1	3.8897	0.5	0.4	-38.1	-29.1	-9	
	3.8775			-41.1	-32.1	-9	
				Avg	-30.6		
				S.E.	1.2		
TR-M	3.9486	1.0	1.0	-23.5	-31.5	8.0	very stable
	3.9451	1	0.9	-24.4	-31.5	7.1	dito
	3.9415	0.9	0.9	-25.3	-31.5	6.2	dito
					Avg	7.1	
					S.E.	0.5	
IMt-1	3.8833	0.4	0.4	-39.7	-30.7	-9	
MB34-M	3.8774	1.2	1	-41.1	-31.5	-9.6	15nA
	3.8394	0.6	0.5	-50.5	-31.5	-19.0	
	3.8609	0.9	0.8	-45.2	-31.5	-13.7	
	3.8725	1	0.7	-42.3	-31.5	-10.8	
	3.8568	1.5	1.2	-46.2	-31.5	-14.7	
	3.8554	0.8	0.8	-46.6	-31.5	-15.1	
	3.8805	0.9	0.7	-40.4	-31.5	-8.9	
	3.8757	0.9	0.7	-41.6	-31.5	-10.1	
	3.8774	1.2	1	-41.1	-31.5	-9.6	

	3.8996	0.7	0.6	-35.6	-31.5	-4.1	
					Avg	-11.6	
					S.E.	1.3	
IMt-1	3.9500			-23.2	-14.2	-9	5nA
	3.9137			-32.1	-23.1	-9	
	3.9203			-30.5	-21.5	-9	
	3.9223			-30.0	-21.0	-9	
				Avg	-20.0		
				S.E.	2.0		
IMt-1	3.8579	0.5	0.4	-45.9	-36.9	-9	3.5nA
	3.8636	0.5	0.4	-44.5	-35.5	-9	
				Avg	-36.2		
ZO-M	3.9740	0.7	0.6	-17.2	-38.1	20.9	10nA
	3.9599	0.8	0.9	-20.7	-38.1	17.4	15nA
	3.9577	0.6	0.5	-21.3	-38.1	16.8	
						18.4	
IMt-1 reck	3.8455	0.5	0.4	-49.0	-40.0	-9	
IMt-1	3.8279	0.5	0.3	-53.4	-44.4	-9	Applied Average of 3 IMF here
	3.8271	0.5	0.3	-53.6	-44.6	-9	
ZO-M	3.9208	0.9	0.7	-30.4	-45	14.6	15nA. Re-check
	3.9555	0.8	0.7	-21.8	-45	23.2	Re-check
IMt-1	3.8212	0.5	0.4	-55.0	-46.0	-9	
					-45.0		
					0.5		
IMt-1	3.8673	0.4	0.3	-43.6	-34.6	-9	Turned up E.M. gain from 2150 to 2250V
	3.8748	0.5	0.3	-41.8	-32.8	-9	
	3.8723	0.5	0.3	-42.4	-33.4	-9	
	3.8752	0.4	0.3	-41.7	-32.7	-9	
				Avg	-33.4		
				S.E.	0.4		
SB01-M	3.9724	0.7	0.6	-17.6	-34.2	16.6	
	3.9833	0.8	0.7	-14.9	-34.2	19.3	
	3.9747	0.9	0.7	-17.1	-34.2	17.1	
					Avg	17.6	
					S.E.	0.8	
IMt-1	3.8704	0.4	0.3	-42.9	-33.9	-9	
SB02-M	4.0200	1.0	0.8	-5.9	-34.2	28.3	
	4.0202	1.1	0.8	-5.8	-34.2	28.4	
	4.0057	0.7	0.6	-9.4	-34.2	24.8	Note change in IMF
					Avg	27.2	Used value below
					S.E.	1.2	
IMt-1	3.8615	0.4	0.3	-45.1	-36.1	-9	
	3.8607	0.3	0.3	-45.3	-36.3	-9	

B31-M	3.8619	0.5	0.6	-45.0	-36.2	-8.8	counts dropping
	3.8677	0.8	0.7	-43.5	-36.2	-7.3	
	3.8643	0.7	0.6	-44.4	-36.2	-8.2	
						-8.1	
						0.4	
IMt-1	3.8682	0.3	0.3	-43.4	-34.4	-9	
	3.8709	0.6	0.4	-42.7	-33.7	-9	
B23-M	3.9863	0.7	0.7	-14.2	-34.2	20.0	counts dropping
	3.9788	0.8	0.7	-16.0	-34.2	18.2	
	3.9591	0.8	0.6	-20.9	-34.2	13.3	
					Avg	17.1	
					S.E.	2.0	
IMt-1	3.8696	0.5	0.4	-43.1	-34.1	-9	
	3.8663	0.5	0.4	-43.9	-34.9	-9.0	inc EM gain
	3.8796	0.4	0.4	-40.6	-31.6	-9.0	
	3.8738	0.5	0.4	-42.0	-33.0	-9.0	50 cycles
				Avg	-33.2		
				S.E.	0.9		
B17-A	3.9253	1.0	1.0	-29.3	-33.3	4.0	50 cycles
	3.9189	1.0	1.0	-30.9	-33.3	2.4	50 cycles
	3.9344	0.8	1.0	-27.0	-33.3	6.3	50 cycles
	3.9324	1.0	1.0	-27.5	-33.3	5.8	50 cycles
	3.9249	1.0	1.0	-29.4	-33.3	3.9	50 cycles
					Avg	4.5	
					S.E.	0.7	
IMt-1	3.8708	0.4	0.3	-42.7	-33.7	-9.0	
ANG-A	3.9216	1.0	0.9	-30.2	-33.3	3.1	100 cycles
	3.9079	1.0	0.9	-33.6	-33.3	-0.3	100 cycles
	3.9182	0.9	0.9	-31.0	-33.3	2.3	100 cycles
					Avg	2.7	
					S.E.	0.6	
SB01-A	3.9189	0.7	0.7	-30.9	-33.3	2.4	100 cycles
	3.9185	1.1	9.8	-31.0	-33.3	2.3	50 cycles
	3.9178	1.3	1.0	-31.1	-33.3	2.2	50 cycles
					Avg	2.3	
					S.E.	0.1	
SB02-A	3.9579	0.8	0.9	-21.2	-33.3	12.1	50 cycles
	3.9577	0.9	0.9	-21.3	-33.3	12.0	50 cycles
	3.9550	0.8	0.9	-21.9	-33.3	11.4	50 cycles
					Avg	11.8	
					S.E.	0.2	
IMt-1	3.8733	0.4	0.3	-42.1	-33.1	-9.0	50 cycles
	3.8918	0.6	0.4	-37.6	-28.5	-9.1	75 IF
	3.8886	0.6	0.6	-38.4	-29.3	-9.1	150 IF

	3.8653	0.8	0.6	-44.1	-35.0	-9.1	150 IF
	3.8799	0.8	0.8	-40.5	-31.4	-9.1	
	3.8838	0.9	0.8	-39.5	-30.4	-9.1	
				Avg	-31		
				S.E.	0.5		
Arg1-A	3.8815	1.7	1.7	-40.1	-31	-9.2	
	3.8739	1.2	1.2	-42.0	-31	-11.1	
	3.8809	1.2	1.1	-40.3	-31	-9.4	
					Avg	-9.9	
					S.E.	0.6	
IMt-1	3.8815	0.5	0.4	-40.1	-31.0	-9.1	MRP 1000
	3.8796	0.6	0.6	-40.6	-31.5	-9.1	
Arg11-A	3.9191	0.6	0.6	-30.8	-31	0.2	100 cycles
	3.9161	0.9	0.8	-31.6	-31	-0.6	50 cycles
					Avg	-0.2	
B23-A	3.7960	0.8	0.8	-61.3	-31	-30.3	100 cycles
	3.7970	1.0	1.1	-61.0	-31	-30.0	50 cycles
					Avg	-30.1	
					S.E.	0.1	
IMt-1	3.8776	0.5	0.5	-41.1	-32.0	-9.1	MRP 1000
BU-A	3.9232	2.0	2.0	-29.8	-32	2.2	50 cycles
	3.9161	1.5	1.4	-31.6	-32	0.4	100 cycles
	3.9106	1.3	1.3	-32.9	-32	-0.9	
					Avg	0.6	
					S.E.	0.9	
IMt-1	3.8781	0.5	0.5	-41.0	-31.9	-9.1	MRP 1000
	3.8668	0.5	0.4	-43.7	-34.6	-9.1	
	3.8716	0.5	0.5	-42.6	-33.5	-9.1	
MB34-A	3.8783	1.2	1.2	-40.9	-34	-6.9	100 cycles
	3.8861	1.6	1.6	-39.0	-34	-5.0	
					Avg	-5.9	
IMt-1	3.8680	0.4	0.4	-43.5	-34.4	-9.1	
TR-A	3.9570	1.2	1.2	-21.4	-34	12.1	100 cycles
	3.9557	1.1	1.1	-21.8	-34	11.7	
	3.9603	1.5	1.5	-20.6	-34	12.9	50 cycles
					Avg	12.2	
IMt-1	3.8737	0.6	0.4	-42.0	-32.9	-9.1	
ZO-A	3.9482	2.3	1.7	-23.6	-33	9.4	
	3.9669	2.1	1.8	-19.0	-33	14.0	
					Avg	11.7	
					S.E.	2.3	
IMt-1	3.8754	0.5	0.4	-41.6	-32.5	-9.1	

CHAPTER EIGHT

8. Conclusions

Bentonites show a bewildering variety of physical-chemical properties and visual appearances caused by a combination of parent material, depositional environment, the bentonite-forming fluids, as well as later diagenetic overprints (Grim & Güven, 1978; Odom, 1984; Christidis & Huff, 2009).

The first aim of this dissertation (chapters 5 and 6) was to determine the formational conditions of bentonite and associated authigenic carbonates in a terrestrial depositional environment in Southern Germany, as well as to trace cation sources and the fluids (salinity, Sr content, Mg/Ca, redox conditions) involved in the bentonitization of the rhyolitic, Mg- and Ca-poor parent material in a strictly non-marine depositional environment (Vogt, 1980; Unger & Niemeyer, 1985a, b; Unger et al., 1990; Ulbig, 1994; Schmid, 2002; Gilg, 2005; Maurer & Buchner, 2007; Aziz et al., 2008, 2010).

The second aim of this dissertation (chapter 7) was to explore the use of the trace element boron in elucidating differences in the fluids (B content, salinity/chlorinity, B and fluid sources) involved in the formation of sodium, magnesium and calcium bentonites using fourteen bentonites from various depositional environments. This was done because the geological, sedimentological, and stable isotope evidence is consistent for some bentonite deposits but contradictory for other bentonite deposits (Table 7.1 and sources in chapter 7).

8.1 The dolomite-bearing Mainburg-Landshut bentonite deposits

The formation of authigenic dolomite and calcite was for the first time systematically examined in distal and non-marine bentonite deposits. Carbonates were found to have formed in distinct formational settings. Whereas dolomite is tied to palustrine and some pedogenic environments such as in wetlands and floodplains, calcite is preferentially found in groundwater and pedogenic dominated deposits located in former riverine channels or oxbow lakes. Dolomites formed from evaporated surface waters consistent with the palustrine wetland setting, whereas calcites formed from largely unmodified meteoric groundwater.

The authigenic dolomite is the most abundant carbonate mineral in Bavarian bentonite deposits. Chemical and mineralogical analyses reveal a calcium-rich (54 to 57 mol-% Mg) and moderately ordered (I_{015}/I_{110}: 0.38–0.68) dolomite, and a Mg-enriched calcite with 4.0 mol-% Mg that places it at

the boundary between high- and low-Magnesian calcite. The Mg/Ca of the carbonates indicate that dolomite formed from waters having a Mg/Ca of 2 – 5 and that calcite formed from waters having a Mg/Ca of about 1.

Dolomites, calcites, and smectites from bentonites have distinct strontium concentrations, with the concentrations in palustrine dolomites exceeding those of most island dolomites (Budd, 1997). The $^{87}Sr/^{86}Sr$ of dolomites are lower than those of calcites and $^{87}Sr/^{86}Sr$ increase down-profile whereas strontium concentration decreases, suggesting dolomite and calcite formation from contrasting fluids: an evaporated fluid dominated by strontium from detrital marine limestone and dolostone, and a largely unmodified groundwater precipitating calcite dominated by more radiogenic strontium sources from silicate detritus in the North Alpine Foreland Basin. Dolomites formed at average salinities of 2 to 6 g/L whereas calcites formed from freshwaters of very low salinity.

The $^{87}Sr/^{86}Sr$ of one smectite from the Mittersberg bentonite and the associated dolomites, together with elevated lithium concentrations in smectites and dolomites, strongly indicate that dolomite and smectite formation was cogenetic at least in palustrine bentonite deposits. The cogenetic smectite-dolomite assemblage has been dated using the Rb-Sr method and yields a formation age identical to primary ash deposition of 14.7 ± 4.1 Ma, and an exchangeable strontium - fixed strontium Rb-Sr age of 11.8 ± 1.5 Ma, indicating a very rapid onset of bentonite formation within 4 Ma after deposition. This is the only illite-poor smectite separate from a bentonite deposit to be directly dated using the Rb-Sr method.

The $^{87}Sr/^{86}Sr$ of exchangeable and fixed strontium in smectites, and of the carbonates, thus reveal contrasting fluid sources and mixing within bentonite deposits. Strontium isotope ratios also reveal that the $^{87}Sr/^{86}Sr$ of the exchangeable strontium is not identical to fixed strontium nor dolomite therefore indicating that the original cation interlayer composition has not been preserved. This is confirmed by the Mg/Ca of the smectite interlayer, dolomites, and calcites that are not in equilibrium with the same fluid thus also pointing to later cation exchange.

The combined chemical, isotopic, mineralogical and sedimentological evidence confirms two distinct depositional and formational settings of bentonites in Southern Germany: a shallow palustrine setting with an asymmetric top-down character of ash-bentonite containing Sr- and Li-bearing dolomite and smectite; and a pedogenic-groundwater setting with the classical bentonite-ash-bentonite order characterised by lower strontium concentrations in carbonates and smectites, and no detectable lithium content.

The results of chapters 5 and 6 suggest that the Rb-Sr geochemistry of smectites and carbonates is a promising method for elucidating bentonitisation and carbonate formation in bentonite deposits, as well as diagenetic alteration processes such as later cation exchange events.

8.2 Boron isotope geochemistry of smectites from bentonite deposits

The trace element boron and its isotope values were for the first time systematically determined for < 0.2 µm fractions (smectites) from fourteen sodium, magnesium and calcium bentonite deposits from various marine and terrestrial depositional environments. Identical sample processing has been applied to all smectites to measure the exchangeable and the fixed boron concentrations using PGAA and SIMS.

The systematic methodology has revealed distinct differences in both boron concentrations and $\delta^{11}B$ values among the examined bentonite deposits. The fixed boron content in smectites (0.2 to 196 µg/g B) spans the entire known range of boron concentrations for montmorillonites (Harder, 1959, 1970). Sodium-bentonites tend to show higher boron concentrations (≥ 30 µg/g B) than Ca- and Mg-bentonites (≤ 30 µg/g B). The boron content indicates that smectite formation occurs in B-poor fresh to brackish waters as well as in B-rich saline waters and brines with several times the chlorinity of seawater.

The $\delta^{11}B$ values of fixed boron show a range of -30.1 ‰ to + 17.6 ‰. There is no systematic variation of $\delta^{11}B$ values with the exchangeable interlayer cation occupancy. Some marine deposited bentonites (Wyoming, Pertek, Tavush, and Lago Pellegrini) and all bentonite deposits in strictly terrestrial depositional settings have $\delta^{11}B$ values smaller or roughly equal to 0 ‰, and thus formed from non-marine waters. Only the Ca- and Mg-bentonites of Milos, Los Trancos, and Otay as well as the Na-bentonite from Askana show $\delta^{11}B$ values possibly consistent with a formation from seawater mixing with other fluids.

A modified fluid-smectite boron partitioning has been developed for smectite based on the boron adsorption onto clay minerals by You et al. (1995, 1996). It has been modified by a potassium correction factor that takes into account the low but almost always present amount of potassium and illitic layers even in the most illite-poor smectites. This boron partitioning coefficient yields realistic boron concentrations for the smectite-forming fluids consistent with the geological and hydrogeological situation of the examined bentonite deposits.

Most smectites showed little variation in boron concentrations of mannitol-treated (i.e. adsorbed and interlayer boron + fixed boron) and cation-exchanged sub-samples (i.e. only the fixed boron),

however, the $\delta^{11}B$ values of some samples that showed little variation in boron content after treatment such as Bahia, Glasgow and La Tranquera dropped by up to 47.2 ‰ points! The systematic approach shows that careful sample processing is a mandatory for reliable boron isotope geochemistry of clay minerals, and that sometimes drastically different results can be obtained from differently treated sub-samples. It is therefore strongly advisable to determine the boron content and the $\delta^{11}B$ values using cation exchanged smectites.

With the exception of Milos, Askana and Pertek all carbonate-bearing bentonite deposits have calcite or dolomite with carbon and oxygen isotope values indicative of non-marine waters such as basinal brines. Carbonate isotope geochemical results thus confirm boron isotope results suggesting bentonite formation predominantly from basinal brines and meteoric waters with a strong influence by water-rock interaction.

8.3 Research outlook

The preceding chapters showed that authigenic carbonates and smectites from bentonites are valuable archives of depositional and formational settings, as well as of the fluids involved in the formation of bentonite deposits. The trace elements strontium and boron are shown to have great potential for tracing the fluids involved in the formation of clay mineral deposits, as well as later cation exchange events, but ought to be refined by future studies on the regional and the deposit scale. The usefulness of the modified boron partitioning coefficients used for the estimation of the boron content of the smectite-precipitating fluids should be verified by experiments under controlled laboratory conditions.

Still, the strontium and boron isotope geochemistry of bentonite-associated carbonates and smectites are highly valuable tools not only for reconstructing fluids involved in the formation or later diagenetic overprint of bentonite deposits, but also for other swelling clay minerals in sedimentary basins or crystalline rocks close to the earth's surface, or in man-made applications such as bentonite buffers used in the insulation of highly active nuclear waste. Strontium and boron can be used to elucidate the fluids and/or processes affecting the bentonite buffers in nuclear disposal sites during water-rock interaction and cation exchange reactions.

They could also be used, after appropriate testing of many more bentonite deposits, as a quality control method, e.g. for discriminating natural from artificial sodium bentonites or to determine the geographic/geologic origin of commercial bentonite products because fixed strontium and boron are

only affected by treatments that strongly attack the octahedral and/or tetrahedral sheets of clay minerals.

Finally, and in addition to the applied and commercial aspects, strontium and especially boron in smectites are excellent tools for palaeoenvironmental studies using clay minerals in ancient and modern sedimentary and hydrothermal environments dominated by authigenic clays here on Earth, and other planets.

References

Adams T., Haynes J., Walker C. (1965) Boron in Holocene illites from the Dovey estuary, Wales, and its relationship to palaeosalinity in cyclothems. Sedimentology, 4, 189–195.

Afshar F.A. (1965) Geology of Tunceli-Bingöl Region of Eastern Turkey. Bulletin of the Mineral Research and Exploration Institute of Turkey, 65, 33–39.

Aggarwal J.K., Palmer M.R., Bullen T.D., Arnórsson S., Ragnarsdóttir K.V. (2000) The boron isotope systematics of Icelandic geothermal waters: 1. Meteoric water charged systems. Geochimica et Cosmochimica Acta, 64, 579–585.

Aguirre-Urreta B., Tunik M., Naipauer M., Pazos P., Ottone E., Fanning M., Ramos V.A. (2010) Malargüe Group (Maastrichtian–Danian) deposits in the Neuquén Andes, Argentina: Implications for the onset of the first Atlantic transgression related to Western Gondwana break-up. Gondwana Research, 19, 482–494.

Akkoca D.B., Kürüm S., Huff, W.D. (2013) Geochemistry of volcanogenic clayey marine sediments from the Hazar-Maden Basin (Eastern Turkey). Geologica Carpathica, 64, 467–482.

Akkoca D.B., Sagiroglu A. (2005) The authigenic dolomite and smectite formations in the Neogene lacustrine-fluvial Çaybağı Basin (Elaziğ, Eastern Turkey). Geologica Carpathica, 56, 531–543.

Aksoy E., Türkmen I., Turan M. (2005) Tectonics and sedimentation in convergent margin basins: an example from the Tertiary Elâzığ basin, Eastern Turkey. Journal of Asian Earth Sciences, 25, 459–472.

Albrecht T. (2011) Geological Mapping and Investigations of Bentonite Deposits in the Area of the Gavião-Block, South-Bahia, Brazil. Master thesis, Technische Universität München, München, Germany, 146 p.

Aleva G.J.J (1994) Laterites. Concepts, geology, geomorphology and chemistry. ISRIC. Wageningen, 169 p.

Alonso-Zarza A.M. (2003) Palaeoenvironmental significance of palustrine carbonates and calcretes in the geological record. Earth-Science Reviews, 60, 261–298.

Alonso-Zarza A.M., Wright, V.P. (2010) Calcretes. Pp. 225–267 in: Carbonates in Continental Settings: Facies, Environments and Processes. Developments in Sedimentology, 61, (A.M. Alonso-Zarza, L.H. Tanner, editors) Elsevier, Amsterdam.

Ames L.L., Sand L.B., Goldich S.S. (1958) Contribution on the Hector, California bentonite deposit. Economic Geology, 53, 22–37.

Ammon L. v. (1901) Die Malgersdorfer Weisserde. Geognostische Jahreshefte, 13, 195–208, München.

Anadón P., Utrilla R., Vázquez A. (2002) Mineralogy and Sr–Mg geochemistry of charophyte carbonates: a new tool for paleolimnological research. Earth and Planetary Science Letters, 197, 205–214.

Andreis R.R., Zalba P.E. (2001) Na-Bentonites and K-Bentonites from Argentina: composition, origin and age. Pp. 21 in: Proceedings of the 12th International Clay Conference, Bahia Blanca, Argentina, July 21st-22nd 2001 (E.A. Dominguez, G.R. Mas, Cravero F., editors), AIPEA , Elsevier, Amsterdam.

Anna L.O., Pollastro R., Gaswirth S.B. (2007) Williston Basin Province–Stratigraphic and structural framework to a geologic assessment of undiscovered oil and gas resources, chap. 2 of U.S. Geological Survey Williston Basin Province Assessment Team, Assessment of undiscovered oil and gas resources of the Williston Basin Province of North Dakota, Montana, and South Dakota, 2010 (ver. 1.1, November 2013), U.S. Geological Survey Digital Data Series 69–W, 17 p.

Argiel A. (1992) Die Lagerstätten smektithaltiger Tone in Argentinien. Doctoral thesis, Friedrich-Alexander-Universität Erlangen-Nürnberg, Germany, 186 p.

Armas P., Sánchez M.L. (2013) Sedimentología y arquitectura de las dunas costeras de la Formación Allen, Grupo Malargüe, cuenca Neuquina - Río Negro, Argentina. Revista Mexicana de Ciencias Geológicas, 30, 65–79.

Armenteros I. (2010) Diagenesis of Carbonates in Continental Settings. Pp. 61–151 in: Carbonates in Continental Settings: Chemistry, Diagenesis and Applications (A.M. Alonso-Zarza, L.H. Tanner, editors), Developments in Sedimentology, 62, Elsevier, Amsterdam.

Armstrong R.L., Ward P. (1993) Late Triassic to earliest Eocene magmatism in the North American Cordillera: Implications for the Western Interior basin. Pp. 49-72 in: Evolution of the Western Interior Basin (Caldwell W.G.E., Kauffman E.G., editors), Geological Association of Canada, Special Papers, 39.

Arnórsson S., Andrésdóttir A. (1995) Processes controlling the distribution of boron and chlorine in natural waters in Iceland. Geochimica et Cosmochimica Acta, 59, 4125–4146.

Arp G., Wiesheu R. (1997) Ein kontinuierliches Profil von Algenbiohermen bis zu Seetonen des miozänen Rieskratersees: Sequenzen, Mikrofazies und Dolomitisierung. Geologische Blätter für Nordost-Bayern, 47, 461–486.

Aziz H.A., Böhme M., Rocholl A., Prieto J., Wijbran J.R., Bachtadse V., Ulbig A. (2010) Integrated stratigraphy and $^{40}Ar/^{39}Ar$ chronology of the early to middle Miocene Upper Freshwater Molasse in western Bavaria (Germany). International Journal of Earth Sciences, 99, 1859–1886

Aziz H.A., Böhme M., Rocholl A., Zwing A., Prieto J., Wijbrans J. R., Heissig K., Bachtadse V. (2008) Integrated stratigraphy and $^{39}Ar/^{40}Ar$ dating of the early to middle Miocene upper freshwater Molasse in eastern Bavaria (Germany). International Journal of Earth Sciences, 97, 115–134

Baier J. (2009) Zur Herkunft und Bedeutung der Ries-Auswurfprodukte für den Impakt-Mechanismus. Jahresberichte und Mitteilungen des Oberrheinischen Geologischen Vereins, N.F., 91, 9–29, Stuttgart.

Banner J.L. (1995) Application of the trace element and isotope geochemistry of strontium to studies of carbonate diagenesis. Sedimentology, 42, 805–824.

Barth S.R. (1993) Boron isotope variations in nature: a synthesis. Geologische Rundschau, 82, 640–651.

Barth S.R. (2000) Stable isotope geochemistry of sediment-hosted groundwater from a Late Paleozoic–Early Mesozoic section in central Europe. Journal of Hydrology, 235, 72–87.

Bassett R. L. (1977) The geochemistry of boron in thermal waters. Ph.D. dissertation, Stanford University, United States of America, 290 p.

Batsche H. (1957) Geologische Untersuchungen in der Oberen Süßwassermolasse Ostniederbayerns (Blatt Landau, Eichendorf, Simbach, Arnstorf der Topographischen Karte 1:25000). Beihefte zum Geologischen Jahrbuch, 26, 261–307

Bau M., Möller P. (1992) Rare earth element fractionation in metamorphogenic hydrothermal calcite, magnesite and siderite. Mineralogy and Petrology, 45, 231–246.

Bauer K. (2014) Stable O and H isotopic composition of hydrous minerals as proxies for paleoclimate and topography: Application to the European Alps. Ph.D. thesis, Université de Lausanne, Switzerland, Pp. 304–305.

Bauer K., Vennemann T.W., Gilg H.A. (2016) Stable isotope composition of bentonites from the Swiss and Bavarian Freshwater Molasse as a proxy for paleoprecipitation. Palaeogeography, Palaeoclimatology, Palaeoecology, 455, 53–64.

Beaudoin N., Bellahsen N., Lacombe O., Emmanuel L., Pironon J. (2014) Crustal-scale fluid flow during the tectonic evolution of the Bighorn Basin (Wyoming, USA). Basin Research, 26, 403–435.

Bell J.W., Caskey S.J., House P.K. (2010) Geologic map of the Lahontan Mountains quadrangle, Churchill County, Nevada, 2nd edition. Nevada Bureau of Mines and Geology Map 168, 1:24,000 scale, 24 p.

Belyankin D.S., Petrov V.P. (1950) Petrographic composition and origin of Askana clays. Bulletin of the Academy of Sciences of the USSR, Series Geology, 1950(2), 33–44.

Berg R.B. (1969) Bentonite in Montana. Montana Bureau of Mines and Geology Bulletin, 74, 34 p.

Berg R.B. (1970) Bentonite deposits in the Ingomar-Vananda area, Treasure and Rosebud Counties, Montana. Montana Bureau of Mines and Geology Special Publication, 51, 5 p.

Bergmann J, Friedel P., Kleeberg R. (1998) BGMN – a new fundamental parameters based Rietveld program for laboratory X-ray sources, it's use in quantitative analysis and structure investigations. International Union of Crystallography Commission on Powder Diffraction Newsletter, 20, 5–8.

Bernard R., Taran Y., Pennisi M., Tello E., Ramirez A. (2011) Chloride and Boron behavior in fluids of Los Humeros geothermal field (Mexico): A model based on the existence of deep acid brine. Applied Geochemistry, 26, 2064–2073.

Berry R.W. (1991) Deposition of Eocene and Oligocene bentonites and their relationship to Tertiary tectonics, San Diego County. In: Eocene geologic history – San Diego region (Abbott P.L., May J.A, editors). SEPM Pacific Section Book, 68, 107–113.

Berry R.W. (1999) Eocene and Oligocene Otay-type waxy bentonites of San Diego county and Baja California: chemistry, mineralogy, petrology and place tectonic implications. Clays and Clay Minerals, 47, 70–83.

Bertog J.L., Huff W.D., Martin J.E. (2007) Geochemical and mineralogical recognition of the bentonites in the lower Pierre Shale Group and their use in regional stratigraphic correlation. Pp. 23–50 in: The Geology and Paleontology of the Late Cretaceous Marine Deposits of the Dakotas, (Martin J.E., Parris D.C., editors), Geological Society of America, Special Papers, 427.

Blondes M.S., Gans K.D., Rowan E.L., Thordsen J.J., Reidy M.E., Engle M.A., Kharaka Y.K., Thomas B. (2016) U.S. Geological Survey National Produced Waters Geochemical Database, Version 2.2. http://eerscmap.usgs.gov/pwapp/.

Blum J.D., Gazis C.A., Jacobsen A.D., Chamberlain C.P. (1998) Carbonate versus silicate weathering in the Raikhot watershed within the High Himalayan Crystalline Series. Geology, 26, 411–414.

Böhme M. (2003) The Miocene Climatic Optimum: Evidence from ectothermic vertebrates of Central Europe. Palaeogeography, Palaeoclimatology, Palaeoecology, 195, 389–401.

Böhme M., Bruch A.A., Selmeier, A. (2007) The reconstruction of Early and Middle Miocene climate and vegetation in Southern Germany as determined from the fossil wood fauna. Palaeogeography, Palaeoclimatology, Palaeoecology, 253, 91–114.

Böhme M., Gregor H.-J., Heissig K. (2001) The Ries and Steinheim meteorite impacts and their effect on environmental conditions in time and space. Pp. 215–235 in: Geological and Biological Effects of Impact Events (Buffetaut E., Koerbel, C., editors.), Springer, Berlin.

Boschetti T. (2011) Application of brine differentiation and Langelier–Ludwig plots to fresh-to-brine waters from sedimentary basins: Diagnostic potentials and limits. Journal of Geochemical Exploration, 108, 126–130.

Boschetti T., Toscani L., Mariani E.S. (2014) Boron isotope geochemistry of Na-bicarbonate, Na-chloride and Ca-chloride waters from the Northern Apennine Foredeep basin: other pieces of the sedimentary basin puzzle. Geofluids, 15, 546–562.

Bottomley D.J., Gregoire D.C., Raven K.G. (1994) Saline groundwaters and brines in the Canadian Shield: Geochemical and isotopic evidence for a residual evaporite brine component. Geochimica et Cosmochimica Acta, 58, 1483–1498.

Bradshaw M.J. (1975) Origin of montmorillonite bands in the middle Jurassic of Eastern England. Earth and Planetary Science Letters, 26, 245-252.

Braun R.E. (1983) The transition from the Judith River Formation to the Bearpaw Shale (Campanian), north-central Montana. Master thesis, Montana State University, United States of America, 66 p.

Breecker D.O., Sharp Z.D., McFadden L.D. (2009) Seasonal bias in the formation and stable isotopic composition of pedogenic carbonate in modern soils from central New Mexico, USA. Geological Society of America Bulletin, 121, 630–640.

Brockamp O. (1973) Borfixierung in authigenen und detritischen Tonen. Geochimica et Cosmochimica Acta, 37, 1339–1351.

Brunnacker K. (1962) Erläuterung zur geologischen Karte von Bayern 1:25000 Blatt Freising 7536 – Nord. Bayerischen Geologisches Landesamt, München, 83 p.

Buchner E., Schmieder M., Schwarz W.H., Trielof M. (2013) Das Alter des Meteoritenkraters Nördlinger Ries – eine Übersicht und kurze Diskussion der neueren Datierungen des Riesimpakts. Zeitschrift der Deutschen Gesellschaft für Geowissenschaften, 164, 433–445.

Budd D.A. (1997) Cenozoic dolomites of carbonate islands: their attributes and origin. Earth-Science Reviews, 42, l–47.

Burtner R.L., Warner M.A. (1986) Relationship between illite/smectite diagenesis and hydrocarbon generation in Lower Cretaceous Mowry and Skull Creek Shales of the Northern Rocky Mountain area Clays and Clay Minerals, 34, 390–402.

Bustillo M.A., Arribas M.E., Bustillo M. (2002) Dolomitization and silicification in low-energy lacustrine carbonates (Paleogene, Madrid Basin, Spain). Sedimentary Geology, 151, 107–126.

Byers C. W., Larson D.W. (1979) Paleoenvironments of Mowry Shale (Lower Cretaceous), western and central Wyoming. American Association of Petroleum Geologist Bulletin, 63, 354–375.

Caballero E., de Cisneros C.J., Huertas F.J., Huertas F., Pozzuoli A., Linares J. (2005) Bentonites from Cabo de Gata, Almería, Spain: a mineralogical and geochemical overview. Clay Minerals, 40, 463–480.

Caballero E., Linares J., Reyes E., Huertas F. (1985) Hydrothermal solutions related to bentonite genesis, Cabo de Gata region, Almeria, SE Spain. Mineralogica et Petrographica Acta, 29-A, 187–199.

Caballero E., Reyes E., Delgado A., Huertas F., Linares J. (1992) The formation of bentonite: mass balance effects. Applied Clay Science, 6, 265–276.

Cadrin A.A.J., Kyser T.K., Caldwell W.G.E., Longstaffe F.J. (1995) Isotopic and chemical compositions of bentonites as paleoenvironmental indicators of the Cretaceous Western Interior Seaway. Palaeogeography, Palaeoclimatology, Palaeoecology, 119, 301–320.

Caldwell W.G.E. (1968) The late Cretaceous Bearpaw Formation in the south Saskatchewan River valley. Saskatchewan Research Council, Geology Division, Report No. 8, 89 p.

Campani M., Mulch A., Kempf O., Schlunegger F., Mancktelow N. (2012) Miocene paleotopography of the Central Alps. Earth and Planetary Science Letters, 337–338, 174–185.

Canadell J., Jackson R.B., Ehleringer J.R., Mooney H.A., Sala O.E., Schulze E.-D. (1996) Maximum rooting depth of vegetation types at the global scale. Oecologia, 108, 583–595.

Capo R.C., Whipkey C.E., Blachère J.R., Chadwick O.A. (2000) Pedogenic origin of dolomite in a basaltic weathering profile, Kohala peninsula, Hawaii. Geology, 28, 271–274.

Cas R., Wright J. (1988) Volcanic Successions, Modern and Ancient. Springer Netherlands, Amsterdam, 528 pp.

Casado A.I., Alonso-Zarza A.M., La Iglesia Á. (2014) Morphology and origin of dolomite in paleosols and lacustrine sequences. Examples from the Miocene of the Madrid Basin. Sedimentary Geology, 312, 50–62.

Cerling T.E. (1984) The stable isotopic composition of soil carbonate and its relationship to climate. Earth and Planetary Science Letters, 71, 229–240.

Cerling T.E. (1991) Carbon dioxide in the atmosphere: Evidence from Cenozoic and Mesozoic paleosols. American Journal of Science, 291, 377–400.

Cerling T. E., Quade J. (1993) Stable carbon and oxygen isotopes in soil carbonates. Geophysical Monograph Series, 78, 217–231.

Chahi A., Duringer P., Ais M., Bouabdelli M., Gauthier-Lafayer F., Fritz B. (1999) Diagenetic transformation of dolomite into stevensite in lacustrine sediments from Jbel Rhassoul, Morocco. Journal of Sedimentary Research, 69, 1123–1135.

Chaudhuri S., Brookins D.G. (1979) The Rb-Sr systematics in acid-leached clay minerals. Chemical Geology, 24, 231–242.

Chaussidon M., Albarede F. (1992) Secular boron isotope variations in the continental crust: an ion microprobe study. Earth and Planetary Science Letters, 108, 229–241.

Chaussidon M., Robert F., Mangin D., Hanon P., Rose E.F. (1997) Analytical procedures for the measurement of boron isotope composition by ion microprobe in meteorites and mantle rocks. Geostandards Newsletter, 21, 7–17.

Chris C.L., Harder H. (1974) Boron. Pp. 5A1–5O3 in: Handbook of Geochemistry (K.H. Wedepohl, editor), Springer-Verlag, Berlin, Heidelberg.

Christidis G.E. (1998) Comparative study of the mobility of major and trace elements during alteration of an andesite and a rhyolite to bentonite, in the islands of Milos and Kimolos, Aegean, Greece. Clays and Clay Minerals, 46, 379–399.

Christidis G.E. (2001) Geochemical correlation of bentonites from Milos Island, Aegean, Greece. Clay Minerals, 36, 295–306.

Christidis G.E. (2006) Genesis and compositional heterogeneity of smectites. Part III: Alteration of basic pyroclastic rocks – A case study from the Troodos Ophiolite Complex, Cyprus. American Mineralogist, 91, 685–701.

Christidis G.E. (2008) Do bentonites have contradictory characteristics? An attempt to answer unanswered questions. Clay Minerals, 43, 515–529.

Christidis G.E., Dunham A.C. (1993) Compositional variations in smectites. Part I. Alteration of intermediate rocks. A case study from Milos Island, Greece. Clay Minerals, 28, 255–273.

Christidis G.E., Dunham A.C. (1997) Compositional variations in smectites; Part II, Alteration of acidic precursors, a case study from Milos Island, Greece. Clay Minerals, 32, 253–270.

Christidis G.E., Huff W.D. (2009) Geological Aspects and Genesis of Bentonites. Elements, 5, 93–98.

Christidis G.E., Scott P.W., Marcopoulos T. (1995) Origin of the bentonite deposits of eastern Milos, Aegean, Greece: Geological, mineralogical and geochemical evidence. Clays and Clay Minerals, 43, 63–77.

Chukhrov F.V. (1968) Some results of the study of clay minerals in the U.S.S.R. Clays and Clay Minerals, 16, 3–14.

Clauer N. (1979) Relationship between the isotopic composition of strontium in newly formed continental clay minerals and their source material. Chemical Geology, 27, 115–124.

Clauer N., Hoffert M., Karpoff A.M. (1982) The Rb-Sr isotope system as an index of origin and diagenetic evolution of southern Pacific red clays. Geochimica et Cosmochimica Acta, 46, 2659–2664.

Clay Minerals Society (2016) The Clay Minerals Society Glossary of Clay Science. The Clay Minerals Society, Chantilly, VA.

Cleveland G.B. (1960) Geology of the Otay bentonite deposits, San Diego County, California. California Division of Mines, Special Report, 64, 16 p.

Clow D.W., Mast M.A., Bullen T.D., Turk J.T. (1997) Strontium 87/strontium 86 as a tracer of mineral weathering reactions and calcium sources in an alpine/subalpine watershed, Loch Vale, Colorado. Water Resources Research, 33, 1335–1351.

Cobban W.A., Kennedy W.J. (1989) The ammonite Metengonoceras Hyatt, 1903, from the Mowry Shale (Cretaceous) of Montana and Wyoming. U.S. Geological Survey Bulletin, 1787–L, 11 p.

Cole T.G., Shaw H.F. (1983) The nature and origin of authigenic smectites in some recent marine sediments. Clay Minerals, 18, 239–252.

Compton J.S., Conrad M.E., Vennemann T.W. (1999) Stable Isotope Evolution of Volcanic Ash Layers during Diagenesis of the Miocene Monterey Formation, California. Clays and Clay Minerals, 47, 84–95.

Congdon R.D., Nash W.P. (1991) Eruptive pegmatite magma: rhyolite of the Honeycomb hills, Utah. American Mineralogist, 76, 1261–1278.

Coolbaugh M.F., Sladek C., Kratt C., Shevenell L., Faulds J.E. (2006) Surface Indicators of Geothermal Activity at Salt Wells, Nevada, USA, Including Warm Ground, Borate Deposits, and Siliceous Alteration. Geothermal Resources Council Transactions, 30, 399–405.

Curtis C.D. (1963) Studies on the use of boron as a paleoenvironmental indicator. Geochimica et Cosmochimica Acta, 28, 1125–1137.

Couch E.L. (1971) Calculation of Paleosalinities from Boron and Clay Mineral Data. American Association of Petroleum Geologists Bulletin, 55, 1829–1837.

Couch E.L., Grim R.E. (1968) Boron fixation by illites. Clays and Clay Minerals, 16, 249–256.

Dabrio C.J., Martin J.M. (1978) Los arrecifes Messinienses de Almería (SE de España). Cuadernos de Geología, 8-9, 83–103.

D'Amore, F., Sergio N. (1977) Notes on the chemistry of geothermal gases. Geothermics, 6, 39–65.

D'Amore F., Truesdell A.H. (1979) Models for steam chemistry at Larderello and The Geysers. Pp. 283–297 in: Proceedings of the 5th Workshop on Geothermal Reservoir Engineering. Stanford University, California.

Darragi F., Tardy Y. (1987) Authigenic trioctahedral smectites controlling pH, alkalinity, silica and magnesium concentrations in alkaline lakes. Chemical Geology, 63, 59–72.

Davis D.A. (2014) Industrial Minerals. Pp. 109–122 in: The Nevada Mineral Industry 2012 (J.L. Muntean, D.A. Davis, L. Shevenell, B. McDonald, editors), Nevada Bureau of Mines and Geology Special Publication, MI-2012, Nevada, Reno, 177 p.

Davis H.R., C.W. Byers, L.M. Pratt (1989) Depositional Mechanisms and Organic Matter in Mowry Shale (Cretaceous), Wyoming. American Association of Petroleum Geologists Bulletin, 73, 1103–1116.

Davis J.C. (1970) Petrology of Cretaceous Mowry Shale of Wyoming. American Association of Petroleum Geologists Bulletin, 54, 487–502.

Decher A., Bechtel A., Echle W., Friedrich G., Hoernes S. (1996) Stable isotope geochemistry of bentonites from the island of Milos (Greece). Chemical Geology, 129, 101–113.

Dehm R. (1955) Die Säugetierfaunen in der Oberen Süßwassermolasse und ihre Bedeutung für die Gliederung. Pp. 81–88 in: Erläuterung der geologischen Übersichtskarte 1:300000 der süddeutschen Molasse, (G. Abele, B. Beschoren, R. Dehm, L. Erb, B. Fuchs, O. Ganss, H. Kiderlen, H. Nathan, F. Neumaier, P. Schmidt-Thomk, W. Stephan, editors), Bayerisches Geologisches Landesamt, München.

Deines P. (2004) Carbon isotope effects in carbonate systems. Geochimica et Cosmochimica Acta, 68, 2659–2679.

de Leeuw, A., Filipescu, S., Matenco, L., Krijgsman, W., Kuiper, K., Stoica, M. (2013) Paleomagnetic and chronostratigraphic constraints on the Middle to Late Miocene evolution of the Transylvanian Basin (Romania): Implications for Central Paratethys stratigraphy and emplacement of the Tisza-Dacia plate. Global and Planetary Change, 103, 82–98.

Delgado A. (1993) Estudio isotópico de los procesos diagenéticos e hidrotermales relacionados con la génesis de bentonitas (Cabo de Gata, Almería). Thesis doctoral, Universidad de Granada, España, 410 p.

Delgado A., Caballero E., Reyes E. (1993) Bentonite deposits at Cabo de Gata (Almeria, Spain). Pp. 81–101 in: 2nd Biennial SGA Meeting Field Trip Guide (P.F. Haeh-Ali, J. Torres-Ruiz, F. Gervilla, F. Velaseo, editors), 9-15 September 1993, Granada, Spain.

Delgado A., Reyes E. (1993) Isotopic study of the diagenetic and hydrothermal origins of the bentonite deposits at Los Escullos (Almería, Spain). Pp. 675–678 in: Current research in Geology Applied to Ore Deposits, (P. Fenoll Hach-Ali, J. Torres-Ruiz, F. Gervilla, editors), University of Granada, Granada.

de Oliveira S.M.B., Trescases J.J., Melfi A.J. (1992) Lateritic nickel deposits of Brazil. Mineralium Deposita, 27, 137–146.

Department of the Interior - Bureau of Land Management (2015) Environmental Assessment of the DOI-BLM-MT-Glasgow Field Office, DOI-BLM-MT-M020-2015-0014-EA, Bent Number Four Amendment.

Deyhle A., Kopf A.J. (2005) The use and usefulness of boron isotopes in natural silicate–water systems. Physics and Chemistry of the Earth, 30, 1038–1046.

Diaz-Hernandez J.L., Sánchez-Navas A., Reyes E. (2013) Isotopic evidence for dolomite formation in soils. Chemical Geology, 347, 20–33.

Dickson A.G. (1990) Thermodynamics of the dissociation of boric acid in synthetic seawater from 273.15 to 318.15 K. Deep-Sea Research, 37, 755–766.

Dohrmann R., Kaufhold S. (2010) Determination of exchangeable calcium of calcareous and gypsiferous bentonites. Clays and Clay Minerals, 58, 513–522.

Dohrmann R., Kaufhold S. (2014) Cation exchange and mineral reactions observed in MX 80 buffers samples of the prototype repository in situ experiment in Äspö, Sweden. Clays and Clay Minerals, 62, 357–373.

Dohrmann R., Kaufhold S. (2017) Characterization of the second package of the alternative buffer material (ABM) experiment – II Exchangeable cation population rearrangement. Clays and Clay Minerals, 65, 104–121.

Dohrmann R., Olsson S., Kaufhold S., Sellin P. (2013) Mineralogical investigations of the first package of the alternative buffer material test – II. Exchangeable cation population rearrangement. Clay Minerals, 48, 215–233.

Donelly W., Thompson G., Salisbury M.H. (1979) The chemistry of altered basalts at Site 417, Deep Sea Drilling Project, Leg 51. Initial Reports of the Deep Sea Drilling Project, 51, 1319–1330.

Doppler G., Heissig K., Reichenbacher B. (2005) Die Gliederung des Tertiärs im süddeutschen Molassebecken. Newsletters on Stratigraphy, 41, 359–375.

Dromgoole E., Walter L. (1990) Iron and manganese incorporation into calcite: Effects of growth kinetics, temperature and solution chemistry. Chemical Geology, 81, 311–336.

Dsotsenidze G.S., Matchabely G.A. (1963) The genesis of bentonites of Georgian SSR. Proceedings of the International Clay Conference, Stockholm 2, 203–210.

Duane M.J., Zammel A. (1999) Modern and ancient sabkha environments – boron isotopes as discriminators of facies and uses in base metal exploration. Qatar University Science Journal, 19, 202–218.

Durum W.J. (1955) The Quality of the Ground Water. Pp. 45–62 in: Geology and Ground-Water Resources of the Missouri River Valley in Northeastern Montana (F.A. Swensen, editor), Geological Survey, Water-Supply Paper, 1263.

Dymond J. (1981) Geochemistry of Nazca Plate surface sediments: an evaluation of hydrothermal, biogenic, detrital, and hydrogenous sources. Pp. 133–174 in: Nazca Plate: Crustal Formation and Andean Convergence (V.D. Kulm, J. Dymond, E.J. Dasch, D.M. Hussong, R. Roderick, editors), Geological Society of America, Memoirs, 154.

Eberl D.D., Środoń J., Northrop H.R. (1986) Potassium fixation in smectite by wetting and drying. Pp. 296–326 in: Geochemical Processes at Mineral Surfaces (J.A. Davis, K.F. Hayes, editors). American Chemical Society Symposium Series, 323, American Chemical Society.

Eberl D.D., Velde B., McCormick T. (1993) Synthesis of illite-smectite from smectite at Earth surface temperatures and high pH. Clay Minerals, 28, 49–60.

Egger R., Eichinger L., Rauert W., Stichler W. (1983) Untersuchung zum Grundwasserhaushalt des Tiefenwassers der Oberen Süßwassermolasse durch Grundwasseraltersbestimmung. Informationsberichte Bayerisches Landesamt für Wasserwirtschaft, 8/83, 99–145.

Eichinger L., Lorenz G., Heidinger M. (2007) Bohrung Uetlibergtunnel: Interpretation der isotopenhydrologischen, hydrochemischen und gasphysikalischen Untersuchungsergebnisse. Nagra Arbeitsbericht, NAB 07–08, 1–59.

Eisenhour D.D., Brown R.K. (2009) Bentonite and its impact on modern life. Elements, 5, 83–88.

Eisenhut S., Heumann K. G. (1997) Identification of ground water contaminations by landfills using precise boron isotope ratio measurements with negative thermal ionization mass spectrometry. Fresenius' Journal of Analytical Chemistry, 359, 375–377.

Ellis A.J., Mahon W.A.J. (1964) Natural hydrothermal systems and experimental hot water/rock interactions. Geochimica et Cosmochimica Acta, 28, 1323–1357.

Ellis A.J., Mahon W.A.J. (1967) Natural hydrothermal systems and experimental hot water/rock interactions (part II). Geochimica et Cosmochimica Acta, 31, 519–538.

Elzea J.M. (1990) Geology, geochemistry, selected physical properties and genesis of the Cretaceous Clay Spur bentonite in Wyoming and Montana. Ph.D. thesis, Indiana University Bloomington, United States of America, 201 p.

Elzea J.M., Murray H.H. (1990) Variation in the mineralogical, chemical, and physical properties of the Cretaceous clay spur bentonite in Wyoming and Montana. Applied Clay Science, 5, 229–248.

Elzea J.M., Murray H. (1994) Bentonite. Pp. 233-46 in: Industrial Minerals and Rocks, 6th edition (D.D. Carr, editor). Society for Mining, Metallurgy and Exploration, Inc., Littleton, Colorado.

Erb L. (1931) Erläuterungen zum Blatt 146 Hilzingen. Geologische Spezial-Karte Baden 1:25000, Badisches Geologisches Landesamt und Schweizer Geologische Kommission, Freiburg im Breisgau, 115 p.

Faust G.T., Hathaway J.C., Millot G. (1959) A restudy of stevensite and allied minerals. American Mineralogist, 44, 342–370.

Fernandez Soler J. M. (1992) El volcanismo calco-alcalino de Cabo de Gata (Almería), Thesis doctoral, Universidad de Granada, 243 p.

Fiest W. (1986) Lithostratigraphie und Schwermineralgehalt der Oberen Süßwassermolasse im Bereich um die Gallenbacher Mülldeponie zwischen Aichach und Dasing. Diploma thesis, Ludwig-Maximilians-Universität München, Germany, 119 p.

Fiest W. (1989) Lithostratigraphie und Schwermineralgehalt der Mittleren und Jüngeren Serie der Oberen Süßwassermolasse Bayerns im Übergangsbereich zwischen Ost- und Westmolasse. Geologica Bavarica, 94, 259–279.

Finn T.M. (2010) New source rock data for the Thermopolis and Mowry Shales in the Wyoming part of the Bighorn Basin. U.S. Geological Survey Digital Data Series DDS–69–V, 16 p.

Fischer R.V., Schmincke H.U. (1984) Pyroclastic Rocks. Springer Verlag, Berlin.

Folinsbee R.E., Baadsgaard H., Gumming G.L., Nascimbee J., Shafiqualla M. (1965) Late Cretaceous radiometric dates from the Cypress Hills of Canada. Alberta Society of Petroleum Geologists 15th Annual Field Conference Guidebook, 162–174.

Folinsbee R.E., Baadsgaard H., Lipson J. (1961) Potassium-argon dates of Upper Cretaceous ash falls, Alberta, Canada: Annals New York Academy of Sciences, 91, 352–359.

Folk R.L., Land L.S. (1975) Mg/Ca ratio and salinity: two controls over crystallization of dolomite. American Association of Petroleum Geologists Bulletin, 59, 60–68.

Foster G.L., Pogge von Strandmann P.A.E., Rae J.W.B. (2010) Boron and magnesium isotopic composition of seawater. Geochemistry, Geophysics, Geosystems, 11, Q08015.

Frederickson A.F., Reynolds R.C. (1960) Geochemical method for determining paleosalinity. Clays and Clay Minerals, 8, 203-213,

Freudenberger W., Schwerd K. (1996) Erläuterungen zur Geologischen Karte von Bayern 1:500000. Bayerisches Geologisches Landesamt, 329 p.

Freytet, P., Verrecchia, E.P. (2002) Lacustrine and palustrine carbonate petrography: an overview. Journal of Paleolimnology, 27, 221-237

Frisch W., Kuhlemann J., Dunkl I., Brügel A. (1998) Palinspastic reconstruction and topographic evolution of the Eastern Alps during late Tertiary tectonic extrusion. Tectonophysics, 297, 1–15.

Furquim S.A.C., Graham R.C., Barbiero L., de Queiroz Neto J.P., Valle V. (2008) Mineralogy and genesis of smectites in an alkaline-saline environments of Pantanal wetland, Brazil. Clays and Clay Minerals, 56, 579–595.

Fyticas M. (1977) Geological and geothermal study of Milos Island. Ph.D. thesis. University of Thessaloniki, Greece, 228 p.

Fyticas M., Innocenti F., Kolios N., Manetti P., Mazzuoli R., Poli G., Rita F., Villari L. (1986) Volcanology and petrology of volcanic products from the Island of Milos and the neighbouring islets. Journal of Volcanology and Geothermal Research, 28, 297–317.

Gac J.Y., Droubi A., Fritz B., Tardy Y. (1977) Geochemical behavior of silica and magnesium during the evaporation of waters in Chad. Chemical Geology, 19, 215–228.

Gaines A.M. (1980) Dolomitization kinetics: recent experimental studies. SEPM Special Publication, 28, 81–86.

Galán E. (2006) Genesis of Clay Minerals. Pp. 1129–1162 in: Handbook of Clay Science, 1st edition, (F. Bergaya, B.K.G. Theng, G. Lagaly, editors), Developments in Clay Science, 1, Elsevier, Amsterdam.

Galán E., Castillo A. (1984) Sepiolite-palygorskite in Spanish Tertiary basins; genetical patterns in continental environments. Pp. 87–124 in: Palygorskite-Sepiolite Occurrences, Genesis and Uses, (A. Singer, E. Galán, editors). Developments in Sedimentology, 37, Elsevier, Amsterdam.

Gao X., Wang P., Li D., Peng Q., Wang C., Ma H. (2012) Petrologic characteristics and genesis of dolostone from the Campanian of the SK-I Well Core in the Songliao Basin, China. Geoscience Frontiers, 3, 669–680.

García del Cura M.A., Calvo J.P, Ordonez S., Jones B.F., Canaveras J.C. (2001) Petrographic and geochemical evidence for the formation of primary, bacterially induced lacustrine dolomite: La Roda `white earth´ (Pliocene, central Spain). Sedimentology, 48, 897–915.

Gasse F., Fontes J.C., Plaziat J.C., Carbonel P., Kaczmarska I., de Deckker P., Soulié-Marsche I., Callot Y., Dupeuble P.A. (1987) Biological remains, geochemistry and stable isotopes for the reconstruction of environmental and hydrological changes in the Holocene lakes from North Sahara. Palaeogeography, Palaeoclimatology, Palaeoecology, 60, 1–46.

Geske A., Zorlu J., Richter D.K., Buhl D., Niedermayr A., Immenhauser A. (2012) Impact of diagenesis and low grade metamorphosis on isotope ($\delta^{26}Mg$, $\delta^{13}C$, $\delta^{18}O$ and $^{87}Sr/^{86}Sr$) and elemental (Ca, Mg, Mn, Fe and Sr) signatures of Triassic sabkha dolomites. Chemical Geology, 332–333, 45–64.

Gilg H.A. (2000) D-H evidence for the timing of kaolinization in Northeast Bavaria, Germany. Chemical Geology, 170, 5–18.

Gilg H.A. (2005) Eine geochemische Studie an Bentoniten und vulkanischen Gläsern des nordalpinen Molassebeckens (Deutschland, Schweiz), Pp. 16–18 in: Berichte der deutschen Ton- und Tonmineralgruppe e.V., Beiträge zur Jahrestagung Celle 10.-12. Oktober 2005 (Dohrmann R., editor), Deutsche Ton- und Tonmineralgruppe, Köln, Germany.

Gilg H.A. (2018) Genesis of bentonite deposits. Pp. 19–22 in: Bentonites – from mine to application (Kaufhold, S., editor), Geologisches Jahrbuch, B107, E. Schweizerbart'sche Verlagsbuchhandlung Nägele u. Obermiller, Stuttgart.

Gilg H.A., Rocholl A. (2009) The bentonite puzzle: a stable isotope and geochemical perspective, Pp. 87 in: Abstracts of the 46th Annual Meeting of the Clay Minerals Society, Clay Minerals Society, Billings.

Gilg H.A., Ulbig A. (2017) Bentonite, Kohlentonsteine und feuerfeste Tone in der Bayerischen Molasse und dem Urnaab-System (Exkursion F am 20. April 2017). Jahresberichte und Mitteilungen des Oberrheinischen Geologischen Vereins, N.F., 99, 191–214.

Gilg H.A., Weber B., Kasbohm J., Frei R. (2003) Isotope geochemistry and origin of illite-smectite and kaolinite from the Seilitz and Kemmlitz kaolin deposits, Saxony, Germany. Clay Minerals, 38, 95-112.

Ginesu, S., Pietracaprina A. (1985) Il Giacimento di bentonite di S'Aliderru ed i suoi rapporti con l'evoluzione delle paleosuperfici della Nurra (Saedegna nord-occidentale). Bollettino della Società sarda di scienze naturali, 24, 49–56.

Goldberg E.D., Arrhenius G.O.S. (1958) Chemistry of Pacific pelagic sediments. Geochimica et Cosmochimica Acta, 13, 153–212.

Goldberg S., Glaubig R.A. (1985) Boron adsorption on aluminium and iron oxide minerals. Soil Science Society of America Journal, 49, 1374–1379.

Goldschmidt V.M., Peters Cl. (1932) Zur Geochemie des Bors. Teil I und II. Nachrichten von der Gesellschaft der Wissenschaften zu Göttingen, Mathematisch-physikalische Klasse, Band 1932, 402–407.

Goldsmith J.R., Graf D.L. (1958) Structural and compositional variations in some natural dolomites. The Journal of Geology, 66, 678–693.

Govindaraju K. (1989) Compilation of working values and sample description for 272 Geostandards. Geostandards and Geoanalytical Research, 13, 1–113.

Graup G., Horn P., Köhler H., Müller-Sohnius D. (1981) Source material for moldavites and bentonites. Naturwissenschaften, 68, 616–617.

Grim R.E., Güven, N. (1978) Origin of bentonites. Pp. 126–137 in: Bentonites: Geology, mineralogy, properties and uses. Developments in Sedimentology, 24, (R.E. Grim, N. Güven, editors) Elsevier, Amsterdam

Gubler T. (2009) Geologischer Atlas Schweiz 1:25000, Erläuterungen zu Blatt 1111 Albis. Bundesanstalt für Landestopografie, 104 p.

Gubler T., Meier M., Oberli F. (1992) Bentonites as time markers for sedimentation of the Upper Freshwater Molasse: geological observations corroborated by high resolution single zircon U-Pb ages. Zusammenfassungen, 172. Jahresversammlung SANW, Basel, 12–13.

Güven N. (2009) Bentonites – Clays for molecular engineering. Elements, 5, 89–92.

Hallam A., Selwood B.W. (1968) Montmorillonite and zeolite in Mesozoic and Tertiary beds of Southern England. Mineralogical Magazine, 37, 945–952.

Handler R., Ebner F., Neubauer F., Bojar A.-V., Hermann S. (2006) $^{40}Ar/^{39}Ar$ dating of Miocene tuffs from the Styrian part of the Pannonian Basin: an attempt to refine the basin stratigraphy. Geologica Carpathica, 57, 483–494.

Hanson R.T, Izbicki J.A., Reichard E.G., Edwards B.D., Land M., Martin P. (2009) Comparison of groundwater flow in Southern California coastal aquifers. Pp. 1–29 in: Earth Science in the Urban Ocean: The Southern California Continental Borderland (Lee H.J., Normark W.R., editors), The Geological Society of America Special Papers, 454.

Hara T., Tamai M. (1968) Some factors affecting the behavior of boron in soil. Soil Science and Plant Nutrition, 14, 215–224.

Harangi S., Mason P. R. D., Lukács R. (2005) Correlation and petrogenesis of silicic pyroclastic rocks in the Northern Pannonian Basin, Eastern-Central Europe: In situ trace element data of glass shards and mineral chemical constraints. Journal of Volcanology and Geothermal Research, 143, 237–257.

Harder H. (1959) Beitrag zur Geochemie des Bors, II. Bor in Sedimenten. Nachrichten von der Gesellschaft der Wissenschaften zu Göttingen, Mathematisch-physikalische Klasse, 6, 123-183.

Harder H. (1970) Boron content of sediments as a tool in facies analysis. Sedimentary Geology, 4, 153–175.

Harder H. (1972) The role of magnesium in the formation of smectite minerals. Chemical Geology, 10, 31–39.

Harder H. (1977) Clay mineral formation under lateritic weathering conditions. Clay Minerals, 12, 281–288.

Harr K. (1976) Mineralogisch-petrographische Untersuchungen an Bentoniten in der Süddeutschen Molasse. Doctoral thesis, University of Tübingen, Germany, 131 p.

Hay R.L. (1966) Zeolites and zeolitic reaction in sedimentary rocks. Pp. 1–130 in: Zeolites and Zeolitic Reactions in Sedimentary Rocks, (Hay R.L., editor), Geological Society of America Special Papers, 85.

Hay R.L., Pexton R.E., Teague T.T., Kyser T.K. (1986) Spring-related carbonate rocks, Mg-clays and associated minerals in Pliocene deposits of the Amargosa Desert, Nevada and California. Geological Society of America Bulletin, 97, 1488–1503.

Hay R.L., Sheppard R.A. (2001) Occurrence of zeolites in sedimentary rocks: An overview. Pp. 217–232 in: Natural Zeolites: Properties Applications and Uses (D.L. Bish, D.W. Ming, editors). Reviews in Mineralogy, 45, Mineralogical Society of America, Chantilly, Virginia, USA.

Heissig K. (1989) Neue Ergebnisse zur Stratigraphie der Mittleren Serie der Oberen Süßwassermolasse Bayerns. Geologica Bavarica, 94, 239–258.

Heissig K. (2006) Biostratigraphy of the “main bentonite horizon” of the upper freshwater molasses in Bavaria. Palaeontographica Abteilung A, 277, 93–102.

Heinzmann E.P.J., Mörs Th. (1994) Neue Wirbeltierfunde aus dem Oberoligozän der Tongrube Kärlich und ihre Bedeutung für die Tertiär-Stratigraphie des Neuwieder Beckens (Rheinland-Pfalz, Deutschland). Neues Jahrbuch für Geologie und Paläontologie, 192, 17–36.

Henry D.J., Dutrow B.L. (1996) Metamorphic Tourmaline and Its Petrologic Applications. Pp. 503–558 in: Boron: Mineralogy, Petrology, and Geochemistry (Anovitz, L.M., Grew E.S, editors), Reviews in Mineralogy, 33, Mineralogical Society of America, Chantilly, Virginia, USA.

Héran M.A., Lécuyer C., Legendre S. (2010) Cenozoic long-term terrestrial climatic evolution in Germany tracked by $\delta^{18}O$ of rodent tooth phosphate. Palaeogeography, Palaeoclimatology, Palaeoecology, 285, 331–342.

Herece E.I., Acar S. (2016) The geology of the Upper Cretaceous-Tertiary sequences in the vicinity of Pertek (Tunceli). Bulletin of the Mineral Research and Exploration Institute of Turkey, 153, 1–43.

Herold R. (1970) Sedimentpetrographische und mineralogische Untersuchungen an pelitischen Gesteinen der Molasse Niederbayerns. Doctoral thesis, Ludwig-Maximilians-Universität München, Germany, 132 p.

Hershey J.P., Fernandez M., Milne P.J., Miller F.J. (1986) The ionization of boric acid in NaCl, Na-Ca-Cl and Na-Mg-Cl solutions at 25 °C. Geochimica et Cosmochimica Acta, 50, 143–148.

Hervig, R.L. (1996) Analyses of geological materials for boron by secondary ion mass spectrometry, Pp. 789–800 in: Boron: Mineralogy, Petrology, and Geochemistry (Anovitz, L.M., Grew E.S, editors), Reviews in Mineralogy, 33, Mineralogical Society of America, Chantilly, Virginia, USA.

Hervig R.L., Moore G.M., Williams L.B., Peacock S.M., Holloway J.R., Roggensack K.R. (2002) Isotopic and elemental partitioning of boron between hydrous fluid and silicate melt. American Mineralogist, 87, 769–774.

Hevia R. (1989) Bentonitas cerámicas de Mogna- Provincia de San Juan (Argentina). Boletín de la Sociedad Española de Cerámica y Vidrio, 28, 195–197.

Hillel D. (1982) Introduction to Soil Physics. Academic Press, New York. Pp. 155–167

Hingston F.J. (1964) Reactions between boron and clays. Australian Journal of Soil Research, 2, 83–95.

Hird K. (1985) Petrography and geochemistry of some Carboniferous and Precambrian dolomites. Doctoral thesis, Durham University, United Kingdom, Pp. 340–343.

Hofmann B. (1973) Geologische Karte von Bayern 1:25000, Erläuterungen zum Blatt Nr. 7439 Landshut Ost, Pp. 44–50.

Hofmann F. (1956a) Sedimentpetrographische und tonmineralogische Untersuchungen an Bentoniten der Schweiz und Südwestdeutschlands. Eclogae Geologicae Helvetiae, 49, 113–133.

Hofmann F. (1956b) Die Obere Süsswassermolasse in der Ostschweiz und im Hegau. Bulletin der Vereinigung Schweizer Petroleum–Geologen und –Ingenieure, 23, 23–34.

Hofmann F. (1965) Die stratigraphische Bedeutung der Bentonite und Tufflagen im Molassebecken. Jahresberichte und Mitteilungen des Oberrheinischen Geologischen Vereins, 47, 79–90.

Hofmann F., Büchl U.P., Iberg R., Peters, T. (1975) Vorkommen, petrographische, tonmineralogische und technische Eigenschaften von Bentoniten im schweizerischen Molassebecken. Beiträge zur Geologie der Schweiz, 54, 1–51.

Hogan J. F., Blum J.D. (2003) Boron and lithium isotopes as groundwater tracers: a study at the Fresh Kills Landfill, Staten Island, New York, USA. Applied Geochemistry, 18, 615–627.

Horn P., Müller-Sohnius D., Köhler H., Graup, G. (1985) Rb-Sr systematics of rocks related to the Ries Crater, Germany. Earth and Planetary Science Letters, 75, 384–392.

Horwitz E.P., Chiarizia R., Dietz M.L. (1992) A novel strontium-selective extraction chromatographic resin. Solvent Extraction and Ion Exchange, 10, 313–336.

Hosterman J.W., Patterson S.H. (1992) Bentonite and Fuller's Earth Resources of the United States. US Geological Survey, Professional Paper, 1522, 45p.

Huber B. (2001) Isotopie und Genese von Karbonatkonkretionen aus der Oberen Süßwassermolasse Bayerns. Diploma thesis, Ludwig-Maximilians-Universität München, Germany, 73 p.

Huff W. (2016) K-Bentonites: A Review. American Mineralogist, 101, 43–70.

Hugget J., Cuadros J. (2005) Low-temperature illitization of smectite in the Late Eocene and Early Oligocene of the Isle of Wight (Hampshire basin), U.K. American Mineralogist, 90, 1192–1202.

Iborra C.V., Cultrone G., Cerezo P., Aguzzi C., Baschini, B.T., Valles, J., Lopez-Galindo, A. (2006) Characterisation of northern Patagonian bentonites for pharmaceutical uses. Applied Clay Science, 31, 272–281.

Imai N., Terashima S., Itoh S., Ando A. (1995) Compilation of analytical data for minor and trace elements in seventeen GSJ geochemical reference samples, "igneous rock series". Geostandards Newsletter, 19 (2), 135–213

Impiccini A. (1995) Mineralogía de la fracción no arcillosa de las bentonitas del Cretácico superior de la región Norpatagonia. Doctoral thesis, Universidad Nacional de La Plata, Argentina, 191 p.

Impiccini A., Valles J. (2011) Bentonitas. Pp. 755-762 in: Relatorio del XVIII Congreso Geológico Argentino, Geología y Recursos Naturales de la provincia del Neuquén (Leanza H.A., Arregui C., Carbone O., Danieli J.C., Vallés J, editors), Asociación Geológica Argentina, Buenos Aires.

Ishikawa T., Nakamura E. (1993) Boron isotope systematics of marine sediments. Earth and Planetary Science Letters, 117, 567–580.

Jensen F.S., Varnes H.D. (1963) Geology of the Fort Peck area, Garfield, McCone, and Valley Counties, Montana. Pp. F1–F48 in: Shorter Contributions to General Geology (Stieff L. R., Stern T. W., Eicher R. N., editors), Geological Survey Professional Paper 414.

Jin L., Williams E.L., Szramek K.J., Walter L.M., Hamilton S.K. (2008) Silicate and carbonate mineral weathering in soil profiles developed on Pleistocene glacial drift (Michigan, USA): Mass balances based on soil water geochemistry. Geochimica et Cosmochimica Acta, 72, 1027–1042.

Jourdan F., Reimold W.U., Deutsch A. (2012) Dating terrestrial impact structures. Elements, 8, 49–53.

Kainzmaier B., Thom P, Wrobel M., Pukowietz C. (2007) Geowissenschaftliche Landesaufnahme in der Planungsregion 13 Landshut, Pp. 81–88 in: Erläuterungen zur Hydrogeologischen Karte 1:100000 (Wagner B., editor), Bayerischen Geologisches Landesamt, Augsburg, Germany.

Kakihana H., Kotaka M. (1977) Equilibrium constants for boron isotope-exchange reactions. Bulletin of the Research Laboratory for Nuclear Reactors, 2, 1–12.

Kakihana H., Kotaka M., Satoh S., Nomura M., Okamoto M. (1977) Fundamental studies on the ion-exchange separation of boron isotopes. Bulletin of the Chemical Society of Japan, 50, 158–163.

Kallis P., Bleich K.E., Stahr K. (2000) Micromorphological and geochemical characterisation of Tertiary 'freshwater carbonates' locally preserved north of the edge of the Miocene Molasse Basin (SW Germany). Catena, 41, 19–42.

Kaufhold S., Dohrmann R. (2008) Detachment of colloids from bentonites in water. Applied Clay Science, 39, 50–59.

Karro E., Upin M. (2013) The occurrence and hydrochemistry of fluoride and boron in carbonate aquifer system, central and western Estonia. Environmental Monitoring and Assessment, 185, 3735–3748.

Kearsey T., Twitchett R.J., Newell A.J. (2012) The origin and significance of pedogenic dolomite from the Upper Permian of the South Urals of Russia. Geological Magazine, 149, 291–307.

Kenward P.A., Goldstein R. H., Gonzáles L. A., Roberts J.A. (2009) Precipitation of low temperature dolomite from an anaerobic microbial consortium: the role of methanogenic Archaea. Geobiology, 7, 556–565.

Keren R., Mezumen U. (1981) Boron Adsorption by Clay Minerals Using a Phenomenological Equation. Clays and Clay Minerals, 29, 198–204.

Keren R., O'Connor G.A. (1982) Effect of exchangeable ions and ionic strength on boron adsorption by montmorillonite and illite. Clays and Clay Minerals, 30, 341–346.

Kharaka Y.K., Gunter W.D., Aggarwal P.K., Perkins E.H., DeBraal, J. D. (1988) SOLMINEQ.88: A Computer Program for Geochemical Modeling of Water–Rock Interactions. US Geological Survey Water Resources Investigations Report, 88–4227.

Kharaka Y.K., Hanor J.S. (2003) Deep Fluids in the Continents: I. Sedimentary Basins. Pp. 499–540 in: Treatise on Geochemistry, Volume 5 (Holland H.D., Turekian K.K., editors), Elsevier, Amsterdam, 605 p.

Kim S.T., O'Neil J.R. (1997) Equilibrium and nonequilibrium oxygen isotope effects in synthetic carbonates. Geochimica et Cosmochimica Acta, 61, 3461–3475.

Kirkland B.L., Lynch F.L., Rahnis M.A., Folk R.L., Molineux I.J., McLean R.J.C. (1999) Alternative origins for nannobacteria-like objects in calcite. Geology, 27, 347–350.

Klappa C.F. (1980) Rhizoliths in terrestrial carbonates: classification, recognition, genesis and significance. Sedimentology, 27, 613–629.

Kloppmann W., Négrel Ph., Casanova J., Klinge H., Schelkes K., Guerrot C. (2001) Halite dissolution derived brines in the vicinity of a Permian salt dome (N German Basin). Evidence from boron, strontium, oxygen, and hydrogen isotopes. Geochimica et Cosmochimica Acta, 65, 4087–4101.

Knechtel M.M., Patterson S.H. (1956) Bentonite deposits in Marine Cretaceous Formations, Hardin District, Montana and Wyoming. US Geological Survey Bulletin, 1023, 1–116.

Knechtel M.M., Patterson S.H. (1962) Bentonite deposits of the Northern Black Hills District, Wyoming, Montana and South Dakota. US Geological Survey Bulletin, 1082–M, 893–1030.

Knight W.C. (1897) Mineral soap. Engineering and Mining Journal, 63, 600–601.

Knight W.C. (1898) Bentonite. Engineering and Mining Journal, 66, 491.

Köhler H., Frank, C., Königsberger T., Schön B. (2008) Isotopische (Sr, Nd) Charakterisierung und Datierung Variskischer Granitoide der Moldanubischen Kruste Nordostbayerns. Geologica Bavarica, 110, 170–203.

Kopf A., Deyhle A., Lavrushin V.Y., Polyak B.G., Gieskes J.M., Buachidze G.I., Wallmann K., Eisenhauer A. (2003) Isotopic evidence (He, B, C) for deep fluid and mud mobilization from mud volcanoes in the Caucasus continental collision zone. International Journal of Earth Sciences, 92, 407–425.

Köster M.H., Gilg H.A. (2015) Pedogenic, palustrine and groundwater dolomite formation in non-marine bentonites (Bavaria, Germany). Clay Minerals, 50, 163–183.

Köster M.H., Hölzl S., Gilg H.A. (2017) A strontium isotope and trace element geochemical study of dolomite-bearing bentonite deposits in Bavaria (Germany). Clay Minerals, 52, 161–190.

Kralik M. (1983) Interpretation of K-Ar and Rb-Sr data from fine fractions of weakly metamorphosed shales and carbonate rocks at the base of the Northern Calcareous Alps (Salzburg, Austria). Tschermaks Mineralogische und Petrographische Mitteilungen, 32, 49–67.

Kretz R. (1982) A model for the distribution of trace elements between calcite and dolomite. Geochimica et Cosmochimica Acta, 46, 1979–1981.

Kürum S., Akgül B., Önal A.Ö., Boztuğ D., Harlavan Y., Ural M. (2011) An Example for Arc-Type Granitoids along Collisional Zones: The Pertek Granitoid, Taurus Orogenic Belt, Turkey. International Journal of Geosciences, 2, 214–226.

LaPointe D.D., Price J.G., Davis D.A., dePolo C. M. (2011) "Life's A Beach" In Search of Ancient Shorelines and Volcanoes in the Grimes Point and Lahontan Mountains Area. Guide for the Earth Science Week Field Trip, October 15 or 16, 2011, Nevada Bureau of Mines and Geology Educational Series E-51, 23 p.

Last W.M. (1980) Sedimentology and postglacial history of Lake Manitoba. PhD thesis, University of Manitoba, Winnipeg, Canada, 687 p.

Last W.M. (1990) Lacustrine dolomite – an overview of modern, Holocene, and Pleistocene occurrences. Earth-Science Reviews, 27, 221–263.

Laudelout H., van Bladel R., Bolt G.H., Page A.L. (1968) Thermodynamics of heterovalent cation exchange reaction in a montmorillonite clay. Transactions of the Faraday Society, 64, 1477–1488.

Lawlor S.M. (2000) Hydrologic and Water-Quality Data for Ground Water along the Milk River Valley, North-Central to North-eastern Montana. Montana Bureau of Mines, Open-File Report 00-79, 24 p.

Leeman W.P., Sisson V.B. (1996) Geochemistry of boron and its implications for crustal and mantle processes. Pp. 645–708 in Boron: Mineralogy, Petrology, and Geochemistry (Anovitz, L.M., Grew E.S, editors), Reviews in Mineralogy, 33, Mineralogical Society of America, Chantilly, Virginia, USA.

Leeman W.P., Sisson V.B., Reid M.R. (1992) Boron geochemistry of the lower crust: evidence from granulite terranes and deep crustal xenoliths. Geochimica et Cosmochimica Acta, 56, 775–788.

Lemarchand D., Gaillardet J., Lewin É., Allègre C.J. (2002) Boron isotope systematics in large rivers: implications for the marine boron budget and paleo-pH reconstruction over the Cenozoic. Chemical Geology, 190, 123– 140.

Lemarchand D., Jacobson A.D., Cividini D., Chabaux F. (2015) The major ion, $^{87}Sr/^{86}Sr$, and $\delta^{11}B$ geochemistry of groundwater in the Wyodak-Anderson coal bed aquifer (Powder River Basin, Wyoming, USA). Comptus Rendus Geoscience, 347, 348–357,

Lemcke K., Engelhardt W., Füchtbauer H. (1953) Geologische und sedimentpetrographische Untersuchungen im Westteil der ungefalteten Molasse des süddeutschen Alpenvorlandes. Beihefte zum Geologischen Jahrbuch, 11, 1–110.

Lemcke K. (1973) Zur nachpermischen Geschichte des nördlichen Alpenvorlandes. Geologica Bavarica, 69, 5–48.

Lemcke K. (1988) Geologie von Bayern. Bd.1. Das bayerische Alpenvorland vor der Eiszeit. Schweizerbart'sche Verlagsbuchhandlung, Stuttgart, 175 p.

Leone G., Reyes E., Cortecci G., Pochini A., Linares J. (1983) Genesis of bentonites from Cabo de Gata, Almeria, Spain: a stable isotope study. Clay Minerals, 18, 227–238.

Levinson A.A. (1980) Introduction to Exploration Geochemistry, 2nd edition. Applied Publishing Ltd., Wilmette, Illinois. 924 p.

Liakopoulos A., Katerinopoulos A., Markopoulos Th., Boulegue J. (1991) A mineralogical petrographic and geochemical study of samples from wells in the geothermal field of Milos Island (Greece). Geothermics, 20, 237–256.

Lico M.S., Seiler R.L. (1994) Ground-Water Quality and Geochemistry, Carson Desert, Western Nevada. U.S. Geological Survey, Open-File Report 94-31, 91 p.

Linares J. (1963) Las bentonitas de Cabo de Gata. Estudio mineralógico y técnico. Ph.D. thesis, Universidad Granada, Spain, 169 p.

Linares J., Caballero E., Reyes E., Huertas F. (1987) Trace elements mobility in bentonite formation. Pp. 230–250 in: The Practical Applications of Trace Elements and Isotopes to Enviromental Biogeochemistry and Mineral Resources Evaluation (Hurst R.W., Davis T.E., Augustithis S.S., editors). Theophrastus Publications, Athens.

Lippolt H.J., Gentner W., Wimmenauer W. (1963) Altersbestimmung nach der Kalium-Argon-Methode an tertiären Eruptivgesteinen Südwestdeutschlands. Jahresheft des Geologischen Landesamtes in Baden-Württemberg, 6, 507–538.

Liu Y., Tossell J.A. (2005) Ab initio molecular orbital calculations for boron isotope fractionations on boric acids and borates. Geochimica et Cosmochimica Acta, 69, 16, 3995–4006.

Lohmann K. C. (1988) Geochemical patterns of meteoric diagenetic systems and their application to studies of paleokarst. Pp. 58–80 in: Paleokarst (James N.P, Choquette P.W., editors). Springer–Verlag, New York, United States.

Lombardi B., Baschini M., Torres-Sánchez R.M. (2002) Characterization of montmorillonites from bentonite deposits of North Patagonia, Argentina: physicochemical and structural parameter correlation. Journal of the Argentine Chemical Society, 90, 87–99.

Lorens R.B. (1981) Sr, Cd, Mn and Co distribution coefficients in calcite as a function of calcite precipitation rate. Geochimica et Cosmochimica Acta, 45, 553–561.

Ludwig K.R. (2008) User's manual for Isoplot 3.70. A geochronological toolkit for Microsoft Excel. Berkeley Geochronology Center Special Publication, 4, 76 p.

Luft E. (1983) Zur Bildung der Moldavite beim Ries-Impakt aus tertiären Sedimente. Ferdinand Encke Verlag, Stuttgart, 202 p.

Lukács R., Harangi S., Bachmann O., Guillong M., Danišik M., Buret Y., v. Quadt A., Dunkl I., Fodor L., Sliwinski J., Soós I., Szepesi J. (2015) Zircon geochronology and geochemistry to constrain the youngest events and magma evolution of the Mid-Miocene ignimbrite flare-up in the Pannonian Basin, eastern central Europe. Contributions to Mineralogy and Petrology, 170:52.

Lumsden D.N., Chimahusky J.S. (1980) Relationship between dolomite nonstoichiometry and carbonate facies parameters, Pp. 123–137 in: Concepts and Models of Dolomitization (Zenger D.H., Dunham J.B., Ethington R.L., editors). Society of Economic Palaeontologists and Mineralogists, Special Publication No. 28.

Luttig G.W., Wiedenbein F.W. (1990) Bentonite and related deposits–world economic significance and situation in Greece. Bulletin of the Geological Society of Greece, 25, 101–111.

Maccioni L., Marchi M., Padalino G., Palomba M., Sistu G. (1995) Bentonite occurrences in the Tertiary volcanic rocks in Central Sardinia, Italy. Exploration and Mining Geology, 4, 74– 79.

Maccioni L., Marchi M., Padalino G., Palomba M., Sistu G., (1998) Occurrence of bentonite in Sardinia: a synthesis about occurrences, geology, mineralogy and properties. Bollettino della Societa Geologica Italiana, 117, 629–642.

Machel H.-G., Mountjoy E.W. (1986) Chemistry and environments of dolomitization – a reappraisal. Earth-Science Reviews, 23, 175–222.

Manuilova N.S., Sukhanova S.M., Varlomov V.P. (1965) Swelling of bentonites. Nauchn. Issled. Mekh. Stroit. Mater. Konstr, 1965(2), 68–85.

Martínez R.N., Colombi C.E. (2011) Evolución litofacial y edad de La Formación Cañón del Colorado (Jurásico Inferior), Precordillera oriental, San Juan. Revista de la Asociación Geológica Argentina, 68, 96 – 108.

Martínez R.N. (1999) The first record of dinosaur-bearing continental strata of Lower Jurassic age in South America. 14° Congreso Geológico Argentino and 2nd Symposium Jurassic of South America, Actas I: 50, Salta.

Martín-Vivaldi J.L., Linares J. (1968) Las bentonitas de Cabo de Gata. I. Yacimientos de Los Trancos y Majada de las Vacas. Boletin Geológico Minero, 79, 513–23.

Maughan E.K. (1966) Environment of deposition of Permian salt in the Williston and Alliance Basins: Cleveland, Ohio. Northern Ohio Geological Society, 2nd Symposium on Salt, 1, 35–47.

Maurer H., Buchner E. (2007) Identification of fluvial architectural elements of meandering systems by paleosols (Upper Freshwater Molasse, North Alpine Foreland Basin, SW-Germany). Zeitschrift der deutschen Gesellschaft für Geowissenschaften, 158, 271–285.

Maurer D.K., Welch A.H. (2001) Hydrogeology and Geochemistry of the Fallen Basalt and Adjacent Aquifers, and Potential Sources of Basalt Recharge, in Churchill County, Nevada. USGS Water-Resources Investigations Report 01-4130, Carson City, Nevada, 72 p.

McArthur J.M., Howarth R. J., Bailey T. R. (2001) Strontium isotope stratigraphy: LOWESS Version 3: Best fit to the marine Sr-isotope curve for 0–509 Ma and accompanying look-up table for deriving numerical age. The Journal of Geology, 109, 155–170.

Menegatti A.P., Früh-Green G.L., Stille P. (1999) Removal of organic matter by disodium peroxodisulphate: effects on mineral structure, chemical composition and physicochemical properties of some clay minerals. Clay Minerals, 34, 247 –257.

Möller P., Morteani G., Dulski P. (1984) The origin of the calcites from the Pb–Zn veins in the Harz Mountains, Federal Republic of Germany. Chemical Geology, 45, 91–112.

Moore D.M., Reynolds R.C. (1997) X-Ray diffraction and the identification and analysis of clay minerals. Oxford University Press, Oxford, 378 p.

Moreira M. (1984) Mineralogical and physico-chemical investigation of a montmorillonite clay from Bahia, Brazil. Master thesis, University of Hull, UK, 95 p.

Morell I., Pulido-Bosch A., Daniele L., Cruz J.V. (2008) Chemical and isotopic assessment in volcanic thermal waters: cases of Ischia (Italy) and São Miguel (Azores, Portugal). Hydrological processes, 22, 4386-4399.

Morrison R.B. (1964) Lake Lahontan: Geology of Southern Carson Desert. Geological Survey Professional Paper 401, 156 p.

Muehlenbach K. (1979) The alteration and ageing of the basaltic layer of the sea-floor: oxygen isotope evidence from DSDP/IPOD 51, 52 and 53. Initial Reports of the Deep Sea Drilling Project, 51-53, Part II, 1159-1167.

Müller G., Irion G., Förstner U. (1972) Formation and diagenesis of inorganic Ca–Mg carbonates in the lacustrine environment. Naturwissenschaften, 59, 158–164.

Murray H.H. (2007) Applied Clay Mineralogy. Developments in Clay Science, 2, Elsevier, Amsterdam.

Muttik N., Kirsimäe K., Newsom H.E., Williams L.B. (2011) Boron isotope composition of secondary smectite in suevites at the Ries crater, Germany: Boron fractionation in weathering and hydrothermal processes. Earth and Planetary Science Letters, 310, 244-251.

Naden J., Kilias S.P., Darbyshire D.P.F. (2005) Active geothermal systems with entrained seawater as modern analogs for transitional volcanic-hosted massive sulfide and continental magmato-hydrothermal mineralization: The example of Milos Island, Greece. Geology, 33, 541–544.

Nahon D., Colin F., Tardy Y. (1982) Formation and distribution of Mg, Fe, Mn-smectites in the first stages of lateritic weathering of forsterite and tephroite. Clay Minerals, 17, 339–348.

Naish T.R., Nelson C.S., Hodder A.P.W. (1993) Evolution of Holocene sedimentary bentonite in a shallow-marine embayment, Firth of Thames, New Zealand. Marine Geology, 109, 267–278.

Nance W.B., Taylor S.R. (1976) Rare earth element patterns and crustal evolution, I, Australian post-Archean sedimentary rocks. Geochimica et Cosmochimica Acta, 40, 1539–1551.

Négrel Ph., Millot R., Guerrot C., Petelet-Giraud E., Brenot A., Malcuit E. (2012) Heterogeneities and interconnections in groundwaters: Coupled B, Li and stable-isotope variations in a large aquifer system (Eocene Sand aquifer, Southwestern France). Chemical Geology 296-297, 83–95.

Nelson C.S., Smith A.M. (1996) Stable oxygen and carbon isotopes composition fields for skeletal and diagenetic components in New Zealand Cenozoic nontropical carbonate sediments and limestones: A synthesis and review. New Zealand Journal of Geology and Geophysics, 39, 93–107.

Nettleton W.D., Olson C.G., Wysocki D.A. (2000) Paleosol classification: Problems and solutions. Catena, 41, 61–92.

Norton J. J. (1965) Lithium-bearing bentonite deposit, Yavapai County, Arizona. Pp. 163–16 in: 6U.S. Geological Survey Professional Papers, 525-D.

Odom I.E. (1984) Smectite clay Minerals: Properties and Uses. Philosophical Transactions of the Royal Society of London. Series A, Mathematical and Physical Sciences, 311, 391–409.

Oeltzschner H. (1965) Geologische und sedimentpetrographische Untersuchungen auf Blatt Vilsbiburg 75406 Niederbayern. Diploma thesis, Ludwig-Maximilians-Universität München, Germany, 101 p.

Pacton M., Gorin G., Vasconcelos C., Gautschi H.P., Barbarand J. (2010) Structural arrangement of sedimentary organic matter: nanometer-scale spheroids as evidence of a microbial signature in early diagenetic processes. Journal of Sedimentary Research, 80, 919–932.

Palmer M.R. (1991) Boron isotope systematics of hydrothermal fluids and tourmalines: a synthesis. Chemical Geology: Isotope Geosciences Section, 94, 111–121.

Palmer M.R., London D., Morgan G.B., Babb H.A. (1992) Experimental determination of fractionation of $^{11}B/^{10}B$ between tourmaline and aqueous vapour: a temperature and pressure dependent isotopic system. Chemical Geology, 101, 123–129.

Palmer M.R., Spivack A.J. Edmond J.M. (1987) Temperature and pH controls over isotopic fractionation during absorption of boron marine clay. Geochimica et Cosmochimica Acta, 51, 2319–2323.

Palmer M.R., Sturchio N.C. (1990) The boron isotope systematics of the Yellowstone National Park (Wyoming) hydrothermal system: A reconnaissance. Geochimica et Cosmochimica Acta, 54, 2319–2323.

Palmer M.R., Swihart G.H. (1996) Boron isotope geochemistry: an overview. Pp. 709–744 in: Boron: Mineralogy, Petrology, and Geochemistry (Anovitz, L.M., Grew E.S, editors), Reviews in Mineralogy, 33, Mineralogical Society of America, Chantilly, Virginia, USA.

Palomba M., Padalino G., Marchi M. (2006) Industrial mineral occurrences associated with Cenozoic volcanic rocks of Sardinia (Italy): Geological, mineralogical, geochemical features and genetic implications. Ore Geology Reviews, 29, 118– 145.

Paris G., Bartolini A., Donnadieu Y., Beaumont V., Gaillardet J. (2010) Investigating boron isotopes in a middle Jurassic micritic sequence: Primary vs. diagenetic signal. Chemical Geology, 275, 117–126.

Passey B.H., Levin N.E., Cerling T.E., Brown F.H., Eiler J.M. (2010) High-temperature environments of human evolution in East Africa based on bond-ordering in palaeosol carbonates. Proceedings of the National Academy of Science, 107, 11245–11249.

Patel P.K. (1987) Lateritization and bentonitization of basalt in Kutch, Gujarat State, India. Sedimentary Geology, 53, 327–346.

Pennisi M., Bianchini G., Kloppmann W., Muti A. (2009) Chemical and isotopic (B, Sr) composition of alluvial sediments as archive of a past hydrothermal outflow. Chemical Geology 266, 114–125.

Pennisi M., Leeman W.P., Tonarini S., Pennisi A., Nabelek P. (2000) Boron, Sr, O, and H isotope geochemistry of groundwaters from Mt. Etna (Sicily)–hydrologic implications. Geochimica et Cosmchimica Acta, 64, 961–974.

Perry E.A., Jr. (1972) Diagenesis and the validity of the boron paleosalinity technique. American Journal of Science, 272, 150–160.

Perry W.J., Jr., Rice D.D., Maughan E.K. (1983) Petroleum Potential of Wilderness Lands in Montana. Pp. G1–G23 in: Petroleum Potential of Wilderness Lands in Montana (Perry W.J., Rice D.D., Maughan E.K., editors), Geological Survey Circular 902-G.

Petrosov I.Kh. (1970) Relative characteristics of conditions of the formation of hydrothermal and diagenetic bentonitic clays as exemplified by the Sarigyukh-Noyemberyan deposits in the Armenian SSR. Investigations and use of clays and clay minerals, Institute of Sciences, Alma-Ata.

Petrosov I.L.M., Tsameryan P.P. (1964) Petrography and mineralogy of bentonite clays in the Noyemberyan deposit. Research of the Academy of Sciences of the Armenian SSR, 22(4), 50–59.

Pichavant M., Valencia Herrera J., Boulmier S., Briqueu L., Joron J.-L., Juteau M., Marin L., Michard A., Sheppard S.M.F., Treuil M., Vernet M. (1987) The Macusani glasses, SE Peru: Evidence of chemical fractionation in peraluminous magmas. Pp. 359–373 in: Magmatic processes: Geochemical principles (Mysen B.O., editor), Geochemical Society Special Publication, 1.

Pietracaprina A., Novelli G., Rinaldi A. (1987) A New Bentonite Deposit in Sardinia. Applied Clay Science, 2, 167–174.

Pin C., Basin C. (1992) Evaluation of a strontium-specific extraction chromatographic method for isotopic analysis in geological materials. Analytica Chimica Acta, 269, 249–255.

Post J.L. (1996) Sodium bentonite from western Nevada. Preprints of the Society for Mining, Metallurgy & Exploration, 23, 1–5.

Post J.L. (1997) Sodium bentonite from western Nevada. Transactions of the Society for Mining, Metallurgy & Exploration, 300, 149–151.

Potter P.E., Shimp N.F., Witters J. (1963) Trace elements in marine and fresh-water argillaceous sediments. Geochimica et Cosmochimica Acta, 5, 669–694.

Quade J., Eiler J., Daëron M., Achyuthan H. (2013) The clumped isotope geothermometer in soil and paleosol carbonate. Geochimica et Cosmochimica Acta, 105, 92–107.

Rahn M.K., Selbekk R. (2007) Absolute dating of the youngest sediments of the Swiss Molasse basin by apatite fission analysis. Swiss Journal of Geosciences, 100, 371–381.

Rateyev M.A. (1968) Authigenic clay formation in volcanic-sedimentary formations. Research at the Academy of Sciences, Kazakh SSR, 1968: 88–94.

Rateyev M.A., Gradusov B.P. (1970) Structural phases in transformation of andesite-trachyte tuffs of Askana in zones of hydrothermal sulphide mineralization. Litologiya i poleznye iskopaemye, 1.

Rateyev M.A., Gradusov B.P., Il'inskaya M.N. (1975) Hydrothermal argillization of upper Santonian volcanogenic rocks and its role in formation of bentonites in the Sarigyukh deposit, Armenian SSR, International Geology Review, 17, 495-508.

Retallack G.J. (1988) Field recognition of palaeosols. Pp. 1–20 in: Paleosols and Weathering Through Geologic Time: Principles and Applications. (Reinhardt J., Sigleo W.R., editors), Geological Society of America Special Papers, 216.

Reyes A.G., Trompetter W.J. (2012) Hydrothermal water–rock interaction and the redistribution of Li, B and Cl in the Taupo Volcanic Zone, New Zealand. Chemical Geology, 314-317, 96–112.

Reyes E., Huertas F., Linares J. (1979) Mineralogía y geoquímica de las bentonitas de la zona norte de Cabo de Gata (Almería). V. Área de Los Trancos. Estudios Geológicos, 35, 363–370.

Rice D.D. (1981) Subsurface cross section from south-eastern Alberta, Canada, to Bowdoin Dome area, north-central Montana, showing correlation of Cretaceous rocks and shallow, gas-productive zones in low-permeability reservoirs: U.S. Geological Survey Oil and Gas Investigations Chart OC-112.

Rimstidt J.D., Balog A., Webb J. (1998) Distribution of trace elements between carbonate minerals and aqueous solutions. Geochimica et Cosmochimica Acta, 62, 1851–1863.

Roberts J. A., Bennett P.C., González L.A., Macpherson G.L., Milliken K.L. (2004) Microbial precipitation of dolomite in methanogenic groundwater. Geology, 32, 277–280.

Robertson J.D., Dyar M.D. (1996) Nuclear methods for analysis of boron in minerals. Pp. 805–820 in: Boron: Mineralogy, Petrology, and Geochemistry (Anovitz, L.M., Grew E.S, editors), Reviews in Mineralogy, 33, Mineralogical Society of America, Chantilly, Virginia, USA.

Robertson R.H.S. (1986) Fuller's Earth, a History. Volturna Press, Hythe, Kent, UK, 421 p.

Rocholl A., Boehme M., Guenther D., Höfer H., Ulbig A. (2008) Prevailing stratospheric easterly wind direction in the Paratethys during the Lower Badenian: Ar-Ar- and Nd-isotopic evidence from rhyolitic ash layers in the Upper Freshwater Molasse, S-Germany. Geophysical Research Abstracts, 10, EGU2008–A-08747; Wien.

Rocholl A., Ovtcharova M., Schaltegger U., Wijbrans J., Pohl J., Harzhauser M., Prieto J., Ulbig A., Boehme M. (2011) A precise and accurate „astronomical" age of the Ries impact crater, Germany: A cautious note on argon dating of impact material. Geophysical Research Abstracts, 13, EGU2011–13322-7; Wien.

Rocholl A., Schaltegger U., Gilg H.A., Wijbrans J., Böhme M. (2017) The age of volcanic tuffs from the Upper Freshwater Molasse (North Alpine Foreland Basin) and their possible use for tephrostratigraphic correlations across Europe for the Middle Miocene. International Journal of Earth Sciences, doi.org/10.1007/s00531-017-1499-0.

Rodríguez M.F., Leanza H.L., Aranguren M.S. (2007) Hoja Geológica 3969-II Neuquén, 1:250000, Provincias del Neuquén, Río Negro y La Pampa. Servicio Geológico Minero Argentino, Instituto de Geología y Recursos Minerales, Boletin 370, Argentina, Buenos Aires, 165 p.

Romanek C.S., Grossmann E.L., Morse J.W. (1992) Carbon isotopic fractionation in synthetic aragonite and calcite: Effects of temperature and precipitation rate. Geochimica et Cosmochimica Acta, 56, 419–430.

Rosenbaum, J., Sheppard, S.M. (1986) An isotopic study of siderites, dolomites and ankerites at high temperatures. Geochimica et Cosmochimica Acta, 50, 1147–1150.

Ross C.S., Shannon E.V. (1926) Minerals of bentonite and related clays and their physical properties. Journal of the American Ceramic Society, 9, 77–96.

Royal J., Branch T. (2014) NI43-101 Independent Geological Report Technical Report prepared for Tigris Resources Ltd. Multiple Exploration Projects in Turkey, CSA Global, 172 p.

Royal J., White G., Branch T. (2015) NI43-101 Independent Geological Report on the Pertek, Uğur Tepe and Gömeç Exploration Projects in Turkey prepared for Tigris Resources Ltd. and Kirkcaldy Capital Corp. CSA Global, 173 p.

Ryan J.G., Langmuir C.H. (1963) The systematics of boron abundances in young volcanic rocks. Geochimica et Cosmochimica Acta, 57, 1489–1498.

Sánchez-Román M., Romanek C.S., Fernández-Remolar D.C., Sánchez-Navas A., McKenzie J.A., Pibernat R.A., Vasconcelos C. (2011) Aerobic biomineralization of Mg-rich carbonates: Implications for natural environments. Chemical Geology, 281, 143–150.

Savci G. (1983) Structure and tectonics of the Keban metamorphics in the northern margin of the Biltis suture zone, South-Eastern Turkey. Master thesis, State University of New York – Albany, United States of America, 201 p.

Savin S.M., Epstein S. (1970) The oxygen and hydrogen isotope geochemistry of clay minerals. Geochimica et Cosmochimica Acta, 34, 25 –42.

Sawatzki G., Schreiner A. (1991) Bentonite und Deckentuffe am Hohenstoffeln/Hegau. Jahreshefte des Geologischen Landesamts Baden-Württemberg, 33, 59–73.

Sayles F.L., Ku T.L., Bowker P.C. (1975) Chemistry of ferromanganoan sediment of the Bauer Deep. Geological Society of America Bulletin, 86, 1423–1431.

Sayles F.L., Mangelsdorf P.C. Jr. (1977) The equilibration of clay minerals with seawater: exchange reactions. Geochimica et Cosmochimica Acta, 41, 951–960.

Sayles F.L., Mangelsdorf P.C. Jr. (1979) Cation-exchange characteristics of Amazon River suspended sediment and its reaction with seawater. Geochimica et Cosmochimica Acta, 43, 767–779.

Scheuenpflug L. (1980) Neue Funde ortsfremder Weißjuragesteine in Horizonten der südbayerischen miozänen Oberen Süßwassermolasse um Augsburg. Jahresberichte und Mitteilungen des Oberrheinischen Geologischen Vereins, N.F., 62, 131–142.

Schieber J., Arnott H.J. (2003) Nanobacteria as a by-product of enzyme-driven tissue decay. Geology, 31, 717–720.

Schmid W. (2002) Ablagerungsmilieu, Verwitterung und Paläoböden feinklastischer Sedimente der

Oberen Süßwassermolasse Bayerns. Doctoral thesis, Ludwig-Maximilians-Universität, Germany, 185 p.

Schmidt R.G., Pecora W.T., Hearn B.C. (1964) Geology of the Cleveland Quadrangle Bearpaw Mountains Blaine County, Montana. Contributions to General Geology (Stieff L. R., Stern T. W., Eicher R. N., editors), Geological Survey Bulletin 1141-P, 26p.

Schreiner A. (1976) Hegau und westlicher Bodensee. Sammlung Geologischer Führer 62, Gebrüder Borntraeger, Stuttgart, 83 p.

Schroll E., Wieden P. (1960) Eine rezente Bildung von Dolomit im Schlamm des Neusiedler Sees. Tschermaks Mineralogische und Petrographische Mitteilungen, 7, 286–289.

Schultz L.G., Tourtelot H.A., Gill J.R., Boerngen J.G. (1980) Composition and Properties of the Pierre Shale and Equivalent Rocks, Northern Great Plains Region. Geological Survey Professional Paper 1064-B, 114 p.

Schulz H. (1926) Morphologie und randliche Bedeckung des Bayerischen Waldes in ihrer Beziehung zum Vorland. Neues Jahrbuch für Mineralogie, 54, 289–346.

Schwarcz H.P., Agyei E.K., McMullen C.C. (1969) Boron isotopic fractionation during clay adsorption from seawater. Earth and Planetary Science Letters, 6, 1–5.

Schwertmann, U. (1964) Differenzierung der Eisenoxide des Bodens durch Extraktion mit Ammoniumoxalat-Lösung. Zeitschrift für Pflanzenernährung, Düngung, Bodenkunde, 105, 194–202.

Sharifabadi M.A. (1992) Mineralogy, geochemistry and genesis of lateritic rocks of mainland Gujarat. Proceedings of the Indian National Science Academy, 58, 43–54.

Shaw D.M., Bugry R. (1966) A Review of Boron Sedimentary Geochemistry in Relation to New Analyses of Some North American Shales. Canadian Journal of Earth Sciences, 3, 49–63.

Shaw D.M., Sturchio N.C. (1992) Boron-lithium relationships in rhyolites and associated thermal waters of young silicic calderas, with comments on incompatible element behaviour. Geochimica et Cosmochimica Acta, 56, 3723–3731.

Sheppard S.M.F., Schwarcz H.P. (1970) Fractionation of carbon and oxygen isotopes and magnesium between coexisting metamorphic calcite and dolomite. Contributions to Mineralogy and Petrology, 26, 161–198.

Shoval S. (2004) Deposition of volcanogenic smectite along the southeastern Neo-Tethys margin during the oceanic convergence stage. Applied Clay Science, 24, 299–311.

Siddiquie N.N., Bahl D.P. (1965) Geology of the bentonite deposits of the Barmer District, Rajasthan. Memoirs of the Geological Survey of India, 96, 36 p.

Siebel W., Reitter E., Wenzel T., Blaha U. (2005) Sr isotope systematics of K-feldspars in plutonic rocks revealed by the Rb–Sr microdrilling technique. Chemical Geology, 222, 183–199.

Siegl W. (1948) Glastuff in der oberbayerischen Molasse und seine Beziehung zur Bleicherde. Neues Jahrbuch für Mineralogie, Monatshefte 1945–48 (5–8). Abt. A, 77–82.

Simon L., Lécuyer C., Maréchal C., Coltice, N. (2006) Modelling the geochemical cycle of boron: Implications for the long-term $\delta^{11}B$ evolution of seawater and oceanic crust. Chemical Geology, 225, 61– 76.

Slaughter M., Earley J.W. (1965) Mineralogy and geological significance of the Mowry bentonites, Wyoming. Pp. 1–95: Mineralogy and geological significance of the Mowry bentonites, Wyoming. (Slaughter M., Earley J.W., editors), Geological Society of America Special Papers, 83.

Smedes H.W. (1966) Geology and Igneous Petrology: of the Northern Elkhorn Mountains Jefferson and Broadwater Counties, Montana. Geological Survey Professional Paper 510, 116 p.

Smellie J. (2001) Wyoming Bentonites Evidence from the geological record to evaluate the suitability of bentonite as a buffer material during the long-term underground containment of radioactive wastes. Technical Report TR-01-26, Swedish Nuclear Fuel and Waste Management Co., Stockholm, Sweden, 24 p.

Smith H.J., Spivack A.J., Staudigel H., Hart S.R. (1995) The boron isotopic composition of altered oceanic crust. Chemical Geology, 126, 119–135.

Southam G., Donald R. (1999) A structural comparison of bacterial microfossils vs. ‘nanobacteria' and nanofossils. Earth-Science Reviews, 48, 251–264.

Spivack A.J. (1986) Boron isotope geochemistry. Ph.D. thesis, Massachusetts Institute of Technology, Cambridge, United States of America, 184 p.

Spivack A.J., Edmond J.M. (1987) Boron isotope exchange between seawater and oceanic crust. Geochimica et Cosmochimica Acta, 51, 1033–1043.

Spivack A. J., Palmer M. R., and Edmond J. M. (1987) The sedimentary cycle of the boron isotopes. Geochimica et Cosmochimica Acta, 51, 1939–1949.

Środoń J. (1980) Precise identification of illite/smectite interstratifications by X-ray powder diffraction. Clays and Clay Minerals, 28, 401–411.

Stanjek H., Marchel C. (2008) Linking the redox cycles of Fe oxides and Fe-rich clay minerals: an example from a palaeosol of the Upper Freshwater Molasse. Clay Minerals, 43, 69–82.

Stichler W. (1997) Isotopengehalte in Tiefengrundwässern aus Erdöl- und Erdgasbohrungen um süddeutschen Molassebecken. Beiträge zur Hydrogeologie, 48, 81–88.

Storzer D., Gentner W. (1970) Spaltspuren – Alter von Riesgläsern, Moldaviten und Bentoniten. Jahresberichte und Mitteilungen des Oberrheinischen Geologischen Vereins, N.F., 52, 97–111.

Swihart G.H., Moore P.B., Callis E.L. (1986) Boron isotopic composition of marine and non-marine evaporite borates. Geochimica et Cosmochimica Acta, 50, 1297–1301.

Taieb R. (1990) Les isotopes de l'hydrogene, du carbone et de l'oxygene dans les ss argileux et les eaux de formation. Doctoral thesis, Institut National Polytechnique de Lorraine, Nancy, France.

Talbot M.R. (1990) A review of the palaeohydrological interpretation of carbon and oxygen isotopic ratios in primary lacustrine carbonates. Chemical Geology, Isotope Geoscience Section, 80, 261–279.

Tan S.S., Kennedy M.P. (2002) Geological map of the Otay Mesa 7.5' quadrangle San Diegeo County, California: a digital database, 1:24000. Digital Preparation by Corriea K. and Jorgensen S., Department of Conservation, California Geological Survey.

Tang Y. (2005) Non-metallic deposits of Xinjiang, China [Zhongguo Xinjiang Fei Jinshu Kuangchuang]. Geological Publishing House, Beijing, 289 p.

Tardy Y. (1997) Petrology of Laterites and Tropical Soils. 1st edition. A.A. Balkema, Rotterdam, 408 p.

Tardy Y., Kobilsek B., Paquet H. (1991) Mineralogical composition and geographical distribution of African and Brazilian periatlantic laterites. The influence of continental drift and tropical paleoclimates during the past 150 million years and implications for India and Australia. Journal of African Earth Sciences, 12, 283–295.

Taucher P., Bartos T.T., Clarey K.E., Quillinan S.A., Hallberg L.L., Clark M.L., Thompson M, Gribb N., Worman B., Gracias T. (2012) Wind/Bighorn River Basin Water Plan Update Groundwater Study Level 1 (2008–2011). Available Groundwater Determination Technical Memorandum (Copeland D., editor). Wyoming State Geological Survey, 381 p.

Thüns N. (2012) Die Bentonite des Neuwieder Beckens und des Westerwaldes. Bachelor thesis, Technische Universität München, Germany, 40 p.

Timofeeff M.N., Lowenstein T.K., Martins da Silva M.A., Harris N.B. (2006) Secular variation in the major-ion chemistry of seawater: Evidence from fluid inclusions in Cretaceous halites. Geochimica et Cosmochimica Acta, 70, 1977–1994.

Tomascak, P.B. (2004) Developments in the understanding and application of lithium isotopes in the Earth and planetary sciences. Pp. 153–195 in: Geochemistry of Non-Traditional Stable Isotopes (Johnson C.M., Beard B.L., Albarede F., editors), Reviews in Mineralogy, 33, Mineralogical Society of America, Chantilly, Virginia, USA.

Tompa É., Nyirő-Kósa I., Rostási Á., Cserny T., Pósfai M. (2014) Distribution and composition of Mg-calcite and dolomite in the water and sediments of Lake Balaton. Central European Geology, 57, 113–136.

Tonarini S., Pennisi M., Leeman W. P. (1997) Precise boron isotopic analysis of complex silicate (rock) samples using alkali carbonate fusion and ion-exchange separation. Chemical Geology, 142, 129–137.

Tourtelot H.A. (1962) Preliminary Investigation of the Geologic Setting and Chemical Composition of the Pierre Shale Great Plains Region. Geological Survey Professional Paper 390, 74 p.

Tourtelot H. A., Schultz L. G., Huffman C.Jr. (1961) Boron in bentonite and shale from the Pierre Shale, South Dakota, Wyoming, and Montana. Short papers in the geologic and hydrologic sciences, U.S. Geological Survey Professional Papers 424-C, C288-C292.

Trescases J.J., Melfi A.J., de Oliveira S.M.B. (1981) Nickeliferous laterites of Brazil. Mineralium Deposita, 27, 137–146.

Tucker M.E., Wright V.P. (1990) Carbonate Sedimentology. Blackwell Science, Oxford. Pp. 168–172.

Tütken T., Vennemann T.W. (2009) Stable isotope ecology of Miocene large mammals from Sandelzhausen, southern Germany. Paläontologische Zeitschrift, 83, 207–226.

Tütken T., Vennemann T.W., Janz H., Heinzmann E.P.J. (2006) Palaeoenvironment and palaeoclimate of the Middle Miocene lake in the Steinheim basin, SW Germany: A reconstruction from C, O, and Sr isotopes of fossil remains. Palaeogeography, Palaeoclimatology, Palaeoecology, 241, 457–491.

Ufer K., Stanjek H., Roth G., Dohrmann R., Kleeberg R., Kaufhold S. (2008) Quantitative phase analysis of bentonites by the Rietveld method. Clays and Clay Minerals, 56, 272–282.

Ulbig A. (1994) Vergleichende Untersuchungen an Bentoniten, Tuffen und sandig-tonigen Einschaltungen in den Bentonitlagerstätten der Oberen Süßwassermolasse. Doctoral thesis, Technische Universität München, Germany, 245 p.

Ulbig A. (1999) Untersuchungen zur Entstehung der Bentonite in der bayerischen Oberen Süßwassermolasse. Neues Jahrbuch Geologisch-Paläontologische Abhandlungen, 214, 497–508.

Underwood M.B., Pickering K., Gieskes J.M., Kastner M., Orr, R. (1993) Sediment geochemistry, clay mineralogy, and diagenesis: a synthesis of data from Leg 131, Nankai Trough. Proceedings of the Ocean Drilling Program, Scientific Results, 13, 343–363.

Unger H.J. (1981) Bemerkungen zur stratigraphischen Stellung, der Lagerung und Genese der Bentonitlagerstätten in Niederbayern. Verhandlungen der Geologischen Bundesanstalt, Wien, 1981/2, 193–203.

Unger H.J. (1983) Geologische Karte von Bayern 1:50000 – Erläuterungen zum Blatt Nr. L 7342 Landau an der Isar. Bayerisches Geologisches Landesamt, München, 141 p.

Unger H.J. (1989) Die Lithozonen der Oberen Süßwassermolasse Südostbayerns und ihre vermutlichen zeitlichen Äquivalente gegen Westen und Osten. Geologica Bavarica, 94, 195–237.

Unger H.J. (1991) Geologische Karte von Bayern 1:50000 – Erläuterungen zum Blatt Nr. L 7538 Landshut. Bayerisches Geologisches Landesamt, München, 213 p.

Unger H.J. (1996) Östliche Vorlandmolasse und Braunkohlentertiär i. w. S., Pp. 168–185 in: Geologische Karte von Bayern 1:500000 (Freudenbacher W., Schwerd K., editors), Bayerisches Geologisches Landesamt, München, Germany.

Unger H. J. (1999) Die tektonischen Strukturen der bayerischen Ostmolasse. Documenta Naturae, 125, 1–16.

Unger H.J., Fiest W., Niemeyer A. (1990) Die Bentonite der ostbayerischen Molasse und ihre Beziehungen zu den Vulkaniten des Pannonischen Beckens. Geologisches Jahrbuch, D96, 55–66.

Unger H.J., Niemeyer A. (1985a) Die Bentonite in Ostniederbayern – Entstehung, Lagerung, Verbreitung. Geologisches Jahrbuch, D71, 3–58.

Unger H.J., Niemeyer A. (1985b) Bentonitlagerstätten zwischen Mainburg und Landshut und ihre zeitliche Einstufung. Geologisches Jahrbuch, D71, 59–93.

Vahrenkamp V. C., Swart P. K. (1990) New distribution coefficient for the incorporation of strontium into dolomite and its implications for the formation of ancient dolomites. Geology, 18, 387–391.

Vallés J.M., Burlando L., Chiachiarini P., Giaveno M., Impiccini A. (1989) Geological and genetical features of the Upper Cretaceous bentonite deposit from North Patagonia. PICG, 24, Cretácico América Latina, Buenos Aires, 79-98.

Vallés J.M., Giusiano A. (2001) Bentonitic and kaolin deposits in extra-Andean Patagonia and soils in the Andean region. Post-conference field excursion July 29-August 1st, 2001. The 12th International clay conference, Universida Nacional de sur Bahia Blanca, Argentina, 59 p.

Valsami-Jones E., Baltatzis E., Bailey E.H., Boyce A.J., Alexander J.L., Magganas A., Anderson L., Waldron S., Ragnarsdóttir K.V. (2005) The geochemistry of fluids from an active shallow submarine hydrothermal system: Milos island, Hellenic Volcanic Arc. Journal of Volcanology and Geothermal Research, 148, 130–151.

van Lith Y., Warthmann R., Vasconcelos C., McKenzie J.A. (2003) Sulphate-reducing bacteria induce low-temperature Ca-dolomite and high Mg-calcite formation. Geobiology, 1, 71–79.

Varnavas S.P., Cronan D.S. (2005) Submarine hydrothermal activity off Santorini and Milos in the Central Hellenic Volcanic Arc: A synthesis. Chemical Geology, 224, 40– 54.

Vasconcelos C., McKenzie J.A., Warthmann R., Bernasconi S.M. (2005) Calibration of the $\delta^{18}O$ paleothermometer for dolomite precipitated in microbial cultures and natural environments. Geology, 33, 317–320.

Vengosh A., Chivas A.R., McCulloch M.T., Starinsky A., Kolodny Y. (1991) Boron isotope geochemistry of Australian salt lakes. Geochimica et Cosmochimica Acta, 55, 2591–2606.

Vengosh A., Chivas A.R., Starinsky A., Kolodny Y., Zhang B.Z., Zhang P.X. (1995) Chemical and boron isotope compositions of non-marine brine from the Qaidam Basin, Qinghai, China. Chemical Geology 120, 135–154.

Vengosh A., Hendry M.J. (2001) Chloride-bromide-$\delta^{11}B$ systematics of a clay-rich aquitard system. Water Resources Research, 37, 1437–1444.

Vengosh A., Starinsky A., Kolodny Y., Chivas A. R., Raab M. (1992) Boron isotope variations during fractional evaporation of sea water: New constraints on the marine vs. non-marine debate. Geology, 20, 799–802.

Voerkelius S., Lorenz G.D., Rummel S., Quétel C.R., Heiss G., Baxter M., Brach-Papa C., Deters-Itzelsberger P., Hoelzl S., Hoogewerff J., Ponzevera E., Bocxstaele M.V., Ueckermann H. (2010) Strontium isotopic signatures of natural mineral waters, the reference to a simple geological map and its potential for authentication of food. Food Chemistry, 118, 933–940.

Vogt K. (1980) Bentonite Deposits in Lower Bavaria. Geologisches Jahrbuch, D39, 47–68.

Vogt K., Köster H.M. (1978) Zur Mineralogie, Kristallchemie und Geochemie einiger Montmorillonite aus Bentoniten. Clay Minerals, 13, 25–43.

Waber H.N., Heidinger M., Lorenz G., Traber D. (2014) Hydrochemie und Isotopenhydrogeologie von Tiefengrundwässern in der Nordschweiz und im angrenzenden Süddeutschland. Nagra Arbeitsbericht, NAB 13–63, 1–247.

Wagner B., Töpfner C., Lischeid G., Scholz M., Klinger R., Klaas P. (2003) Hydrogeochemische Hintergrundwerte der Grundwässer Bayerns. GLA-Fachberichte, 21, 1–250.

Walker C.T., Price N.B. (1963) Departure Curves for Computing Paleosalinity from Boron in Illites and Shales. American Association of Petroleum Geologists Bulletin, 47, 833–841.

Walsh S.L., Demere T.A. (1991) Age and stratigraphy of the Sweetwater and Otay formations, San Diego County, California. Pp. 131-148 in: Eocene Geologic history, San Diego region (Abbott P.L., May J.A., editors). Society of Economic Paleontologists and Mineralogists Pacific Section Book 68.

Walz W. (1991) Chemisch-mineralogische und physikalisch-technische Untersuchungen an bayerischen Bentoniten sowie Betrachtungen zur Genese der bayerischen Bentonitlagerstätten. Doctoral thesis, Friedrich-Alexander-Universität Erlangen-Nürnberg, Erlangen, 289 p.

Warner M.A. (1982) Source and time of generation of hydrocarbons in the Fossil basin, western Wyoming thrust belt. Pp. 805–815 in: Geologic Studies of the Cordilleran Thrust Belt, Volume 2 (Powers R.B., editor), Rocky Mountain Association of Geologists, Denver.

Warr L.N., Hofmann H., van der Pluijm B.A. (2016) Constraining the alteration history of a Late Cretaceous Patagonian volcaniclastic bentonite–ash–mudstone sequence using K–Ar and $^{40}Ar/^{39}Ar$ isotopes. International Journal of Earth Sciences, 106, 255–268.

Warthmann R., van Lith Y., Vasconcelos C., McKenzie J.A., Karpoff A.M. (2000) Bacterially induced dolomite precipitation in anoxic culture experiments. Geology, 28, 1091–1094.

Weaver C.E. (1989) Clays, Muds, and Shales. 1st Editon. Developments in Sedimentology, 44, Elsevier, Amsterdam, 818 p.

Weaver C.E., Pollard L.D. (1973) The Chemistry of Clay Minerals. Elsevier, Amsterdam, 213 p.

Webster J.D., Holloway J.R., Hervig R.L. (1989) Partitioning of lithophile trace elements between H_2O and H_2O+CO_2 fluids and topaz rhyolite melt. Economic Geology, 84, 116–134.

Weinig H. (1987) Bentonit (Bleicherde). Geologica Bavarica, 91, 135–142.

Wetzenstein W. (1972) Die Bentonitlagerstätten im Ostteil der Insel Milos und ihre mineralogische Zusammensetzung. Bulletin of the Geological Society of Greece, 9, 144–171.

Williams L.B. (2000) Boron isotope geochemistry during burial diagenesis. Ph.D. dissertation, University of Calgary, Alberta, Canada, 168 p.

Williams L.B., Hervig R.L. (2002) Exploring intra-crystalline B-isotope variations in mixed-layer illite-smectite. American Mineralogist, 87, 1564–1570.

Williams L.B., Hervig R.L. (2004) Boron isotope composition of coals: a potential tracer of organic contaminated fluids. Applied Geochemistry, 19, 1625–1636.

Williams L.B., Hervig R.L. (2005) Lithium and boron isotopes in illite/smectite: The importance of crystal size. Geochimica et Cosmochimica Acta, 69, 5705–5716.

Williams L.B., Hervig R.L. (2006) Crystal size dependence of illite-smectite isotope equilibration with changing fluids. Clays and Clay Minerals, 54, 531–540.

Williams L. B., Hervig R. L., Holloway J. R., Hutcheon I. (2001a) Boron isotope geochemistry during diagenesis: Part I. Experimental determination of fractionation during illitization of smectite. Geochimica et Cosmochimica Acta, 65, 1769–1782.

Williams L. B., Hervig R. L., Hutcheon I. (2001b) Boron isotope geochemistry during diagenesis: Part II. Applications to organic-rich sediments. Geochimica et Cosmochimica Acta, 65, 1783–1794.

Williams L.B., Weiser M.E., Hutcheon I., Hervig R.L., (2001c) Application of boron isotopes to understanding fluid/rock interactions in a hydrothermally stimulated oil-reservoir in the Alberta basin, Canada. Geofluids, 1, 229–240.

Williams L.B., Turner A., Hervig R.H. (2007) Intracrystalline boron isotope partitioning in illite–smectite: testing the geothermometer. American Mineralogist, 92, 1958–1965.

Wostatek T. (2014) Geochemische Analyse der eisenreichen Tone der Carl Heinrich-Grube. Bachelor thesis, Technische Universität München, Germany, 54 p.

Wright V.P., Tucker M.E. (Eds.) (1991) Calcretes: An Introduction. Pp. 1–25. In: Calcretes. (V.P. right, Tucker M.E., editors) Blackwell Scientific Publications, Oxford.

Wu S.F, You C.F., Lina Y.P., Valsami-Jones E., Baltatzis E. (2016) New boron isotopic evidence for sedimentary and magmatic fluid influence in the shallow hydrothermal vent system of Milos Island (Aegean Sea, Greece). Journal of Volcanology and Geothermal Research, 310, 58–71.

Xiao J., Xiao Y.K., Jin Z.D., He M.Y., Liu C.Q. (2013) Boron isotope variations and its geochemical application in nature. Australian Journal of Earth Sciences, 60, 431–447.

You C.F., Spivack A.J., Gieskes J.M., Rosenbauer R., Bischoff J.L. (1995) Experimental study of boron geochemistry: Implications for fluid processes in subduction zones, Geochimica et Cosmochimica Acta, 59, 2435–2442.

You C.F., Spivack A.J., Gieskes J.M., Martin J.B., Davisson M.L. (1996) Boron contents and isotopic compositions in pore waters: a new approach to determine temperature induced artifacts – geochemical implications. Marine Geology, 129, 351–361.

Zeebe R.E. (2005) Stable boron isotope fractionation between dissolved $B(OH)_3$ and $B(OH)_4^-$. Geochimica et Cosmochimica Acta, 69, 2753–2766.

Zeibig G., Kubanek F., Luck J. (1989) Pressure leaching of boron from argillaceous sediments for facies analysis. Chemical Geology, 74, 343–349.

Zhang L., Chan L.H., Gieskes J.M. (1998) Lithium isotope geochemistry of pore waters from Ocean Drilling Program Sites 918 and 919, Irminger Basin. Geochimica et Cosmochimica Acta, 62, 2437–2450.

Zorlu J. (2007) Sedimentpetrographische und geochemische Untersuchungen an unterschiedlich überprägten Triasdolomiten der Ost- und Südalpen. Doctoral thesis, Ruhr-Universität Bochum, Germany, Pp. 123–146.